

UC Riverside

UC Riverside Electronic Theses and Dissertations

Title

Development of NMR Methods for the Characterization of Heparin and its Impurities

Permalink

<https://escholarship.org/uc/item/4884z4xc>

Author

Lintiaco, John Francis Kuper

Publication Date

2011

Peer reviewed|Thesis/dissertation

University of California
Riverside

Development of NMR Methods for the Characterization of Heparin and its Impurities

A Dissertation submitted in partial satisfaction
of the requirement for the degree of

Doctor of Philosophy

in

Chemistry

by

John Kuper Limtiaco

June 2011

Dissertation Committee:

Dr. Cynthia K. Larive, Chairperson

Dr. Dallas Rabenstein

Dr. Yinsheng Wang

Copyright by
John Kuper Limtiaco
June 2011

The Dissertation of John Kuper Limtiaco is approved:

Committee Chairperson

University of California, Riverside

Acknowledgements

Looking back on my life it is quite hard for me to imagine that I would have made it this far in my academic pursuits. I often felt that goals such as this were too difficult for me to achieve, however with the encouragement and support from so many individuals this unattainable goal has become a reality. I would like to start off by thanking my undergraduate mentor, Dr. Maika Vuki, for taking me under his wing as an ill-equipped student at the University of Guam. Dr. Vuki introduced me to the many joys of research, guiding and motivating me to pursue an advanced degree in chemistry. His vision for me far exceeded my own.

I want to extend a sincere thanks to my graduate advisor, Dr. Cynthia Larive, I am marveled by her patience and her unending support for me and all her students. Cindy has often pushed me far beyond my comfort zone in an effort to broaden my horizons, making me a better scientist and person. I believe that the most important thing Cindy has taught me over the last five years is that people are the most important consideration. I would also like to thank Christopher Jones for all his help in both NMR and MS. My friend, one day we will meet up again and have some excellent stories to tell about graduate school. To all my former but most especially my present labmates, thank you for making everyday an entertaining one.

I would like to acknowledge my parents whose unconditional love and support continues to inspire me to become a more productive and caring person. You both stressed the importance of a college education as witnessed in the success of both of your children. Thank you both for setting an example and encouraging me to chase my dreams of becoming a doctor and scientist.

Above all else, I want to thank my fiancé, Angela Laygo, for her unconditional support, understanding, patience, and friendship. Though she was also working on completing her doctorate degree she still found time to care for me while I worked to complete this dissertation. I would not have gotten through these years without your love and encouragement, I am eternally grateful to have you by my side and in my life.

I Love You Neni!

This dissertation is dedicated to my parents for their unwavering love, encouragement,
and support throughout the 28 years of my life.

You've always lead me to believe that anything is possible.

To my love and fiancé, Angela Jane Laygo, for comforting me when times got tough and
never letting me give up.

I am so very excited to start our lives together!

ABSTRACT OF THE DISSERTATION

Development of NMR Methods for the Characterization of Heparin and its Impurities

by

John Kuper Limtiaco

Doctor of Philosophy, Graduate Program in Chemistry
University of California, Riverside, June 2011
Dr. Cynthia K. Larive, Chairperson

The goal of this dissertation is to develop and apply NMR methods for the analysis of heparin and its impurities. As a result of the intentional contamination of heparin with oversulfated chondroitin sulfate (OSCS), significant efforts have been placed on the development of analytical methods to evaluate heparin purity. To advance the suite of analytical methods available for heparin analysis, HPLC-NMR and diffusion NMR methods were developed for its characterization. Our HPLC-NMR method focuses on the WAX separation of intact glycosaminoglycans (GAGs) coupled to on-line UV and NMR spectroscopy for detection and identification of heparin contaminants. The weak anion exchange (WAX) method developed allows for the timely separation of heparin and its impurities, OSCS, dermatan sulfate, and chondroitin sulfate A. In addition to the study of heparin impurities using WAX-HPLC, the characterization of intact and digested heparin samples was investigated using diffusion NMR. Because the diffusion behavior of the intact biopolymers can be dominated by viscosity and molecular crowding effects even in dilute GAG solutions, NMR diffusion results must only be interpreted qualitatively. These limitations can be largely overcome by digesting heparin to low molecular weight oligosaccharides, significantly improving the resolution of heparin and its biopolymer impurities.

The second part of this dissertation is on the characterization of heparin-derived oligosaccharides. Because of the structural complexity and heterogeneity of heparin and heparan sulfate, extensive or partial digestion of the full length polysaccharides is a common practice. Size-exclusion chromatography was used to separate digested heparin oligosaccharides into size-based fractions while SAX-HPLC was used to further purify individual oligosaccharides for NMR characterization. Although, NMR spectroscopy is a powerful tool for structure determination, it trails other analytical techniques in sensitivity. Microcoil NMR is an inexpensive method for enhancing the mass sensitivity of NMR allowing structure elucidation with 5-10 μg of isolated material. Results are presented showing the utility of microcoil NMR for the structure characterization of microgram amounts of heparin-derived tetrasaccharides, reducing the NMR sample requirements by 2-fold when compared to analysis in a Shigemi tube.

In Chapter 6, an IMPACT-HNMBC experiment was used in the detection of ^{15}N in amino sugars through long-range couplings to carbon-bound protons of the sugar ring. Comparison of the ge-HMBC, IMPACT-HMBC and a modified IMPACT-HNMBC pulse sequence revealed improved sensitivity, resolution and reduced F_1 noise with the IMPACT-HNMBC experiment.

TABLE OF CONTENTS

ABSTRACT OF THE DISSERTATION	vii
TABLE OF CONTENTS	ix
LIST OF FIGURES	xvi
LIST OF TABLES	xxii
CHAPTER ONE: Introduction	1
1.1 Heparin Structure	3
1.1.2 Heparin and HS Biosynthesis	5
1.1.3 Biological Function and Protein Binding	8
1.2 Heparin Impurities	10
1.2.1 OSCS Adulteration of Heparin	11
1.3 Analytical Challenges for Heparin Analysis	17
1.3.1 Enzymatic Depolymerization of Heparin	18
1.3.2 Role of NMR Spectroscopy in Heparin Impurity Analysis	20
1.4 Nuclear Magnetic Resonance Theory	23
1.4.1 Origin of the NMR Signal	23
1.4.2 Vector Description of NMR	26
1.5 Improving the Sensitivity of NMR	29
1.5.1 Microcoil NMR	31
1.6 Oligosaccharide Structure Assignment by NMR Spectroscopy	32
1.7 Diffusion NMR	35
1.7.1 Diffusion NMR with the BPPSTE Pulse Sequence	43
1.7.2 Diffusion-Ordered Spectroscopy (DOSY)	46

1.7 References	54
CHAPTER TWO: Characterization of Heparin and its Impurities with HPLC-NMR using Weak Anion Exchange Chromatography	61
2.1 Introduction: Identification of pharmaceutical contaminants and degradants using high performance liquid chromatography coupled to NMR (HPLC-NMR)	61
2.1.1 Identification of heparin contaminants using weak-anion exchange chromatography coupled to NMR (WAX-HPLC-NMR)	62
2.2 Experimental Section	64
2.2.1 Chemicals	64
2.2.2 OSCS Synthesis	64
2.2.3 RPIP-HPLC Analysis	65
2.2.4 WAX-HPLC Analysis	66
2.2.4.1 WAX-HPLC Separation in Protonated Buffers	66
2.2.4.2 WAX-HPLC Separation in Deuterated Buffers	67
2.2.5 Trapping of OSCS	67
2.2.6 On-flow ¹H NMR Analysis	68
2.2.7 Stop-flow ¹H NMR Analysis	68
2.2.8 High pD Stability Experiments	69
2.3 Results and Discussion	70
2.3.1 RPIP-HPLC in the Separation of Heparin and OSCS	70
2.3.2 WAX-HPLC	74
2.3.2.1 Optimization of Heparin Retention and Elution with WAX-HPLC	74
2.3.3 Separation of DS, CSA, Heparin and OSCS in D₂O Solution	75
2.3.4 Analytical Figures-of-Merit	76
2.3.5 On-flow and Stop-flow Analysis Following WAX-HPLC	80

2.3.6 Sensitivity Enhancement Through Peak-trapping of OSCS	85
2.4 Summary	91
2.5 References	92
CHAPTER THREE: Diffusion NMR Measurements of Heparin and its Contaminants	96
3.1 Introduction	96
3.1.1 <i>In-Situ</i> Analysis of Solutions	96
3.1.2 DOSY-NMR Analysis of Heparin and its Impurities	99
3.1.3 Spectral Editing by Molecular Diffusion	98
3.1.4 Application of NMR Diffusion Editing Strategies in Heparin Purity Analysis	99
3.2 Experimental Section	100
3.2.1 Chemicals	100
3.2.2 Heparinase Depolymerization of Heparin	101
3.2.3 Cocktail Digestion of Heparin	102
3.2.4 NMR Spectroscopy	102
3.2.5 Viscosity Measurements	103
3.3 Results and Discussion	105
3.3.1 DOSY Analysis of Intact GAGs	106
3.3.1.1 Diffusion Analysis of Solutions of Heparin and DS	108
3.3.1.2 Diffusion Analysis of Solutions of Heparin and OSCS	115
3.3.2 DOSY Analysis of Heparin Digest Solutions	119
3.3.3 Diffusion-Edited NMR Spectroscopy	123
3.4 Summary	126
3.5 References	129

CHAPTER FOUR: NMR Methods to Monitor the Enzymatic Depolymerization of Heparin	132
4.1 Introduction: Depolymerization of Heparin	132
4.2 Experimental Section	134
4.2.1 Chemicals	134
4.2.2 Enzymatic Depolymerization of Heparin	134
4.2.3 Monitoring the Progress of the Enzymatic Depolymerization with UV Absorption	135
4.2.4 SEC Fractionation	135
4.2.5 ¹ H NMR Experiments	135
4.3 Results and Discussion	138
4.3.1 Monitoring the Enzymatic Depolymerization with UV Absorption	138
4.3.2 Monitoring the Enzymatic Depolymerization of Heparin with ¹ H NMR	141
4.3.3 Monitoring the Enzymatic Depolymerization of Heparin using DOSY	144
4.4 Summary	152
4.5 References	153
CHAPTER FIVE: Structurally unique heparin-derived tetrasaccharide isomers: separation, isolation and identification using microcoil NMR	156
5.1 Introduction: Structural Properties of Heparin and Heparan Sulfate	157
5.1.1 Depolymerization of Heparin and HS	159
5.1.2 Separation of Heparin-Derived Oligosaccharides	161
5.1.2.1 SEC Separation of Heparin Depolymerization Products	161
5.1.2.2 SAX-HPLC Separation of Size-Uniform Heparin Oligosaccharide Fractions	162

5.1.2.3 RPIP-HPLC Separation of Size-Uniform Heparin Oligosaccharides	163
5.1.3 Characterization of Heparin Components by NMR	164
5.1.3.1 Two-dimensional NMR Analysis of Heparin Oligosaccharides	165
5.2 Experimental Section	166
5.2.1 Chemicals	166
5.2.2 Enzymatic Depolymerization of Heparin	168
5.2.3 SEC Separation	168
5.2.4 SAX-HPLC Separation	169
5.2.5 Desalting Procedure	170
5.2.6 Microcoil NMR Analysis	170
5.2.7 NMR Sensitivity Measurements	172
5.2.8 RPIP-UPLC Separation	173
5.2.9 Mass Spectrometry	174
5.3 Results and Discussion	174
5.3.1 Separation and Isolation of Heparin-Derived Tetrasaccharides	175
5.3.2 RPIP-UPLC-MS Analysis of the SEC Tetrasaccharide Fraction	178
5.3.3 ¹ H NMR Characterization of Saccharides	181
5.3.4 Microcoil NMR	182
5.3.5 NMR Sensitivity Comparison	183
5.3.6 NMR Characterization of Heparin Tetrasaccharides	185
5.4 Summary	204
5.5 References	206
CHAPTER SIX: IMPACT-HNMBC Measurements of Amino Sugars	211

6.1 Introduction: Inverse Detected NMR Experiments for Heteronuclear Correlation	212
6.1.1 Single-bond heteronuclear [¹H-¹⁵N] correlation experiments in GAG analysis	212
6.1.2 Multiple-bond heteronuclear [¹H-¹⁵N] correlation experiments in GAG analysis	215
6.2 Experimental Section	215
6.2.1 Chemicals	215
6.2.2 NMR Experiments	216
6.2.2.1 ¹H NMR experiments	216
6.2.2.2 [¹H-¹⁵N]-HMBC experiments	216
6.2.2.3 Characterization of the α and β anomers of GalNAc	217
6.3 Results and Discussion	218
6.3.1 HMBC Pulse Sequence	218
6.3.2 HMBC pulse sequence comparison	222
6.3.3 IMPACT-HNMBC of <i>N</i>-modified glucosamines	225
6.3.4 ¹⁵N-²H splitting with IMPACT-HNMBC	232
6.4 Summary	237
6.5 Acknowledgment	238
6.6 References	239
CHAPTER SEVEN: Conclusions and Future Directions	242
7.1 Conclusions	242
7.2 Future Directions	245
7.2.1 Capillary Isotachopheresis (cITP)-NMR	245
7.2.2 Heteronuclear Hartmann-Hahn (HEHAHA)	246
7.2.3 Hyperpolarization	247

LIST OF FIGURES

Figure		Page
Figure 1.1	Structures of the possible disaccharide subunits of heparin showing the substitution sites on the uronic acid and glucosamine residues and the orientation of the carboxylate moiety in the the iduronic and glucuronic acid epimers.	4
Figure 1.2	Schematic illustration of the origin of heparin's microheterogeneous structure.	6
Figure 1.3	Major repeating disaccharide units of heparin-like GAGs (A) CS, (B) DS, (C) OSCS.	12
Figure 1.4	NMR spectra of contaminated heparin. (A) Comparison of anomeric and acetyl regions of the ¹ H NMR spectra of standard heparin, heparin containing natural dermatan sulfate (DS) and contaminated heparin. (B) Comparison of carbonyl (i), sugar (ii) and <i>N</i> -acetyl regions (iii) of the ¹³ C NMR spectra of standard heparin, heparin containing natural dermatan sulfate, and contaminated heparin. (C) HSQC spectrum of the contaminated sample overlaid on control heparin sample.	15
Figure 1.5	Scheme illustrating the enzymatic depolymerization of heparin with the enzyme heparinase I. The heparin-derived oligosaccharide contains a $\Delta^{4,5}$ double bond introduced into the uronic acid at the non-reducing end. R ₁ : H or SO ₃ ⁻ , R ₂ : H or SO ₃ ⁻ , and R ₃ : H, SO ₃ ⁻ , or COCH ₃ .	19
Figure 1.6	HSQC spectrum of heparin containing 10% (w/w) OSCS prepared using a 20 mg/mL D ₂ O solution of the USP system suitability standard.	21
Figure 1.7	Field dependence of the nuclear spin states, α and β , for the spin quantum number $I=1/2$.	25
Figure 1.8	Vector diagrams for the orientation of the bulk magnetization M , (A) at equilibrium aligned with the static magnetic field, B ₀ , (B) following the application of a RF pulse with length (t_p) applied along the x-axis, and (C) following the application of an RF pulse along the x-axis of sufficient length to place the bulk magnetization along the y-axis.	28
Figure 1.9	(A) CapNMR ¹ H survey spectrum measured with 192 μ g of Δ UA(2S)-GlcNS(6S)-GlcA-GlcNS(6S). Portions of the (B) COSY, (C) TOCSY spectra showing cross peaks to the well-resolved anomeric resonances used to establish the structure of the	33

	tetrasaccharide. (D) Structure of the heparin-derived tetrasaccharide.	
Figure 1.10	(A) Spin-echo pulse sequence for the measurement of T_2 relaxation introduced by Edwin Hahn in 1950. (B) Diagram of the formation of the spin echo.	37
Figure 1.11	(A) PGSE pulse sequence used for PFG-NMR diffusion measurements and (B) the effect on the magnetization.	39
Figure 1.12	(A) The PFG-STE pulse and (B) the effect on the magnetization.	42
Figure 1.13	Bipolar pulse pair stimulated echo (BPPSTE) used in the diffusion experiments in this dissertation	45
Figure 1.14	(A) The structure of the pyridine ligand and ^1H NMR spectrum of 1:1 mixture of ligand and cluster. (B) Stacked plot of cluster resonances (left) and ligand resonances (right) collected as a function of increased gradient strength. (C) Molecular diffusion by the attenuation of the NMR resonances as the gradient amplitude is increased.	47-48
Figure 1.15	DOSY spectrum of a 1:1 mixture of the pyridine ligand and cluster acquired in $\text{DMSO}-d_6$.	52
Figure 2.1	Proposed mechanisms for the separation of a negatively charged analyte with the cationic IRP and the competing cationic ammonium ion.	72
Figure 2.2	NMR detected chromatogram for the separation of (A) heparin and (B) OSCS using RPIP-HPLC as well as the (C) UV detected chromatogram for the separation of OSCS.	73
Figure 2.3	UV-detected WAX chromatograms of DS, CSA, heparin and OSCS. (A) Measured using deuterated buffers and no isocratic delay. (B) Measured using deuterated buffers and employing a 10 min isocratic delay between the elution of heparin and OSCS.	77
Figure 2.4	UV-detected WAX chromatogram for a sample containing (top) 0.25 mg/mL DS and OSCS in the presence of 40 mg/mL heparin and (bottom) blank measured using protonated buffers.	79
Figure 2.5	On-flow ^1H NMR-detected WAX chromatogram of heparin and OSCS.	81
Figure 2.6	Stop-flow ^1H NMR spectra of (A) heparin, (B) OSCS, (C) DS, and (C) CSA.	83-84

Figure 2.7	¹ H NMR spectra of heparin at pD 10.25, (A) day 1, (B) day 2, and (C) after 1 week.	86
Figure 2.8	¹ H NMR spectra of OSCS at pD 10.25, (A) day 1, (B) day 2, and (C) after 1 week.	87
Figure 2.9	¹ H NMR spectra of DS at pD 10.25, (A) day 1, (B) day 2, and (C) after 1 week.	88
Figure 2.10	(A) Stop-flow ¹ H NMR spectrum of OSCS measured for a single injection of a sample containing 40 mg/mL of heparin and 2 mg/mL OSCS acquired with 1024 scans. (B) Stop-flow ¹ H NMR spectrum of OSCS measured for a single injection of a sample containing 40 mg/mL heparin and 2 mg/mL OSCS acquired with 4608 scans. (C) Stop-flow ¹ H NMR spectrum of OSCS measured for a single injection of a sample containing 40 mg/mL of heparin and OSCS. (D) Stop-flow ¹ H NMR spectrum of OSCS measured for 10 repeated injections of a sample containing 40 mg/mL heparin and 2 mg/mL OSCS using peak trapping.	89
Figure 3.1	Diffusion results obtained by fitting a mono-exponential decay to the intensities of the <i>N</i> -acetyl resonances of (A) heparin and (B) OSCS for a heparin/OSCS solution with a total GAG concentration of 12.5 mg/mL.	104
Figure 3.2	¹ H NMR spectra measured for (A) heparin/DS and (B) heparin/OSCS solutions.	109
Figure 3.3	Comparison of <i>N</i> -acetyl region of the ¹ H NMR spectra measured for (A) heparin/DS and (B) heparin/OSCS solutions.	111
Figure 3.4	Diffusion NMR spectra for a solution of intact heparin and DS. (A) Stacked plot showing the decrease in the <i>N</i> -acetyl resonance intensity as a function of applied gradient. (B) DOSY spectrum.	112
Figure 3.5	DOSY NMR spectrum measured for a solution containing intact heparin and OSCS.	116
Figure 3.6	¹ H NMR BPPSTE spectra showing the attenuation of the <i>N</i> -acetyl resonances of heparin and DS (A) after digestion and (B) before digestion with the enzyme heparinase I.	120
Figure 3.7	The <i>N</i> -acetyl region of the DOSY spectra measured for heparinase I digest solutions of (A) heparin/DS and (B) heparin/OSCS.	121
Figure 3.8	¹ H NMR spectra of (A) heparin API digest solution, (B) diffusion-edited spectrum of the DS contained in the heparin digest	124

solution, (C) DS standard solution.

- Figure 3.9** ^1H NMR spectra of (A) heparin/OSCS digest solution (B) diffusion-edited spectrum of the OSCS and CSA contained in the heparin digest solution, (C) OSCS solution prepared in our laboratory, and (D) CSA standard solution. **125**
- Figure 3.10** *N*-acetyl region of the ^1H NMR spectra of (A) heparin/OSCS digest solution (B) diffusion-edited spectrum of the OSCS and CSA contained in the heparin digest solution, (C) OSCS solution prepared in our laboratory, and (D) CSA standard solution. **127**
- Figure 4.1** Production and size-fractionation of heparin derived oligosaccharides. (A) Progression of the enzymatic digestion measured at 232 nm using a 1 mm path length. Aliquots were taken at regular intervals (20 min to 6 hr). (B) Preparative SEC of heparin oligosaccharides following the enzymatic depolymerization of heparin with heparinase I. **139**
- Figure 4.2** ^1H NMR spectra measured as a function of time for the depolymerization solution. **142**
- Figure 4.3** DOSY spectra for the anomeric and H-4 protons of the ΔUA residues of the heparin digest solution at (A) 1 hr and (B) 66 hr. **146**
- Figure 4.4** ^1H NMR spectra of the anomeric region (A) standard IS disaccharide of heparin measured in depolymerization buffer and (B) heparin depolymerization solution at time 66 hr. **150**
- Figure 4.5** The diffusion coefficients for the H-4 protons of the ΔUA residues at 5.973, 5.981, 5.990, and 5.998 formed during heparinase I digestion. **151**
- Figure 5.1** Disaccharide subunits of heparin showing the common substitution sites on the uronic acid and glucosamine residues as well as the orientation of the carboxyl moiety of the (A) iduronic acid and (B) glucuronic acid epimers. **158**
- Figure 5.2** Diagram illustrating the ^1H correlations observed using the pulse sequences (A) COSY, (B) TOCSY, and (C) ROESY. **167**
- Figure 5.3** (A) SEC separation of heparin digest with off-line detection at 232 nm. Well-resolved peaks corresponding to size-uniform depolymerization products (dp) are detected for di- (dp2) to hexadecasaccharides (dp16). (B) UV-detected SAX chromatogram at 232 nm for the SEC fraction of heparin-derived tetrasaccharides using a 2.0 M NaCl gradient for elution. **176**

Figure 5.4	Total ion chromatogram of an optimized RPIP-UPLC/MS separation for the SEC fraction of heparin-derived tetrasaccharides. RPIP-UPLC resolves the α and β anomers of the reducing end residue, complicating the separation and contributing to the poor resolution of this separation.	179
Figure 5.5	^1H NMR spectra comparing the observed S/N and line shapes for 20 μg of sucrose in D_2O using (A) CapNMR probe using solvent push volume technique, (B) CapNMR probe using sample focusing with chloroform- <i>d</i> , and (C) a Bruker 1 mm MicroProbe with disposable capillary insert.	184
Figure 5.6	CapNMR ^1H spectra measured for the tetrasaccharide peaks isolated using SAX-HPLC.	186
Figure 5.7	CapNMR spectra measured with 21 μg of $\Delta\text{UA}(2\text{S})\text{-GlcNS-IdoA}(2\text{S})\text{-GlcNS}(6\text{S})$ isolated as SAX peak 4. Portions of the (A) COSY, (B) TOCSY and (C) ROESY spectra showing cross peaks to the well-resolved anomeric resonances used to establish the structure of the tetrasaccharide.	188
Figure 5.8	^1H NMR spectrum for SAX peak 2 showing the anomeric and $\Delta\text{UA}_{\text{H}4}$ chemical shift region. The measured integrals displayed above each peak were normalized to the area of the $\Delta\text{UA}_{\text{H}4}$ resonance.	193
Figure 5.9	CapNMR ^1H spectra measured for $\Delta\text{UA}(2\text{S})\text{-GlcNS}(6\text{S})\text{-IdoA}(2\text{S})\text{-GlcNS}$ isolated as SAX peak 3. Portions of the (A) TOCSY and (B) ROESY spectra measured for this sample.	194
Figure 5.10	CapNMR ^1H spectra measured for SAX peak 2 Portions of the (B) TOCSY and (C) ROESY spectra measured for this sample. The spectrum was acquired within a 24 hr period for a sample containing 49 μg of isolated sample. Cross peaks due to $\Delta\text{UA}(2\text{S})\text{-GlcNS}(6\text{S})\text{-IdoA}(2\text{S})\text{-GlcNS}$ (labeled P3) are assigned in Figure 5.9.	196
Figure 5.11	(A) Total ion chromatogram of the RPIP-UPLC/MS separation of SAX peak 2 containing tetrasaccharides $\Delta\text{UA}(2\text{S})\text{-GlcNS}(6\text{S})\text{-IdoA}(2\text{S})\text{-GlcNS}$ and $\text{IdoA}(2\text{S})\text{-GlcNS}(6\text{S})\text{-IdoA}(2\text{S})\text{-GlcNS}(6\text{S})$ along with their mass spectra (B) and (C), respectively.	199
Figure 6.1	Structure of GlcN along with the ^1H numbering scheme used to represent the peaks in the 2D NMR spectra.	214
Figure 6.2	The NMR pulse sequences for the (A) ge-HMBC, (B) IMPACT-	219

HMBC, and (C) IMPACT-HNMBC experiments.

Figure 6.3	Two dimensional HMBC NMR spectra of GlcNAc recorded on a 600 MHz NMR spectrometer using the (A) ge-HMBC, (B) IMPACT-HMBC, and (C) IMPACT-HNMBC pulse sequences.	223-224
Figure 6.4	(A) ^1H NMR spectrum and (B) IMPACT-HNMBC of a mixture containing GlcN, GlcNS, and GlcNAc each at a concentration of 100 mM in D_2O .	226
Figure 6.5	Two dimensional NMR spectra of GalNAc: (A) IMPACT-HNMBC at 500 mM GalNAc in D_2O , (B) portion of the HSQC, and (C) DQF-COSY in 90% $\text{H}_2\text{O}/10\%$ D_2O .	230-231
Figure 6.6	IMPACT-HNMBC spectrum of GalNAc in 90% $\text{H}_2\text{O}/10\%$ D_2O .	233
Figure 6.7	IMPACT-HNMBC spectra of (A) GlcNAc and (B) GlcNAc6S in D_2O .	234

LIST OF TABLES

Table		Page
Table 3.1	Effect of heparin concentration on diffusion coefficients and solution viscosities.	107
Table 5.1	Structures of commercially available heparin disaccharide standards; IA-IVA, IS-IIIS, and IH-IVH.	160
Table 5.2	¹ H Chemical shifts of the tetrasaccharides isolated using SAX-HPLC.	190-191
Table 5.3	SAX retention times, RPIP-UPLC retention times, m/z of the molecular ion [M-2H] ²⁻ , the mass used in the microcoil NMR experiments and the identities of the heparin-derived tetrasaccharides determined, and references previously reporting this compound.	201
Table 6.1	Amino sugar ¹⁵ N chemical shifts and long-range ¹ H correlations observed in the IMPACT-HNMBC spectra measured in D ₂ O solution.	236

CHAPTER ONE

Introduction

The research presented in this dissertation focuses on the development and application of NMR methods, including HPLC-NMR, diffusion NMR and microcoil NMR, for the characterization of heparin and its impurities. The adulteration of pharmaceutical heparin in late 2007 and early 2008 drew attention to the need for improvements to the analytical methods used for the rapid identification of glycosaminoglycans (GAGs) and their potential impurities. The key role of NMR spectroscopy in the identification of oversulfated chondroitin sulfate (OSCS) as the contaminant in adulterated batches of heparin demonstrated the value of NMR as an essential analytical technique for the rapid and efficient screening for heparin and its related impurities.

The structural diversity and heterogeneity of the GAG biopolymers complicates the analysis of heparin and heparan sulfate (HS). Because these biologically-derived samples are often available in limited amounts, obtaining sufficient quantities of pure oligosaccharides, especially those that constitute rare protein binding motifs, requires labor-intensive isolation protocols involving several orthogonal separation steps. Since heparin and HS are at the forefront of drug discovery, both as targets and as candidates for new therapeutics, assembling a more complete knowledge of the microstructure of these biopolymers is crucial.

The goal of this dissertation is to demonstrate improved analytical methods and approaches that address the challenges of separating and characterizing heparin impurities and heparin-derived oligosaccharides. This goal is accomplished through the following objectives:

Objective 1: Develop an HPLC-NMR method coupled to weak-anion exchange chromatography for the on-line detection and characterization of heparin impurities including OSCS, CSA, and DS (Chapter 2).

Objective 2: Employ DOSY-NMR and diffusion-editing for the in-situ analysis of heparin and its impurities and investigate the effects of viscosity on diffusion coefficients measured for the intact polysaccharides (Chapter 3).

Objective 3: Apply DOSY-NMR to monitor the enzymatic depolymerization of heparin using heparinase I (Chapter 4).

Objective 4: Use microcoil NMR in the characterization of mass-limited amounts of heparin-derived tetrasaccharides isolated by SAX-HPLC (Chapter 5).

Objective 5: Design and apply a novel heteronuclear NMR experiment to structurally characterize *N*-modified amino sugars via long-range couplings of ^{15}N to carbon bonded protons at ^{15}N natural abundance (Chapter 6).

The first part of this introductory chapter presents background information about heparin's structure and function. This is followed by a discussion of the application of various NMR techniques to the challenges of heparin impurity analysis and the structural characterization of heparin and HS oligosaccharides.

1.1 Heparin Structure

Heparin is a member of the GAG family of carbohydrates which also includes HS, dermatan sulfate (DS), keratan sulfate, chondroitin sulfate, and hyaluronic acid (HA). Heparin is a polydisperse mixture of sulfonated linear polysaccharides consisting of 1→4 linked and variously modified uronic acid and D-glucosamine repeating disaccharide subunits as presented in Figure 1.1.¹ Heparin and HS are the most structurally complex members of the GAG family. Their structural complexity arises from varying levels of sulfonation as well as epimerization at the C-6 position of the uronic acid residues.

The uronic acid residue of heparin and HS may be either α -L-iduronic (IdoA) or β -D-glucuronic acid (GlcA) and can be unsubstituted or sulfonated at the 2-O position. The glucosamine residue may be unmodified (GlcN), *N*-sulfonated (GlcNS) or *N*-acetylated (GlcNAc), and can contain variable patterns of *O*-sulfonation at the 3-O and 6-O positions. The major disaccharide sequence of heparin is the trisulfonated α -L-IdoA(2S)-D-GlcNS(6S) which comprises over 70% of heparin isolated from porcine intestinal mucosa.^{1, 2} The related GAG, HS, is commonly found as a proteoglycan located at the cellular surface and the extracellular matrix (ECM).³ Although heparin and HS are constructed from the same disaccharide subunit, the sulfonate content of HS is considerably lower than heparin. Consequently, a GAG qualifies as heparin only if the content of *N*-sulfo groups largely exceeds that of *N*-acetyl groups and the concentration of *O*-sulfo groups exceeds those of GlcNS.⁴

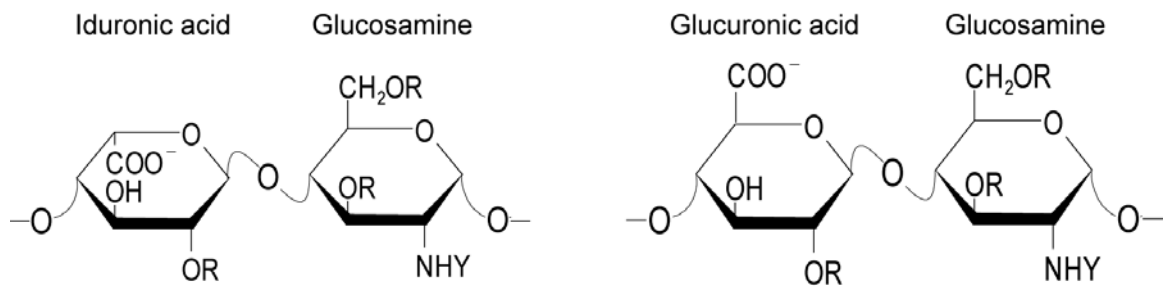


Figure 1.1. Structures of the possible disaccharide subunits of heparin showing the substitution sites on the uronic acid and glucosamine residues and the orientation of the carboxylate moiety in the the iduronic and glucuronic acid epimers; R: H or SO₃⁻ and Y: H, SO₃⁻, or COCH₃.

1.1.2 Heparin and HS Biosynthesis

Heparin is biosynthesized as a proteoglycan in a multistep process involving various enzymes in the endoplasmic reticulum and the Golgi apparatus of the mast cells of connective tissues.^{1, 3} Chain initiation begins with the step-wise addition of a xylose (Xyl) residue, two galactose (Gal) residues and a GlcA residue that attach to serine residues of serglycin, the core structural protein of heparin, to form the tetrasaccharide linker β -GlcA-(1 \rightarrow 3)- β -Gal-(1 \rightarrow 3)- β -Gal-(1 \rightarrow 4)- β -Xyl-Ser.^{1, 5} Chain initiation proceeds similarly for HS, however for HS several different core proteins are also involved including: the syndecans (transmembrane proteins), the glypicans (cell membrane proteins), and other core proteins located in the extracellular matrix.⁶ Polymerization of the heparin and HS chain involves the alternating addition of GlcA and GlcNAc monosaccharide residues via a 1 \rightarrow 4 linkage to the linker tetrasaccharides to form polysaccharide chains of various length ([GlcA-(1 \rightarrow 4)-GlcNAc]_n), where n can range from 5 to 50. For most commercial heparin preparations n is in the range of 20 to 26.⁷ The disaccharide addition is performed by two glycosyl transferases (EXT1 and EXT2), forming a stable heterodimeric complex in the Golgi.⁸

The next stage of heparin and HS biosynthesis is polymer modification. The modification process begins with the sequential modification of the [GlcA-(1 \rightarrow 4)-GlcNAc]_n chains by a series of enzyme-catalyzed reactions, as shown in Figure 1.2. The *N*-deacetylase enzyme removes the *N*-acetyl groups from the glucosamine residue and *N*-sulfotransferase replaces them with sulfate groups (GlcNS). *N*-sulfonation is initiated randomly along the polymer chains and it is believed that these two enzymes operate in parallel. This step occurs in a more localized fashion in HS resulting in a smaller ratio of GlcNS/GlcNAc than in heparin which has a significantly higher amount of GlcNS. The *N*-

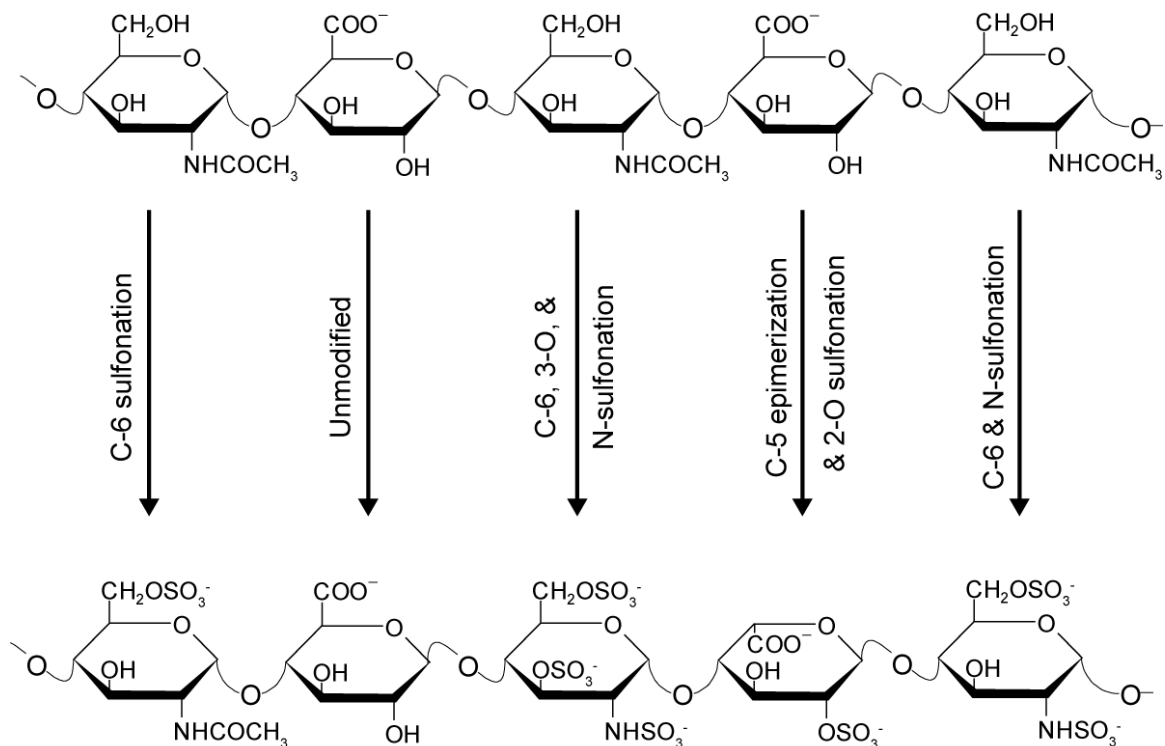


Figure 1.2. Schematic illustration of the origin of heparin's microheterogeneous structure. The final structure of heparin is the result of incomplete sequential modifications of the $[\text{GlcA}-(1,4)\text{-GlcNAc}]_n$ polymer by *N*-deacetylase/*N*-sulfotransferase-, C5 epimerase-, and 2-*O*-, 3-*O*-, and 6-*O*-sulfotransferase-catalyzed reactions. Shown at the bottom is the unique pentasaccharide sequence responsible for the antithrombin binding activity of heparin.

deacetylation/*N*-sulfonation reactions are followed by the conversion of GlcA to IdoA through the action of the C5 epimerase. The requirement for this modification is that the GlcA must be attached to the reducing end of a GlcNS residue. IdoA residues are then 2-*O*-sulfonated by the enzyme 2-*O*-sulfotransferase and this reaction is limited by the substrate specificity of the enzyme. 2-*O*-sulfotransferase cannot bind to IdoA residues that contain a C1-attached GlcNS(6S) (IdoA-(1→4)GlcNS(6S)). This suggests that the 2-*O* modification must occur first, followed by *O*-sulfation at the C-6 position of the GlcNS and unmodified GlcNAc residues by 6-*O*-sulfotransferase. Finally, certain GlcNS(6S) residues can act as a substrate for 3-*O*-sulfotransferase. The resulting 3-*O*-sulfonation (GlcNS(3,6S)) is a modification that is required in the pentasaccharide sequence responsible for the anticoagulant activity of heparin (Figure 1.2). *O*-sulfonation can also occur at other sites, such as the 2-*O*-sulfonation of GlcA residues and 6-*O*-sulfonation of isolated GlcNAc residues, but sulfonation at these sites occurs to a much smaller extent. As with the glycosyl transferases, it is also likely that the modifying enzymes, *N*- and *O*-sulfotransferases and the C5 epimerase, also associate to form a hetero-oligomeric complex in the Golgi resulting in the concomitant modification of several sequences at a time.⁸ Several tissue-specific isoforms of the biosynthetic enzymes give this system an additional level of complexity.⁸ Overall, HS contains fewer *O*- and *N*-sulfo modifications (0.2-0.7 per disaccharide) compared to heparin (2.0-2.5 per disaccharide).¹ The abundance of sulfonate and carboxylate groups associated with heparin contributes to its negative charge density making it the most anionic of any known biological macromolecule. Although the enzymatic modifications are believed to be performed in an organized and regulated way, not all of the potential substrate residues are modified.

As a result, the resulting polysaccharide chains are structurally complex and heterogeneous.

Following polymer modification, the polysaccharide chains of heparin are cleaved at select GlcA residues by the *endo*- β -D-glucuronidase enzyme yielding shorter, unbound chains of heparin. Because cleavage does not occur at all GlcA residues, heparin is polydisperse with regard to chain length and molecular weight. Chain cleavage also occurs for HS chains, but to a lesser degree. Most HS chains remain attached to their core proteins constituting the HS proteoglycan. The additive effect of microheterogeneity and polydispersity in heparin and HS contribute to the difficulty in the evaluation of important binding motifs that may be responsible for their biological functions.

1.1.3 Biological Function and Protein Binding

Following biosynthesis, heparin is stored along with histamine and basic proteases in the secretory granules of mast cells and is released into the extracellular matrix upon immunoglobulin-E-receptor stimulation via an immunogenic response.^{9, 10} Heparin is involved in the mediation of many biological functions such as cell differentiation, proliferation and migration, adhesion and host-pathogen interactions mainly through interactions with basic amino acid rich motifs of proteins.¹¹⁻¹⁴ Despite its involvement in these various biological processes, heparin is best known as an intravenous anticoagulant. Heparin was introduced into medical practice in the 1930s, making it one of the oldest drugs currently in widespread clinical use.¹⁵ Heparin's anticoagulant activity is due to binding of a unique pentasaccharide sequence (Figure 1.2) containing a 3-O-sulfo moiety, to the protease inhibitor antithrombin III (ATIII).

Heparin binding causes a conformational change in ATIII that increases the flexibility of its reactive site loop and as a result, its binding affinity for thrombin and Factors IXa and Xa.^{16, 17}

The large-scale industrial production of pharmaceutical heparin begins with its isolation from porcine intestinal mucosa or whole intestine. As the sources of unfractionated heparin are diverse and the production of raw heparin is under-regulated, variability observed in the chemical profile of raw heparin is not surprising. Consequently, some variability is preserved in pharmaceutical-grade heparin, even after well-regulated purification processes.¹⁸ The molecular weight of unfractionated heparin is in the range of 5-40 kDa, although the vast majority of commercial preparations are a heterogeneous mixture of molecules with a mean mass between 12 and 15 kDa.¹⁹

The main drawback of heparin administration resides in the poor predictability of coagulation parameters. To overcome this limitation, low molecular weight heparins (LMWHs) were introduced into clinical use.²⁰ A further success of the clinical application of LMWHs resides in their enhanced subcutaneous bioavailability and improved pharmacokinetics.²¹ LMWHs are manufactured from unfractionated heparin by controlled depolymerization resulting in average molecular weights of 4-6 kDa.²² Among the currently marketed LMWH's, tinzaparin is processed via digestion of heparin using heparinase lyase enzymes, while nadroparin and dalteparin are prepared by nitrous acid depolymerization. Enoxaparin is prepared by benzylation and alkaline hydrolysis, while ardeparin and cantaxarin are produced by oxidative fragmentation of the parent polysaccharide using hydrogen peroxide and periodate, respectively.^{23, 24}

1.2 Heparin Impurities

Considering the sources of pharmaceutical heparin, the numbers of potential impurities are relatively large compared with a synthetic therapeutic agent. The range of possible biological contaminants is quite extensive including viruses, bacterial endotoxins, Transmissible Spongiform Encephalopathy (TSE) agents, lipids, proteins and DNA.^{25, 26} During the preparation of pharmaceutical grade heparin from animal tissues, impurities such as solvents, heavy metals and extraneous cations can be introduced. However, methods to identify and/or eliminate process-related contaminants are well established and listed in guidelines and pharmacopoeias. The major challenge in the analysis of heparin impurities is the detection and identification of structurally related impurities, for example other GAGs.

The most prevalent impurity present in heparin is DS²⁷, also known as chondroitin sulfate B. The building block of DS is a disaccharide comprised of *N*-acetyl galactosamine (GalN) 1→3 linked to an uronic acid residue. The disaccharide subunits are connected via 1→4 linkages to form the polymer. DS is composed of three possible uronic acid (GlcA, IdoA or IdoA2S) and four possible hexosamine (GalNAc, GalNAc4S, GalNAc6S or GalNAc4S6S) building blocks. The occurrence of IdoA in DS distinguishes it from chondroitin sulfate A and C, likening it to heparin and HS.²⁸ DS has an overall lower negative charge density compared to heparin. A commonly occurring natural contaminant, DS is present at 1-7% in heparin API, but has no proven biological activity that influences the anticoagulation effect of heparin.

The chondroitin sulfate class of GAGs is comprised of 1→3 linked GlcA and GalNAc residues. The pattern of sulfonation helps to classify the GAGs into CSA (GalNAc4S), CSC (GalNAc6S), CSD (GlcA2S and GalNAc6S), and CSE (GalNAc4S6S).

The terms highly or fully-sulfonated chondroitin sulfate (FSCS) refer to a naturally occurring sequence, bearing 3 sulfonates per disaccharide unit. However, oversulfated chondroitin sulfate (OSCS) is a semi-synthetic compound containing 4 sulfonate groups per building blocks.^{29, 30} The structural differences between DS, CS, and OSCS are illustrated in Figure 1.3.

1.2.1 OSCS Adulteration of Heparin

In late 2007, contaminated lots of pharmaceutical heparin were associated with the acute and rapid onset of a potentially fatal allergic reaction.^{29, 31} Because the adulterant produced anticoagulant activity similar to that of heparin, it was not detected in the clotting-time assays used to screen heparin efficacy. The contaminant resulted in anaphylactic-type events observed following administration of contaminated lots of heparin to surgery and dialysis patients. These adverse reactions resulted in over 200 deaths, which were attributed to hypotension as a result of anaphylactic shock.³²

A detailed description of events related to the OSCS adulteration of heparin is summarized on the US Food and Drug Administration (FDA) website.³³ The first observation of serious adverse events in patients receiving heparin therapy was made on November 19, 2007 at the Children's Hospital in St. Louis, MO, USA followed by additional cases in January 2008. The marked increase in allergic reactions following heparin administration was reported to the Centers for Disease Control and Prevention (CDC). The CDC alerted the FDA to this problem on January 4, 2008. Five days later, a connection between the suspected lots of heparin and Baxter Healthcare emerged and Baxter initiated a voluntary recall of 9 lots of single and multi-dose heparin vials on

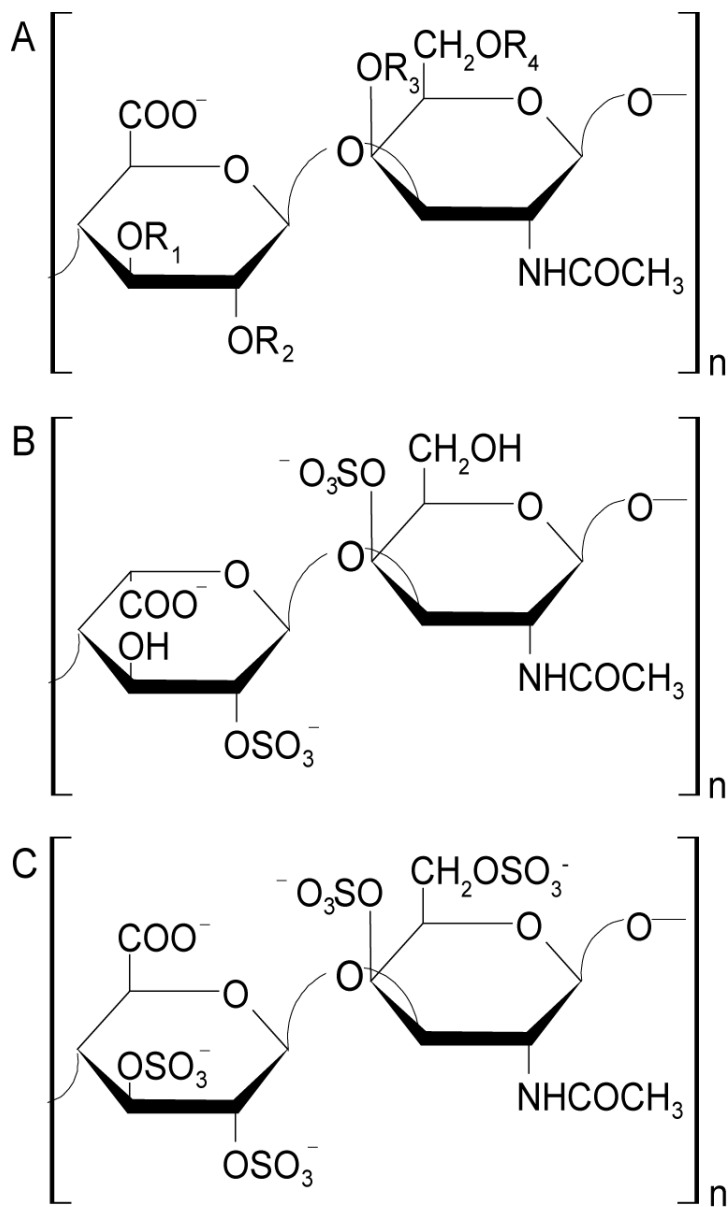


Figure 1.3. Major repeating disaccharide units of heparin-like GAGs (A) CS, (B) DS, (C) OSCS. The backbone of DS is not homogeneous; the vast majority of the uronic acid residues are IdoA, but DS also contains minor amounts of GlcA. The backbone of CS and OSCS are homogeneously composed of GlcA. For CS, R_1 - R_4 can be either sulfonated or unsubstituted.

January 17 followed by a recall of all its heparin products on February 28, when it ultimately ceased heparin production. On February 14, Changzhou SPL was identified as the origin of contaminated heparin that had been distributed to over 10 countries. In addition to Changzhou SPL, the contaminant was traced by the FDA to 11 other Chinese companies in the heparin API supply chain, broadening the heparin crisis.³³

The administration of contaminated heparin lots was associated with the acute, rapid onset of a potentially fatal allergic reaction.^{29, 32} These adverse reactions resulted in over 200 deaths, which were attributed to hypotension triggered by anaphylactic shock^{18, 29, 32} prompting the FDA to identify the contaminant in collaboration with scientists in industry and academia. By March 5, 2008, equipped with preliminary data obtained by combined use of optical rotation, capillary electrophoresis (CE), and ¹H NMR, the FDA announced that the contaminant was a “heparin-like” molecule. The following day the FDA posted protocols for using NMR and CE to screen heparin batches for the contaminant. After these safeguards were put into place, the number of adverse reactions returned to background levels. In a matter of weeks, the multidisciplinary team led by Ram Sasisekharan at the Massachusetts Institute of Technology identified and presented the structure of the contaminant to the FDA. Two days later, on March 19 the agency announced that the contaminant was OSCS, a structurally unique glycosaminoglycan with an unnatural sulfonation pattern. The physico-chemical properties of the isolated contaminant were in good agreement with that of chemically synthesized OSCS.³⁰ According to our present knowledge OSCS is not a natural product arising from animal sources. Therefore, it must be concluded that this was not a case of accidental contamination, but that OSCS was intentionally added to the raw heparin product as an act of purposefully adulteration.

The detection and the subsequent identification of OSCS as the heparin contaminant relied heavily on capillary electrophoresis (CE) and NMR spectroscopy, especially ^{13}C and multidimensional NMR methods (Figure 1.4). The first information about the contaminant's structure was provided by simple ^1H and ^{13}C NMR experiments. In addition to the *N*-acetyl resonances belonging to heparin (2.04 ppm) and DS (2.08 ppm), a known heparin impurity,²⁷ an unusual *N*-acetyl signal at 2.16 ppm was also observed in heparin lots associated with the adverse events (Figure 1.4A). The ^{13}C NMR spectrum of contaminated heparin lots also contained signals at 25.6 ppm and 53.5 ppm indicative of an *O*-substituted *N*-acetylgalactosamine moiety of unknown origin and distinctly different from DS (Figure 1.4B). The ^{13}C signals in the range of 103-105 ppm suggested a beta glycosidic linkage between the monosaccharides. The results of homonuclear (COSY, TOCSY, ROESY) and heteronuclear (HSQC, HMBC) 2D NMR experiments were consistent with a structure containing a polymeric repeat of *N*-acetyl galactosamine linked to glucuronic acid. Though a preliminary identification of the contaminant was possible by NMR, conclusive assignment was achieved only following the enzymatic depolymerization of heparin and DS followed by the subsequent isolation of the intact OSCS polysaccharide. Parallel to the enrichment of the contaminant by enzymatic degradation, alcohol-based selective precipitation and chromatographic separations were also used to purify the contaminant. Taken together, the results unequivocally proved the structure of OSCS as a polymer of the unusual tetrasulfonated disaccharide composed of GlcA2S3S and GalNAc4S6S with a 1→3 linkage between the two sugars and 1→4 linkage between adjacent disaccharide units. Because OSCS is a semi-synthetic polysaccharide, the direct comparison of the NMR spectra of the isolated

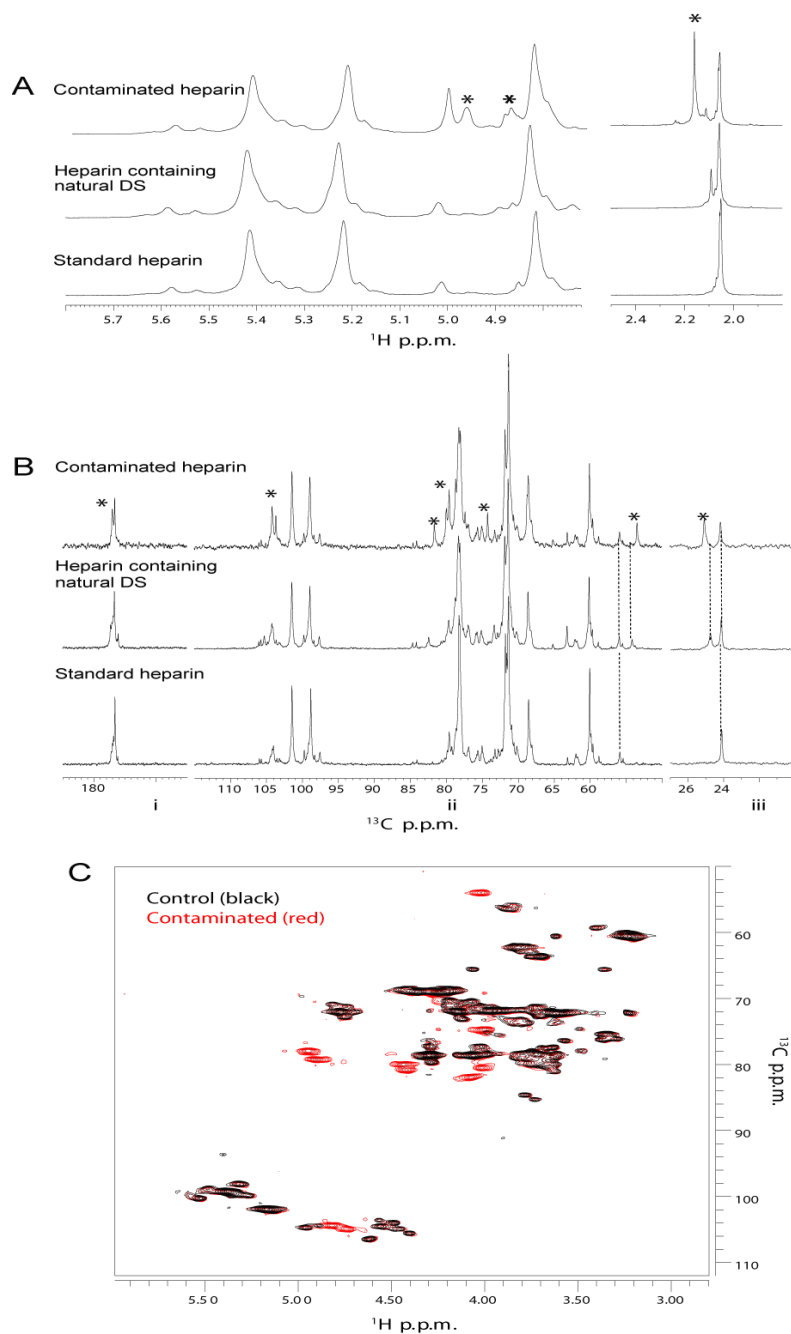


Figure 1.4. NMR spectra of contaminated heparin. (A) Comparison of anomeric and acetyl regions of the ^1H NMR spectra of standard heparin, heparin containing natural dermatan sulfate (DS) and contaminated heparin. (B) Comparison of carbonyl (i), sugar (ii) and *N*-acetyl regions (iii) of the ^{13}C NMR spectra of standard heparin, heparin containing natural dermatan sulfate, and contaminated heparin. Signals due to the contaminant are highlighted by asterisks. (C) HSQC spectrum of the contaminated sample overlaid on control heparin sample. Reprinted by permission from Macmillan Publishers Ltd: Nature Biotechnology [24] copyright (2008).

material with a synthesized OSCS standard confirmed the identity of the contaminant.^{18,}

29, 30, 34

Shortly after the structural studies, the biological investigation began in late March 2008, to find the missing link between OSCS and the adverse reactions. The high charge density of OSCS resulted in its strong anti-factor IIa activity allowing the contaminated sample lots to pass the anticoagulation potency screens used to determine heparin efficacy and purity. Highly charged anionic polysaccharides similar to heparin and OSCS have also been shown to be potent mediators of the immune response system which may explain the severe anaphylactic response observed upon administration of the contaminated heparin.^{18, 32} A study to determine the biological link between the presence of OSCS in heparin and anaphylactic events established that concentrations of 2.5 and 25 µg/mL of OSCS in heparin activated the kinin-kallikrein pathway and its complement pathways through the fluid-phase activation of FXII in the coagulation pathway.³¹ Kinin-kallikrein pathway activation results in the formation of bradykinin peptides responsible for the enlargement of blood vessels and subsequent drop in blood pressure. A strong correlation has been reported between the OSCS concentration in the contaminated heparin and the released bradykinin concentration.³⁵

Identification of OSCS paved the way for the establishment of authentic standards and analytical protocols to guard against future problems resulting from heparin contamination by this compound. With the introduction of an OSCS standard, NMR, HPLC, and CE methods were quickly developed to screen heparin lots to prevent further exposure of patients to contaminated heparin.³⁶ The health crisis created by the intentional adulteration of heparin stimulated the analytical chemistry community to rapidly introduce a number of new methods for heparin impurity analysis.

1.3 Analytical Challenges of Heparin Analysis

Heparin is one of the most challenging pharmaceutical agents to analyze and characterize. Compared to small drug molecules, the molecular properties of pharmaceutical heparin have traditionally been pushed into the background due to its polydisperse nature and complex microheterogeneous structure. As a result of its structural microheterogeneity, studies of heparin at the molecular level are initiated by the depolymerization of the raw/pharmaceutical material into smaller, more manageable, oligosaccharide fragments using enzymatic or chemical methods.^{37, 38} The enzymatic depolymerization of heparin can be achieved by heparin lyases I, II and III produced by *Flavobacterium heparinum*.³⁹ Each class has different substrate specificity with respect to the uronic acid moiety and sulfonation pattern, as discussed in Section 1.3.1, but in all cases the cleavage of the glycosidic linkage between the glucosamine and uronic acid residues is accomplished through β -elimination. The enzymatic depolymerization of heparin generates a double bond between the C-4 and C-5 of the uronate residue, allowing for the detection of the generated fragments at 232 nm with an approximate molar absorption coefficient of $5500 \text{ M}^{-1} \text{ cm}^{-1}$.⁴⁰ In chemical reactions used in the conversion of heparin to smaller oligosaccharides either the oxidative instability of the polymer is exploited, or the enzymatic reaction is mimicked chemically.²² The primary focus of chemical depolymerization is the preparation of LMWHs for pharmaceutical application.

The activity of pharmaceutical heparin is specified by clotting-time assays in the pharmacopoeias. Since OSCS exhibits anticoagulation activity similar to that of heparin,³⁰ contaminated heparin samples passed the whole-blood coagulation screens performed by the manufacturer. Although the bio- and physico-chemical behavior of

OSCS is similar to heparin in many ways, NMR spectroscopy can be effectively used to detect structural differences necessary to discriminate the impurity from heparin.

1.3.1 Enzymatic Depolymerization of Heparin

Exhaustive digestions of heparin and HS are typically carried out by use of a cocktail containing the enzymes heparinase I, II, and III to selectively cleave the biopolymer at the glucosamine-(1→4)-uronic acid glycosidic bonds. The enzymatic reaction inserts a double bond at the nonreducing end of each cleaved chain to create an ultraviolet (UV) chromophore that absorbs at a wavelength of 232 nm, thereby facilitating detection.⁴¹ Such heparin lyase enzymes, produced by *Flavobacterium heparinum*, are highly specific to heparin and HS and are classified according to their substrate specificity.⁴² Heparinase I cleaves the polymer chain between GlcNS and 2-O-sulfonated IdoA residues, the most common substitution motif in most forms of intact heparin. The specificity of heparinase I and the structure of the resulting cleavage products is illustrated in Figure 1.5. Heparinase II is less specific than heparinase I and III cleaving heparin and HS between glucosamine residues that can be *N*-sulfonated or *N*-acetylated and 2-O-sulfonated IdoA, unsubstituted IdoA, or GlcA residues.⁴² Heparinase III cleaves specifically at sites between *N*-acetylated or *N*-sulfonated glucosamine and 2-O-unsubstituted IdoA or GlcA. Because the disaccharide GlcNAc(1→4)GlcA is commonly found in HS, heparinase III is often used for HS digestions.

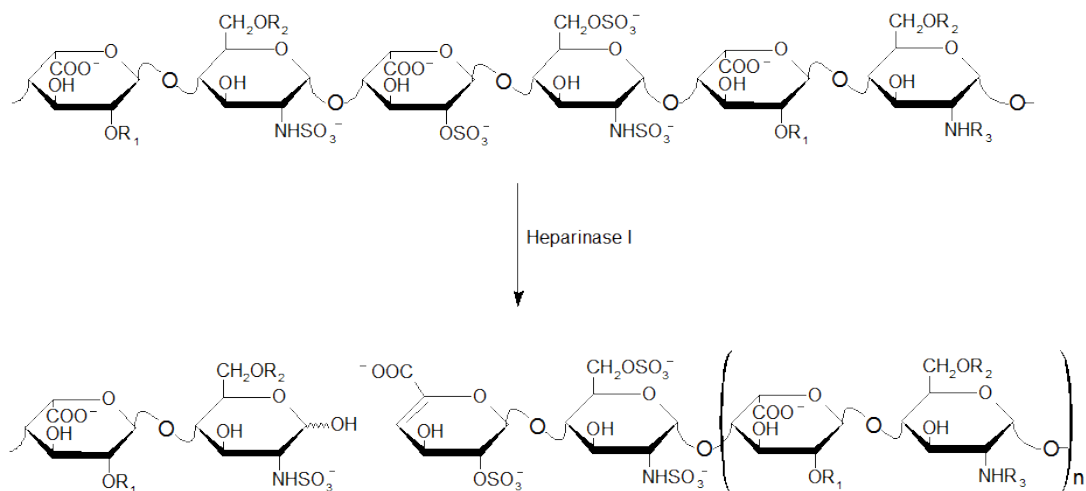


Figure 1.5. Scheme illustrating the enzymatic depolymerization of heparin with the enzyme heparinase I. The heparin-derived oligosaccharide contains a $\Delta^{4,5}$ double bond introduced into the uronic acid at the non-reducing end; R_1 : H or SO_3^- , R_2 : H or SO_3^- , and R_3 : H, SO_3^- , or COCH_3 .

1.3.2 Role of NMR Spectroscopy in Heparin Impurity Analysis

As demonstrated in Section 1.2.1, NMR played a decisive role in the structure determination of OSCS during the heparin crisis, although the exceptionally high concentration of OSCS in the adulterated samples likely contributed to its successful identification by this method. The complete ^1H NMR assignment of OSCS has been reported in several publications^{29, 36, 43, 44} and in the original work by Maruyama et al.³⁰ It is also important to note that Holzgrabe et al. published ^1H NMR spectra of heparin in 1998 which already contained OSCS.⁴⁵ In addition to the ^1H and ^{13}C NMR spectra, the heteronuclear HSQC and HMBC experiments were important for the conclusive molecular level characterization of OSCS (Figure. 1.4C). Signals associated with the characteristic OSCS moieties are easily detectable in the HSQC spectrum of OSCS contaminated heparin (Figure 1.6).

Due to its high sensitivity to minor structural variations, ^1H NMR spectroscopy has been used previously to detect variations in the chemical composition of heparin,^{27, 46, 47} low molecular weight heparins,⁴⁸ heparin-derived oligosaccharides,^{49, 50} and as a screening tool for GAG impurities.^{27, 51} As ^1H NMR has also been recommended by the FDA as one of the analytical techniques for rapid screening of OSCS, intense efforts are being made to improve the NMR-based characterization of heparin API. To obtain a satisfactory NMR spectrum for correct identification, several factors should be considered. As demonstrated by McEwen et al., the chemical shift of the OSCS *N*-acetyl methyl signal is dependent on counter ion type and concentration, varying linearly from 2.13 ppm to 2.18 ppm with increasing amounts of Ca^{2+} until reaching a saturation point of four Ca^{2+} per tetrasulfonated disaccharide unit.⁵² Paramagnetic transition metal ions, present as production residuals, can cause line broadening through paramagnetic

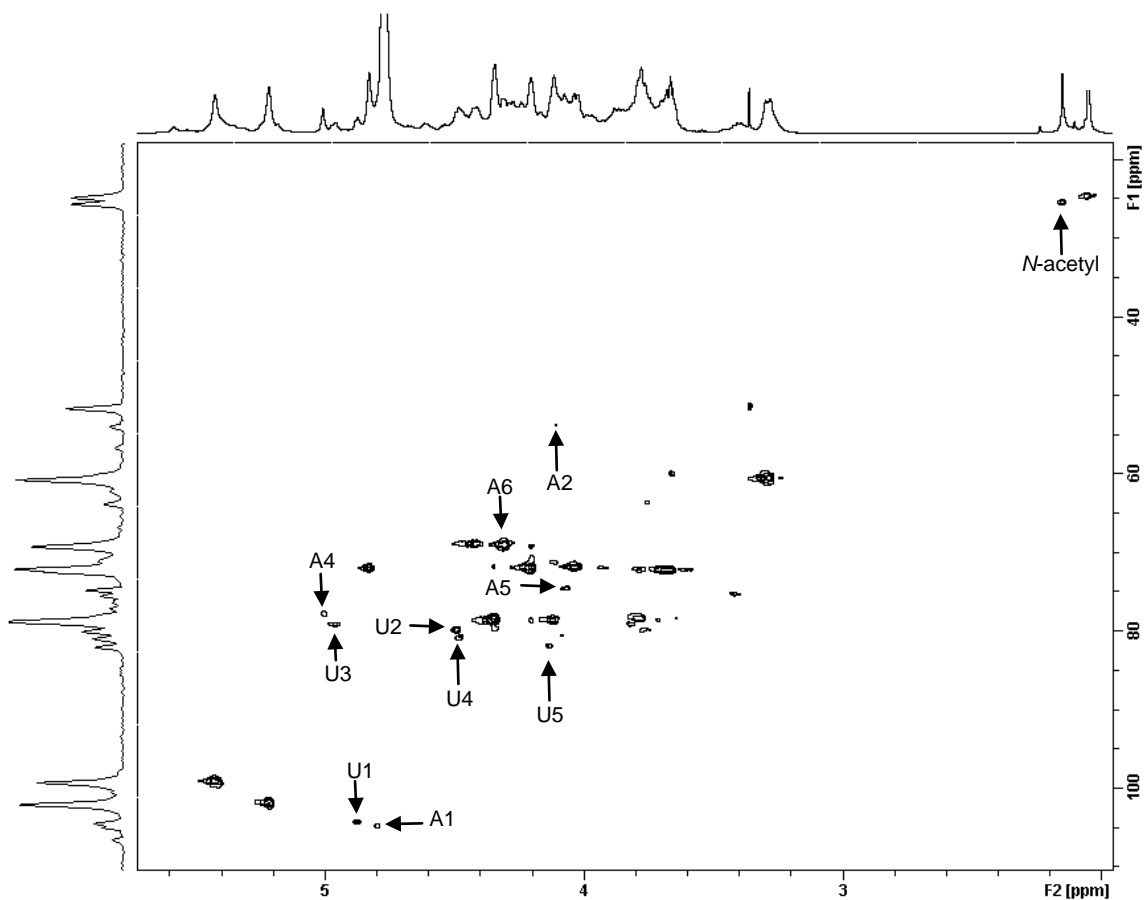


Figure 1.6. HSQC spectrum of heparin containing 10% (w/w) OSCS prepared using a 20 mg/mL D_2O solution of the USP system suitability standard at pD 6.6 and 298.2 K. To improve the line shape 1% $\text{EDTA-}d_{16}$ was added. The spectrum was acquired using 32 scans per increment with 2560 and 512 data points in F2 and F1, respectively, using a 600 MHz NMR equipped with a broad band inverse probe. The polarization transfer delay was set using a $^1\text{J}_{\text{C-H}}$ coupling value of 155 Hz. The spectrum was referenced to internal TMSP. The characteristic OSCS signals for GalNAc4S6S and GlcA2S3S are labeled as A and U, respectively.

relaxation enhancement, even within the range of allowed quantities.⁵³ Manganese (Mn^{2+}) was found to present the most pronounced effect on the heparin IdoA H1 (5.22 ppm) and H5 (5.42 ppm) protons and the OSCS methyl protons, the signal recommended for OSCS quantification. Passing the solution through a cation exchange resin prior to measurement or adding 300 μ g EDTA per gram of heparin can eliminate the unwanted broadening.⁵³

Acquisition of spectra at elevated temperatures can also improve the 1H resonance line shape of GAG solutions.⁵⁴ Measuring spectra at 333 K (or even 353 K) enables clear isolation of the H5 proton of the sulfonated IdoA residue from other proton signals in the fingerprint region, including the water/HDO resonance due to its temperature-induced upfield shift.⁵⁵ Caution should be used in making measurements using unbuffered heparin solutions which can produce pH-dependent chemical shift differences of the carboxylate adjacent H5 proton of uronic acid residue.⁴⁴

Low-level contaminant peaks can be masked by the ^{13}C satellite peaks of the *N*-acetyl methyl peak of heparin and in these cases ^{13}C decoupling is recommended to discriminate the satellite peak from those of the contaminants.⁵⁶ Although it can be difficult to detect certain GAG impurity signals by visual inspection of the 1H survey spectrum, multidimensional NMR can easily detect and distinguish between analogous sulfonated polysaccharides.⁵⁷ To obtain more contaminant-specific signals from the crowded fingerprint region and improve the reliability of impurity identification, the 2D NOESY experiment can provide a highly informative 1H fingerprint.⁵⁸

The accurate quantification of 1H NMR signals requires a high quality spectrum, which can be typically achieved using a high magnetic field (≥ 500 MHz), optimum solution conditions and appropriate NMR parameters.⁴⁴ Beyer and coworkers have

shown that even using 300 or 400 MHz NMR spectrometers, the OSCS LOD can be as low as 0.1%.⁵⁴ These authors analyzed over 100 heparin API samples using the standard addition method of monitoring the *N*-acetyl region. They developed a routine ¹H NMR-based screening method for heparin API, quantified both OSCS and DS and proved the lack of correlation between these signals. In addition to quantification of OSCS and DS, Beyer et al. also reported other impurities present in varying amounts in pharmaceutical heparin, including methanol, ethanol and acetate.⁵⁴ In a subsequent study, this group also scrutinized the German heparin market and analyzed 145 representative samples from 2008.⁵⁹ The samples tested by ¹H NMR were found to contain DS (51%) and OSCS (19%), as well as process-related impurities such as ethanol, methanol, acetone, formic acid and acetate in considerable amounts. Many of these process-related impurities are undetectable by conventional CE and LC methods. Keire et al. have also reported a 0.1% LOD for OSCS on a 500 MHz instrument using 25 mg/700 μ L heparin solutions.⁶⁰ This group has also identified additional native and oversulfated GAGs as possible economically-motivated adulterants based on their characteristic chemical shifts in the *N*-acetyl and 3.0-6.0 ppm spectral regions.⁶¹ CSA, DS, OSCS and oversulfated dermatan sulfate (OSDS) showed unique signal patterns when spiked into the heparin sample, while HS, oversulfated heparan sulfate (OSHS) and oversulfated heparin were difficult to identify.⁶¹

1.4 Nuclear Magnetic Resonance Theory

1.4.1 Origin of the NMR Signal

In the quantum mechanical description of NMR, a nucleus with spin quantum number **I** in a magnetic field **B**₀ can exist in 2**I**+1 distinct energy levels. For nuclei with a

spin quantum number $I = 1/2$, such as ^1H , ^{13}C , and ^{15}N , there are two distinct energy levels designated as the α and the β spin states. In the absence of an applied magnetic field, where $\mathbf{B}_0=0$, both the α and β spin states are equivalent in energy and excitation of the spins is not possible. However, in the presence of an applied magnetic field of strength, \mathbf{B}_0 , the difference between the two energy states, ΔE , is given by equation 1.1,

$$\Delta E = \frac{h\gamma B_0}{2\pi} \quad (1.1)$$

where h is Planck's constant, γ is the gyromagnetic ratio of the nucleus being studied, for protons, $\gamma = 2.67510 \times 10^8 \text{ rad } T^{-1} s^{-1}$. The potential energy of the two spin states, as given by equation 1.1, is dependent on the external magnetic field, as illustrated in Figure 1.7. The lower energy state (α), $m_I=+1/2$, occurs when the magnetic moment of the nuclear spin is aligned parallel to the magnetic field and the upper energy state (β), $m_I=-1/2$, occurs when the magnetic moment of the nuclear spin is aligned anti-parallel to the magnetic field.

As with other spectroscopic methods, including NMR, the signal observed is a result of the difference between the energy absorbed by the spins which make a transition from the lower energy state to the higher energy state. The sensitivity is also proportional to the difference in the population of the excited (N_β) and ground (N_α) energy states as given by the Boltzmann distribution (equation 1.2),

$$\frac{N_\beta}{N_\alpha} = e^{\frac{-\Delta E}{k_B T}} \quad (1.2)$$

Because the energy difference, ΔE , between the α and β spin states is small the difference in the populations of the upper and lower energy levels is also expected to be

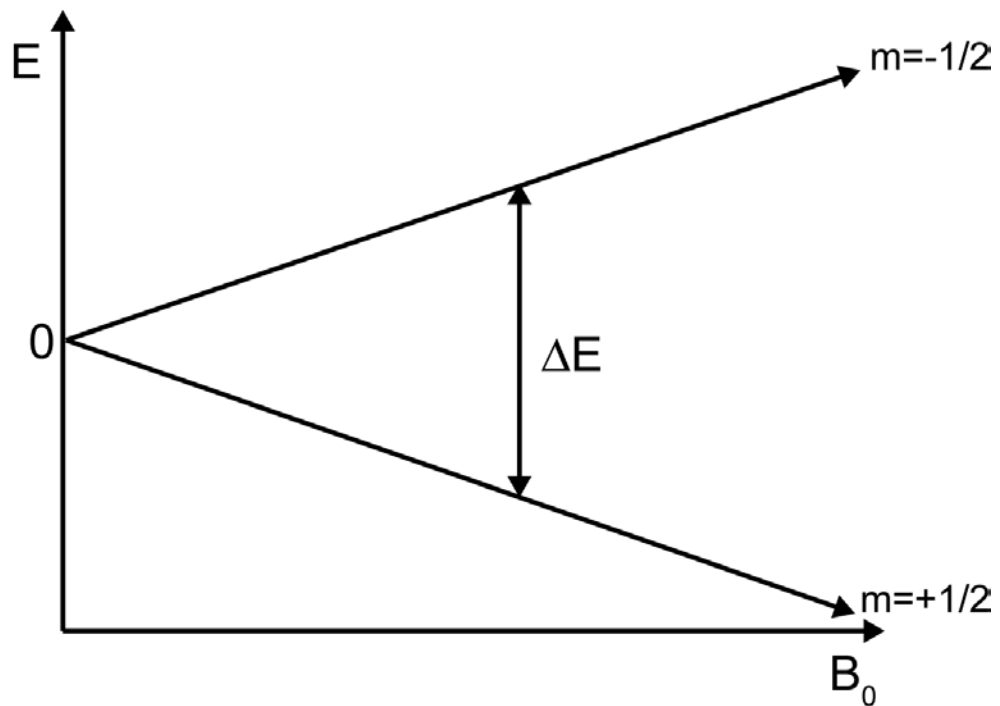


Figure 1.7. Field dependence of the nuclear spin states, α and β , for the spin quantum number $I=1/2$. For the lower energy state (α), the magnetic moment of the nuclear spin is aligned parallel to the magnetic field and for the upper energy state (β), the magnetic moment of the nuclear spin is aligned anti-parallel to the magnetic field, \mathbf{B}_0 .

small. For protons in a 14 T magnet field at 25° C the population difference is of the order of 1 in 10⁴. From the Boltzmann distribution (equation 1.2), the population difference is quite small wherein the population of spins in the excited state is only slightly larger than the population of spins in the ground state. Though the difference in population is small, the bulk magnetization aligned with **B**₀, corresponding to the slight excess of spins in the lower energy state, can be measured. In NMR, we measure the transitions of nuclei between the two energy states as measured by their frequency of transitions expressed in equation 1.3;

$$\Delta E = \frac{h\omega}{2\pi} \quad (1.3)$$

where ω is the transition (or resonant) frequency expressed as Hz s⁻¹ and h is Planck's constant. These transitions are observed in the radio-frequency (RF) region of the electromagnetic spectrum corresponding to a frequency of 10⁸ Hz. In more sensitive optical spectroscopic methods such as UV and IR spectroscopy, transition frequencies on the order of ~3x10¹³ and ~3x10¹⁶, respectively, are observed thus leading to a higher sensitivity than NMR. Because ΔE is linearly dependent on magnetic field strength, as illustrated in Figure 1.7, increasing the field strength of the magnet increases the resonant frequency and thus the sensitivity of the NMR measurement.

1.4.2 Vector Description of NMR

In order to understand the experiments used in this dissertation it is necessary to introduce the vector description of the NMR experiment. This approach is a non-mathematical system used in describing the behavior of the magnetization under the influence of magnetic fields. Because there is a slight excess of spins in the lower

energy (α) spin state, a net magnetic moment aligned with the \mathbf{B}_0 field is observed. At equilibrium, this bulk or macroscopic magnetization (\mathbf{M}) is aligned parallel to the static magnetic field (\mathbf{B}_0) (Figure 1.8). \mathbf{M} is represented as a single vector which corresponds to the sum of all the individual magnetic moments of the nuclei in the higher energy (β) and lower energy (α) spin states. Displacement of \mathbf{M} away from equilibrium is accomplished by the application of a second magnetic field (\mathbf{B}_1) perpendicular to that of the static magnetic field. This magnetic field (\mathbf{B}_1) oscillates at an appropriate frequency, equivalent to the difference in the energies between the two energy states, stimulating the transition of spins between the α and β spin states. This \mathbf{B}_1 field is generated from a current that is passed through a coil oriented perpendicular to the \mathbf{B}_0 field.

The interaction of the excitation field (\mathbf{B}_1) with the bulk magnetization \mathbf{M} produces a torque on \mathbf{M} which moves the magnetization away from the z-axis creating a vector component in the transverse (xy) plane, as shown in Figure 1.8. The final position of the bulk magnetization depends on the length (t_p) and field strength (B_1) of the excitation pulse where the tip angle, φ , is calculate by equation 1.4;

$$\varphi = \gamma B_1 t_p \quad (1.4)$$

If the pulse is applied for a sufficient period of time, \mathbf{B}_1 , can tip \mathbf{M} from the z-axis so that it lies entirely along the x- or y-axis. A pulse that efficiently tips \mathbf{M} to the transverse plane is considered a 90° or $\pi/2$ pulse as shown in Figure 1.8C. Following the application of the \mathbf{B}_1 pulse, the magnetization will precess about \mathbf{B}_0 at the Larmor frequency. This precession of the transverse magnetization produces a detectable signal by inducing a current in the coil wound about the sample generating the free induction decay (FID). The FID is the time domain signal that contains all of the amplitude and frequency information of each resonance in the NMR spectrum.

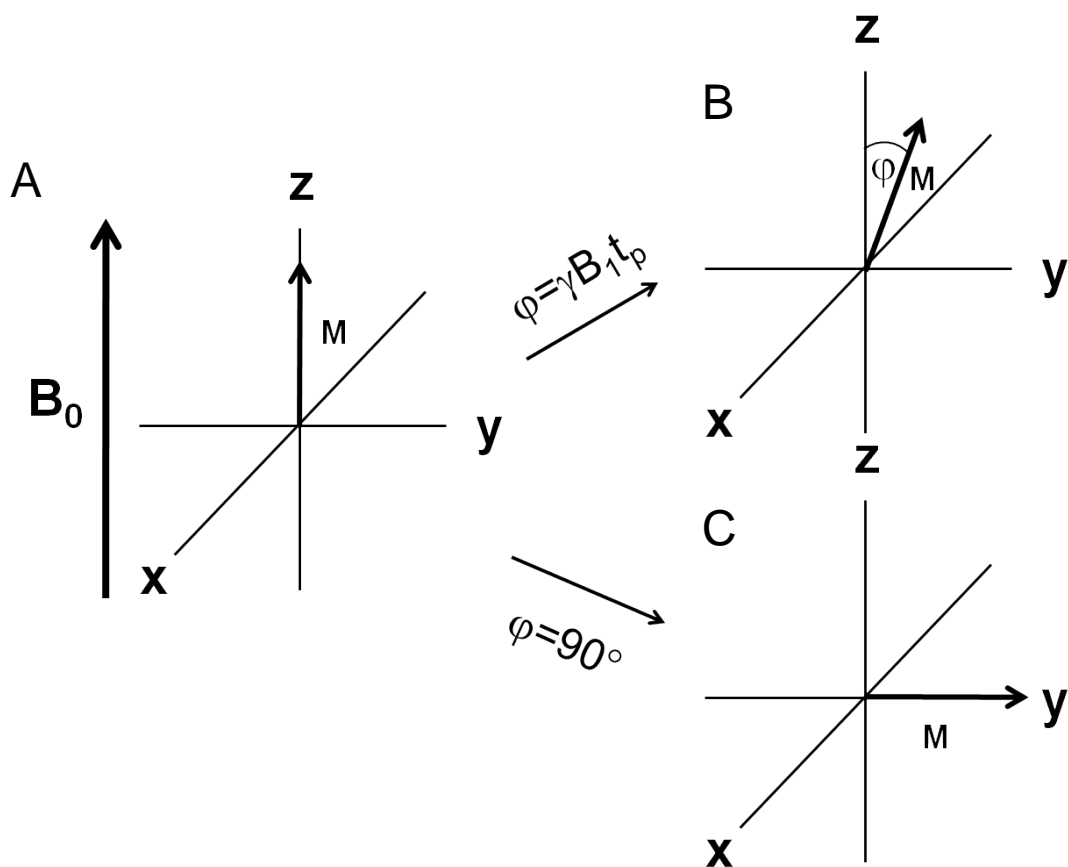


Figure 1.8. Vector diagrams for the orientation of the bulk magnetization \mathbf{M} , (A) at equilibrium aligned with the static magnetic field, \mathbf{B}_0 , (B) following the application of a RF pulse with length (t_p) applied along the x-axis, and (C) following the application of an RF pulse along the x-axis of sufficient length to place the bulk magnetization along the y-axis.

Following excitation, the perturbed nuclear spin system relaxes to its equilibrium state by first-order processes characterized by two separate relaxation times. The first is the spin-lattice (T_1) relaxation time. Spin-lattice relaxation is a set of mechanisms by which the excited magnetization returns to equilibrium along the z-axis and represents the lifetime of the magnetization in an NMR experiment. The mechanisms responsible for T_1 relaxation are dipole-dipole interactions, quadrupolar relaxation, paramagnetic relaxation, and chemical shift anisotropy. The other relaxation time is the spin-spin (T_2) relaxation time, also known as transverse relaxation. Spin-spin relaxation occurs as a result of through bond interactions between neighboring nuclei with identical precessional frequencies but different magnetic quantum states.

1.5 Improving the Sensitivity of NMR

Although NMR spectroscopy is a powerful technique for structure elucidation and is capable of providing dynamic information, its relatively low sensitivity, compared with other techniques, hinders its use for the study of compounds for which limited amounts of material are available. This disadvantage is most commonly encountered when the target of the measurement is available only in limited quantities, as is the case for heparin and HS oligosaccharides isolated from biological samples through lengthy and often tedious procedures. To address this limitation, several approaches can be used to improve NMR sensitivity and enhance its limits-of-detection (LOD). These methods include increasing the strength of the static magnetic field (which has the added advantage of improving resonance dispersion), use of cryogenically cooled probes (to decrease Johnson noise), hyperpolarization techniques to increase the population difference between the spin states, and reduced size RF coils (microcoils). Although the

benefits of increased magnetic field strength are well recognized, investigators are generally limited by the available instrumentation. Cryogenically cooled NMR probes and receivers can provide significant improvements in signal-to-noise ratios (S/N), generally by a factor of two to four, depending on the solvent and ionic strength.^{62, 63} A 4-fold increase in sensitivity may not seem significant, but for mass-limited samples it can make a significant difference in spectral quality, especially in 2D NMR spectra. In cryogenic technology, the preamplifier and the RF coil is cooled to about 20 – 30 K to reduce the electronic noise of the probe thus increasing the signal sensitivity. Although the introduction of cryogenically cooled probes promises to improve the concentration sensitivity of NMR experiments, for aqueous solutions of lossy samples, such as GAG enzymatic digests, the sensitivity gains can be significantly less than the theoretical maximum. Although signal averaging can also be used to improve S/N, it rapidly becomes impractical in 2D NMR experiments, given that a 4-fold gain in S/N requires a 16-fold increase in experiment time.

The poor sensitivity of NMR spectroscopy arises from the small population differences of nuclear spin states, as demonstrated in Section 1.4.1, even at extremely high magnetic fields >1 GHz. A notable way to improve the sensitivity of NMR is to use hyperpolarization techniques in which an independent physical means is used to bring the nuclear spin system into a nonequilibrium state before each measurement.⁶⁴ One promising technique is dynamic nuclear polarization (DNP), in which a sample aliquot is polarized in its solid state at low (~1 K) temperatures. Following polarization, the sample is dissolved in a stream of hot solvent before being transferred directly into the NMR spectrometer for acquisition. Compared with spectra acquired at thermal equilibrium in a 9.4 T magnetic field⁶⁵, DNP polarization yields signal enhancements of up to 44,400 for

^{13}C and 23,500 for ^{15}N . A drawback of DNP lies in the short lifetimes associated with the hyperpolarized state, which has restricted the application of DNP to one-dimensional spectra.⁶⁶ With the introduction of single-scan 2D NMR experiments,⁶⁷ DNP has allowed the acquisition of fast heteronuclear multiple quantum correlation experiments, thereby permitting the measurement of heteronuclear 2D spectra in a matter of seconds.⁶⁸

1.5.1 Microcoil NMR

Despite the advantages of cryogenically cooled NMR probes, not every NMR laboratory can accommodate such instrumentation, either because its initial cost and ongoing maintenance expenses or because the diversity of NMR experiments performed requires frequent probe changes. For compounds with high solubility, such as heparin oligosaccharides, microcoil NMR probes can provide sensitivity enhancements similar to those offered by cryogenically cooled probes at a fraction of the cost. A comprehensive review on microcoil NMR technology and its application to mass-limited samples has been previously published.⁶⁹ The smaller active volume of microcoil NMR probes can enable 2D NMR analysis using smaller sample amounts than required by conventional probes. Gains in sensitivity from the use of microcoil probes are roughly similar to that provided by cryoprobes, albeit at a fraction of the cost. Therefore, microcoil NMR was used in the structural characterization of heparin derived oligosaccharides isolated using SAX-HPLC, presented in Chapter 5.

It has been shown that for RF microcoils with dimensions less than 2 mm, the signal-to-noise ratio (SNR) is expressed in equation 1.5,

$$SNR = \eta \frac{\omega_0^2 \frac{B_1}{i} V_S}{V_{noise}} \quad (1.5)$$

where η is the proportionality constant dependent on the nucleus density, nucleus type, and temperature, ω_0 is the Larmor frequency of the nucleus under observation, B_1 is the RF field, i is the current produced in the coil by the B_1 pulse, V_S is the sample volume, and V_{noise} is the noise voltage from the coil and the sample. The sensitivity of an RF coil is defined as the magnitude of the magnetic field, B_1 , in the coil volume produced by a unit current i , also known as the quality or q factor. For solenoidal coils, this is mathematically expressed in equation 1.6,

$$\frac{B_1}{i} = \frac{\mu_0 n}{d_{\text{coil}} \sqrt{1 + \left[\frac{h}{d_{\text{coil}}}\right]^2}} \quad (1.6)$$

where μ_0 is the permeability of free space, n is the number of turns, d_{coil} is the coil diameter, and h is the length of the coil. Solenoidal microcoils intrinsically have 2-3 times higher mass sensitivity than Helmholtz coils. Equation 1.6 shows that coil sensitivity is inversely proportional to the diameter of the coil provided h/d_{coil} is kept constant. Therefore, additional mass sensitivity can be expected with a decreased coil diameter.

1.6 Oligosaccharide Structure Assignment by NMR Spectroscopy

NMR spectroscopy is highly sensitive to minor variations in molecular structure, making it an important technique for heparin characterization. A simple ^1H NMR survey spectrum can both reveal the number of monosaccharide residues present and provide a tentative compositional analysis based on the comparison of ^1H chemical shifts and reference data as shown in Figure 1.9A for a heparin derived tetrasaccharide.^{50, 70} Although the ^1H survey spectrum can provide important information about sample purity

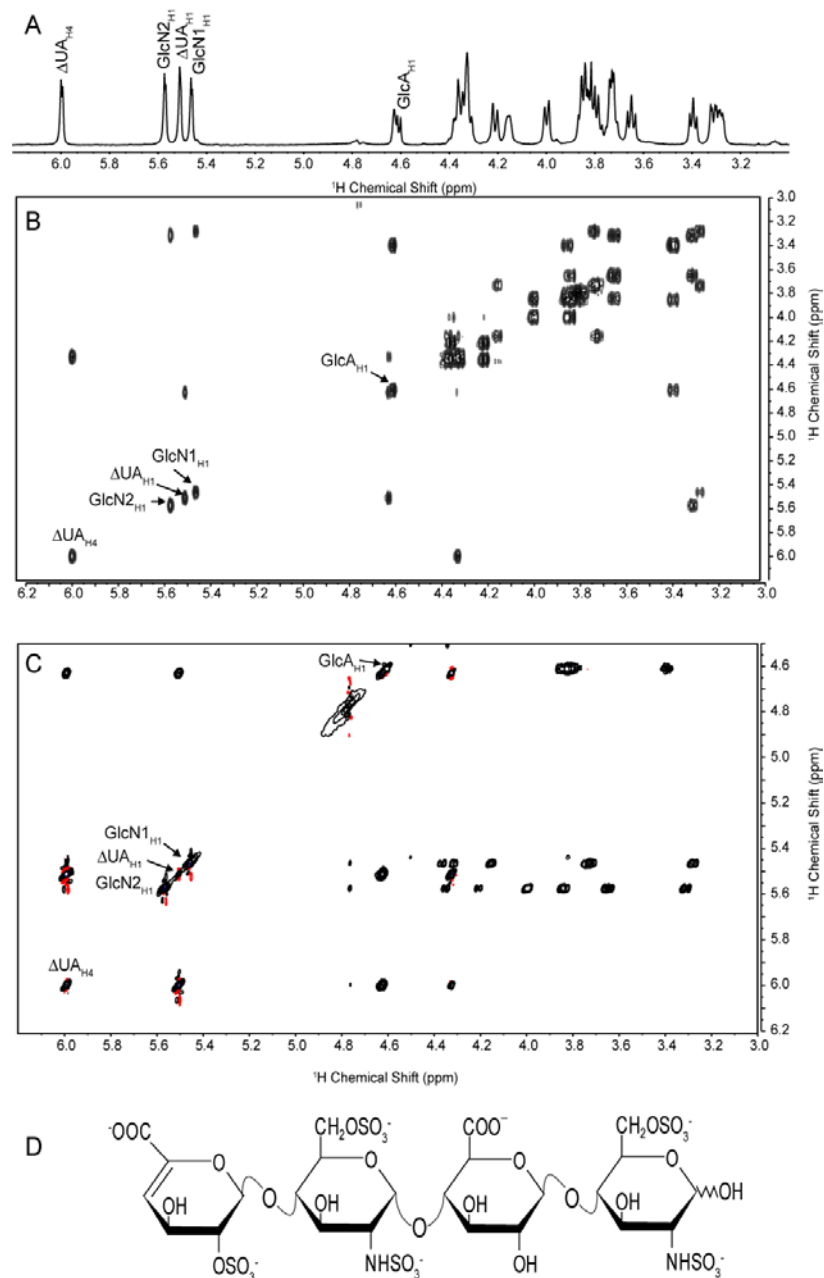


Figure 1.9. (A) CapNMR ^1H survey spectrum measured with 192 μg of $\Delta\text{UA}(2\text{S})\text{-GlcNS}(6\text{S})\text{-GlcA-GlcNS}(6\text{S})$. Portions of the (B) COSY, (C) TOCSY spectra showing cross peaks to the well-resolved anomeric resonances used to establish the structure of the tetrasaccharide. All spectra were acquired within a 12 hr period. (D) Structure of the heparin-derived tetrasaccharide.

and composition, complete structural characterization of isolated oligosaccharides requires two-dimensional NMR experiments such as correlation spectroscopy (COSY), total correlation spectroscopy (TOCSY), and rotating-frame Overhauser effect spectroscopy (ROESY).⁷¹ With the powerful arsenal of two-dimensional experimental techniques available, NMR spectroscopy can be used to determine the sequence of the component monosaccharide residues and unambiguously assign sites of *N*-acetylation as well as of *N*- and *O*-sulfonation along the oligosaccharide chain. Most importantly, NMR spectroscopy can also specify the orientation of the anomeric linkage connecting the various disaccharide subunits and easily distinguishes IdoA and GlcA residues that may be important for specific protein binding.

Structural characterization of heparin-derived oligosaccharides is typically initiated by identification of the individual monosaccharide subunits in the oligosaccharide chain using scalar couplings to provide through-bond connectivities. These connectivities can be obtained through a number of 2D NMR experiments, including homonuclear correlation spectroscopy (COSY) and homonuclear total correlation spectroscopy (TOCSY) experiments, as well as heteronuclear single (HSQC) and multiple quantum coherence (HMQC) spectroscopy experiments.⁷²⁻⁷⁵ Through the COSY spectrum (Figure 1.9B), connections between coupled protons on adjacent carbon atoms within a monosaccharide ring can be identified. The well-resolved anomeric resonances and the H4 resonance of the $\Delta^{4,5}$ UA residue of oligosaccharides produced by enzymatic cleavage provide an entry point for analysis of the COSY spectrum. However, the limited ¹H NMR chemical shift dispersion of carbohydrates can make interpretation of the COSY data challenging, even for medium-sized oligosaccharides. Because the TOCSY experiment transfers ¹H scalar coupling

information throughout a spin system, the TOCSY spectrum allows detection of the connectivity of all the protons within each monosaccharide residue through the anomeric resonances. The TOCSY spectrum in Figure 1.9C was used to assign resonances of a heparin-derived tetrasaccharide, whose structure is shown in Figure 1.9D. Through comparison of the ^1H chemical shift data obtained from the TOCSY spectrum with reference data, the structural identities of the monosaccharide residues can be deduced. For complicated spectra with extensive overlap in the anomeric region of the ^1H NMR spectrum, the band-selective homonuclear-decoupled (BASHD)-TOCSY experiment can provide improved resolution.⁵⁰

Following assignment of the resonances of the individual monosaccharide residues, the oligosaccharide sequence is determined through dipolar coupling information obtained by the ROESY experiment. The ROESY spectrum can also distinguish IdoA and GlcA through unique interresidue cross peaks. In the ROESY spectrum, cross peaks arise between resonances of the H1 and the H4 protons of adjacent residues connected via the glycosidic bond, which reveals the relative positions of the monosaccharide residues within the full chain.

1.7 Diffusion NMR

Because of the non-invasive nature of NMR spectroscopy it is a unique tool in the study of molecular dynamics in chemical and biological systems, preserving the chemical environment of the system thus providing a more realistic means to probe component interactions such as aggregation and partitioning. Diffusion NMR is a spectroscopic technique used for the *in situ* analysis of mixtures differing from HPLC and other conventional methods of separation in that the components of the mixture are not physically separated, but are resolved spectroscopically according to differences in their

diffusion coefficients. The ease in implementation with modern spectrometers and the non-destructive nature of NMR, make diffusion NMR an excellent technique in the routine screening of mixtures.⁷⁶

Molecules present in solution are in a constant state of motion experiencing both rotational and translational motions. The random translational motion of molecules in solution is commonly referred to as self-diffusion and is driven by its internal kinetic energy, known as Brownian motion. The rate at which a molecule moves is expressed by its diffusion coefficient, D , and may be approximated by the Stokes-Einstein equation (equation 1.7):

$$D = \frac{kT}{f} \quad (1.7)$$

where k is the Boltzmann constant, T is the temperature and f is the friction coefficient. In the case of a spherical molecule, $f = 6\pi\eta r_s$ where r_s is the effective hydrodynamic radius (Stokes radius) and η is the solution viscosity. The Stokes-Einstein equation presented above is effective in approximating the diffusion coefficients for spherical molecules in non-viscous solutions, however, when working with non-spherical molecules such as heparin and others GAGs, structural constraints such as aggregation and charge state may affect free diffusion in solution. Because the diffusional behavior of components in solution are related to hydrodynamic properties such as size, shape, and charge, individual components in the solution can be distinguished provided that the species have resolved resonances or, in cases of resonance overlap, significantly different diffusion coefficients.

The application of NMR spectroscopy in the investigation of the self-diffusion properties of molecules was first introduced by Stejskal and Tanner⁷⁷ in 1965 using a modified version of the Hahn spin-echo experiment (Figure 1.10) introduced by Erwin

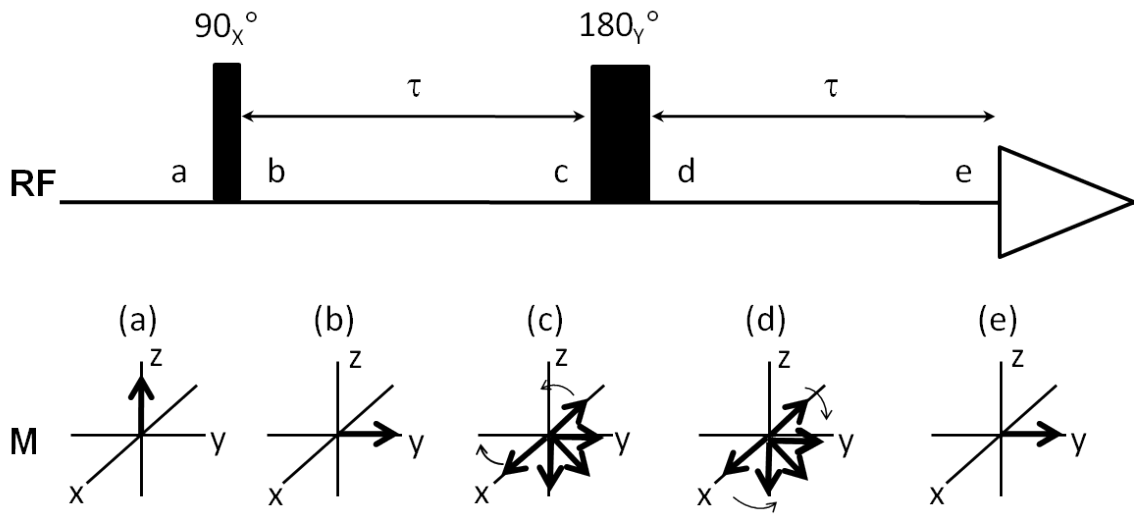


Figure 1.10. (A) Spin-echo pulse sequence for the measurement of T_2 relaxation introduced by Edwin Hahn in 1950. (B) Diagram of the formation of the spin echo. Following the application of a 90° RF pulse, the resonance signal decays as a result of dephasing by T_2 relaxation. The 180° RF pulse at the center of the τ delays reverses the relative positions of the precessing spins. The NMR signal is reestablished as the different spins converge on the y -axis before detection.

Hahn in 1950 to measure transverse relaxation time (T_2) resulting from magnetic field inhomogeneities.⁷⁸ Therefore, it is necessary to explain the spin-echo experiment before talking about the pulsed field gradient experiments which are used to measure molecular diffusion. Following the 90_x° excitation pulse which places the magnetization along the y-axis, the NMR signal is observed to decay due to dephasing of the transverse magnetization. The dephasing of the magnetization vector results from inhomogeneities of precessional frequencies in the ensemble of nuclei due to magnetic field inhomogeneities. As a result, some of the nuclei precess faster than the Larmor frequency while some precess at a slower rate. After time period τ , a 180_y° pulse is applied which rotates the spins about the y-axis and the relative positions of the fast and slow spins is reversed. After a second τ period, the NMR signal is refocused along the y-axis for detection as shown in vector diagram (e) in Figure 1.9. This process is known as a spin-echo and is a building block in numerous pulse sequences.

In the pulsed field gradient spin-echo (PGSE) pulse sequence (Figure 1.11A) developed by Stejskal and Tanner, attenuation of the echo as a result of the applied magnetic field gradient in each of the evolution periods, τ , is used to measure the displacement of the observed spins. The magnetic field gradient is generated by the application of current to a coil specially wound to produce a regularly varying magnetic field gradient across the length of the sample.

In NMR experiments, nuclear spins are observed to precess about the static magnetic field, B_0 , at a frequency defined by the chemical identity of the nucleus (in this study ^1H) and its local electronic environment. Provided that the static magnetic field is

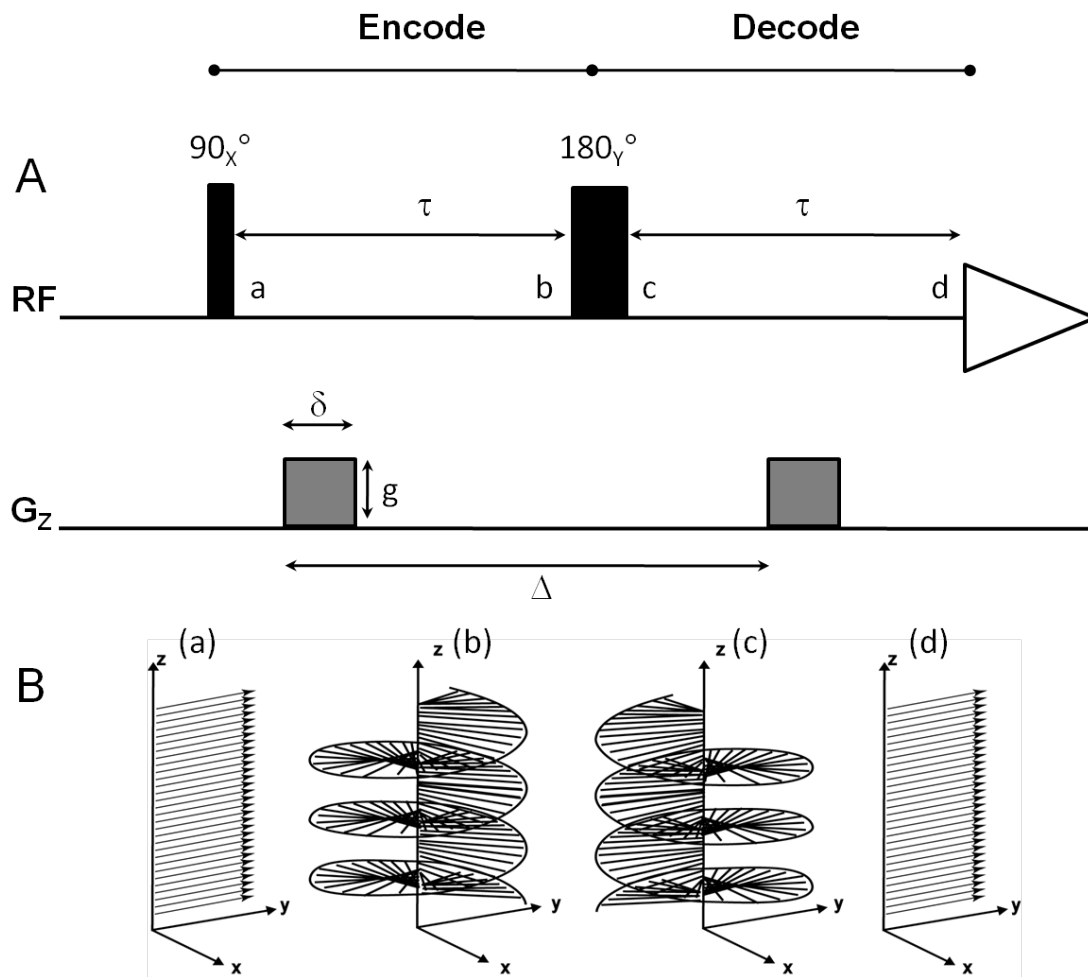


Figure 1.11. (A) PGSE pulse sequence used for PFG-NMR diffusion measurements and (B) the effect on the magnetization.

homogenous within the NMR probe coil, all spins within the sample experience an identical magnetic field despite their location within the sample. The application of a magnetic field gradient has the effect of making the magnetic field inhomogenous in a linearly dependent fashion along the direction of the applied gradient pulse and therefore, induces a translational dependent phase shift in the spins. The resulting phase shift is expressed by the equation 1.8,

$$\theta_i(t) = \gamma B_0 \tau + \gamma g \int_{t_1}^{t_1+\Delta} z_i(t) dt \quad (1.8)$$

where the first term, $\gamma B_0 \tau$, is the phase shift due to the static magnetic field, B_0 , under the influence of the Larmor precessional frequency and the second term in the expression above, $\gamma g \int_{t_1}^{t_1+\Delta} z_i(t) dt$, is the phase shift as a result of the applied magnetic field gradient pulse. The application of a well-defined magnetic field gradient can therefore be used to label the position of spins through their Larmor frequencies. Figure 1.11B illustrates how the magnetic field gradients in the PGSE experiment label nuclei according to their spatial position within the sample tube. The magnetization vectors are wound into a helix along the z-axis during encoding as shown in Figure 1.11B.

Provided that translational diffusion does not occur during the diffusion delay time (Δ), the spatial encoding of the spins in the system is fully reversible by the application of a second magnetic field gradient pulse following the 180° echo pulse with no attenuation of the NMR signal. The second gradient pulse unwinds the magnetization vectors during the decoding period. However, if translational diffusion does occur the second gradient pulse will not realign the previously encoded phases of the spins and the resulting NMR signal will appear attenuated. Because the NMR signal intensity following the PGSE pulse sequence is related to both the amplitude and duration of the applied gradient

pulse and the diffusion delay time, the diffusion coefficients for the components in the solution can be determined using the Stejskal-Tanner equation (equation 1.9),

$$I = I_0 \exp \left[-D(\gamma g \delta)^2 \left(\Delta - \frac{\delta}{3} \right) \right] \quad (1.9)$$

where I and I_0 are the intensity of the NMR signal in the presence and absence of the gradient pulse, respectively, D is the diffusion coefficient of the molecule, Δ is the diffusion delay time, γ is the nuclear gyromagnetic ratio, and g and δ are the amplitude and duration of the gradient pulses, respectively. For non-exchanging protons, the diffusion coefficient D can be obtained by an exponential fit of the signal intensity I to the Stejskal-Tanner equation as a function of the applied gradient amplitude, g .

Because the calculation of diffusion coefficients is dependent on the attenuation of the resonances, experiments requiring longer delay times, for example in the analysis of macromolecules such as proteins or highly viscous solutions suffer from magnetization loss as a result of T_2 relaxation. In addition, for coupled spin systems, phase modulation due to heteronuclear couplings reduces the applicability of diffusion NMR. To overcome these limitations, Tanner introduced the pulsed-field gradient stimulated echo (PFG-STE) experiment in 1970.⁷⁹ The PFG-STE (Figure 1.12) pulse sequence is a more versatile experiment for diffusion measurements. In the pulse sequence shown in Figure 1.12A, the encode and decode periods are separated by a pair of 90° pulses, which allows for the majority of the diffusion period to occur while the magnetization is stored along the longitudinal axis. The resulting echo attenuation therefore occurs by T_1 relaxation during the diffusion period and phase distortion as a result of J_{HH} coupling evolution, which is not refocused by the spin echo experiment, is

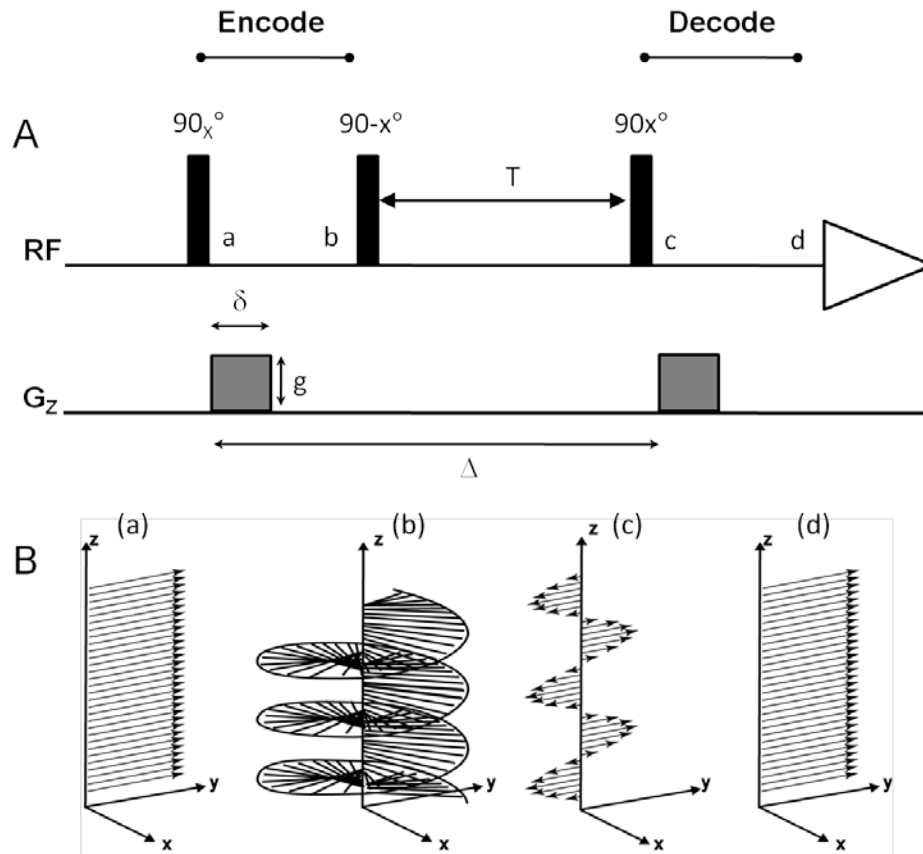


Figure 1.12. (A) The PFG-STE pulse and (B) the effect of magnetization. After the first 90° pulse (a) the gradient pulse spatially encodes spins along the length of the sample (b). Shortly following the gradient pulse, a 90° pulse is applied which places z components of the spatially encoded magnetization along the longitudinal axis. A delay time (T) follows which allows the molecules to diffuse. A 90° pulse is applied following the diffusion delay time returning the spatially encoded magnetization back along the transverse axis (c). From the magnetization vectors (b) and (c), it is evident that half of the magnetization is eliminated as a result of magnetization storage during the diffusion delay time (T). A final gradient pulse refocuses magnetization of the components (d) where the efficiency of refocusing is dependent on the extent of diffusion during the delay time.

eliminated. Because the time in which the magnetization is held in the transverse plane is short in the PFG-STE experiment, as long as the diffusion delay time is shorter than T_1 , translational diffusion dominates the measured signal decay rather than T_2 relaxation. A drawback of the stimulated echo experiment is that half of the potential signal is lost, as illustrated in Figure 1.12B. Signal loss is due to the second 90_x° pulse only stores the y-component of the transverse onto the z-axis, while the magnetization along the x-axis is destroyed by the homospoil gradient pulse. Therefore, only half of the signal can be refocused with the stimulated echo experiment.

1.7.1 Diffusion NMR with the BPPSTE Pulse Sequence

Following the introduction of the PGSE and the PFG-STE experiments by Stejskal and Tanner, numerous other pulse sequences have been developed for the measurement of diffusion of components in liquid and even solid mixtures. For large slow moving species the phase-encoding gradient pulses must have large amplitudes, and the resulting eddy-current fields can cause significant errors in the phase encoding.⁸⁰ Eddy currents are induced in the metal structures of the NMR magnet and probe by the magnetic field gradient pulses. Eddy currents can significantly distort NMR signals especially when stronger gradient pulses are used. With the introduction of better shielded gradient probes and bipolar gradient pulses there is a reduced need for the eddy current delays and diffusion experiments designed with delays to reduce eddy current distortions, such as LED, have largely fallen out of use.⁸⁰ The PFG-BPPSTE experiment used in this dissertation incorporates bipolar gradient pulses to effectively eliminate eddy currents.

The BPPSTE pulse sequence used in this dissertation is shown in Figure 1.13. The behavior of the proton magnetization as a result of the pulse sequence can be explained visually using vector diagrams, as demonstrated in Section 1.4.2. The magnetization vector, \mathbf{M} , is tipped away from the z-axis and onto the transverse (xy) plane with the initial 90° pulse. A gradient pulse of duration δ is then applied to encode for the spatial position of the molecules within the NMR sample tube as demonstrated in Figures 1.11 and 1.12. The gradient pulse is followed immediately by the application of a 180° pulse which inverts the magnetization about the y- or x-axis. A second gradient pulse, equal in amplitude but opposite in phase to the first gradient pulse, is applied to further encode the molecules in the NMR tube. A 90° pulse then stores the spatially encoded magnetization along the longitudinal axis during the diffusion time, Δ . As mentioned above, storing magnetization on the longitudinal axis helps to reduce magnetization loss as a result of T_2 relaxation as well as J-coupling modulations which lead to signal loss and phase distortions. This first half of the pulse sequence is considered the encode period. Following the encode period, a homospoil gradient pulse is applied to destroy magnetization remaining in the transverse plane. During the allowed diffusion time, molecular diffusion leads to a decrease in the amplitude of the stored magnetization. The second half of the BPPSTE pulse program refocuses the remaining magnetization stored along the z-axis resulting in the formation of the NMR echo. The intensity of specific resonances I and the diffusion coefficient D are related according to the modified Stejskal-Tanner equation (equation 1.10):

$$I = I_0 \exp \left[-D(\gamma\delta g)^2 \left(\Delta - \frac{\delta}{2} - \frac{\tau}{3} \right) \right] \quad (1.10)$$

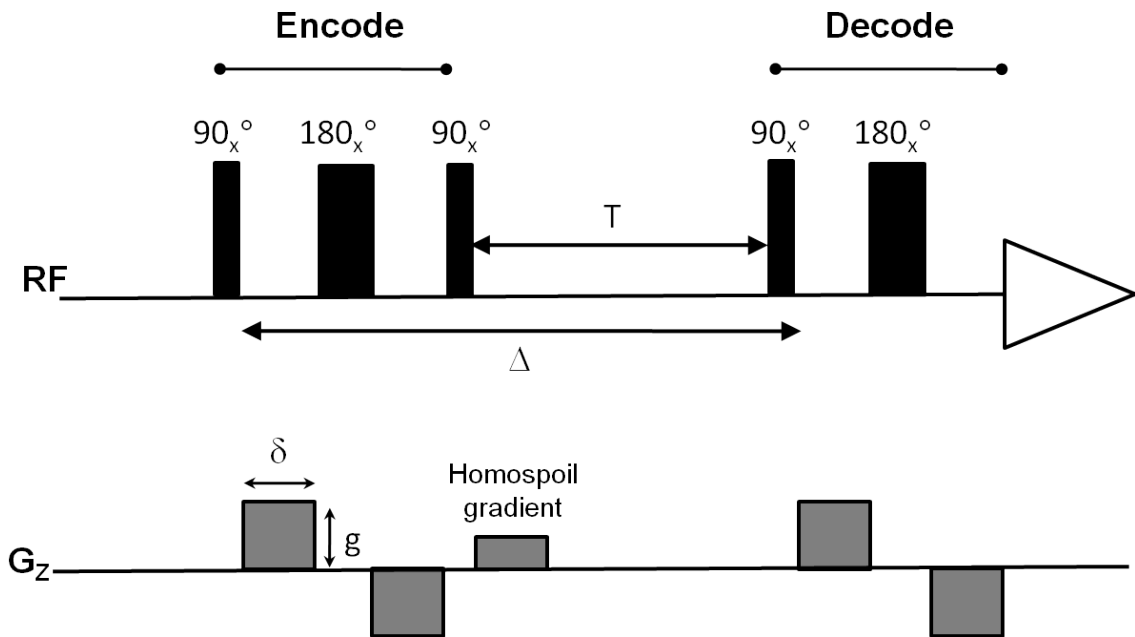


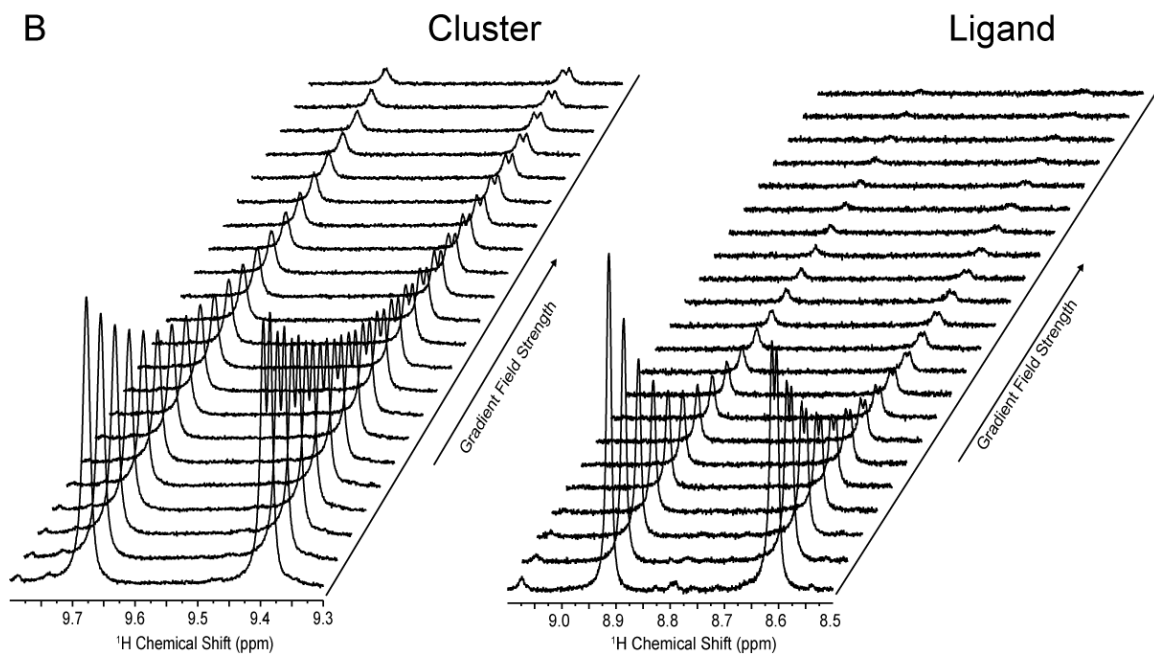
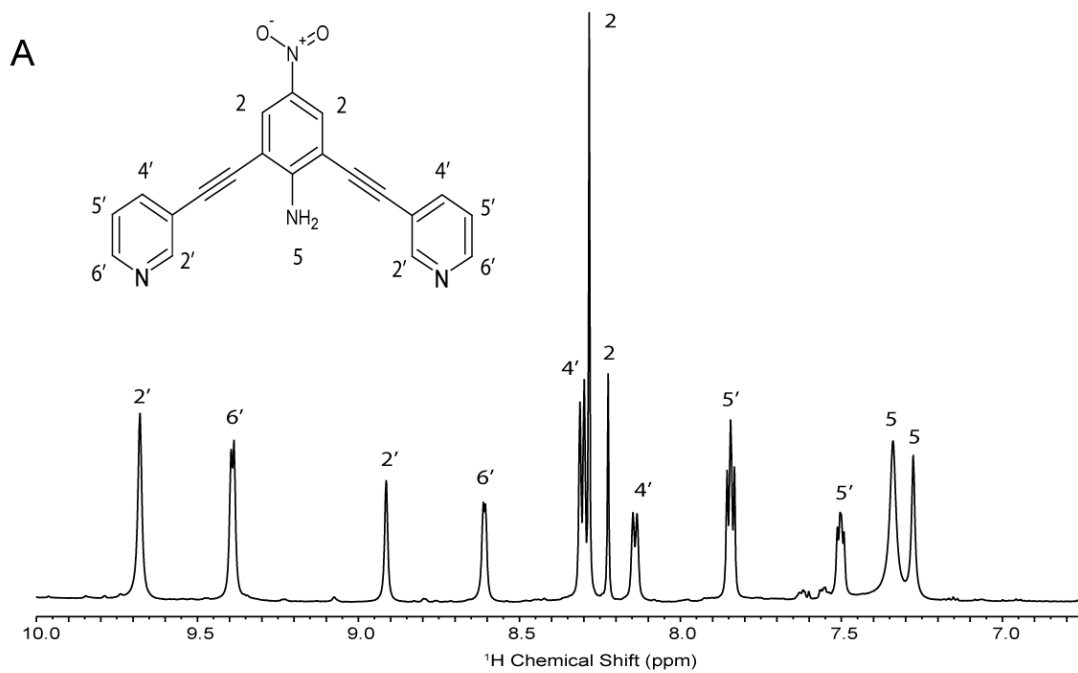
Figure 1.13. Bipolar pulse pair stimulated echo (BPPSTE) used in the diffusion experiments in this dissertation.

Equation 1.10 differs from the original Stejskal-Tanner equation (equation 1.9) by the introduction of the term τ , which accounts for the short gradient recovery delay following all gradients during which time relaxation and spin-spin coupling evolution are not significant.

Figure 1.14 illustrates the application of BPPSTE in the separation of a 1:1 mixture of a pyridine ligand and cluster. The pyridine ligand structure and ^1H NMR spectrum are shown in Figure 1.14A. The diffusion coefficients for the two components can be extracted by fitting the decay of the resonance intensities between 8.5 – 9.8 ppm measured as a function of the square of the gradient amplitude according equation 1.10. A stacked plot comparing the attenuation of the well-resolved resonances at 8.92 and 8.61 ppm corresponding to the free ligand and the resonances at 9.68 and 9.39 ppm corresponding to the cluster is shown in Figure 1.14B. From the stacked spectra shown in Figure 1.14B, it is visually evident that the ligand cluster diffuses slower than the smaller free ligand, as illustrated by the more gradual attenuation of the cluster resonances (9.68 and 9.39 ppm). Figure 1.14C shows the exponential fits of the resonances for the free ligand and ligand cluster as well as the residuals from the fit. Non-linear least squares fit of a model based on equation 1.10 produced diffusion coefficients for the free ligand of $2.60 \pm 0.05 \times 10^{-10} \text{ m}^2\text{s}^{-1}$, whereas the diffusion constant for the ligand cluster was $1.35 \pm 0.01 \times 10^{-10} \text{ m}^2\text{s}^{-1}$. The other peaks for the cluster and ligand gave rise to similar diffusion constants.

1.7.2 Diffusion-Ordered Spectroscopy (DOSY)

DOSY processing of NMR diffusion data produces a pseudo-2D spectrum with NMR chemical shifts on the horizontal axis and calculated self-diffusion coefficients



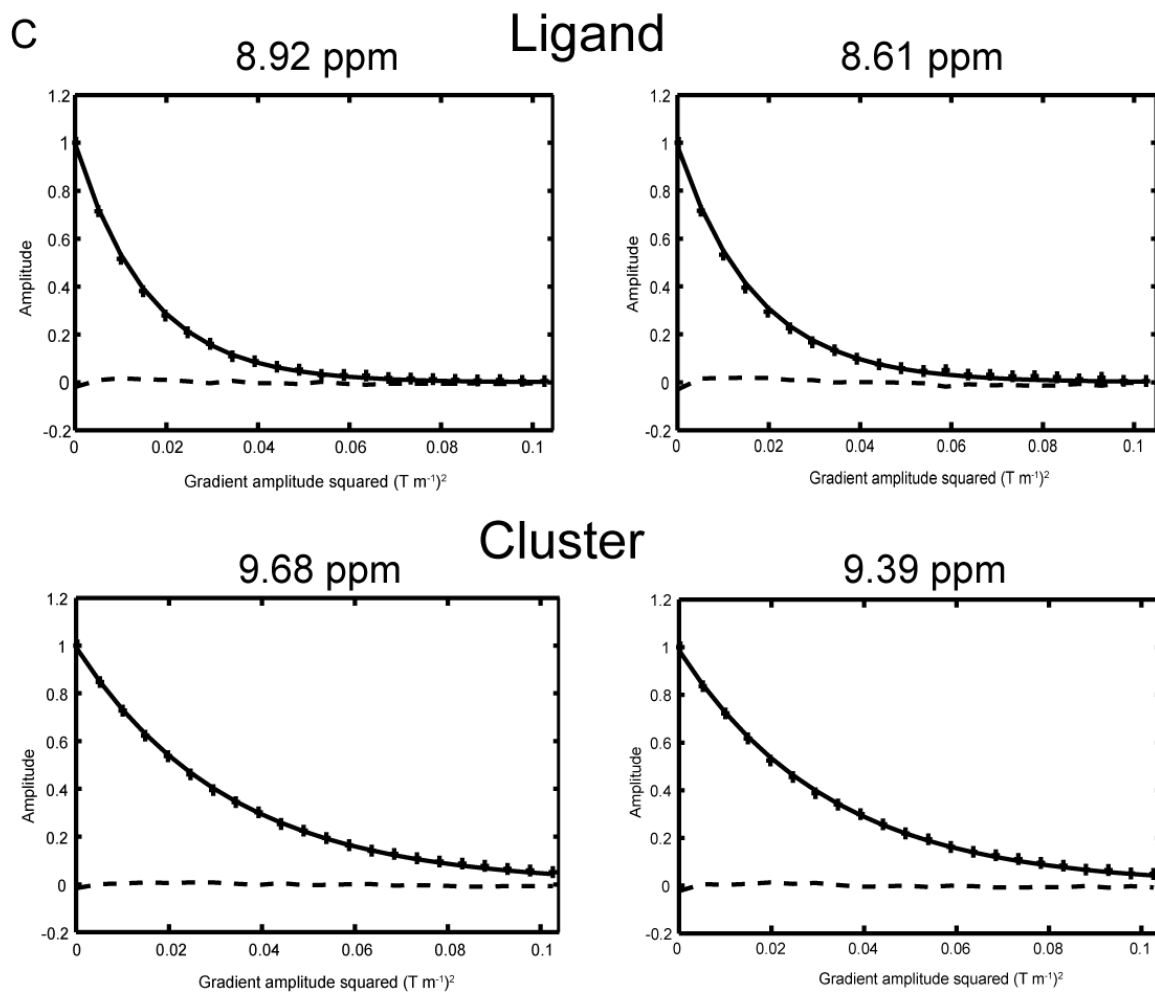


Figure 1.14. (A) The structure of the pyridine ligand and ^1H NMR spectrum of 1:1 mixture of ligand and cluster. (B) Stacked plot of cluster resonances (left) and ligand resonances (right) collected as a function of increased gradient strength. (C) Molecular diffusion is illustrated by the attenuation of the NMR resonances as the gradient amplitude is increased. The intensity of the integrated region is plotted against the square of the gradient amplitude, and the resulting curve can be fit to derive the diffusion coefficient.

along the vertical axis. DOSY has been used for the analysis and characterization of mixtures and aggregates,⁸¹⁻⁸⁵ as well as in the study of intermolecular interactions.⁸⁶⁻⁹¹

The advantage of DOSY in the analysis of PFG-NMR data measured for mixtures is its ability to order resonances in a two-dimensional format according to their chemical shift, effectively resolving the spectra of individual components based on differences in their diffusion coefficients. Like all NMR techniques, DOSY is a non-invasive technique that is used to obtain both physical and chemical information and therefore can be considered a cheap alternative to LC-NMR for mixture analysis.

DOSY is comprised of a collection of methods used in the processing and displaying of PFG-NMR data. In a DOSY experiment, a series of ¹H NMR spectra are acquired using either a PGSE or PFGSTE experiment where the intensities of the resonances vary as a function of the applied gradient pulse. The observed rate by which the NMR signal decay is governed by the translational diffusion of the molecule as expressed by its diffusion coefficient. Because translational diffusion is a property of the molecule as a whole, the diffusion coefficient carries information that can be used to distinguish between signals of the different molecular species in the mixture.

Processing of PFG-NMR data using DOSY techniques involves the step-wise analysis of the individual frequencies in a spectrum or groups of frequencies represented as baseline resolved resonances having discrete diffusion coefficients where the diffusion coefficients of the individual components in the mixture are extracted using a non-linear curve fit of the experimental data to the Stejskal-Tanner equation (equation 1.9 or 1.10).⁷⁶ A more effective method for DOSY processing was pioneered by Johnson and Morris by which the acquisition is easily analyzed by Fourier transformation yielding spectral intensities of the pure components in the frequency dimension (F2) along with a

spectrum of the diffusion coefficients, determined by solving the inverse Laplace transforms (ILT) of the signal intensities of the diffusion-attenuated spectra, in the diffusion dimension (F1).^{81, 92} Because DOSY processing involves the fitting of the decay data to the ILT, it is more strongly influenced by the quality of the experimental data than 2D NMR experiments such as COSY and TOCSY whose processing is based on Fourier transformation of the time dependent FID.

There are two main methods used in the data processing, they are univariate processing^{81, 93-96} where each resonance in the spectrum is processed individually and multivariate processing⁹⁷⁻¹⁰⁰ where the whole spectrum or regions of the spectrum are processed simultaneously. In this dissertation, univariate processing was exclusively used in the processing of PFG-NMR data and therefore for the sake of simplicity, I will restrict the remainder of this section to processing by univariate methods.

The most basic and effective univariate processing method is high resolution DOSY (HR-DOSY).⁹³ In HR-DOSY, the decay of each resonance is fitted to a monoexponential decay and the data is presented in a pseudo-2D DOSY plot. To better interpret the data, a set of calculations is performed to group the diffusion coefficients measured for a given resolved resonance. Statistical analysis is performed for the calculated diffusion coefficients and a single “cross-peak” is created having a width in the diffusion dimension representative of its standard deviation.⁷⁶

When using HR-DOSY in the processing of PFG-NMR data, an assumption is made that each resonance interrogated arises from only one species in the mixture (i.e. there are no overlapping resonances). When the resonances are in fact composed of only one component, HR-DOSY provides exceptional resolution in the diffusion dimension, capable of differentiating between components with differences in their

diffusion coefficients as small as 0.5%.¹⁰¹ However when resonance overlap is encountered, the measured diffusion coefficient will likely be a weighted average of the components comprising that peak, complicating spectral interpretation.⁹³

Identification of resonances with signal decays containing contributions from more than one species is often difficult in that the average of two exponentials with similar decay constants is almost indistinguishable from that of a single exponential with an intermediate decay. Close examination of the fitting residuals, a plot which presents the deviation of the experimental data from the calculated exponential fit, may help to indicate the presence of overlapping resonances, but care must be taken as deviations can also be easily attributed to system errors such as non-uniform gradients.^{95, 101} A seemingly straightforward way to overcome complications resulting from resonance overlap is to fit the data to multi-exponential decays such as bi- and tri-exponential decays. But in order to do this, the data must be of high quality and high signal-to-noise ratio (SNR). The multi-exponential approach put very high demands on the data and as a rule of thumb for data with a SNR of 10,000:1 the lower limit for detection of differences in diffusion coefficients is around 30%.¹⁰¹ This is significantly less sensitive than the 0.5% resolution attainable with fully resolved resonances.

DOSY spectra for the pyridine ligand and cluster presented in Figure 1.14 are calculated using an approximation to the ILT from a series of pulsed-field gradient NMR spectra acquired using gradient pulses with varying amplitudes as shown in Figure 1.14B. Shown in Figure 1.15 is the DOSY spectrum obtained by the mono-exponential fitting of the BPPSTE data.

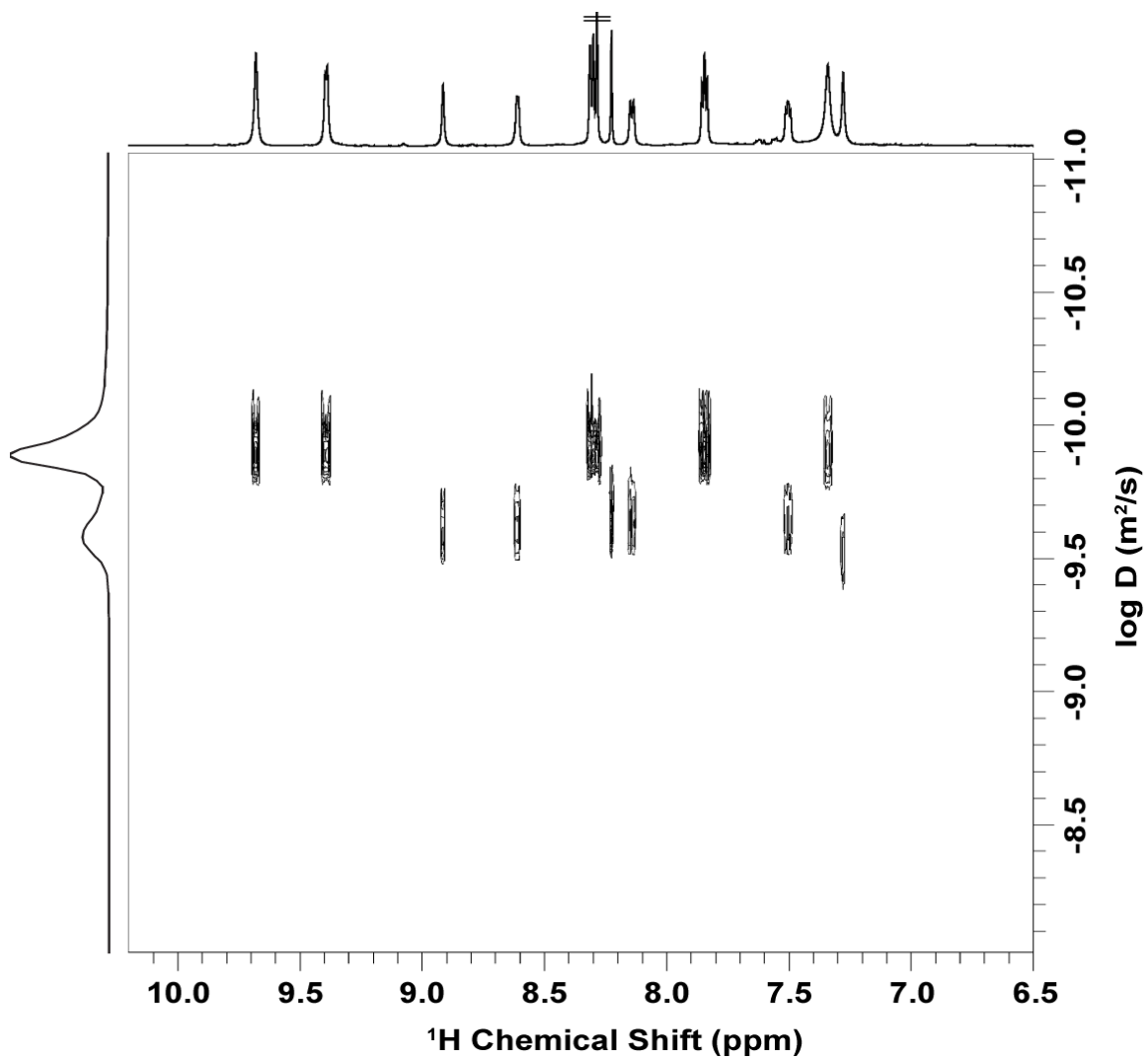


Figure 1.15. DOSY spectrum of a 1:1 mixture of the pyridine ligand and cluster acquired in $\text{DMSO-}d_6$ at 298 K. A diffusion delay of 200 msec and a gradient pulse length 2 msec was used in the BPPSTE experiment. The projection in the diffusion dimension (F1) corresponds to peaks in the chemical shift region (F2) between 10 ppm and 8.5 ppm. This region was selected to remove the contribution from the large singlet at 8.283 ppm belonging to the cluster and more easily resolve the peaks from ligand in the diffusion projection plotted along the y-axis.

NMR spectroscopy is a powerful tool in the analysis of heparin solutions as demonstrated in the detection and identification of OSCS in pharmaceutical heparin preparations as presented in section 1.2.3. However, the structural and solution complexity of GAG samples can present a daunting task in the interpretation of the NMR spectra. This compounded by the lower inherent sensitivity of NMR complicates the detection and identification of small amounts of impurities which may be present in pharmaceutical heparin preparations. A goal of this dissertation is in the development and application of NMR methods to simplify the characterization of heparin solutions through the use of hyphenated- and diffusion-NMR techniques. In this work we also address sensitivity limitations of NMR through the use of microcoil NMR technology in the structure characterization of mass-limited heparin-derived oligosaccharides.

1.8 References

1. Rabenstein, D. L. Heparin and heparan sulfate: structure and function. *Nat. Prod. Rep.* **2002**, *19*, 312-331.
2. Gatti, G.; Casu, B.; Hamer, G. K.; Perlin, A. S. Studies on the Conformation of Heparin by ¹H and ¹³C NMR Spectroscopy. *Macromolecules* **1979**, *12*, 1001-1007.
3. Whitelock, J. M.; Iozzo, R. V. Heparan Sulfate: A Complex Polymer Charged with Biological Activity. *Chem Rev* **2005**, *105*, 2745-2764.
4. Gallagher J T., W. A. Molecular distinctions between heparan sulphate and heparin. *Biochem J.* **1985**, *230*, 665-674.
5. Sugahara, K.; Kitagawa, H. Heparin and Heparan Sulfate Biosynthesis. *IUBMB Life* **2002**, *54*, 163-175.
6. Rosenberg, R. D.; Shworak, N. W.; Liu, J.; Schwartz, J. J.; Zhang, L. Heparan sulfate proteoglycans of the cardiovascular system. Specific structures emerge but how is synthesis regulated? *The Journal of Clinical Investigation* **1997**, *99*, 2062-2070.
7. Jing, P.; Kim, Y.; Amemiya, S. Voltammetric Extraction of Heparin and Low-Molecular-Weight Heparin across 1,2-Dichloroethane/Water Interfaces. *Langmuir* **2009**, *25*, 13653-13660.
8. Sasisekharan, R.; Venkataraman, G. Heparin and heparan sulfate: biosynthesis, structure and function. *Current Opinion in Chemical Biology* **2000**, *4*, 626-631.
9. Feyerabend, T. B.; Li, J.-P.; Lindahl, U.; Rodewald, H.-R. Heparan sulfate C5-epimerase is essential for heparin biosynthesis in mast cells. *Nat. Chem. Biol.* **2006**, *2*, 195-196.
10. Kolset, S. O.; Prydz, K.; Pejler, G. Intracellular proteoglycans. *Biochem J.* **2004**, *379*, 217-227.
11. Capila, I.; Linhardt, R. J. Heparin-Protein Interactions. *Angew Chem Int Ed Engl* **2002**, *41*, 390-412.
12. Folkman, J.; Weisz, P. B.; Joullie, M. M.; Li, W. W.; Ewing, W. R. Control of Angiogenesis with Synthetic Heparin Substitutes. *Science* **1989**, *243*, 1490-1493.
13. Sasisekharan, R.; Shriver, Z.; Venkataraman, G.; Narayanasami, U. Roles of heparan-sulphate glycosaminoglycans in cancer. *Nat. Rev. Cancer* **2002**, *2*, 521-528.
14. Tyrrell, D. J.; Kilfeather, S.; Page, C. P. Therapeutic uses of heparin beyond its traditional role as an anticoagulant. *Trends Pharmacol. Sci.* **1995**, *16*, 198-204.
15. Jorpes, E. The chemistry of heparin. *Biochem J.* **1935**, *29*, 1817-1830.
16. Lindahl, U.; Bäckström, G.; Thunberg, L.; Leder, I. G. Evidence for a 3-O-sulfated D-glucosamine residue in the antithrombin-binding sequence of heparin. *Proc. Natl. Acad. Sci. U. S. A.* **1980**, *77*, 6551-6555.
17. Björk, I.; Lindahl, U. Mechanism of the anticoagulant action of heparin. *Mol. Cell. Biochem.* **1982**, *48*, 161-182.
18. Liu, H. Y.; Zhang, Z. Q.; Linhardt, R. J. Lessons learned from the contamination of heparin. *Nat. Prod. Rep.* **2009**, *26*, 313-321.
19. Khorana, A. A.; Sahni, A.; Altland, O. D.; Francis, C. W. Heparin Inhibition of Endothelial Cell Proliferation and Organization Is Dependent on Molecular Weight. *Arterioscler Thromb Vasc Biol* **2003**, *23*, 2110-2115.

20. Barrowcliffe, T. W. Low Molecular Weight Heparin(s). *British Journal of Haematology* **1995**, *90*, 1-7.
21. Linhardt, R. J. 2003 Claude S. Hudson Award Address in Carbohydrate Chemistry. Heparin: Structure and Activity. *J. Med. Chem.* **2003**, *46*, 2551-2564.
22. Linhardt, R. J.; Gunay, N. S. Production and chemical processing of low molecular weight heparins. *Semin Thromb Hemost* **1999**, *25*, 5-16.
23. Fareed, J.; Jeske, W.; Hoppensteadt, D.; Clarizio, R.; Walenga, J. M. Low-molecular-weight heparins: pharmacologic profile and product differentiation. *Am J Cardiol* **1998**, *82*, 3L-10L.
24. Zhang, Z. Q.; Weiwer, M.; Li, B. Y. Z.; Kemp, M. M.; Daman, T. H.; Linhardt, R. J. Oversulfated chondroitin sulfate: Impact of a heparin impurity, associated with adverse clinical events, on low-molecular-weight heparin preparation. *J. Med. Chem.* **2008**, *51*, 5498-5501.
25. Concannon, S.; Wimberley, P.; Workman, W. A quantitative PCR method to quantify ruminant DNA in porcine crude heparin. *Analytical and Bioanalytical Chemistry* **2010**, *399*, 757-762.
26. Kokubo, S.; Horii, T.; Yonekawa, O.; Ozawa, N.; Mukaide, M. A phylogenetic-tree analysis elucidating nosocomial transmission of hepatitis C virus in a haemodialysis unit. *Journal of Viral Hepatitis* **2002**, *9*, 450-454.
27. Neville, G. A.; Mori, F.; Holme, K. R.; Perlin, A. S. Monitoring the purity of pharmaceutical heparin preparations by high-field ¹H-nuclear magnetic resonance spectroscopy. *J. Pharm. Sci.* **1989**, *78*, 101-104.
28. Trowbridge, J. M.; Gallo, R. L. Dermatan sulfate: new functions from an old glycosaminoglycan. *Glycobiology* **2002**, *12*, 117R-125R.
29. Guerrini, M.; Beccati, D.; Shriver, Z.; Naggi, A.; Viswanathan, K.; Bisio, A.; Capila, I.; Lansing, J. C.; Guglieri, S.; Fraser, B.; Al-Hakim, A.; Gunay, N. S.; Zhang, Z. Q.; Robinson, L.; Buhse, L.; Nasr, M.; Woodcock, J.; Langer, R.; Venkataraman, G.; Linhardt, R. J.; Casu, B.; Torri, G.; Sasisekharan, R. Oversulfated chondroitin sulfate is a contaminant in heparin associated with adverse clinical events. *Nature Biotechnol* **2008**, *26*, 669-675.
30. Maruyama, T.; Toida, T.; Imanari, T.; Yu, G.; Linhardt, R. J. Conformational changes and anticoagulant activity of chondroitin sulfate following its O-sulfonation. *Carbohydr. Res.* **1998**, *306*, 35-43.
31. Kishimoto, T. K.; Viswanathan, K.; Ganguly, T.; Elankumaran, S.; Smith, S.; Pelzer, K.; Lansing, J. C.; Sriranganathan, N.; Zhao, G. L.; Galcheva-Gargova, Z.; Al-Hakim, A.; Bailey, G. S.; Fraser, B.; Roy, S.; Rogers-Cotrone, T.; Buhse, L.; Whary, M.; Fox, J.; Nasr, M.; Dal Pan, G. J.; Shriver, Z.; Langer, R. S.; Venkataraman, G.; Austen, K. F.; Woodcock, J.; Sasisekharan, R. Contaminated heparin associated with adverse clinical events and activation of the contact system. *N. Engl. J. Med.* **2008**, *358*, 2457-2467.
32. Blossom, D. B.; Kallen, A. J.; Patel, P. R.; Elward, A.; Robinson, L.; Gao, G. P.; Langer, R.; Perkins, K. M.; Jaeger, J. L.; Kurkjian, K. M.; Jones, M.; Schillie, S. F.; Shehab, N.; Ketterer, D.; Venkataraman, G.; Kishimoto, T. K.; Shriver, Z.; McMahon, A. W.; Austen, K. F.; Kozlowski, S.; Srinivasan, A.; Turabelidze, G.; Gould, C. V.; Arduino, M. J.; Sasisekharan, R. Outbreak of Adverse Reactions Associated with Contaminated Heparin. *N. Engl. J. Med.* **2008**, *359*, 2674-2684.

33. FDA's Ongoing Heparin Investigation
<http://www.fda.gov/NewsEvents/Testimony/ucm115242.htm> Accessed 21 June 2010.
34. Sasisekharan, R.; Shriver, Z. From crisis to opportunity: A perspective on the heparin crisis. *Thromb Haemost* **2009**, *102*, 854-858.
35. Adam, A.; Montpas, N.; Keire, D.; Désormeaux, A.; Brown, N. J.; Marceau, F.; Westenberger, B. Bradykinin forming capacity of oversulfated chondroitin sulfate contaminated heparin in vitro. *Biomaterials* **2010**, *31*, 5741-5748.
36. Trehy, M. L.; Reepmeyer, J. C.; Kolinski, R. E.; Westenberger, B. J.; Buhse, L. F. Analysis of heparin sodium by SAX/HPLC for contaminants and impurities. *J. Pharm. Biomed. Anal.* **2009**, *49*, 670-673.
37. Lohse, D. L.; Linhardt, R. J. Purification and characterization of heparin lyases from *Flavobacterium heparinum*. *J. Biol. Chem.* **1992**, *267*, 24347-24355.
38. Shively, J. E.; Conrad, H. E. Formation of anhydrosugars in the chemical depolymerization of heparin. *Biochemistry* **1976**, *15*, 3932-3942.
39. Galliher, P. M.; Cooney, C. L.; Langer, R.; Linhardt, R. J. Heparinase production by *Flavobacterium heparinum*. *Appl. Environ. Microbiol.* **1981**, *41*, 360-365.
40. Linker, A.; Hovingh, P. Isolation and characterization of oligosaccharides obtained from heparin by the action of heparinase. *Biochemistry* **1972**, *11*, 563-568.
41. Jandik, K. A.; Gu, K.; Linhardt, R. J. Action pattern of polysaccharide lyases on glycosaminoglycans. *Glycobiology* **1994**, *4*, 289-296.
42. Desai, U. R.; Wang, H. M.; Linhardt, R. J. Specificity studies on the heparin lyases from *Flavobacterium heparinum*. *Biochemistry* **1993**, *32*, 8140-8145.
43. Viskov, C.; Bouley, E.; Hubert, P.; Martinez, C.; Herman, F.; Jeske, W.; Hoppensteadt, D.; Walenga, J. M.; Fareed, J. Isolation and Characterization of Contaminants in Recalled Unfractionated Heparin and Low-Molecular-Weight Heparin. *Clinical and Applied Thrombosis-Hemostasis* **2009**, *15*, 395-401.
44. Guerrini, M.; Shriver, Z.; Naggi, A.; Casu, B.; Linhardt, R. J.; Torri, G.; Sasisekharan, R. Reply to Oversulfated chondroitin sulfate is not the sole contaminant in heparin. *Nat Biotech* **2010**, *28*, 207-211.
45. Holzgrabe, U.; Diehl, B. W. K.; Wawer, I. NMR spectroscopy in pharmacy. *J. Pharm. Biomed. Anal.* **1998**, *17*, 557-616.
46. Holme, K. R.; Perlin, A. S. Nuclear magnetic resonance spectra of heparin in admixture with dermatan sulfate and other glycosaminoglycans. 2-D spectra of the chondroitin sulfates. *Carbohydr. Res.* **1989**, *186*, 301-312.
47. Toida, T.; Huang, Y.; Washio, Y.; Maruyama, T.; Toyoda, H.; Imanari, T.; Linhardt, R. J. Chemical Microdetermination of Heparin in Plasma. *Anal. Biochem.* **1997**, *251*, 219-226.
48. Atha, D. H.; Coxon, B.; Reipa, V.; Gaigalas, A. K. Physicochemical characterization of low molecular weight heparin. *J. Pharm. Sci.* **1995**, *84*, 360-364.
49. Sugahara, K.; Tsuda, H.; Yoshida, K.; Yamada, S.; de Beer, T.; Vliegenthart, J. F. G. Structure Determination of the Octa- and Decasaccharide Sequences Isolated from the Carbohydrate-Protein Linkage Region of Porcine Intestinal Heparin. *J. Biol. Chem.* **1995**, *270*, 22914-22923.
50. Chuang, W.-L.; Christ, M. D.; Rabenstein, D. L. Determination of the Primary Structures of Heparin- and Heparan Sulfate-Derived Oligosaccharides Using

- Band-Selective Homonuclear-Decoupled Two-Dimensional ^1H NMR Experiments. *Anal. Chem.* **2001**, *73*, 2310-2316.
51. Ruiz-Calero, V.; Saurina, J.; Galceran, M. T.; Hernandez-Cassou, S.; Puignou, L. Potentiality of proton nuclear magnetic resonance and multivariate calibration methods for the determination of dermatan sulfate contamination in heparin samples. *Analyst* **2000**, *125*, 933-938.
 52. McEwen, I.; Rundlof, T.; Ek, M.; Hakkarainen, B.; Carlin, G.; Arvidsson, T. Effect of Ca^{2+} on the H-1 NMR chemical shift of the methyl signal of oversulphated chondroitin sulphate, a contaminant in heparin. *J. Pharm. Biomed. Anal.* **2009**, *49*, 816-819.
 53. McEwen, I. Broadening of ^1H NMR signals in the spectra of heparin and OSCS by paramagnetic transition metal ions. The use of EDTA to sharpen the signals. *J. Pharm. Biomed. Anal.* **2010**, *51*, 733-735.
 54. Beyer, T.; Diehl, B.; Randel, G.; Humpfer, E.; Schafer, H.; Spraul, M.; Schollmayer, C.; Holzgrabe, U. Quality assessment of unfractionated heparin using H-1 nuclear magnetic resonance spectroscopy. *J. Pharm. Biomed. Anal.* **2008**, *48*, 13-19.
 55. Tachibana, S.; Nishiura, S.; Ishida, S.; Kakehi, K.; Honda, S. Quality check of heparin injections by ^1H -nuclear magnetic resonance spectroscopy. *Chem. Pharm. Bull.* **1990**, *38*, 2503-2506.
 56. Yamaguchi, H.; Shinagawa, M.; Shimba, N.; Miyano, H.; Suzuki, E. NMR analysis of a contaminant in heparin. *Yakugaku Zasshi-J. Pharm. Soc. Jpn.* **2008**, *128*, 1513-1515.
 57. Guerrini, M.; Shriver, Z.; Bisio, A.; Naggi, A.; Casu, B.; Sasisekharan, R.; Torri, G. The tainted heparin story: An update. *Thromb Haemost* **2009**, *102*, 907-911.
 58. Bigler, P.; Brenneisen, R. Improved impurity fingerprinting of heparin by high resolution H-1 NMR spectroscopy. *J. Pharm. Biomed. Anal.* **2009**, *49*, 1060-1064.
 59. Beyer, T.; Matz, M.; Brinz, D.; Rädler, O.; Wolf, B.; Norwig, J.; Baumann, K.; Alban, S.; Holzgrabe, U. Composition of OSCS-contaminated heparin occurring in 2008 in batches on the German market. *Eur. J. Pharm. Sci.* **2010**, *40*, 297-304.
 60. Keire, D. A.; Trehy, M. L.; Reepmeyer, J. C.; Kolinski, R. E.; Ye, W.; Dunn, J.; Westenberger, B. J.; Buhse, L. F. Analysis of crude heparin by ^1H NMR, capillary electrophoresis, and strong-anion-exchange-HPLC for contamination by over sulfated chondroitin sulfate. *J. Pharm. Biomed. Anal.* **2010**, *51*, 921-926.
 61. Keire, D. A.; Mans, D. J.; Ye, H.; Kolinski, R. E.; Buhse, L. F. Assay of possible economically motivated additives or native impurities levels in heparin by ^1H NMR, SAX-HPLC, and anticoagulation time approaches. *J. Pharm. Biomed. Anal.* **2010**, *52*, 656-664.
 62. Serber, Z.; Richter, C.; Moskau, D.; Bohlen, J.-M.; Gerfin, T.; Marek, D.; Haberli, M.; Baselgia, L.; Laukien, F.; Stern, A. S.; Hoch, J. C.; Dotsch, V. New Carbon-Detected Protein NMR Experiments Using CryoProbes. *J. Am. Chem. Soc.* **2000**, *122*, 3554-3555.
 63. Spraul, M.; Freund, A. S.; Nast, R. E.; Withers, R. S.; Maas, W. E.; Corcoran, O. Advancing NMR Sensitivity for LC-NMR-MS Using a Cryoflow Probe: Application to the Analysis of Acetaminophen Metabolites in Urine. *Anal. Chem.* **2003**, *75*, 1536-1541.

64. Korir, A.; Larive, C. On-line NMR detection of microgram quantities of heparin-derived oligosaccharides and their structure elucidation by microcoil NMR. *Anal. Bioanal. Chem.* **2007**, *388*, 1707-1716.
65. Ardenkjaer-Larsen, J. H.; Fridlund, B.; Gram, A.; Hansson, G.; Hansson, L.; Lerche, M. H.; Servin, R.; Thaning, M.; Golman, K. Increase in signal-to-noise ratio of > 10,000 times in liquid-state NMR. *Proc. Natl. Acad. Sci. U.S.A.* **2003**, *100*, 10158-10163.
66. Bowen, S.; Hilty, C. Time-resolved dynamic nuclear polarization enhanced NMR spectroscopy. *Angew. Chem. Int. Ed.* **2008**, *47*, 5235-5237.
67. Frydman, L.; Lupulescu, A.; Scherf, T. Principles and features of single-scan two-dimensional NMR spectroscopy. *J. Am. Chem. Soc.* **2003**, *125*, 9204-9217.
68. Zeng, H.; Bowen, S.; Hilty, C. Sequentially acquired two-dimensional NMR spectra from hyperpolarized sample. *J. Magn. Reson.* **2009**, *199*, 159-165.
69. Kautz, R. A.; Lacey, M. E.; Wolters, A. M.; Foret, F.; Webb, A. G.; Karger, B. L.; Sweedler, J. V. Sample Concentration and Separation for Nanoliter-Volume NMR Spectroscopy Using Capillary Isotachopheresis. *J. Am. Chem. Soc.* **2001**, *123*, 3159-3160.
70. Chuang, W.-L.; McAllister, H.; Rabenstein, D. L. Hexasaccharides from the histamine-modified depolymerization of porcine intestinal mucosal heparin. *Carbohydr. Res.* **2002**, *337*, 935-945.
71. Pervin, A.; Gallo, C.; Jandik, K. A.; Han, X.-J.; Linhardt, R. J. Preparation and structural characterization of large heparin-derived oligosaccharides. *Glycobiology* **1995**, *5*, 83-95.
72. Pervin, A.; Gallo, C.; Jandik, K. A.; Han, X. J.; Linhardt, R. J. Preparation and Structural Characterization of Large Heparin-Derived Oligosaccharides. *Glycobiology* **1995**, *5*, 83-95.
73. Mascellani, G.; Guerrini, M.; Torri, G.; Liverani, L.; Spelta, F.; Bianchini, P. Characterization of di- and monosulfated, unsaturated heparin disaccharides with terminal N-sulfated 1,6-anhydro-beta-D-glucosamine or N-sulfated 1,6-anhydro-beta-D-mannosamine residues. *Carbohydr. Res.* **2007**, *342*, 835-842.
74. Yamada, S.; Yoshida, K.; Sugiura, M.; Sugahara, K. One-Dimensional and 2-Dimensional H-1-Nmr Characterization of 2 Series of Sulfated Disaccharides Prepared from Chondroitin Sulfate and Heparan-Sulfate Heparin by Bacterial Eliminasin Digestion. *J. Biochem.* **1992**, *112*, 440-447.
75. Yates, E. A.; Santini, F.; Guerrini, M.; Naggi, A.; Torri, G.; Casu, B. H-1 and C-13 NMR spectral assignments of the major sequences of twelve systematically modified heparin derivatives. *Carbohydr. Res.* **1996**, *294*, 15-27.
76. Antalek, B. Using pulsed gradient spin echo NMR for chemical mixture analysis: how to obtain optimum results. *Concepts in Magnetic Resonance* **2002**, *14*, 225-258.
77. Stejskal, E. O.; Tanner, J. E. Spin Diffusion Measurements: Spin Echoes in the Presence of a Time-Dependent Field Gradient. *J. Chem. Phys.* **1965**, *42*, 288-292.
78. Hahn, E. L. Spin Echoes. *Physical Review* **1950**, *80*, 580.
79. Tanner, J. E. Use of Stimulated Echo in NMR-Diffusion Studies. *J. Chem. Phys.* **1970**, *52*, 2523-&.

80. Gibbs, S. J.; Johnson, C. S. A PFG NMR experiment for accurate diffusion and flow studies in the presence of eddy currents. *Journal of Magnetic Resonance (1969)* **1991**, *93*, 395-402.
81. Morris, K. F.; Johnson, C. S. Diffusion-ordered two-dimensional nuclear magnetic resonance spectroscopy. *J. Am. Chem. Soc.* **1992**, *114*, 3139-3141.
82. Morris, K. F.; Stilbs, P.; Johnson, C. S. Analysis of mixtures based on molecular size and hydrophobicity by means of diffusion-ordered 2D NMR. *Anal. Chem.* **1994**, *66*, 211-215.
83. Huo, R.; Wehrens, R.; Duynhoven, J. v.; Buydens, L. M. C. Assessment of techniques for DOSY NMR data processing. *Analytica Chimica Acta* **2003**, *490*, 231-251.
84. Balayssac, S.; Trefi, S.; Gilard, V.; Malet-Martino, M.; Martino, R.; Delsuc, M.-A. 2D and 3D DOSY ¹H NMR, a useful tool for analysis of complex mixtures: Application to herbal drugs or dietary supplements for erectile dysfunction. *J. Pharm. Biomed. Anal.* **2009**, *50*, 602-612.
85. Politi, M.; Groves, P.; Chávez, M. I.; Cañada, F. J.; Jiménez-Barbero, J. Useful applications of DOSY experiments for the study of mushroom polysaccharides. *Carbohydrate Research* **2006**, *341*, 84-89.
86. Derrick, T. S.; McCord, E. F.; Larive, C. K. Analysis of Protein/Ligand Interactions with NMR Diffusion Measurements: The Importance of Eliminating the Protein Background. *Journal of Magnetic Resonance* **2002**, *155*, 217-225.
87. Uccello-Barretta, G.; Nazzi, S.; Balzano, F.; Di Colo, G.; Zambito, Y.; Zaino, C.; Sansò, M.; Salvadori, E.; Benvenuti, M. Enhanced affinity of ketotifen toward tamarind seed polysaccharide in comparison with hydroxyethylcellulose and hyaluronic acid: A nuclear magnetic resonance investigation. *Bioorganic & Medicinal Chemistry* **2008**, *16*, 7371-7376.
88. Lin, M.; Shapiro, M. J.; Wareing, J. R. Diffusion-Edited NMR-Affinity NMR for Direct Observation of Molecular Interactions. *Journal of the American Chemical Society* **1997**, *119*, 5249-5250.
89. Orfi, L.; Lin, M.; Larive, C. K. Measurement of SDS Micelle-Peptide Association Using ¹H NMR Chemical Shift Analysis and Pulsed-Field Gradient NMR Spectroscopy. *Anal. Chem.* **1998**, *70*, 1339-1345.
90. Gounarides, J. S.; Chen, A.; Shapiro, M. J. Nuclear magnetic resonance chromatography: applications of pulse field gradient diffusion NMR to mixture analysis and ligand-receptor interactions. *Journal of Chromatography B: Biomedical Sciences and Applications* **1999**, *725*, 79-90.
91. Lin, M.; Jayawickrama, D. A.; Rose, R. A.; DelViscio, J. A.; Larive, C. K. Nuclear magnetic resonance spectroscopic analysis of the selective complexation of the cis and trans isomers of phenylalanylproline by [beta]-cyclodextrin. *Analytica Chimica Acta* **1995**, *307*, 449-457.
92. Johnson Jr, C. S. Diffusion ordered nuclear magnetic resonance spectroscopy: principles and applications. *Prog. Nucl. Magn. Reson. Spectrosc.* **1999**, *34*, 203-256.
93. Barjat, H.; Morris, G. A.; Smart, S.; Swanson, A. G.; Williams, S. C. R. High-Resolution Diffusion-Ordered 2D Spectroscopy (HR-DOSY) - A New Tool for the Analysis of Complex Mixtures. *Journal of Magnetic Resonance, Series B* **1995**, *108*, 170-172.

94. Morris, K. F.; Johnson, C. S. Resolution of discrete and continuous molecular size distributions by means of diffusion-ordered 2D NMR spectroscopy. *Journal of the American Chemical Society* **1993**, *115*, 4291-4299.
95. Nilsson, M.; Connell, M. A.; Davis, A. L.; Morris, G. A. Biexponential Fitting of Diffusion-Ordered NMR Data: Practicalities and Limitations. *Anal. Chem.* **2006**, *78*, 3040-3045.
96. Delsuc, M. A.; Malliavin, T. E. Maximum Entropy Processing of DOSY NMR Spectra. *Anal. Chem.* **1998**, *70*, 2146-2148.
97. Windig, W.; Antalek, B. Direct exponential curve resolution algorithm (DECRA): A novel application of the generalized rank annihilation method for a single spectral mixture data set with exponentially decaying contribution profiles. *Chemometrics and Intelligent Laboratory Systems* **1997**, *37*, 241-254.
98. Nilsson, M.; Morris, G. A. Speedy Component Resolution: An Improved Tool for Processing Diffusion-Ordered Spectroscopy Data. *Anal. Chem.* **2008**, *80*, 3777-3782.
99. Huo, R.; Wehrens, R.; Buydens, L. M. C. Improved DOSY NMR data processing by data enhancement and combination of multivariate curve resolution with non-linear least square fitting. *Journal of Magnetic Resonance* **2004**, *169*, 257-269.
100. Van Gorkom, L. C. M.; Hancewicz, T. M. Analysis of DOSY and GPC-NMR Experiments on Polymers by Multivariate Curve Resolution. *Journal of Magnetic Resonance* **1998**, *130*, 125-130.
101. Nilsson, M. The DOSY Toolbox: A new tool for processing PFG NMR diffusion data. *Journal of Magnetic Resonance* **2009**, *200*, 296-302.

CHAPTER TWO

Characterization of Heparin and its Impurities with HPLC-NMR using Weak Anion Exchange Chromatography

Based on a paper published in Analytical Chemistry

Anal. Chem., 2009, 81, 10116-10123.

This chapter describes the application of weak-anion exchange (WAX)-HPLC-NMR in the separation and characterization of heparin and its contaminants including oversulfated chondroitin sulfate (OSCS), dermatan sulfate (DS), and chondroitin sulfate A (CSA). The goals of this study were (1) to design an analytical method that permits quality assurance (QA) monitoring of samples using a simple and robust method like HPLC and (2) allows for easy transfer to deuterated buffers for the efficient ^1H NMR analysis of sample lots flagged as suspect in the QA HPLC runs. The results described herein demonstrate the ability of WAX-HPLC to completely separate intact heparin from DS, CSA, and OSCS biopolymers with on-line detection using both UV absorbance and ^1H NMR.

2.1 Introduction: Identification of pharmaceutical contaminants and degradants using high performance liquid chromatography coupled to NMR (HPLC-NMR)

High-resolution NMR spectroscopy is demonstrably one of the most important methods for structure elucidation having an extensive range of biochemical and chemical applications.¹ Hyphenated NMR techniques, such as LC-NMR, are used in the

pharmaceutical industry as a standard tool for the quality assurance of pharmaceuticals.²⁻⁴ Though high-performance liquid chromatography (HPLC) is routinely used in the analysis of chemical mixtures, conventional detectors to monitor the separation based on refractive index, UV, fluorescence, and electrochemical properties can only provide limited information on molecular structure.⁵ The analysis of components that are true unknowns or for which authentic standards are not available can be especially challenging. The hyphenation of HPLC to mass spectrometry (HPLC-MS) has proven indispensable in the identification and quantification of drug impurities and metabolites, but mass spectrometry does not always provide unambiguous structural identification and NMR data are often required for complete structural characterization.¹ The on-line coupling of HPLC to high-resolution NMR spectrometers offers a powerful tool for the analysis and unambiguous identification of complex chemical mixtures when the components of interest are present at relatively high concentrations.

Advances in flow-probe design, increases in magnetic field strength, and better solvent suppression pulse sequences have furthered HPLC-NMR from a tool used exclusively in research laboratories to the stage where it can be routinely used in pharmaceutical analysis.^{6, 7} The direct coupling of HPLC to high-resolution NMR greatly enhances the characterization of pharmaceutical impurities thus speeding up production chemistry processes and quality assurance compliance.

2.1.1 Identification of heparin contaminants using weak-anion exchange chromatography coupled to NMR (WAX-HPLC-NMR)

As discussed in Chapter 1, the identification and structural characterization of OSCS as the contaminant in pharmaceutical preparations of heparin required (1) that

heparin and its minor impurity DS be exhaustively digested using a cocktail of heparinase and chondroitinase depolymerization enzymes and (2) the contaminant be isolated for subsequent ^1H and ^{13}C NMR analysis.⁸ This approach can be quite expensive, time-consuming and requires that the contaminant be resistant to the depolymerization methods used in the removal of heparin and DS. This study explored the use of LC-NMR for the identification and characterization of heparin impurities following their separation using WAX chromatography. Separations of the intact biopolymers heparin, DS, CSA, and OSCS were performed on an amino-bonded column using a NaCl gradient to effect their elution. The WAX separation was selected as it required significantly less salt than comparable strong-anion exchange chromatography, facilitating NMR detection using a Bruker flow probe and thus making this method amenable to commercially available hardware.

The retention and elution of solution components was found to be highly dependent on pH/pD and salt concentration. Because the separation was determined to be through a displacement-based mechanism, the elution time of each analyte could be controlled simply by adjusting an isocratic solvent delay prior to introduction of the appropriate salt concentration, with little impact of the extent of the delay on chromatographic peak shape. This is especially important when performing stop-flow analysis for signal averaging, in order to improve spectral quality, as well as for characterization using longer 2D NMR experiments. For comparison, the separation of the polymeric components by reverse-phase ion-pair (RPIP)-HPLC was also examined; however this approach was much less effective than the WAX separation.

2.2 Experimental Section

2.2.1 Chemicals

Heparin sodium salt from porcine intestinal mucosa (>140 USP units/mg, grade 1-A), chondroitin sulfate A sodium salt from bovine trachea, chondroitin sulfate B sodium salt (dermatan sulfate) from porcine intestinal mucosa, and pyridine-sulfur trioxide were purchased from Sigma (St. Louis, MO, USA). Sodium phosphate dibasic heptahydrate, tributylammonium (TrBA) acetate, *N,N*-Dimethylformamide (DMF), sodium chloride (NaCl), and sodium hydroxide were purchased from Fisher Scientific (Pittsburgh, PA, USA). Deuterium oxide (D, 99%), sodium deuterioxide (D, 99.5%) in D₂O, sodium-3-trimethylsilylpropionic acid (D, 98%), and deuterated EDTA-*d*₁₆ (D, 98%) were purchased from Cambridge Isotope Laboratories (Andover, MA, USA). HPLC grade water (Burdick and Jackson) was purchased from VWR (West Chester, PA, USA). Syringe filters, 0.2 μm nylon, were purchased from MicroSolv (Eatontown, NJ). Vacuum filters, 0.2 μm cellulose nitrate membrane filters were purchased from Fisher Scientific (Pittsburgh, PA, USA).

2.2.2 OSCS synthesis

OSCS was prepared by Christopher J. Jones by modification of the method of Maruyama et al.^{9, 10} The starting material was chondroitin sulfate A (CSA) sodium salt from bovine trachea. The CSA sodium salt was first converted to a protonated form using the hydrogen form of a strong cation-exchange column of Bio-Rad AG 50W-X8 resin to replace the sodium ions with a proton. TrBA was added to the protonated CSA to produce the TrBA salt and the sample was lyophilized. TrBA acts as an ion-pairing reagent (IPR) to increase the solubility of CSA in the DMF reaction solvent. Addition of

pyridine-sulfur trioxide to the CSA DMF solution followed by heating for 75 minutes at 40°C produced OSCS. The reaction was quenched with water and the final product precipitated by addition of ethanol saturated with anhydrous sodium acetate. The product was centrifuged and the OSCS pellet lyophilized and stored at -20°C.

2.2.3 RPIP-HPLC Analysis

RPIP-HPLC separations were performed with an Agilent 1100 HPLC controlled by Bruker Hystar software. Heparin and OSCS were separated on a Waters Symmetry C18 column purchased from Waters Corp. (Milford, MA). The column temperature was maintained at 30 °C throughout the separation and a flow rate of 0.4 mL/min was used to obtain an optimal separation while reducing the consumption of expensive deuterated solvents. A binary solvent system was used for gradient elution. Both solvents contained the same concentration of TrBA and consisted of 5% acetonitrile in an aqueous solution of 15% D₂O and 85% H₂O. In addition to TrBA, buffer B also contained 50 mM ammonium acetate. A sample volume of 50 µL of a 50 mg/mL OSCS or heparin solution prepared in solvent A was injected for each separation. Separations were effected using an ammonium acetate gradient. The gradient profile consisted of a 5 min isocratic step of 100% solvent A after which the fraction of solvent B was increased to 10% over the next 5 min and maintained at 10% for 5 min before it was further increased to 20% in 2 min. Solvent B was held at 20% for 2 min to rinse any highly retained species from the column before returning to 100% A for a total run time of 22 min. Elution of the retained heparin and OSCS was monitored using UV absorbance at 210 nm^{11, 12} as well as by on-flow NMR spectroscopy.

2.2.4 WAX-HPLC Analysis

Separations were performed with an Agilent 1100 HPLC controlled by Bruker Hystar software. Glycosaminoglycans, GAGs, were separated on an Asahipak NH2P-50E amino-bonded column purchased from Thomson Instrument Company (Oceanside, CA). A flow rate of 0.65 mL/min was used for the separation as it provided adequate retention of the GAGs while reducing the consumption of separation buffers, which is especially important when working with expensive deuterated solvents. In our experience, the required equilibration time for the column is approximately 4 min, however longer times were used in this WAX separation method to insure equilibration before sample injection. Equilibration of the column with the initial NaCl composition was essential in order to retain the lesser charged DS and CSA which elute at a much lower salt concentration than either heparin or OSCS. GAGs were detected using UV absorption at 215 nm.¹³ The resulting UV chromatogram was used to identify peaks for analysis using on-flow or stop-flow NMR spectroscopy.

2.2.4.1 WAX-HPLC Separation in Protonated Buffers

HPLC buffer solutions were prepared to 0.1 M HPO_4^{2-} . NaCl was added to the phosphate buffer to make 0.1 M and 1.0 M NaCl solutions for the separation of DS, CSA, heparin and OSCS. Buffer solutions were titrated to a pH of 9.65 using 5 M NaOH. Stock DS, CSA, heparin and OSCS solutions were prepared in water at 100 mg/mL. Samples for HPLC analysis were prepared by diluting the stock solutions with the 0.1 M NaCl separation buffer. A 25 μL injection was used and separations were effected using a NaCl gradient: 0-4 min 0.1 M NaCl, a 10 min linear gradient to 1.0 M NaCl, hold for 6 min, a linear gradient for 2 min to 0.1 M NaCl, equilibrate for 8 min. Total run time was

30 minutes. Experiments to determine the linearity and limits of detection for DS and OSCS were performed using a constant heparin concentration of 40 mg/mL and analyte concentrations ranging from 0.25 to 40 mg/mL. Samples were analyzed in triplicate.

2.2.4.2 WAX-HPLC Separation in Deuterated Buffers

Buffers and stock solutions were prepared as described above except D₂O was used as the solvent. Buffers were titrated to pD 10.25 using a 5 M solution of NaOD in D₂O, where pD was calculated using the pH meter reading (pH*) and the equation: $pD = pH^* + 0.4$.¹⁴ Sample solutions up to 40 mg/mL were prepared by diluting the stock solutions into 0.1 M NaCl buffer. A 25 μ L injection was used and separations were effected using a NaCl gradient: 0-4 min 0.1 M NaCl, a 2 min linear gradient to 0.65 M NaCl, hold for 10 min, linear gradient for 2 min to 1.0 M NaCl, hold for 6 min, a 1 min linear gradient to 0.1 M NaCl, hold for 5 min. Total run time was 30 min.

2.2.5 Trapping of OSCS

Peak trapping of OSCS was accomplished by performing 10 injections, 25 μ L each of a solution containing 2 mg/mL OSCS and 40 mg/mL heparin using an isocratic HPLC method at 0.6 M NaCl. Using this salt concentration heparin was observed to elute in the column void while the OSCS was retained on the WAX column. The separation was monitored using both UV and NMR. The trapped OSCS was eluted from the column with the gradient method using the deuterated buffer described above. Following elution from the column, the OSCS peak was stopped within the active volume of the probe for ¹H NMR analysis.

2.2.6 On-flow ^1H NMR Analysis

Following their separation, GAGs were detected on-flow using a Bruker Avance NMR spectrometer operating at 599.84 MHz. All NMR experiments were performed with a 3 mm Bruker SEI flow probe with a detection volume of (60 μL) and a total cell volume of (120 μL) using *tert*-butanol as a chemical shift reference (1.256 ppm relative to trimethylsilylpropionic acid). The probe could be effectively tuned and matched even at the high salt concentrations required for the elution of the charged GAGs. On-flow ^1H NMR spectra were acquired with WET solvent suppression using the preprogrammed on-flow WET NMR pulse program lc2wetdc.¹⁵ The automated Bruker shape tool was used to create the sinc pulse for the selective excitation of the HOD resonance. For on-flow analysis, spectra were acquired with 8 scans per free-induction decay (FID) at a temperature of 25°C. A relaxation delay of 1.5 s was used and FIDs were acquired into 12 288 data points following the application of a 90° pulse. Prior to Fourier transformation the FIDs were zero-filled to 65 536 points and apodized by multiplication by an exponential decay equivalent to 10 Hz line broadening.

2.2.7 Stop-flow ^1H NMR analysis

In order to measure high quality ^1H NMR spectra, the heparin, DS, CSA and OSCS chromatographic peaks were stopped within the active volume of the flow probe for signal averaging. The stop-flow delay time required to position the analyte within the active volume of the NMR flow probe was determined in a separate experiment using a concentrated fructose solution. Stop-flow NMR spectra for heparin, DS, CSA, and OSCS were acquired using WET solvent suppression by coaddition of 1024 transients. A relaxation delay of 2.0 s was used and FIDs were acquired into 26 452 data points

following the application of a 90° pulse. Prior to Fourier transformation, the FIDs were zero-filled to 65 536 points and apodized by multiplication with an exponential decay equivalent to 1 Hz line broadening.

Excessive broadening of the ^1H NMR resonances of heparin and OSCS was especially noticeable in our initial stop-flow NMR spectra. We attributed this broadening to the presence of paramagnetic metal ions present in trace amounts in our buffer components. To reduce the effects of paramagnetic broadening, EDTA- d_{16} was added to the separation solvents at a concentration of 5 μM , producing significant sharpening of the heparin and OSCS resonances.¹⁶

2.2.8 High pD Stability Experiments

Samples containing 33 mg/mL heparin, OSCS or DS were prepared by diluting a 200 μL aliquot of a 100 mg/mL stock solution prepared in D_2O with 400 μL of a D_2O solution containing 0.1 M NaCl and *tert*-butanol as a chemical shift reference at a pD of 10.25.

^1H NMR spectra were measured in 5 mm NMR tubes using a Bruker Avance spectrometer operating at 599.84 MHz with a broadband inverse probe temperature that was controlled to 25°C. The chemical shifts were referenced to a *tert*-butanol internal standard (1.256 ppm relative to trimethylsilylpropionic acid). Spectra were acquired by the coaddition of 128 transients. A relaxation delay of 2 sec was used and the FIDs were acquired into 24 576 data points following the application of a 90° pulse, calibrated for each solution. Prior to Fourier transform, the FIDs were zero-filled to 65 536 points and apodized by multiplication by an exponential decay equivalent to 0.5 Hz line broadening.

2.3 Results and Discussion

Although HPLC is a standard tool for quality assurance of pharmaceuticals,¹⁷ its application for heparin characterization is not straightforward. Heparin is itself a heterogeneous substance, comprised of linear polysaccharides of varying length and charge.¹⁸ Therefore, an ideal HPLC separation method for impurity profiling of heparin samples would give baseline chromatographic resolution of heparin and potential contaminants while eluting the heparin as a single sharp peak. Further, the separation method should produce good retention of heparin to allow its resolution from early eluting contaminants as well as the column void peak.

2.3.1 RPIP-HPLC in the Separation of Heparin and OSCS

Initial attempts in our laboratory to separate intact heparin and OSCS focused on the use of RPIP-HPLC using a C18 column. TrBA was added as the IPR in an attempt to retain the negatively charged heparin and OSCS on the hydrophobic column. The RPIP-HPLC separation is based on electrostatic interactions between the negatively charged sulfonate (SO_3^-) and carboxylate (COO^-) functional groups of the GAG with the positively charged, hydrophobic TrBA ions permitting the retention of the hydrophilic polysaccharide on the hydrophobic column.¹⁹ The exact mechanism of retention in RPIP-HPLC is a matter of debate but there are currently two proposed mechanisms to explain RPIP-HPLC. In the classical model of retention, the hydrophobic IPR and the analyte ion of opposite charge combine in the mobile phase forming a neutral species which can partition into the hydrophobic stationary phase.^{20, 21} In the second model of retention, the dynamic ion-exchange model, the IPR is first absorbed onto the surface of the stationary phase creating charged sites which can then interact as an ion-exchange

site for oppositely charged heparin and OSCS.^{22, 23} Shown in Figure 2.1 is a schematic illustrating the two proposed mechanisms of separation using RPIP-HPLC.

As mentioned in section 2.2.3, in contrast to traditional RPIP-HPLC methods in which an increase in organic buffer composition is responsible for eluting the retained complex, in the separation of heparin and OSCS using RPIP-HPLC, an ammonium acetate gradient was effective in eluting heparin and OSCS. Using this method, it is believed that the ammonium ion competes with the IPR TrBA for electrostatic interactions with heparin and OSCS.²⁴ As the ammonium ion concentration increases, there are fewer available sites for the TrBA to bind to heparin and OSCS resulting in the elution of the hydrophilic compounds from the hydrophobic column.

Though RPIP-HPLC has been shown to be effective for the separation of depolymerized heparin di-^{24, 25} and tetrasaccharides²⁶⁻²⁸, it did not provide adequate retention for intact heparin. Figure 2.2 illustrates the separation of the intact polysaccharides, heparin and OSCS, using RPIP-HPLC coupled to NMR for detection. As can be seen from the on-flow NMR and the UV chromatograms, while OSCS is retained slightly on the hydrophobic column, heparin elutes very near to the column void. Because heparin has less negative charge density than OSCS, it is expected that lesser charged species such as DS and CSA would coelute with heparin complicating their analysis by ¹H NMR. Additionally, an excessive amount of IPR was needed to retain OSCS resulting in unstable back pressures (>350 bar) and run-to-run variability in retention times. Furthermore, although these samples were sufficiently concentrated for detection by UV and NMR, the large TrBA concentration reduced the potential to detect contaminants present at low levels by limiting the NMR receiver gain that could be used.

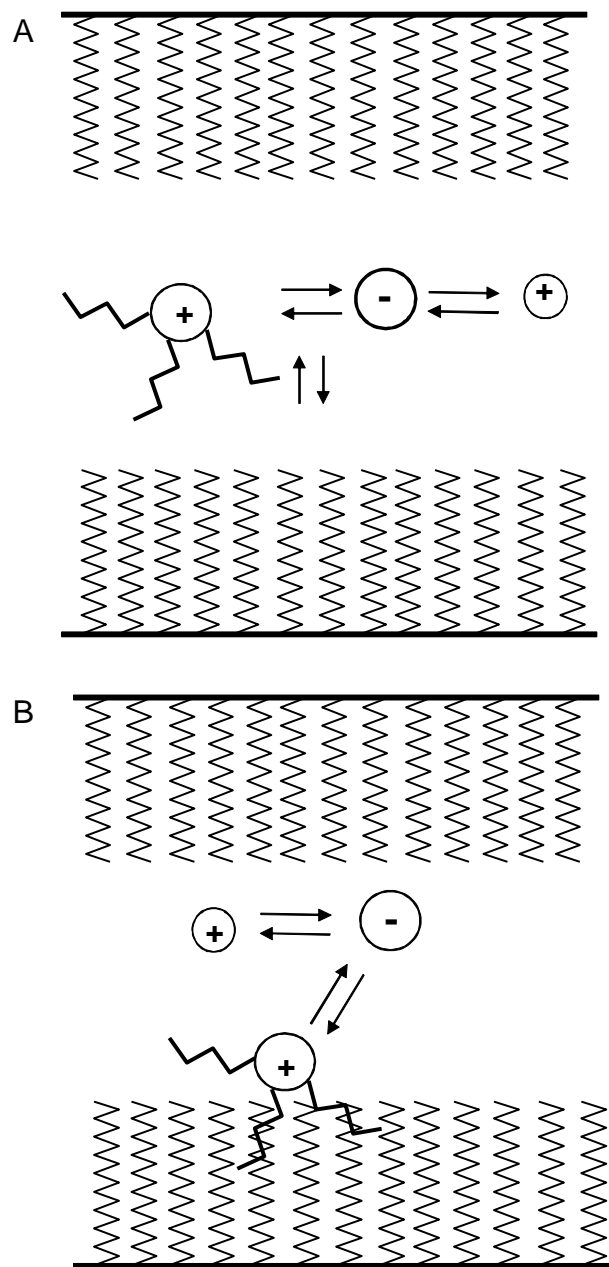


Figure 2.1. Proposed mechanisms for the separation of a negatively charged analyte with the cationic IPR and the competing cationic ammonium ion. (A) Ion pairing occurs in the mobile phase and the pair then partitions into the stationary phase. (B) The IPR is adsorbed onto the surface of the stationary phase creating charge sites that act as ion exchange sites for the analyte.

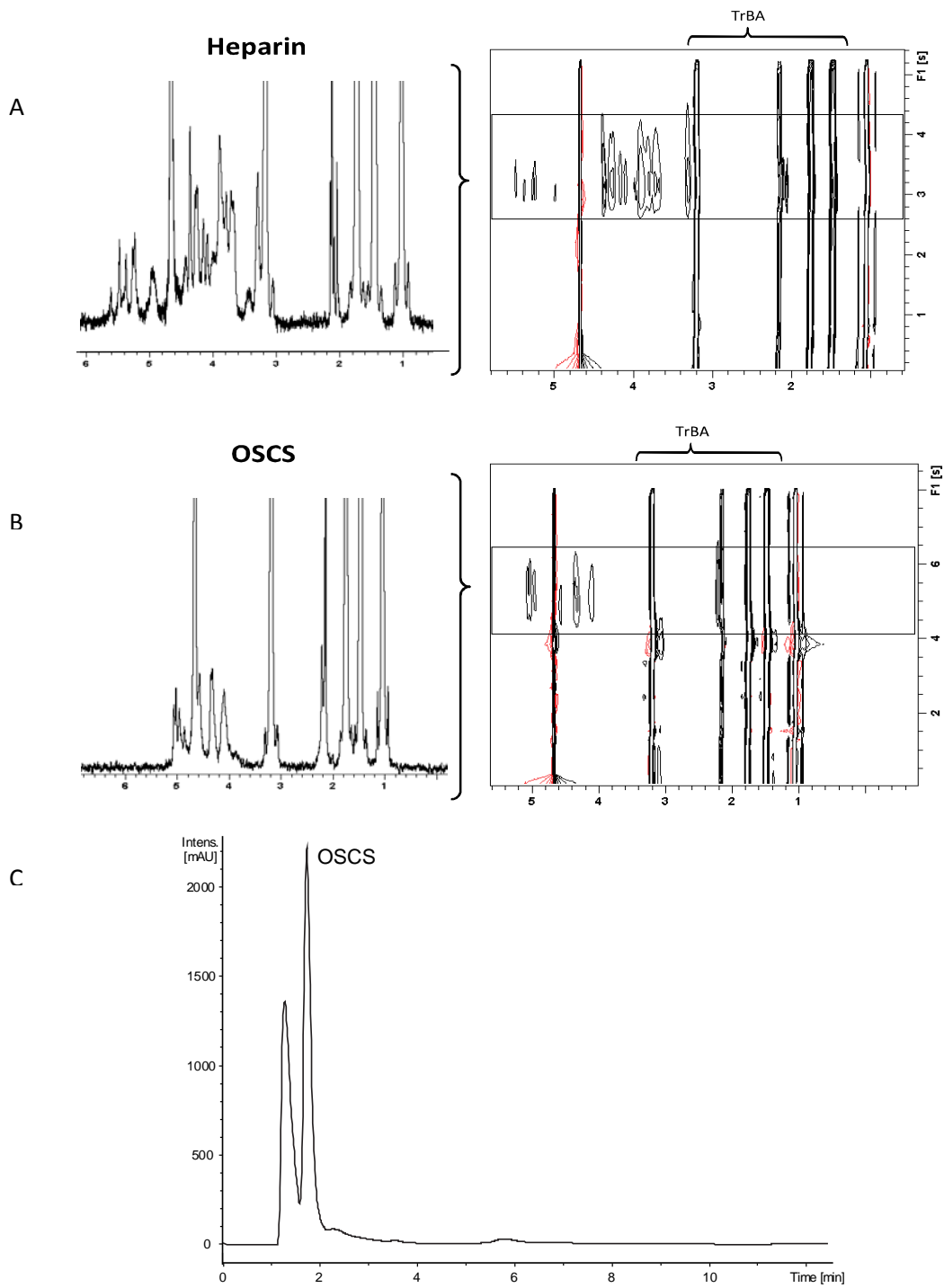


Figure 2.2. NMR detected chromatogram for the separation of (A) heparin and (B) OSCS using RPIP-HPLC as well as the (C) UV detected chromatogram for the separation of OSCS.

2.3.2 WAX-HPLC

To address the limitations encountered with RPIP-HPLC, we turned to WAX chromatography using a Shodex Asahipak NH2P-50E amino-bonded column. A NaCl gradient (0.1 M – 0.5 M) as reported by Huang et al.²⁹ was initially tested, however, using these conditions we were not able to displace the heparin and OSCS from the amino functional groups of the column. It was therefore necessary to determine conditions that would allow both retention and elution of these highly charged polymers.

Because the alkalinity of the separation buffers was reported to play a significant role in the elution of intact GAGs²⁹, it was necessary to carry out experiments to identify pH conditions that would permit the displacement of heparin and OSCS from the amino functional groups of the WAX column while utilizing a salt concentration compatible with our HPLC system and NMR flow probe. Given the nature of the column we hypothesized that increasing the pH of the elution buffer could reduce the net positive charge of the bonded amino groups and thus the capacity of the column to retain the negatively charged GAGs.

2.3.2.1 Optimization of Heparin Retention and Elution with WAX-HPLC

Separation of heparin on the Asahipak column was found to be highly pH dependent. This investigation involved the injection of heparin as a single component using isocratic elution with an aqueous (80% H₂O/20% D₂O) 0.8 M NaCl buffer. Solution pH values from 9.55 to 10.00 were examined. Elution of the heparin was monitored using UV absorbance at 215 nm and on-flow ¹H NMR. Detection using both UV and ¹H NMR spectroscopy was useful for optimizing the chromatographic conditions for heparin retention and elution, as peaks due to non-GAG sample components were also

observed in the UV-detected chromatograms. Using NMR, we were able to identify one early eluting component as acetate. Other UV-active peaks produced no detectable ^1H NMR spectra, even when analyzed using lengthy stop-flow acquisitions. This suggested that the components giving rise to these UV peaks either had extremely high molar absorptivities or more likely were due to inorganic ions, such as carbonate, that do not contain NMR active protons.

From these experiments, we determined that heparin was not retained at pH values above 9.65 at a NaCl concentration of 0.8 M, and eluted with the column void. A pH of 9.65 was determined to be optimal, and was used in all subsequent separations. It is interesting to note that reducing the NaCl concentration to less than 0.6 M at pH 9.65 resulted in the complete retention of heparin. This observation suggested that the mechanism of this separation is based on displacement chromatography.^{30, 31} It became apparent that heparin could be retained indefinitely as long as a lower salt concentration (i.e. < 0.6 M) was used and could be eluted as desired simply by increasing the NaCl concentration to 0.6 M. A separation method was developed that applied 0.4 M NaCl isocratically to retain heparin with application of a 0.1 M/min salt gradient to 0.6 M NaCl to cause heparin to elute as a single sharp peak. A more shallow elution gradient of 0.08 M NaCl/ min was tested, but broadening of the heparin peak resulted, most likely due to partial separation of individual heparin components.

2.3.3 Separation of DS, CSA, Heparin and OSCS in D₂O Solution

Although WET solvent suppression can effectively reduce the H₂O resonance intensity and allow acquisition of ^1H NMR spectra in protonated aqueous solutions, a large region of the ^1H NMR spectrum around the water resonance is also suppressed.

This is an especially significant limitation for carbohydrate samples which have limited ^1H peak dispersion. This problem can be reduced through the use of deuterated solvents, although this adds greatly to the expense of LC-NMR experiments. The translation of a chromatographic method from aqueous to deuterated solvents often requires some modification of the separation parameters. In this case it was necessary to fine tune the solution pD to obtain effective retention and elution of DS, CSA, heparin and OSCS. A pD of 10.25 and a salt gradient from 0.1 to 1.0 M NaCl provided an effective separation, as observed in the UV-detected chromatogram shown in Figure 2.3A. As was the case for the separations conducted with protonated buffers, in separations using D_2O the proper choice of buffer pD was extremely important for effective retention and elution of the polysaccharides. Using a linear gradient, CSA and DS coelute with a salt concentration of 0.4 M NaCl, but are well separated from heparin which elutes at a concentration of 0.6 M NaCl followed by OSCS at a NaCl concentration of 0.8 M. As shown in Figure 2.3B, this method can be adjusted to introduce a long delay between elution of the heparin and the OSCS with no degradation of the OSCS peak. This proved to be important to avoid carryover of heparin in the LC-NMR flowcell by allowing for a longer NMR flow-cell rinse time before the introduction of OSCS.^{32, 33}

2.3.4 Analytical Figures-of-Merit

Retention times were found to be highly reproducible; with a deviation of 3-4 sec run-to-run and 4-6 sec day-to-day. Standard solutions containing DS and OSCS at 0.5, 5.0, 10.0, 20.0, and 40.0 mg/mL were prepared in an aqueous solution containing 40 mg/mL heparin. The standards were analyzed at least in triplicate with UV detection at 215 nm. The calibration plot for the DS standard solution was found to be linear over the

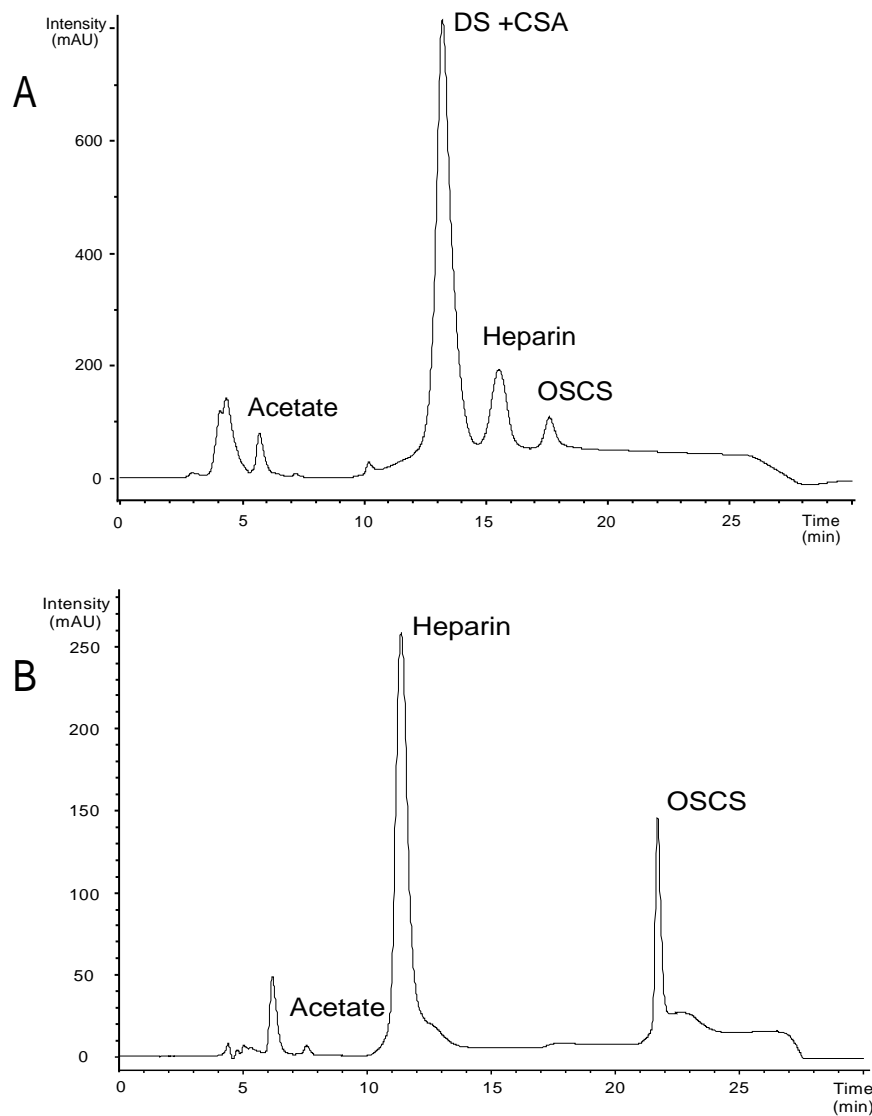


Figure 2.3 UV-detected WAX chromatograms of DS, CSA, heparin and OSCS. (A) Measured using deuterated buffers and no isocratic delay. (B) Measured using deuterated buffers and employing a 10 min isocratic delay between elution of heparin and OSCS.

range of 0.5 mg/mL to 20 mg/mL with a correlation coefficient of 0.9999. The slope of the calibration plot determined for DS with a concentration ranging from 0.5 to 20.0 mg/mL is 14.5 with an intercept of 33.4. The LOD calculated for DS was 0.22 mg/mL corresponding to an injection amount of 5.6 μ g equivalent to 0.51% of the heparin concentration. The calibration plot for OSCS was found to be linear over the range of 0.5 mg/mL to 20 mg/mL with a correlation coefficient of 0.9949. The slope of the calibration plot determined for the OSCS standard solutions ranging from 0.5 to 20.0 mg/mL was 3.04 with an intercept of 51.2. The calculated LOD for OSCS was higher than that of DS at 1.0 mg/mL corresponding to an injection amount of 25 μ g equivalent to 2.5% in heparin. The higher calculated LOD for OSCS is attributed to the higher background and greater variance in the blank absorbance.

The separation of a standard solution containing 0.25 mg/mL DS and OSCS in 40 mg/mL heparin is shown in Figure 2.4. Compared with the blank chromatogram, DS is clearly above the limit of detection at this concentration, and even the smaller OSCS peak can be detected above the blank. Although the WAX-HPLC method is not as sensitive as those published by Trehy¹³ using SAX-HPLC and Wielgos¹¹ and Somsen¹² using CE, the strength of this approach is in its ability to conclusively identify unknown contaminants using on-line ¹H NMR analysis when standards are unavailable. Because NMR is less sensitive than UV detection, we benefit from the ability of the WAX column to accommodate larger amounts of material than other separation methods. Additionally, because both SAX-HPLC and CE also separate components based on charge, it should be relatively straight-forward to adapt a WAX separation by building on the other methods when a sample containing an unknown component is identified.

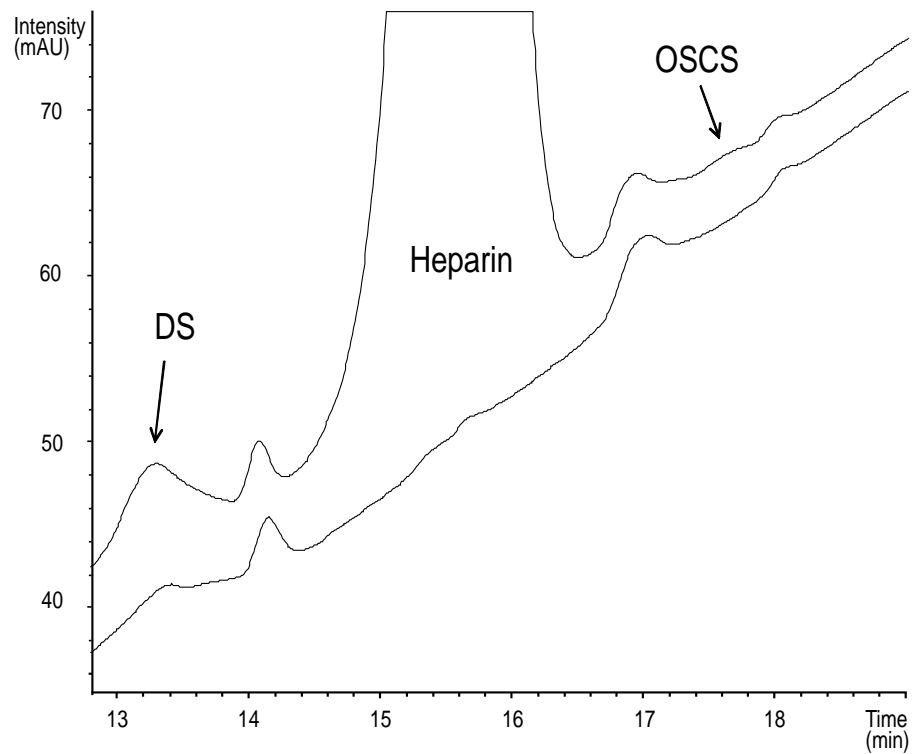


Figure 2.4 UV-detected WAX chromatograms for a sample containing (top) 0.25 mg/mL DS and OSCS in the presence of 40 mg/mL heparin and (bottom) blank measured using protonated buffers.

2.3.5 On-flow and Stop-flow Analysis Following WAX-HPLC

Although the UV-detected chromatograms shown in Figure 2.3 provide evidence for the presence or absence of heparin impurities, especially when standards of known contaminants are available, UV absorbance provides little structural information about the identity of the contaminants. Because of the high salt content used for elution, mass spectrometry is not a good option for on-line identification of heparin impurities using the available SAX¹³ or WAX separations. In contrast, NMR is a very useful method for distinguishing GAGs,³⁴⁻³⁶ and was integral for the identification of commercial heparin lots adulterated with OSCS.³⁷ Although LC-NMR has become a well-established analytical technique especially for pharmaceutical analyses,^{1, 3, 4, 7, 38, 39} to our knowledge it has not been used as an on-line detection method in the HPLC characterization of intact heparin or related GAGs. The on-flow WAX-NMR chromatogram for the separation of heparin and OSCS is shown in Figure 2.5. The slices through the chromatographic peaks show the ¹H NMR spectra of acetate, heparin and OSCS obtained by coaddition of 8 transients. Heparin and OSCS can be clearly identified by their unique ¹H NMR fingerprints. The peaks marked with an asterisk in the on-flow NMR spectra are due to residual protonated acetonitrile. The chemical shift of the residual acetonitrile peak was observed to shift in the NMR on-flow spectrum as a result of the change in NaCl concentration during separation. Although acetonitrile was not used in this separation, the column was shipped with a storage solution of 70% acetonitrile/ 30% water. Despite extensive use and repeated cleanings, a small amount of acetonitrile remains in eluates from this column, although the intensity of this resonance is decreasing over time.

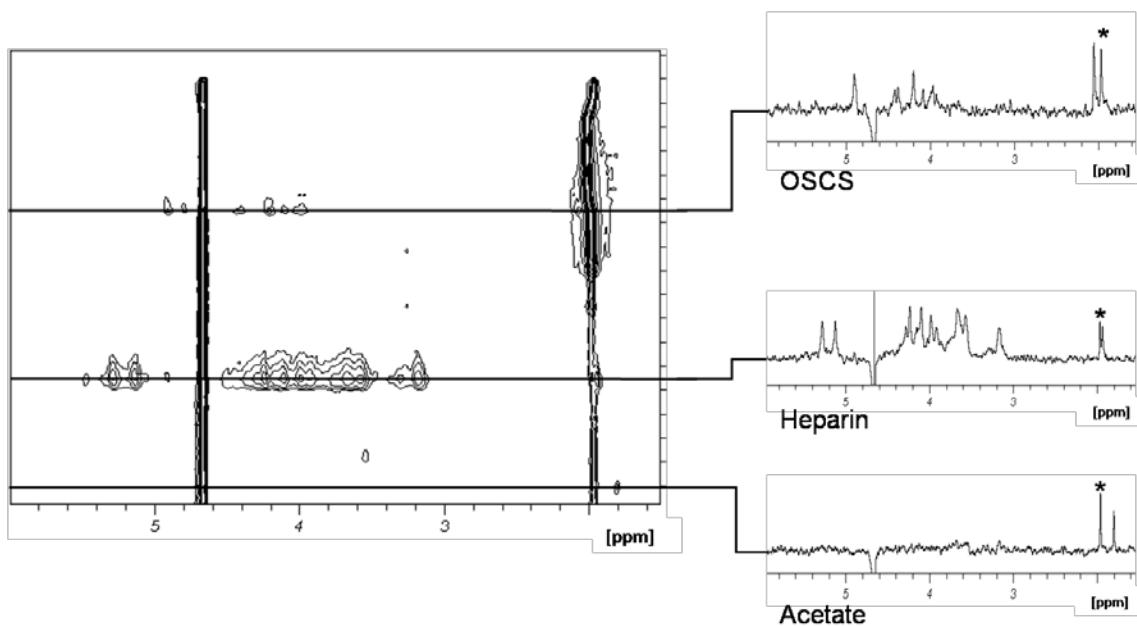
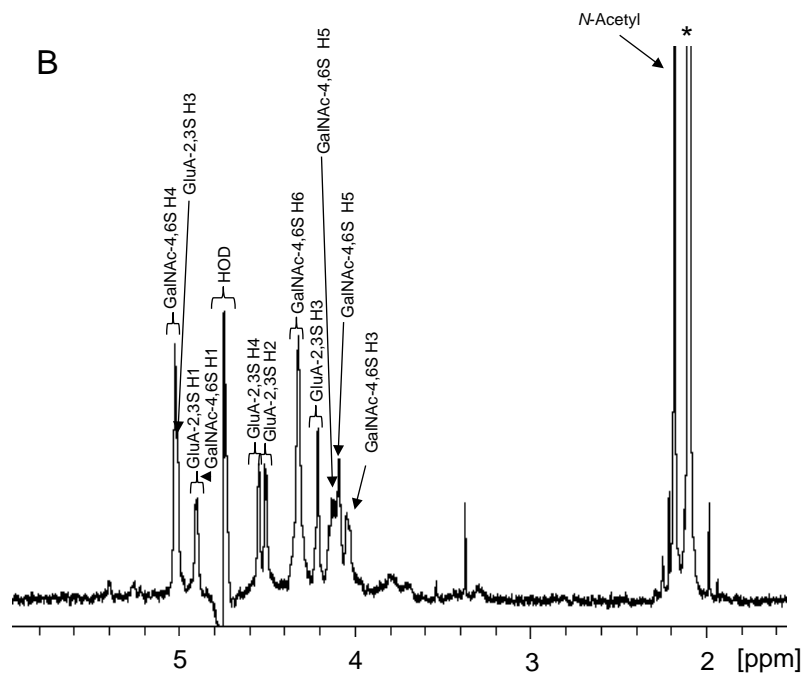
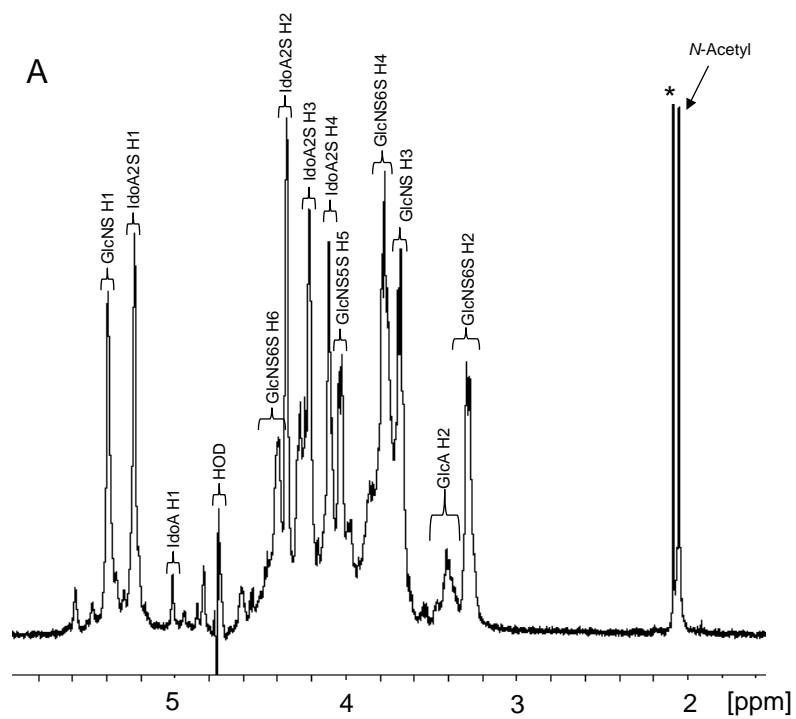


Figure 2.5. On-flow ^1H NMR-detected WAX chromatogram of heparin and OSCS. The slices taken through the chromatographic peaks show the ^1H NMR spectra of OSCS, heparin and acetate, which was present as an unexpected impurity. The resonance marked with an asterisk (*) is due to residual acetonitrile, present as a column contaminant.

Although on-flow NMR spectra can be informative, as shown by Figure 2.5, impurities present at low levels typically require more extensive signal averaging to obtain high quality NMR spectra. Furthermore, the power of NMR as a tool for chemical analysis lies in its ability to provide structural information, such as that provided by 2D NMR spectra. Therefore, HPLC-NMR experiments are often conducted in stop-flow mode in which peaks detected in the UV-chromatogram are used to stop the pumps at an appropriate time, trapping the chromatographic peak in the NMR flow cell. Using the separation method developed for on-flow NMR analysis produced stop-flow NMR spectra of OSCS that were contaminated by heparin due to peak carryover in the NMR flowcell. To reduce this problem, a 10 min isocratic step of 0.65 M NaCl was added between the elution of heparin and initiation of the salt gradient used to elute OSCS, as shown in the UV-detected chromatogram in Figure 2.3B. Although this step lengthened the separation, it significantly reduced the intensity of the heparin resonances observed in the NMR spectrum of OSCS without noticeable broadening of the OSCS peak.

Stop-flow ^1H NMR spectra (Figure 2.6) were measured for samples containing equivalent concentrations (40 mg/mL) of heparin (A), OSCS (B), DS (C), and CSA (D), following their elution from the Asahipak column. Chromatographic peaks corresponding to these GAGs were sequentially stopped within the active volume of the NMR flow probe to obtain the results shown in Figure 2.6. Because DS and CSA coelute in this separation, the stop-flow ^1H NMR spectra of these analytes were obtained in separate injections containing either DS or CSA along with heparin and OSCS. These spectra, which were acquired in 1 hr, have much better S/N than were obtained in the on-flow LC-NMR analysis. Again, protonated acetonitrile is detected in these spectra, and is indicated with an asterisk. Diffusional broadening of peaks left on the column during



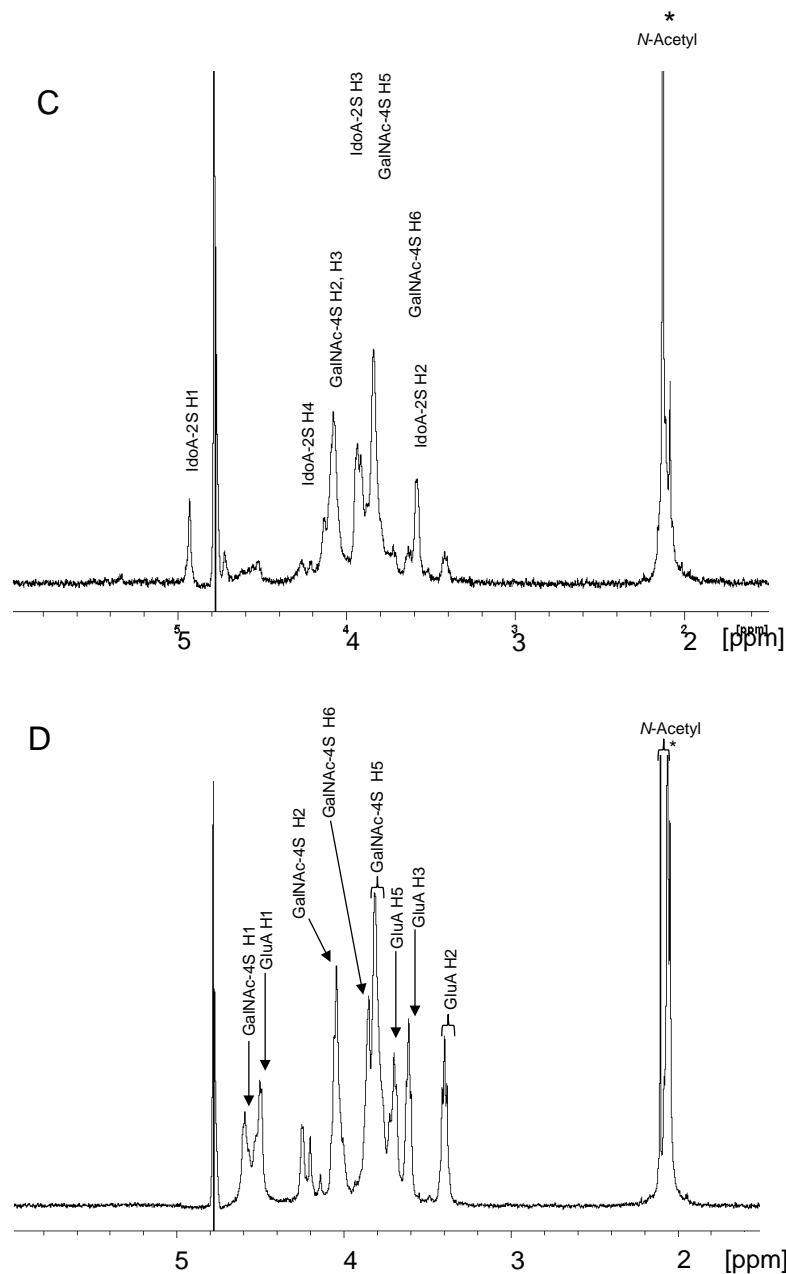


Figure 2.6. Stop-flow ^1H NMR spectra of (A) heparin, (B) OSCS, (C) DS and (D) CSA. Spectra were acquired from a single 25 μL injection of a sample containing 40 mg/mL of each GAG. Spectra were acquired by coaddition of 1024 transients using WET suppression of the HOD resonance. The resonance marked with an asterisk (*) is due to residual acetonitrile, present as a column contaminant. Spectral assignments are taken from literature reports for heparin, OSCS, DS and CSA.

lengthy stop-flow acquisitions is a common problem encountered in HPLC-NMR experiments. However, in this separation, conditions for elution of heparin leave OSCS trapped on the column, and essentially no broadening of the OSCS was observed in the stop-flow experiments.

We were concerned about the stability of the GAGs over the long acquisition periods used in stop-flow analysis due to the high pH required for elution. An experiment was performed in which a heparin sample was stopped in the NMR flow cell and a spectrum was acquired. The solution was left in the NMR overnight, and an identical spectrum was acquired the next morning, suggesting sufficient sample stability for long NMR acquisitions. As described in section 2.2.7, solutions of 33 mg/mL DS, heparin, and OSCS were prepared in 0.1 M NaCl buffer, pH 10.25 to monitor their stability in the high pH separation buffer used in these experiments. As seen by the ^1H NMR spectra presented in Figures 2.7, 2.8, and 2.9, no changes were apparent in these spectra over a 1 week period. However, we advise caution in the use of this method for the separation of GAG components or impurities having poor stability in basic solution.

2.3.6 Sensitivity Enhancement Through Peak-trapping of OSCS

The UV and NMR-detected chromatograms presented in Figures 2.3, 2.4, and 2.5 were measured using samples containing roughly equivalent concentrations of heparin and the OSCS impurity. To explore the ability of this method to detect and characterize impurities present at much lower levels, a sample was prepared containing 40 mg/mL of heparin and 2 mg/L OSCS (5 wt%). Although it was possible to detect OSCS in the UV chromatogram and position it in the NMR flow cell, as shown in Figures 2.10A and B extensive signal averaging is required to produce a ^1H NMR spectrum with

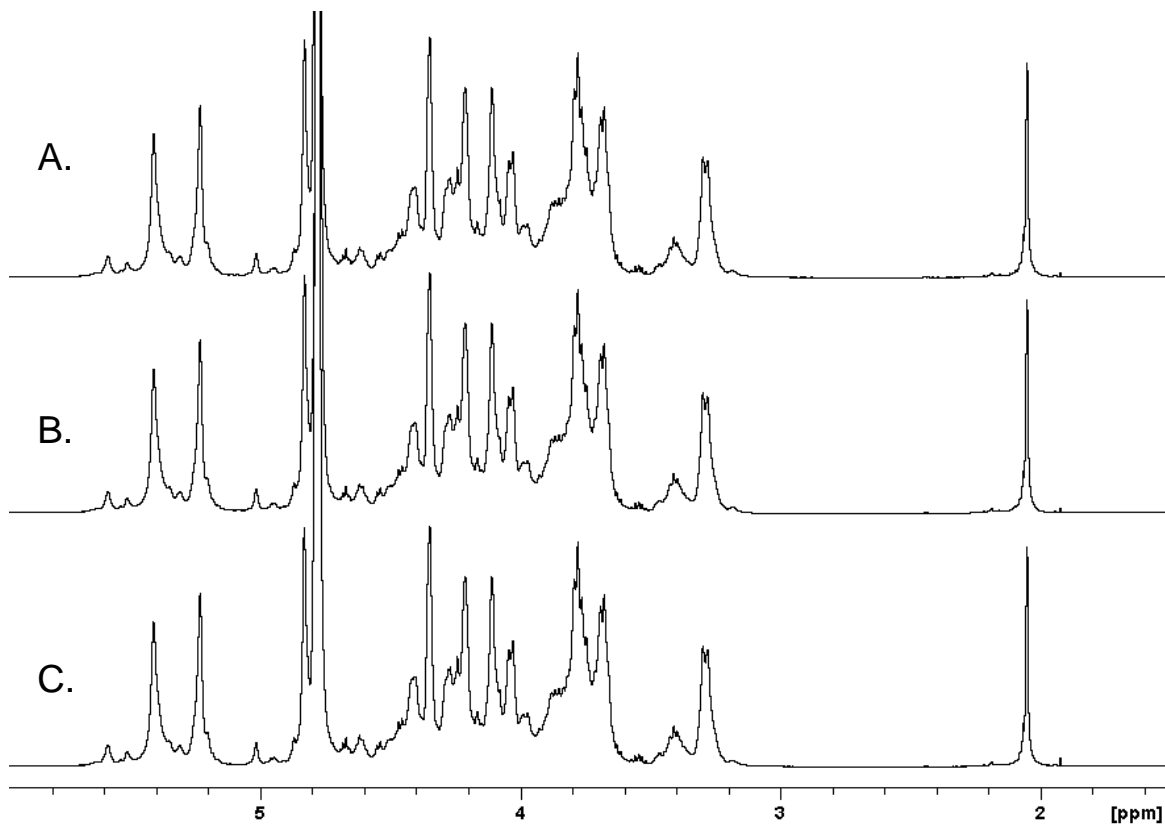


Figure 2.7. ^1H NMR spectrum of heparin at pD 10.25, (A) day 1, (B) day 2, and (C) after 1 week.

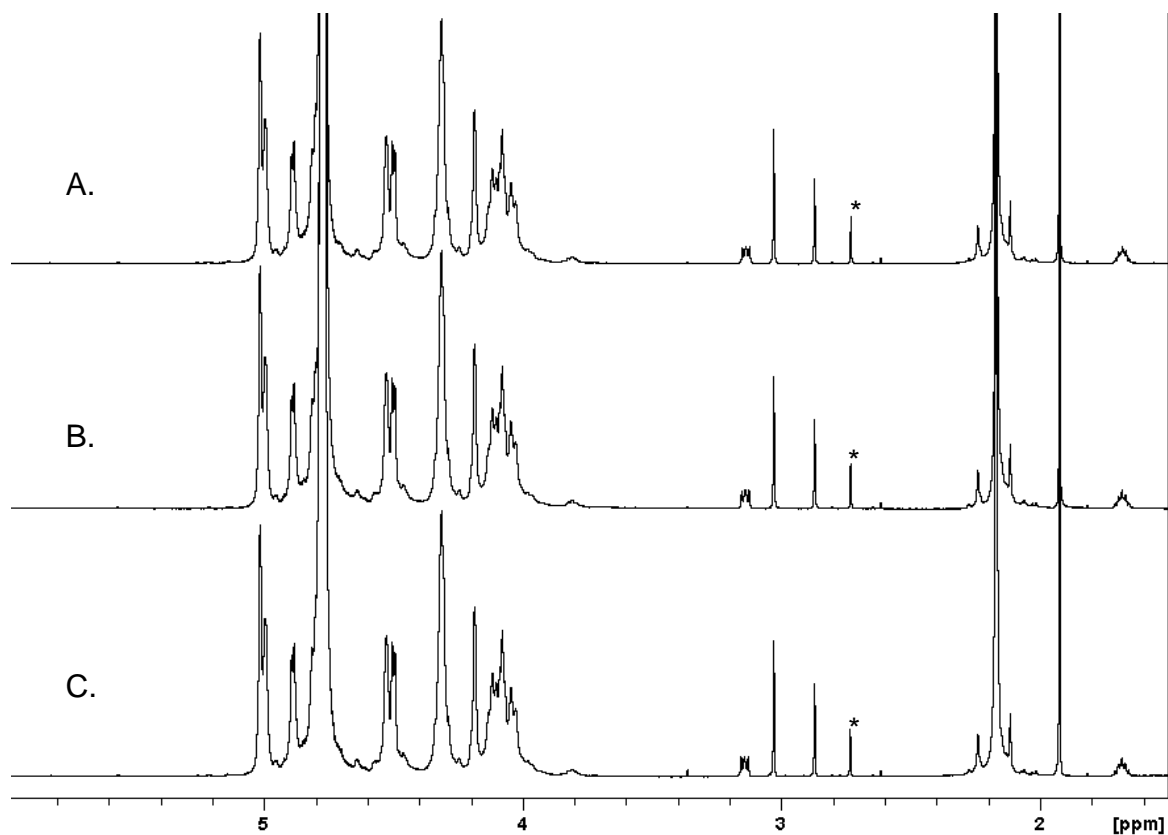


Figure 2.8. ^1H NMR spectrum of 33 mg/mL of OSCS at pD 10.25, (A) day 1, (B) day 2, and (C) after 1 week. The resonances at 1.682 and 3.142 ppm are due to tributylamine and those at 2.871 and 3.027 ppm are due to DMF remaining from our synthesis of OSCS. The peak at 2.737 ppm is an unknown impurity. These impurity resonances do not appear in our LC-NMR spectra because the OSCS is resolved from its impurities by the WAX separation.

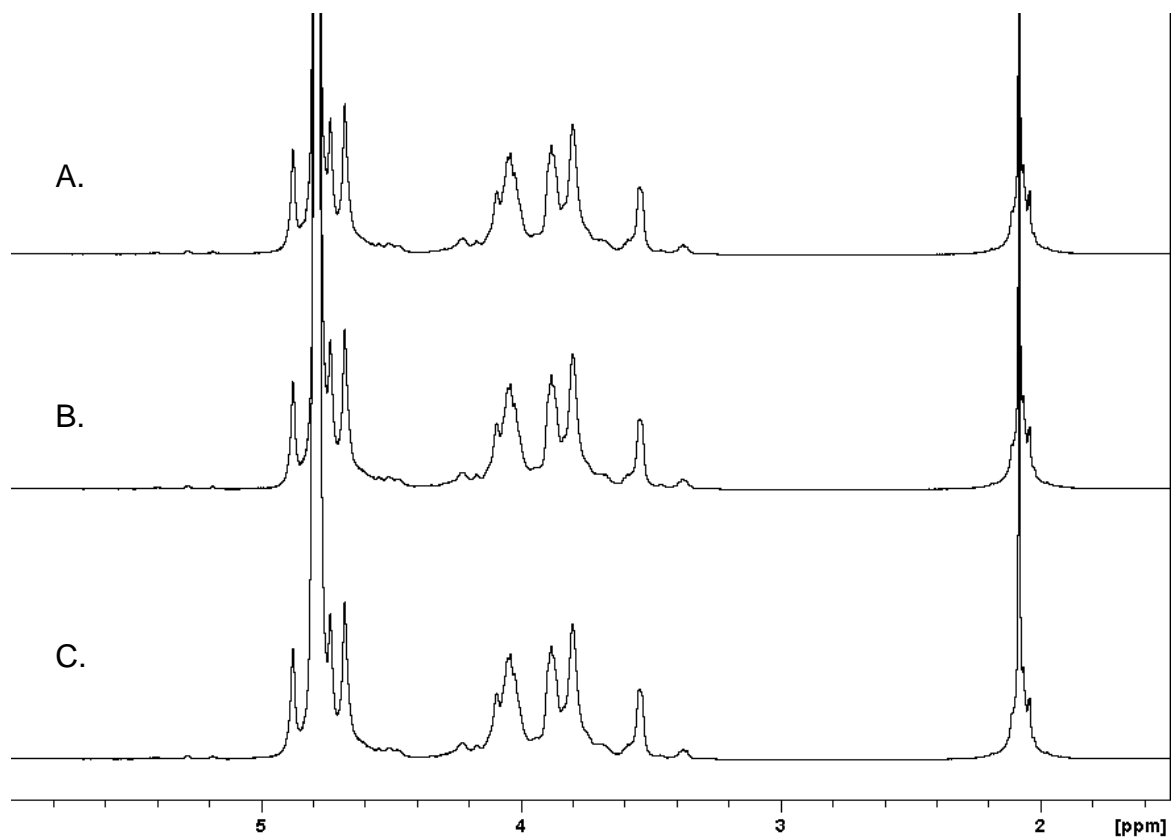


Figure 2.9. ^1H NMR spectrum of 33 mg/mL of DS at pD 10.25, (A) day 1, (B) day 2, and (C) after 1 week.

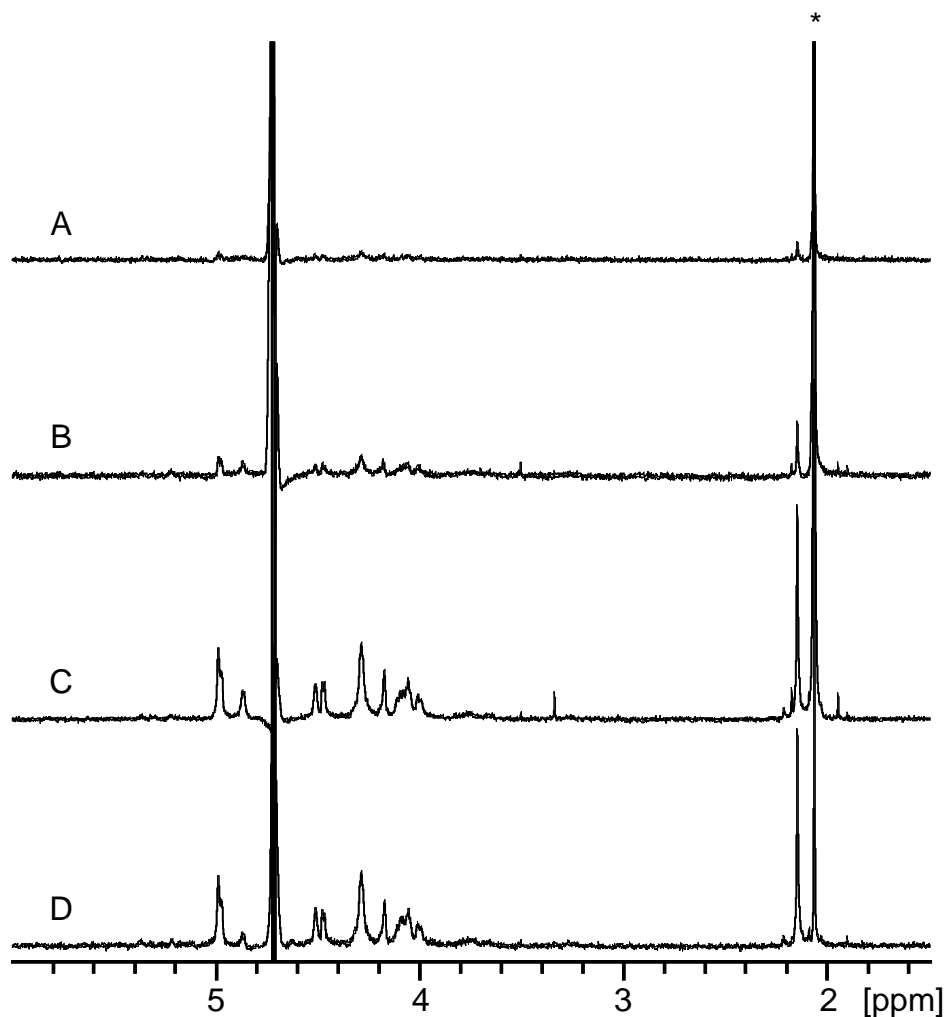


Figure 2.10. (A) Stop-flow ^1H NMR spectrum of OSCS measured for a single injection of a sample containing 40 mg/mL of heparin and 2 mg/mL OSCS acquired with 1024 scans. (B) Stop-flow ^1H NMR spectrum of OSCS measured for a single injection of a sample containing 40 mg/mL of heparin and 2 mg/mL OSCS acquired with 4608 scans. (C) Stop-flow ^1H NMR spectrum of OSCS measured for a single injection of a sample containing 40 mg/mL of heparin and OSCS. (D) Stop-flow ^1H NMR spectrum of OSCS measured for 10 repeated injections of a sample containing 40 mg/mL of heparin and 2 mg/mL OSCS using peak trapping. The resonance marked with an asterisk (*) is due to residual acetonitrile, present as a column contaminant.

adequate quality for this sample. In early experiments, like the one shown in Figure 2.10C, we encountered some problems with carryover of heparin in the NMR flowcell which resulted in contamination of the OSCS spectra. As shown in the spectra in Figures 2.10A and B, this problem could be eliminated by introducing a 10 min isocratic delay following the elution of heparin and by shunting the heparin peak to waste, rather than to the NMR flow probe. This eliminated the problem of heparin carryover and allowed for the acquisition of a clean OSCS spectrum.

Because our WAX separation method allowed us to dictate the retention and elution of analytes with different charges based on the concentration of NaCl in the elution buffer, we investigated the applicability of this method for on-line concentration of OSCS through peak trapping. Because OSCS has a greater net negative charge than heparin, it could be retained on the column through repeated injections, as long as the NaCl concentration of the elution buffer was below 0.8 M NaCl. This allowed the heparin, present at a 20-fold excess in these samples, to be eluted following each injection while OSCS was nearly quantitatively trapped on the WAX column. After the final injection, the OSCS was eluted as a single peak using a salt gradient to 0.8 M NaCl. Figure 2.10C compares the ^1H NMR spectra obtained for a single injection of a sample containing 40 mg/mL of both heparin and OSCS with that obtained in Figure 2.10D using peak trapping for 10 replicate injections of a sample containing 40 mg/mL heparin and 2 mg/mL OSCS. Based on the relative intensities of resonances in these spectra, we estimate a trapping efficiency of about 89% for OSCS. Trapping of the OSCS peak provided a route to concentrate the contaminant on-line prior to detection and thus present a more concentrated sample for ^1H NMR measurements.

2.4 Summary

The WAX-HPLC separation developed in this work provides an efficient and effective method for the resolution of the intact GAG polymers DS, CSA, heparin and OSCS, as well as acetate which was present as an extraneous impurity. WAX-NMR proved to be useful in both on-flow and stop-flow modes, and could be used for on-line peak trapping of OSCS to increase its effective concentration for NMR measurements. Although HPLC-NMR is not practical for routine quality assurance experiments, screening of samples could be conducted on a routine basis using LC-UV or CE-UV and when unexpected peaks are encountered, WAX-NMR exploited for identification and structure elucidation of new or novel impurities.

Though WAX-HPLC-NMR effectively separated heparin and its contaminants, it requires specialized equipment and flow-probes. In addition, LC-NMR experiments often require the use of expensive deuterated solvents to obtain high quality NMR spectra for structural characterization of the eluting components. As with other chromatographic techniques, LC-NMR requires extensive method development for the effective separation of mixture components. In Chapter 3, I investigate DOSY NMR in the routine screening of heparin solutions. The ease of implementation and the non-destructive nature of NMR, permits further analysis by other methods such as MS.

2.5 References

1. Lindon, J. C.; Nicholson, J. K.; Wilson, I. D. Directly coupled HPLC-NMR and HPLC-NMR-MS in pharmaceutical research and development. *J. Chromatogr., B: Anal. Technol. Biomed. Life Sci.* **2000**, *748*, 233-258.
2. Albert, K. Liquid chromatography-nuclear magnetic resonance spectroscopy. *J. Chromatogr., A* **1999**, *856*, 199-211.
3. Keifer, P. A. In *Modern Magnetic Resonance*; Webb, G. A., Ed.; Springer: Netherlands, 2006, pp 1213-1219.
4. Spraul, M. In *Modern Magnetic Resonance*; Webb, G. A., Ed.; Springer: Netherlands, 2006, pp 1221-1228.
5. Albert, K. On-line use of NMR detection in separation chemistry. *J. Chromatogr., A* **1995**, *703*, 123-147.
6. Subramanian, R.; Kelley, W. P.; Floyd, P. D.; Tan, Z. J.; Webb, A. G.; Sweedler, J. V. A Microcoil NMR Probe for Coupling Microscale HPLC with On-Line NMR Spectroscopy. *Anal. Chem.* **1999**, *71*, 5335-5339.
7. Lindon, J. C.; Nicholson, J. K.; Wilson, I. D. Direct coupling of chromatographic separations to NMR spectroscopy. *Prog. Nucl. Magn. Reson. Spectrosc.* **1996**, *29*, 1-49.
8. Guerrini, M.; Beccati, D.; Shriver, Z.; Naggi, A.; Viswanathan, K.; Bisio, A.; Capila, I.; Lansing, J. C.; Guglieri, S.; Fraser, B.; Al-Hakim, A.; Gunay, N. S.; Zhang, Z.; Robinson, L.; Buhse, L.; Nasr, M.; Woodcock, J.; Langer, R.; Venkataraman, G.; Linhardt, R. J.; Casu, B.; Torri, G.; Sasisekharan, R. Oversulfated chondroitin sulfate is a contaminant in heparin associated with adverse clinical events. *Nat Biotech* **2008**, *26*, 669-675.
9. Nagasawa, K.; Uchiyama, H.; Wajima, N. Chemical sulfation of preparations of chondroitin 4- and 6-sulfate, and dermatan sulfate. Preparation of chondroitin sulfate E-like materials from chondroitin 4-sulfate. *Carbohydr. Res.* **1986**, *158*, 183-190.
10. Maruyama, T.; Toida, T.; Imanari, T.; Yu, G.; Lindhardt, R. J. Conformational changes and anticoagulant activity of chondroitin sulfate following its O-sulfonation. *Carbohydr. Res.* **1998**, *306*, 35-43.

11. Wielgos, T.; Havel, K.; Ivanova, N.; Weinberger, R. Determination of impurities in heparin by capillary electrophoresis using high molarity phosphate buffers. *J. Pharm. Biomed. Anal.* **2009**, *49*, 319-326.
12. Somsen, G. W.; Tak, Y. H.; Toraño, J. S.; Jongen, P. M. J. M.; de Jong, G. J. Determination of oversulfated chondroitin sulfate and dermatan sulfate impurities in heparin by capillary electrophoresis. *J. Chromatogr., A* **2009**, *1216*, 4107-4112.
13. Trehy, M.; Reepmeyer, J.; Kolinski, R.; Westenberger, B.; Bushe, L. Analysis of heparin sodium by SAX/HPLC for contaminant and impurities. *J. Pharm. Biomed. Anal.* **2009**, *49*, 670-673.
14. Glasoe, P. K.; Long, F. A. Use of Glass Electrodes to Measure Acidities in Deuterium Oxide. *J. Phys. Chem.* **1960**, *64*, 188-190.
15. Smallcombe, S. H.; Patt, S. L.; Keifer, P. A. WET Solvent Suppression and Its Application to LC NMR and High-Resolution NMR Spectroscopy. *J. Magn. Reson., Ser. A* **1995**, *117*, 295-303.
16. McEwen, I. Broadening of ¹H NMR signals in the spectra of heparin and OSCS by paramagnetic transition metal ions. The use of EDTA to sharpen the signals. *J. Pharm. Biomed. Anal.* **2010**, *51*, 733-735.
17. Dantus, M. M.; Wells, M. L. Regulatory Issues in Chromatographic Analysis in the Pharmaceutical Industry. *J. Liq. Chromatogr. Relat. Technol.* **2005**, *27*, 1413 - 1442.
18. Noti, C.; Seeberger, P. H. Chemical Approaches to Define the Structure-Activity Relationship of Heparin-like Glycosaminoglycans. *Chemistry & Biology* **2005**, *12*, 731-756.
19. Cecchi, T.; Pucciarelli, F.; Passamonti, P. Extended Thermodynamic Approach to Ion Interaction Chromatography. *Anal. Chem.* **2001**, *73*, 2632-2639.
20. Horvath, C.; Melander, W.; Molnar, I.; Molnar, P. Enhancement of retention by ion-pair formation in liquid chromatography with nonpolar stationary phases. *Anal. Chem.* **1977**, *49*, 2295-2305.
21. Wittmer, D. P.; Nuessle, N. O.; Haney, W. G. Simultaneous analysis of tartrazine and its intermediates by reversed phase liquid chromatography. *Anal. Chem.* **1975**, *47*, 1422-1423.

22. Hoffman, N. E.; Liao, J. C. Reversed phase high performance liquid chromatographic separations of nucleotides in the presence of solvophobic ions. *Anal. Chem.* **1977**, *49*, 2231-2234.
23. Kissinger, P. T. Reverse-phase ion-pair partition chromatography. Comments. *Anal. Chem.* **1977**, *49*, 883-883.
24. Jones, C. J.; Membreno, N.; Larive, C. K. Insights into the mechanism of separation of heparin and heparan sulfate disaccharides by reverse-phase ion-pair chromatography. *J. Chromatogr., A* **2010**, *1217*, 479-488.
25. Korir, A. K.; Limtiaco, J. F. K.; Gutierrez, S. M.; Larive, C. K. Ultrapformance ion-pair liquid chromatography coupled to electrospray time-of-flight mass spectrometry for compositional profiling and quantification of heparin and heparan sulfate. *Anal. Chem.* **2008**, *80*, 1297-1306.
26. Eldridge, S. L.; Korir, A. K.; Gutierrez, S. M.; Campos, F.; Limtiaco, J. F. K.; Larive, C. K. Heterogeneity of depolymerized heparin SEC fractions: to pool or not to pool? *Carbohydr. Res.* **2008**, *343*, 2963-2970.
27. Thanawiroon, C.; Linhardt, R. J. Separation of a complex mixture of heparin-derived oligosaccharides using reversed-phase high-performance liquid chromatography. *J. Chromatogr., A* **2003**, *1014*, 215-223.
28. Yang, B.; Solakyildirim, K.; Chang, Y.; Linhardt, R. Hyphenated techniques for the analysis of heparin and heparan sulfate. *Anal. Bioanal. Chem.* **2011**, *399*, 541-557.
29. Huang, Y.; Toyoda, H.; Koshiishi, I.; Toida, T.; Imanari, T. Determination of a depolymerized holothurian glycosaminoglycan in plasma after i.v. administration by postcolumn HPLC. *Chem. Pharm. Bull.* **1995**, *43*, 2182-2186.
30. Buchanan, D. L. Carrier Displacement Chromatography on Ion Exchange Resins. *Anal. Chem.* **1959**, *31*, 833-836.
31. Ramsey, R.; Katti, A. M.; Guiochon, G. Displacement chromatography applied to trace component analysis. *Anal. Chem.* **2002**, *62*, 2557-2565.
32. Keifer, P. A. Flow injection analysis NMR (FIA-NMR): a novel flow NMR technique that complements LC-NMR and direct injection NMR (DI-NMR). *Magn. Reson. Chem.* **2003**, *41*, 509-516.

33. Keifer, P. A. Flow NMR applications in combinatorial chemistry. *Curr. Opin. Chem. Biol.* **2003**, *7*, 388-394.
34. Beyer, T.; Diehl, B.; Randel, G.; Humpfer, E.; Schäfer, H.; Spraul, M.; Schollmayer, C.; Holzgrabe, U. Quality assessment of unfractionated heparin using ¹H nuclear magnetic resonance spectroscopy. *J. Pharm. Biomed. Anal.* **2008**, *48*, 13-19.
35. Guerrini, M.; Naggi, A.; Guglieri, S.; Santarsiero, R.; Torri, G. Complex glycosaminoglycans: profiling substitution patterns by two-dimensional nuclear magnetic resonance spectroscopy. *Anal. Biochem.* **2005**, *337*, 35-47.
36. Torri, G.; Guerrini, M. In *NMR Spectroscopy in Pharmaceutical Analysis*; Holzgrabe, U., Wawaer, I., Diehl, B., Eds.; Elsevier: Amsterdam, 2008, pp 407-427.
37. Guerrini, M.; Beccati, D.; Shriver, Z.; Naggi, A.; Viswanathan, K.; Bisio, A.; Capila, I.; Lansing, J. C.; Guglieri, S.; Fraser, B.; Al-Hakim, A.; Gunay, N. S.; Zhang, Z. Q.; Robinson, L.; Buhse, L.; Nasr, M.; Woodcock, J.; Langer, R.; Venkataraman, G.; Linhardt, R. J.; Casu, B.; Torri, G.; Sasisekharan, R. Oversulfated chondroitin sulfate is a contaminant in heparin associated with adverse clinical events. *Nat. Biotechnol.* **2008**, *26*, 669-675.
38. Lindon, J. C.; Nicholson, J. K.; Wilson, I. D. In *On-line LC-NMR and Related Techniques*; Albert, K., Ed.; John Wiley and Sons Ltd.: West Sussex, 2002, pp 45-87.
39. Olson, D. L.; Norcross, J. A.; O'Neil-Johnson, M.; Molitor, P. F.; Detlefsen, D. J.; Wilson, A. G.; Peck, T. L. Microflow NMR: Concepts and Capabilities. *Anal. Chem.* **2004**, *76*, 2966-2974.

CHAPTER THREE

Diffusion NMR Measurements of Heparin and its Contaminants

This chapter describes the application of diffusion NMR techniques in the characterization of heparin and its impurities. The goals of this study are to characterize mixtures of heparin, and the impurities DS, and OSCS using diffusion NMR and investigate the effect of analyte concentration on both solution viscosity as well as the measured diffusion coefficients.

3.1 Introduction

As presented in Chapter 1, there are numerous techniques that can be used for heparin purity analysis. The current U.S. Pharmacopeia monograph, monograph 2, recommends analysis of heparin using ^1H NMR and HPLC. NMR spectroscopy is effective in the detection and quantification of heparin contaminants provided they have resonances that are well-resolved from those of heparin and other GAG impurities that may be present.¹⁻³ In comparison to other analytical techniques such as HPLC and MS, NMR is a simple technique requiring relatively little sample preparation and is highly reproducible allowing direct comparisons across multiple labs.^{4, 5} Although NMR is less sensitive than some other techniques, it allows for the complete structural identification of contaminants, which is especially important when standards are unavailable.

3.1.1 *In-Situ* Analysis of Solutions

In addition to the application of NMR spectroscopy for the structural characterization of molecules, it also provides numerous options for the analysis of

biological mixtures often without requiring a physical separation of the mixture components. Several NMR parameters can be measured in order to gain information about molecular structure and size, including chemical shifts, nuclear relaxation rates, correlation times, and diffusion coefficients.⁶ One major advantage of using NMR spectroscopy to study complex biological mixtures is the minimal sample preparation required and the detailed analytical profile that can be obtained on the whole biological sample. Therefore, a significant amount of effort has been devoted to discovering new NMR pulse sequence techniques for spectral simplification or spectral editing. A number of methods have been used for NMR spectral editing based on the NMR parameters listed above.

The diffusional behaviors of components in the solution are related to hydrodynamic properties such as size, shape, and charge. Therefore, individual components in the solution can be distinguished based on diffusion provided that the species have resolved resonances or, in cases of resonance overlap, significantly different diffusion coefficients.⁷⁻⁹ Diffusion NMR differs from HPLC and other conventional methods of separation in that the components of the mixture are not physically resolved, but are distinguished spectroscopically according to differences in their diffusion behavior.^{6, 9-11} Because of the non-invasive nature of diffusion NMR it is a unique tool that can be used in the study of molecular dynamics in chemical and biological systems, preserving the chemical environment of the system and thus providing a means to probe component interactions such as aggregation and partitioning.⁶

3.1.2 DOSY-NMR Analysis of Heparin and its Impurities

Shortly following the identification of OSCS as the heparin adulterant, Sitkowski and coworkers investigated the utility of DOSY-NMR as a routine screening method for OSCS in LMW and unfractionated heparin.¹² Because the chemical shifts of the *N*-acetyl resonances of heparin, DS, and OSCS are well-resolved, the DOSY plots obtained by Sitkowski et al. could resolve the diffusion coefficients of OSCS and DS from both LMW and unfractionated heparin. They also observed that in mixtures containing both LMW and unfractionated heparin, the components could not be resolved on the basis of diffusion, and the diffusion coefficient measured using the heparin resonances was a weighted average of both components. In a recent study by the same group, diffusion NMR was used for the separation and characterization of contaminants in pharmaceutical heparin.¹³ These authors noted resonances of currently unidentified contaminants which produced diffusion coefficients that were different from those observed for heparin, DS, and OSCS.

3.1.3 Spectral Editing by Molecular Diffusion

NMR spectral editing methods are useful in simplifying NMR spectra which are complicated by resonance overlap. Two methods of spectral editing are spectral editing based on signal relaxation and spectral editing based on molecular diffusion. Relaxation based spectral editing techniques rely on differences in either the T_1 or T_2 relaxation times of the different resonances in a complex spectrum. In the analysis of complex mixtures, different pulse sequences such as the spin-echo pulse sequence (Section 1.6.1) and the Carr-Purcell-Meiboom-Gill (CPMG) pulse sequence exploit differences in the molecules T_2 relaxation times, while the inversion recovery pulse sequence exploit

differences in the T_1 relaxation times, effectively eliminating resonances that relax away allowing for the selective detection of only the resonances that remain.^{6, 14-17}

The diffusion edited 1D NMR experiment is carried out using a single field gradient which selectively encodes spins base on the translational position in the NMR sample tube, as demonstrated in Section 1.6.1. The single gradient is used to exploit differences in the diffusional properties of molecules in a mixture for the purpose of spectral editing. The pseudo-separation of different molecules on the basis of molecular diffusion can simplify ^1H spectra by eliminating resonances of the smaller rapidly diffusing components of the mixture while permitting the selective observation of the higher molecular weight components.¹⁴ The resulting NMR spectrum contains only the resonances of the slowly diffusing components of the sample.^{6, 17-19} In addition to the advantages of diffusion based discrimination against smaller rapidly diffusing molecules without complex data transformations, diffusion-edited spectra require significantly shorter experiment times than conventional diffusion NMR experiments where multiple diffusion experiments is necessary to measure diffusion coefficients.

3.1.4 Application of NMR Diffusion Editing Strategies in Heparin Purity Analysis

The first study which used diffusion NMR in the characterization of heparin was by Kellenbach and coworkers where they used the pulsed-field gradient longitudinal encode-decode (PFG-LED) experiment to identify signals of low molecular weight impurities in a synthetic heparin pentasaccharide solution.²⁰ Because of the large difference in size between the heparin pentasaccharide and its impurities, a simple “gradient on/ gradient off” experiment was capable of discriminating between the

pentasaccharide-related and low-molecular weight molecules in the solution.²⁰ A stimulated-echo experiment was used to achieve a “diffusion weighing” of the NMR signal intensities. The resolution in the diffusion dimension was traded for sensitivity and therefore only two points were acquired corresponding to the gradient being off where no attenuation of the NMR signals was observed and gradient on where the NMR signals of the low-molecular weight impurities were eliminated. Because the goal of the study was the qualitative identification of resonances belonging to the low-molecular weight impurities in the sample they were uninterested in determining the diffusion coefficients of the components in the solution.

3.2 Experimental Section

3.2.1 Chemicals

Heparin, DS, and a system suitability standard containing both heparin and OSCS were provided by the U.S. Pharmacopeia (Rockville, MD). Low paramagnetic deuterium oxide (D, 99.9%) and sodium acetate-*d*3 (D3, 99%) was purchased from Cambridge Isotope Laboratories (Andover, MA). Tert-butanol was purchased from Fisher Scientific (Pittsburgh, PA). Tris(hydroxymethyl)aminomethane (Tris), CSA sodium salt from bovine trachea, calcium acetate hydrate, and porcine heparin grade 1-A were purchased from Sigma-Aldrich (St. Louis, MO). Porcine heparin from Sigma-Aldrich was used to prepare an 83 mg/mL solution used in our initial experiments to determine the appropriate solution concentrations for the DOSY measurements. The enzyme heparinase I used in the partial digestion of heparin for DOSY analysis of solutions of heparin/DS and heparin/OSCS was purchased from IBEX Technologies Inc. (Montreal, Quebec, Canada). The enzymes heparinase I, II, and III used in the cocktail digestion of

heparin in the diffusion edited analysis of a heparin/OSCS solution were purchased from Iduron (Manchester, UK).

Individual stock solutions containing 50 mg/mL of heparin sodium salt, DS or CSA were prepared by reconstitution of the lyophilized solid into 1 mL D₂O according to the procedure described by the U.S. Pharmacopeia (USP) monograph 2 for heparin analysis. A stock solution of the system suitability standard, which contains 10% OSCS and 90% heparin by weight, was also prepared by dilution to 1 mL to yield a solution with a total GAG concentration of 50 mg/mL. Solutions containing either 10% DS or 10% CSA and 90% heparin were prepared at a concentration of 12.5 mg/mL total GAG by dilution of the stock solutions to a volume of 1 mL in D₂O with addition of 8 μ L of 100 mM *tert*-butanol as a chemical shift reference. Additional D₂O solutions containing only heparin at 6.25, 12.5, 25 and 83 mg/mL were prepared for measurements to probe the effect of concentration on heparin diffusion and viscosity. Solutions at concentrations of 6.25, 12.5, and 25 mg/mL were prepared with USP heparin while the 83 mg/mL solution was prepared with porcine heparin from Sigma-Aldrich.

3.2.2 Heparinase I Depolymerization of Heparin

USP porcine intestinal mucosa heparin was digested with heparinase I. The depolymerization solutions contained 0.1 M Tris and 2.5 mM calcium acetate. Solutions containing heparin and DS or OSCS in 600 μ L buffered D₂O, pD 7.2, were digested with 0.05 IU of heparinase I at 28°C. In addition to monitoring the depolymerization reaction with ¹H NMR, the reaction was also monitored using UV absorption at λ =232 nm.

3.2.3 Cocktail Digestion of Heparin

Porcine intestinal mucosa heparin from Sigma-Aldrich was digested with a cocktail of the enzymes heparinase I, II, and III. The depolymerization solutions contained 0.1 M sodium acetate-*d*3 and 1 mM calcium acetate. A solution containing 25 mg/mL heparin and 1.25 mg/mL OSCS in 600 μ L buffered D₂O, pD 7.0, were digested with 0.01 IU of each enzyme at 32°C.

3.2.4 NMR Spectroscopy

NMR spectra were acquired at 298.15 K using a Bruker Avance NMR spectrometer operating at 599.84 MHz equipped with a broad-band inverse probe with x, y, and z-gradient coils. The z gradient coil used in the diffusion measurements was calibrated using the known diffusion coefficient for lysozyme ($1.07 \times 10^{-10} \text{ m}^2/\text{s}$).²¹ ¹H NMR chemical shifts were referenced to *tert*-butanol (1.253 ppm) in D₂O. ¹H NMR spectra were acquired using the single pulse (zg) pulse program while diffusion spectra were acquired with the stimulated echo experiment using bipolar gradients (stebpgp1s).²²⁻²⁴ Diffusion (Δ) and gradient pulse times (δ) were optimized for the individual solutions using a one-dimensional version of the stimulated echo pulse program, stebpgp1s1d. Diffusion experiments were acquired with 26624 data points and a spectral width of 6009 Hz. To achieve adequate signal-to-noise, a relaxation delay of 2.0 s was used and 80 transients were coadded for each of 20 gradient amplitudes incremented as a square dependence from 1.686 to 32.030 G/cm. Complete diffusion data sets were typically collected in approximately 2 hr.

Following acquisition, the FIDs were apodized by multiplication with an exponential decay equivalent to 1.5 Hz line broadening and baseline corrected before

DOSY processing^{8, 10, 24} using the DOSY Toolbox software.²⁵ Diffusion coefficients were calculated using a monoexponential fit of the well-resolved *N*-acetyl and anomeric resonances of the intact GAGs using the DOSY Toolbox software. Peaks above a manually set threshold were automatically picked by the software for DOSY processing. Shown in Figures 3.1A and B are the exponential fits plotted using the Stejskal-Tanner equation.^{22, 26} and residual plots of the diffusion data measured for the *N*-acetyl resonances of heparin and OSCS, respectively. Although heparin, DS, and OSCS are heterogenous, we were able to achieve acceptable fits of the diffusion coefficients of the individual analytes using a single exponential decay. Fitting errors for the monoexponential fit of the Stejskal-Tanner equation (equation 1.10) were determined and displayed following DOSY processing. The variance in the calculated diffusion coefficients was evaluated through duplicate measurements. Replicate diffusion data sets were acquired with the same solution and parameters to ensure comparability across the measurements. Stacked plots were processed using the Mestrec MNova NMR processing suite. Spectra for the stacked plots were apodized by multiplication with an exponential decay equivalent 1.0 Hz line broadening.

3.2.5 Viscosity Measurements

Viscosity measurements were performed using a calibrated Cannon-Manning semi-micro viscometer purchased from Cannon Instruments Co. (State College, PA). Following each measurement, the viscometer was cleaned thoroughly with water and dried. The temperature was controlled at 298 ± 0.05 K using a Fisher Scientific Isotemp 1013S scientific temperature regulator. The kinematic viscosity (ν) was calculated by

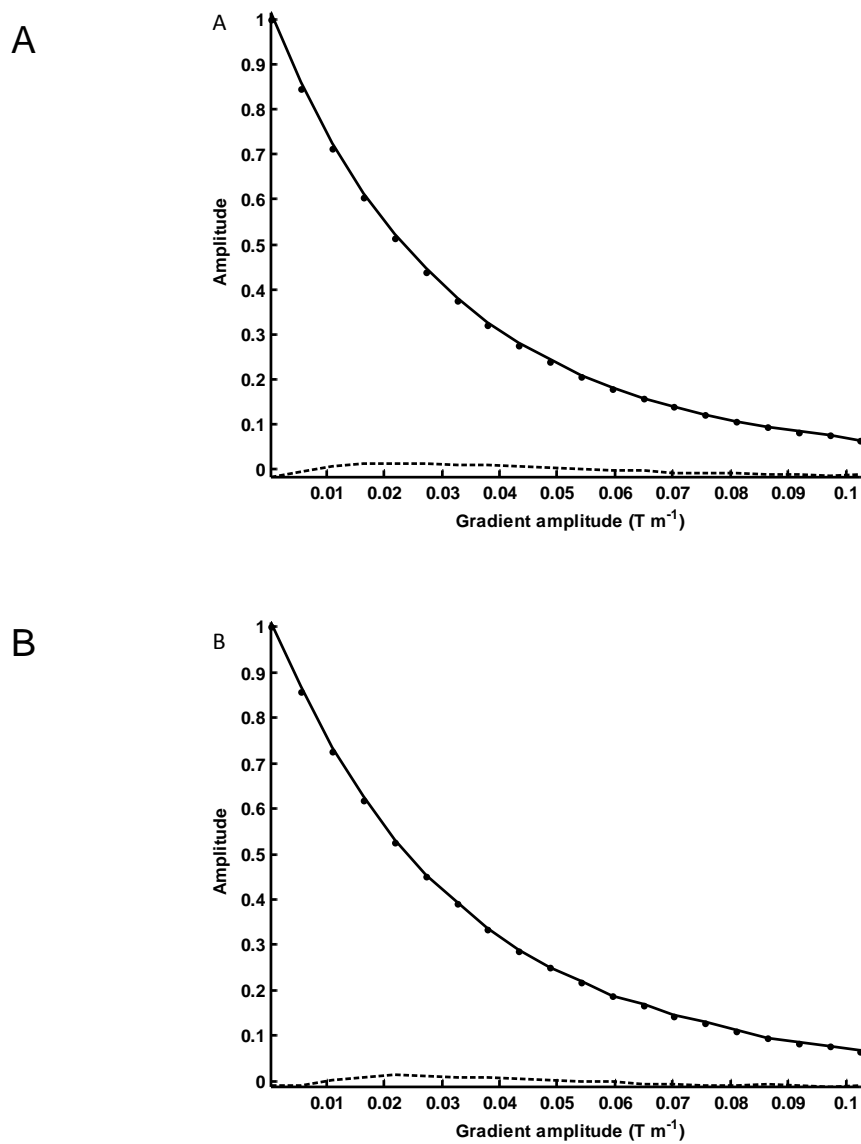


Figure 3.1. Diffusion results obtained by fitting a mono-exponential decay to the intensities of the *N*-acetyl resonances of (A) heparin and (B) OSCS for a heparin/OSCS solution with a total GAG concentration of 12.5 mg/mL. The fitted decay curves and residuals were calculated using the DOSY Toolbox software.

measuring the total efflux time (t) with a stopwatch and the viscometer constant (B) using Eq.3.2.

$$V = tB \quad \text{Eq. 3.2}$$

The viscometer was calibrated using the known viscosity of water at 20°C. Because of the limited sample volumes available, viscosity was measured for each solution following the NMR experiments using the same sample. Replicate measurements (n=4) were performed for each solution.

3.3 Results and Discussion

Diffusion NMR experiments were performed using dilute aqueous solutions of both intact and digested heparin containing the contaminants DS or OSCS. Because the diffusion behavior of solution components is related to properties such as size, shape, and charge, each component within a mixture may be distinguished providing that the species have resolved resonances, or in the case of spectral overlap, have significantly different diffusion coefficients.²⁷⁻²⁹

The diffusion coefficient of a molecule is dependent on its hydrodynamic radius, which is in turn governed by the molecular size, shape, and solvation.^{30, 31} For samples such as those investigated in this study, solution dynamics including electrostatic interactions between sodium ions and the sulfate and carboxyl moieties of the polyanion, hydrogen bonding and molecular crowding can all affect the apparent diffusion coefficient.^{29, 32} Therefore, the diffusion coefficients measured for samples of GAG polyanions such as heparin and OSCS are not expected to follow simple Stokes-Einstein behavior.³³⁻³⁵

In addition to DOSY analysis, viscosity measurements were performed for each of the solutions used for the NMR diffusion experiments. Diffusion coefficients were found to be inversely correlated to solution viscosities, but did not vary in a linear fashion. Therefore, it was important to monitor viscosities as increases in the viscosity of the solution could affect the ability of diffusion NMR to resolve components in the solution.

3.3.1 DOSY Analysis of Intact GAGs

Because GAG solutions can be viscous, experiments were performed to determine appropriate solution concentrations for these measurements. We desired a GAG concentration sufficiently low to allow unhindered diffusion of the sample components yet high enough to allow acquisition of the BPPSTE spectra within a reasonable time. NMR diffusion measurements were performed using D₂O solutions containing heparin at concentrations of 6.25, 12.5, 25 and 83 mg/mL to determine the effect of concentration on the apparent diffusion coefficient. As summarized in Table 3.1, the diffusion coefficients measured using the heparin *N*-acetyl resonance decreased as the concentration was increased from $5.75 \pm 0.01 \times 10^{-11} \text{ m}^2/\text{s}$ at 6.25 mg/mL to $3.62 \pm 0.01 \times 10^{-11} \text{ m}^2/\text{s}$ at 83 mg/mL. This concentration dependent decrease in the diffusion coefficient was accompanied by a corresponding increase in the solution viscosity from $1.29 \pm 0.01 \text{ cSt}$ at 6.25 mg/mL to $4.46 \pm 0.01 \text{ cSt}$ at 83 mg/mL. Higher sugar concentrations result in viscous solutions. In addition, because heparin is a linear long-chain polysaccharide molecular crowding can also be expected to have a significant effect on diffusion, especially in concentrated solutions. Based on these measurements, a total GAG concentration of 12.5 mg/mL was selected as a suitable concentration for

Table 3.1. Effect of Heparin Concentration on Diffusion Coefficients and Solution Viscosities.

Concentration	Diffusion Coefficient	Solution Viscosity
6.25 mg/mL	$5.75 \pm 0.01 \times 10^{-11} \text{ m}^2/\text{s}$	$1.29 \pm 0.01 \text{ cSt}$
12.5	$5.52 \pm 0.01 \times 10^{-11}$	1.49 ± 0.01
25.0	$5.15 \pm 0.01 \times 10^{-11}$	1.86 ± 0.01
83.0	$3.62 \pm 0.01 \times 10^{-11}$	4.46 ± 0.01

the analysis of the subsequent heparin/OSCS and heparin/DS mixtures. At this concentration heparin diffusion did not appear to be unduly hindered, yet the solution was sufficiently concentrated to permit the acquisition of diffusion data sets in an acceptable amount of time, approximately 2 hr. In addition, the concentration of 12.5 mg/mL is similar to the concentrations used in previous studies by Bednarek¹³ and Sitkowski¹².

Single-pulse ¹H NMR spectra were acquired for each sample prior to performing the diffusion measurements. The spectra of the heparin/DS and heparin/OSCS solutions are shown in Figures 3.2A and B, respectively. The components of the two mixtures can be readily identified by their characteristic *N*-acetyl resonances, as shown in Figure 3.3. The *N*-acetyl resonances of heparin, DS, and OSCS are observed at chemical shifts of 2.045, 2.079, and 2.144 ppm, respectively. The spectral resolution of the *N*-acetyl resonances of the GAG components greatly facilitates their *in situ* analysis by diffusion NMR.

3.3.1.1 Diffusion Analysis of Solutions of Heparin and DS

Although it does not have known adverse health effects, analysis of DS is important as it is a natural occurring contaminant of pharmaceutical heparin.^{1, 36} Because DS is less sulfated, containing on average only 1.5 sulfate moieties per disaccharide subunit, it exhibits only minimal anti-clotting activity when compared to more highly charged species such as heparin and OSCS.³⁷ A stacked plot comparing the attenuation of the *N*-acetyl resonances of heparin (11.25 mg/mL) and DS (1.25 mg/mL) as a function of gradient amplitude is shown in Figure 3.4A. From this figure, it is visually evident that DS diffuses more slowly than heparin, as illustrated by the more gradual attenuation of

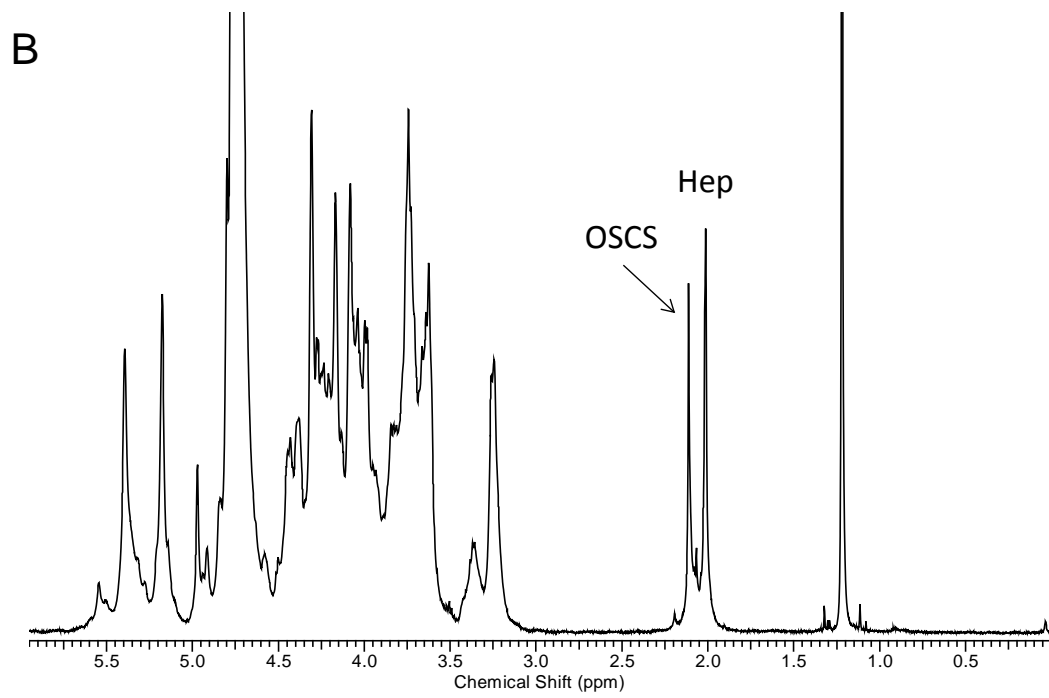
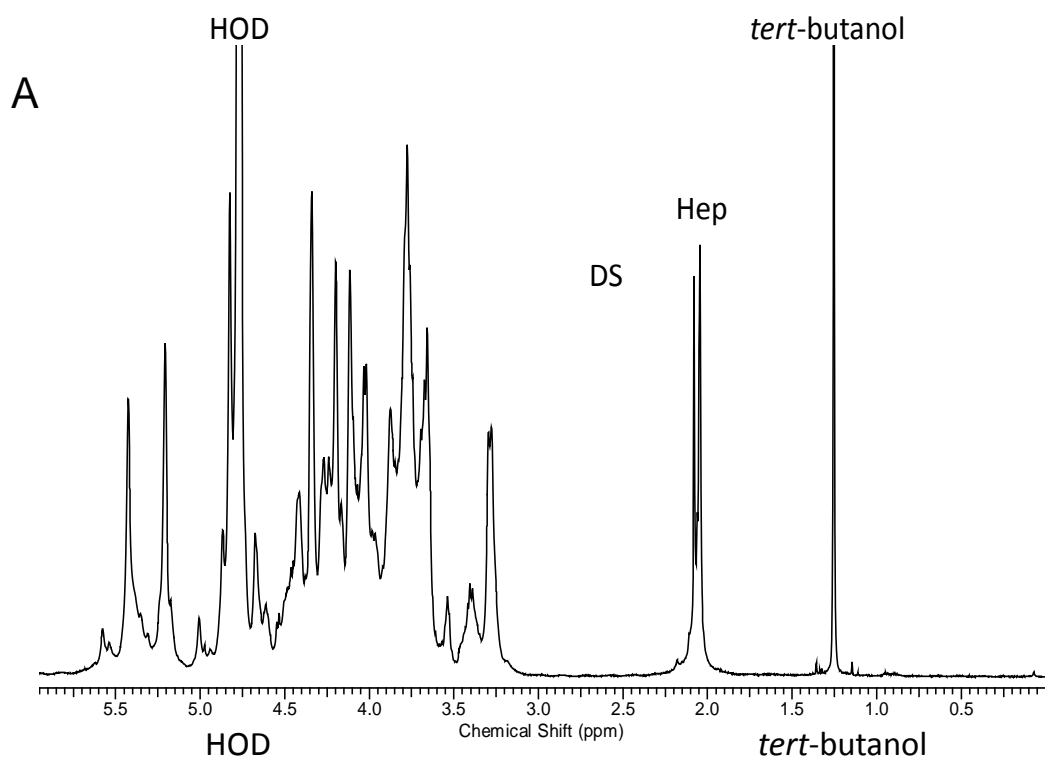


Figure 3.2. ^1H NMR spectra measured for (A) heparin/DS and (B) heparin/OSCS solutions. Both solutions were prepared to a total GAG concentration of 12.5 mg/mL containing 10% of the impurity by mass. Spectra were acquired by coaddition of 64 transients. Resolved resonances of dermatan sulfate (DS), oversulfated chondroitin sulfate (OSCS), and heparin (Hep) are labeled.

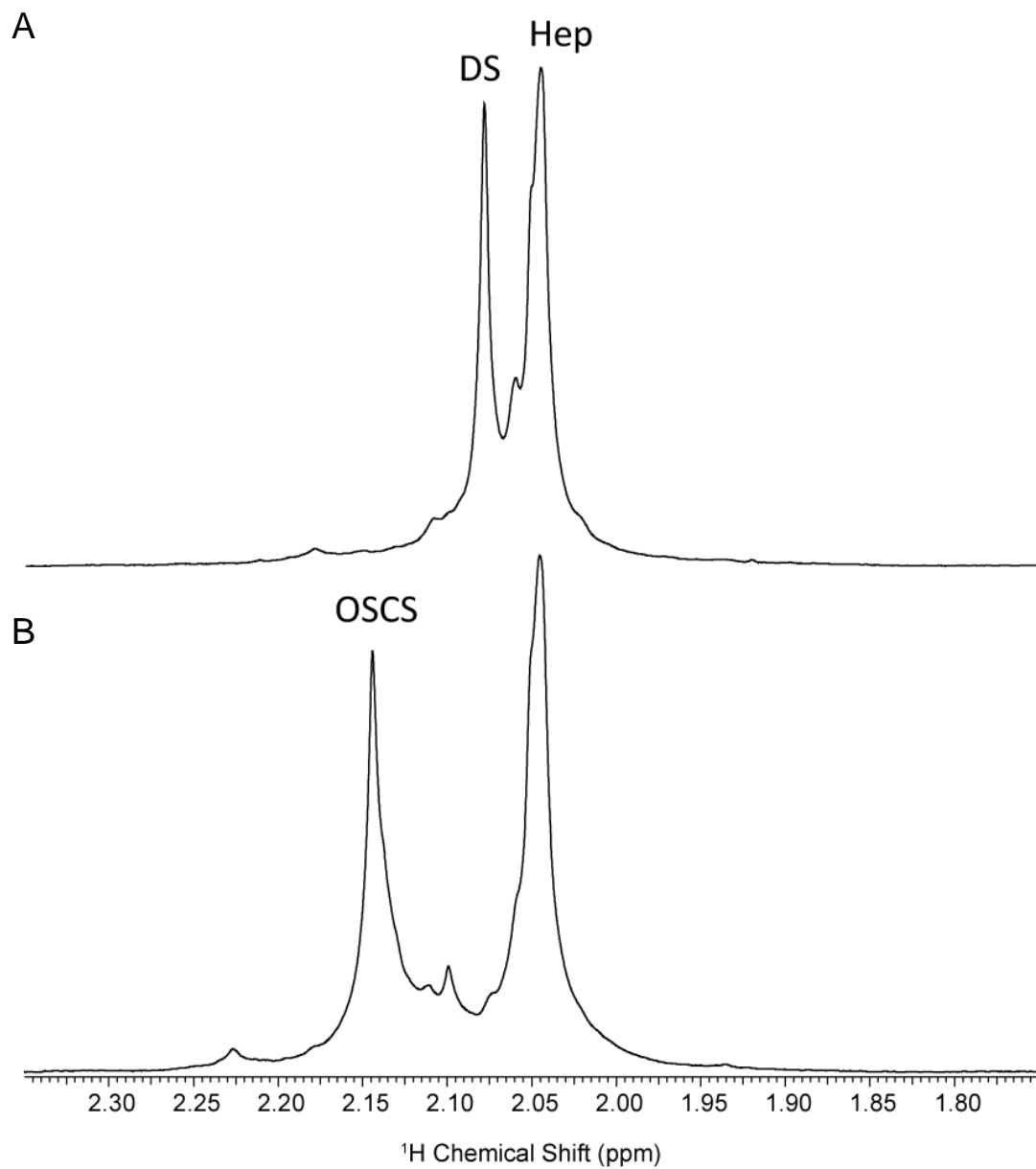


Figure 3.3. Comparison of *N*-acetyl region of the ¹H NMR spectra measured for (A) heparin/DS and (B) heparin/OSCS solutions. The *N*-acetyl resonances of dermatan sulfate (DS), oversulfated chondroitin sulfate (OSCS), and heparin (Hep) are labeled.

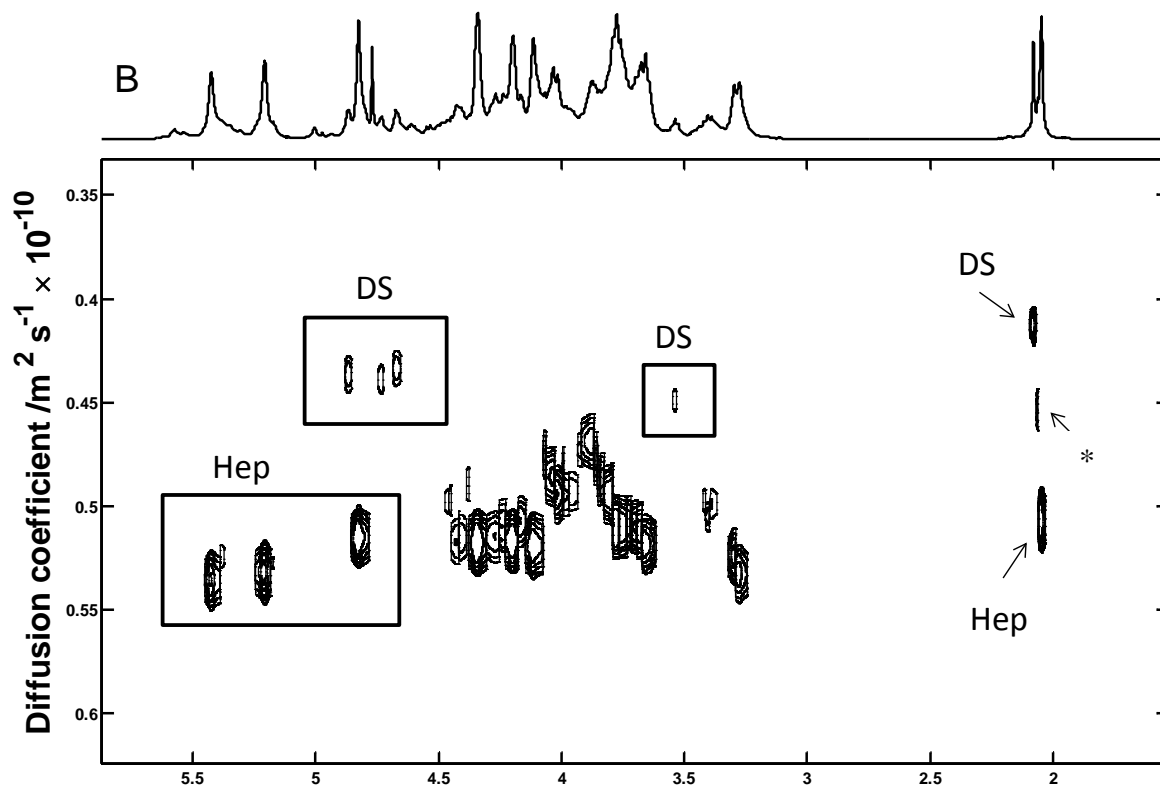
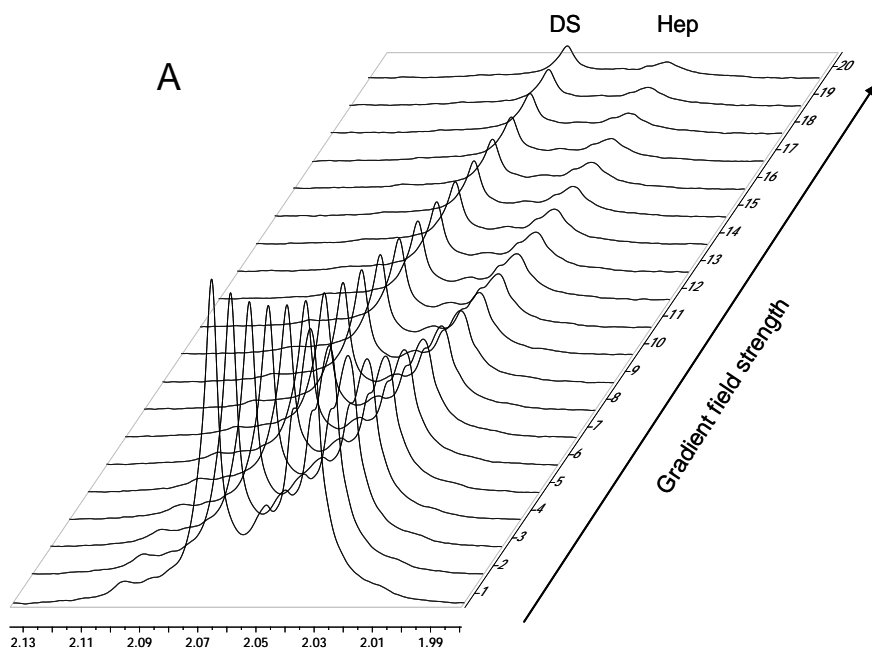


Figure 3.4. Diffusion NMR spectra for a solution of intact heparin and DS. (A) Stacked plot showing the decrease in the *N*-acetyl resonance intensity as a function of applied gradient. (B) DOSY spectrum. Spectra were acquired with 80 scans and 20 gradient increments from 5-95% with the spacing determined using squared function. Diffusion parameters were $\Delta = 300$ ms and $\delta = 2.5$ ms.

the DS *N*-acetyl resonance. The DOSY spectrum obtained for this data set is shown in Figure 3.4B. The diffusion coefficients calculated using the *N*-acetyl resonances of the two components are $5.12 \pm 0.01 \times 10^{-11} \text{ m}^2/\text{s}$ and $4.11 \pm 0.01 \times 10^{-11} \text{ m}^2/\text{s}$ for heparin and DS, respectively. The viscosity measured for this solution is $1.56 \pm 0.01 \text{ cSt}$, slightly larger than the value of $1.49 \pm 0.01 \text{ cSt}$ obtained for heparin alone at the same total GAG concentration. The peak that appears between DS and heparin at 2.060 ppm, is present in the DOSY plot at a diffusion value that is intermediate between that of heparin and DS. This diffusion value is likely not reliable and instead results from overlap of the heparin and DS resonances leading to an apparent diffusion coefficient that is a weighted average of the individual values for the two species.

In addition to the *N*-acetyl resonance, additional resonances of DS at chemical shifts of 4.675, 4.733, and 4.869 ppm were also resolved from the resonances of heparin in the DOSY spectrum in Figure 5B. The diffusion coefficients calculated using these three anomeric DS resonances are $4.29 \pm 0.01 \times 10^{-11}$, $4.36 \pm 0.01 \times 10^{-11}$, and $4.30 \pm 0.01 \times 10^{-11} \text{ m}^2/\text{s}$, respectively. These values are slightly larger than the value calculated using the DS *N*-acetyl resonance. Because the diffusion coefficients of heparin and DS are similar, overlapped resonances of the two GAGs give rise to a single peak in the diffusion dimension of the DOSY spectrum. Using a monoexponential fit, these spectrally overlapped resonances produce diffusion coefficients that are a weighted average of the values for heparin and DS.⁸ Although we attempted biexponential fitting using the DOSY tool box, in our hands the diffusion coefficients determined were physically unreasonable, although fits with lower residuals were obtained.

The smaller diffusion coefficient measured for DS is expected as it has a larger average chain length and molecular weight (25.6 kDa) than porcine heparin (11.6

kDa).^{28, 37} The slower rate of DS diffusion may also result from its lower extent of sulfation and greater molecular rigidity in aqueous solution.³⁸⁻⁴⁰ As was observed by Ogston and co-workers in their study of hyaluronic acid, the diffusion coefficient of the GAG biopolymer may depend on its size, rigidity and on aggregation, which can hinder the free diffusion of solution components.^{34, 41} Therefore, it should be stressed that the reported diffusion coefficients are conditional values depending on the solute concentration and other solution parameters.

3.3.1.2 Diffusion Analysis of Solutions of Heparin and OSCS

A solution containing 12.5 mg/mL of intact heparin containing OSCS, prepared using the heparin system suitability standard available through the USP was also analyzed using DOSY. OSCS was present in the standard sample at a concentration of upwards of 10% as indicated by its MSDS. The ¹H NMR spectrum of this solution is presented in Figure 3.2B, with the expansion of the *N*-acetyl region of the spectrum shown in Figure 3.3B. The resonance at 2.045 ppm in Figure 3.3B corresponds to the *N*-acetyl group of heparin while the resonance at 2.144 ppm corresponds to OSCS. No DS was observed in this sample as indicated by the absence of a peak at 2.079 ppm. The DOSY spectrum measured for this heparin/OSCS solution is shown in Figure 3.5. As was observed for DS, for the well-resolved resonances of heparin and OSCS, the species are also separated according to the differences in their diffusion coefficients. Using the *N*-acetyl resonances, the measured diffusion coefficient for heparin in this solution was $5.45 \pm 0.01 \times 10^{-11} \text{ m}^2/\text{s}$ while the diffusion coefficient for OSCS was $5.25 \pm 0.01 \times 10^{-11} \text{ m}^2/\text{s}$. The viscosity of the heparin/OSCS solution was $1.49 \pm 0.01 \text{ cSt}$, the same as determined for the USP heparin solution at 12.5 mg/mL. In the anomeric region

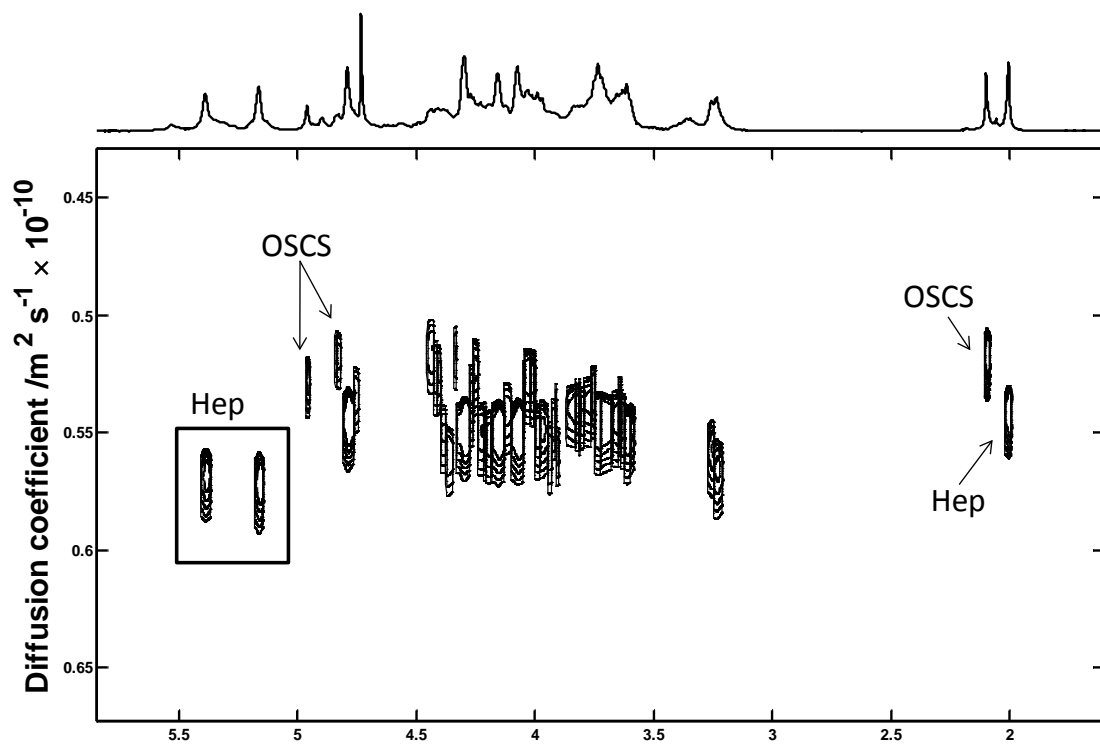


Figure 3.5. DOSY NMR spectrum measured for a solution containing intact heparin and OSCS; spectrum acquired with 80 scans and 20 gradient increments from 5-95%, spaced using a squared function. Diffusion parameters were $\Delta = 300$ ms and $\delta = 2.5$ ms.

of the spectrum, the well-resolved resonances of heparin at 5.209 and 5.426 ppm produced diffusion coefficients of $5.50 \pm 0.01 \times 10^{-11} \text{ m}^2/\text{s}$ and $5.49 \pm 0.01 \times 10^{-11} \text{ m}^2/\text{s}$ within error of the value determined using the *N*-acetyl resonance. The diffusion coefficients calculated for the OSCS peaks at 4.946 and 5.003 ppm, indicated by the arrows in Figure 3.5, are $4.73 \pm 0.01 \times 10^{-11} \text{ m}^2/\text{s}$ and $5.14 \pm 0.01 \times 10^{-11} \text{ m}^2/\text{s}$, respectively.

The previous publications by Sitkowski et al.¹² and Bednarek et al.¹³ relied only on the analysis of the *N*-acetyl region of the DOSY plots producing diffusion coefficients of $3.90 \times 10^{-11} \text{ m}^2/\text{s}$ for a solution of unfractionated heparin (UFH A) at 16.16 mg/mL and $4.49 \times 10^{-11} \text{ m}^2/\text{s}$ for a different unfractionated heparin solution (UFH B) at 16.23 mg/mL. Samples in this study were supplied to investigators by the UK National Institute for Biological Standards and Control. Because the anomeric resonances of heparin, DS, and OSCS are better resolved than the *N*-acetyl resonances, they likely provide a more reliable diffusion coefficient for the solutions studied. The *N*-acetyl resonances, however, have the advantage of greater intensity, so for solutions containing a low concentration of a contaminant the *N*-acetyl region could provide the most robust determination for the impurity.

All GAG components within the sample can contribute to viscosity effects and to molecular crowding, but a larger contribution to molecular crowding should be expected for the larger biopolymers DS and OSCS. Additional barriers to free diffusion can be attributed to the rigidity of the biopolymer and to aggregation. Because DS is thought to be a more rigid molecule in aqueous solutions, it should hinder the diffusion of heparin to a greater extent than OSCS. This may explain the differences in the heparin diffusion coefficients measured for these solutions. Due to its lower average charge, DS could

also have a greater tendency to aggregate providing an additional barrier to the diffusion of both heparin and DS. Because both heparin and OSCS are highly negatively charged, repulsion likely prevents their aggregation. To test these ideas, measurements were performed for a solution containing 10% CSA and 90% heparin at a total GAG concentration of 12.5 mg/mL. The naturally occurring CSA is a precursor in the synthesis of OSCS, and has a sulfation level similar to DS.⁷ The average molecular weight of heparin is 11.6 kDa while the molecular weight average for DS and CSA are 25.6 and 26.1 kDa, respectively.⁴⁵ The diffusion coefficient measured using the *N*-acetyl resonance of CSA, $4.85 \pm 0.01 \times 10^{-11} \text{ m}^2/\text{s}$, is slightly less than that measured for intact heparin in this solution, $4.95 \pm 0.01 \times 10^{-11} \text{ m}^2/\text{s}$, but higher than the value measured for DS $4.11 \pm 0.01 \times 10^{-11} \text{ m}^2/\text{s}$ in the heparin/DS sample. The viscosity for the solution of heparin and CSA was $1.53 \pm 0.01 \text{ cSt}$.

Even though DS, CSA and OSCS have similar average molecular weights, the diffusion coefficients of DS and CSA, and of intact heparin in solutions containing DS and CSA, were lower than the values determined for either heparin or OSCS in the intact heparin/OSCS solution. We attribute the slower diffusion of heparin in the DS and CSA solutions to the greater rigidity of DS and CSA. The larger viscosities of the heparin/DS, $1.56 \pm 0.01 \text{ cSt}$, and heparin/CSA, $1.53 \pm 0.01 \text{ cSt}$, solutions compared with the value measured for the heparin/OSCS solution, $1.49 \pm 0.01 \text{ cSt}$, supports this hypothesis. These observations highlight the potential difficulties of using diffusion coefficients as a means of characterizing heparin or its contaminants. Although DOSY provides a mechanism for distinguishing components, especially those having resolved resonances, the diffusion coefficients determined for solutions of the intact biopolymers

should be considered as apparent diffusion coefficients that are dependent on solution conditions and do not provide a rigorous basis for identification.

3.3.2 DOSY Analysis of Heparin Digest Solutions

To improve the *in situ* diffusion-based separation of heparin and its impurities, intact heparin was enzymatically digested with the enzyme heparinase I. This heparinase enzyme is selective for heparin, leaving both DS and OSCS unaffected.^{42, 43} As shown in Figure 1.5, the enzymatic reaction introduces a double bond into the non-reducing end of the heparin uronic acid residue at the cleavage site allowing the progress of the reaction to be monitored using UV absorbance at 232 nm or by following the resonance of the proton adjacent to the double-bond.^{44, 45} Following extensive digestion, the solutions were analyzed using ¹H and diffusion NMR to evaluate the extent of depolymerization and to separate the components of the digest solution based on differences in diffusion. The diffusion spectra measured for solutions containing 11.25 mg/ mL heparin and 1.25 mg/ mL DS, shown in Figure 3.6, highlight the greater attenuation of the heparin resonances following enzymatic digestion (A) compared with intact heparin (B).

The DOSY spectrum of the digest solution of heparin and DS is shown in Figure 3.7A. As a result of the enzymatic digestion of the heparin, the *N*-acetyl resonances of the two components are better resolved in the diffusion dimension than in the corresponding spectrum of the intact heparin/DS solution (Figure 3.4B). The diffusion coefficient for heparin following digestion was $2.04 \pm 0.05 \times 10^{-10} \text{ m}^2/\text{s}$ while the diffusion coefficient for DS was $7.63 \pm 0.01 \times 10^{-11} \text{ m}^2/\text{s}$. Along with the increase in the diffusion coefficients measured for each species, the solution viscosity also decreased

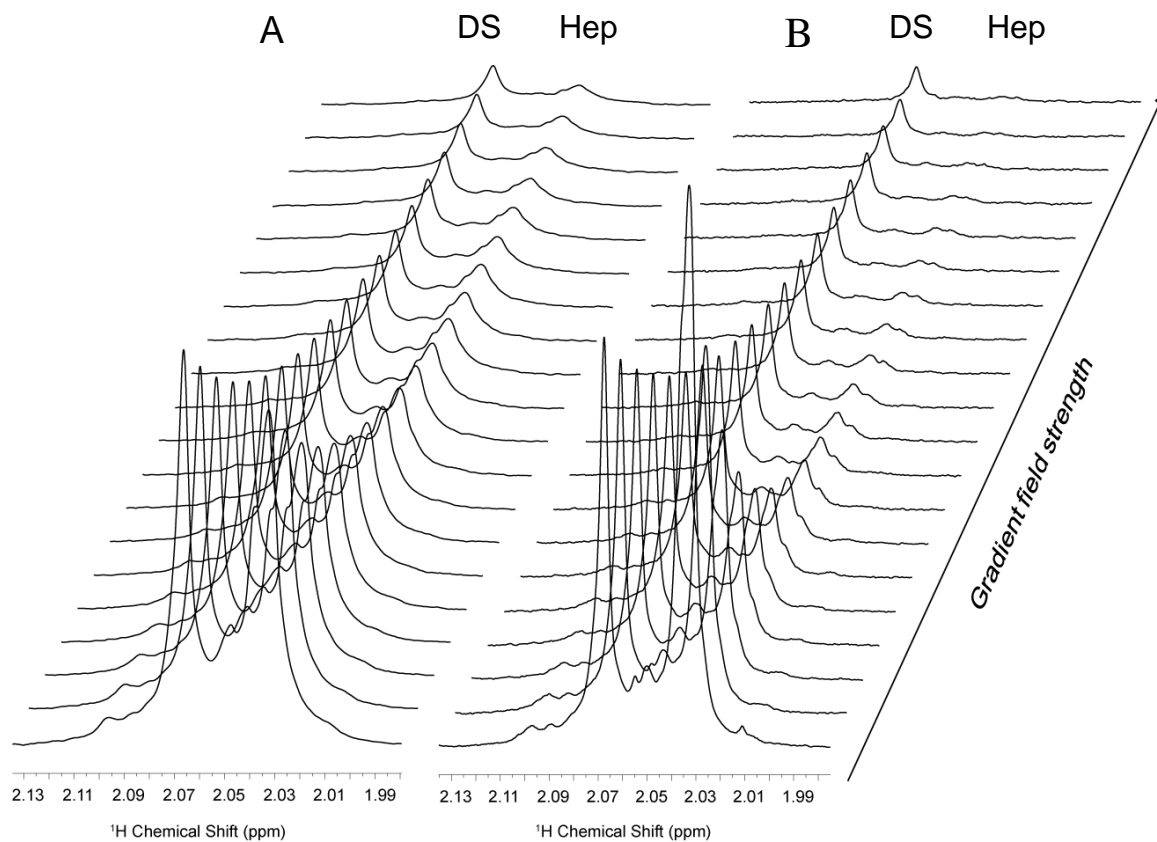


Figure 3.6. ^1H NMR BPPSTE spectra showing the attenuation of the *N*-acetyl resonances of heparin and DS (A) after digestion and (B) before digestion with the enzyme heparinase I.

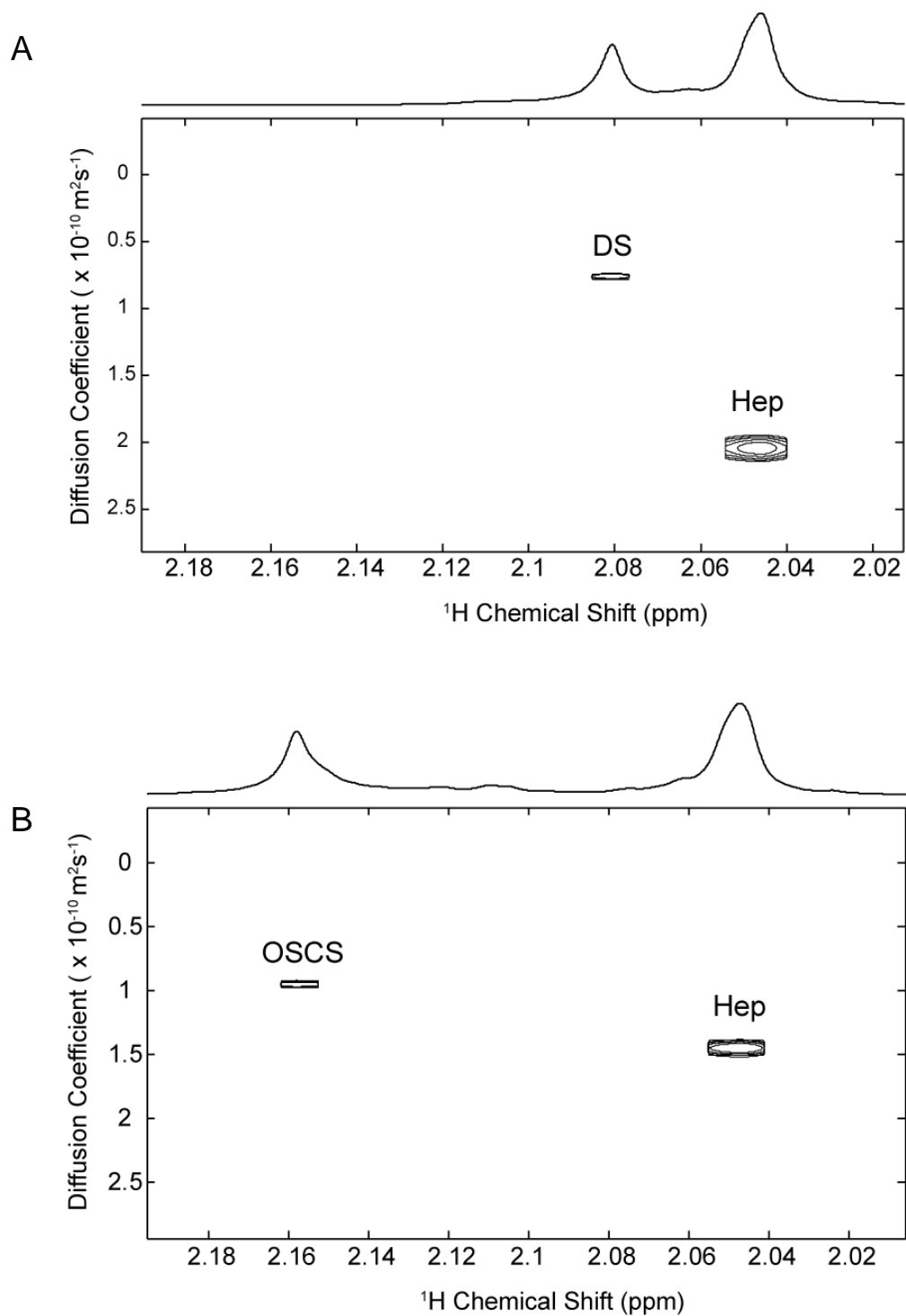


Figure 3.7. The *N*-acetyl region of the DOSY spectra measured for heparinase I digest solutions of (A) heparin/DS and (B) heparin/OSCS. Spectra were acquired with 80 scans and 20 gradient increments from 5-95% using a squared function. Diffusion parameters were $\Delta = 200$ ms and $\delta = 2.4$ ms.

significantly from 1.56 ± 0.01 to 1.09 ± 0.01 cSt following heparin digestion. Because the low molecular weight heparin fragments produced by enzymatic digestion diffuse much more quickly than the DS polymer, the resolution between the components in the diffusion dimension is significantly improved.

As OSCS is also resistant to the action of the heparinase enzyme. To improve the resolution between the heparin and OSCS a similar digestion with heparinase I was performed using the solution prepared using the USP system suitability sample. As with DS, the diffusivity of the digested heparin increased substantially, improving the resolution between heparin and OSCS in the DOSY plot shown in Figure 3.7B. Following digestion, the diffusion coefficient of heparin increased to $1.45 \pm 0.03 \times 10^{-10}$ m²/s while that of OSCS increased to $9.50 \pm 0.01 \times 10^{-11}$ m²/s. The solution viscosity decreased from 1.49 ± 0.01 cSt to 1.08 ± 0.01 cSt following digestion. Interestingly, the heparin diffusion coefficient in this solution was 29% smaller than in the corresponding heparin/DS digest solution, evidence that the enzymatic depolymerization of heparin was inhibited by OSCS consistent with the observations of Zhang et al.⁴²

The large increase in the DS and OSCS diffusion coefficients following enzymatic digestion clearly indicates the extent to which the intact heparin polysaccharide contributed to the viscosity of the solution and to the hindrance of diffusion through molecular crowding effects. In these solutions, DS and OSCS were present at 10% of the total GAG by mass. Depolymerization of intact heparin can assist in the detection of contaminants by diffusion, especially for biopolymer contaminants that have hydrodynamic properties similar to those of heparin. The advantage provided by enzymatic digestion would be especially important for contaminants that do not have resonances well-resolved from those of heparin.

3.3.3 Diffusion-Edited NMR Spectroscopy

A heparin API (Active Pharmaceutical Ingredient) sample containing a small amount of DS as a naturally occurring impurity was digested with a cocktail of heparinase enzymes to completely depolymerize the intact heparin leaving the DS unaffected. The pulse program `stebpgp1s1d`, a one-dimensional version of the BPPSTE experiment, was used to obtain a diffusion-edited spectrum containing just the resonances of the DS contaminant. Figure 3.8 shows an overlay of (A) the ^1H NMR spectrum of the digest solution, (B) the clean diffusion-edited DS spectrum measured for the digest solution using the `stebpgp1s1d` pulse program, and (C) the ^1H NMR spectrum of a standard solution containing only DS. In this case, rather than using differences in diffusion coefficients to resolve the resonances of heparin and DS in a DOSY plot, a single spectrum was acquired using a constant gradient amplitude and diffusion time to selectively eliminate the resonances of the digested heparin. In addition to the removal of the resonances of the low molecular weight heparin oligosaccharides in Figure 3.8B, the resonances of HOD and *tert*-butanol were also selectively suppressed on the basis of their rapid diffusion.

A heparinase cocktail digestion of heparin in the presence of OSCS was performed using a 25 mg/mL heparin sample containing 1.25 mg/mL OSCS to completely depolymerize the intact heparin leaving the OSCS unaffected. The one-dimensional BPPSTE experiment was used to obtain a diffusion-edited spectrum containing just the resonances of the OSCS contaminant. Figure 3.9 shows an overlay of (A) the ^1H NMR spectrum of the digest solution, (B) the diffusion-edited spectrum measured for the digest solution using the `stebpgp1s1d` pulse program, and (C) the ^1H

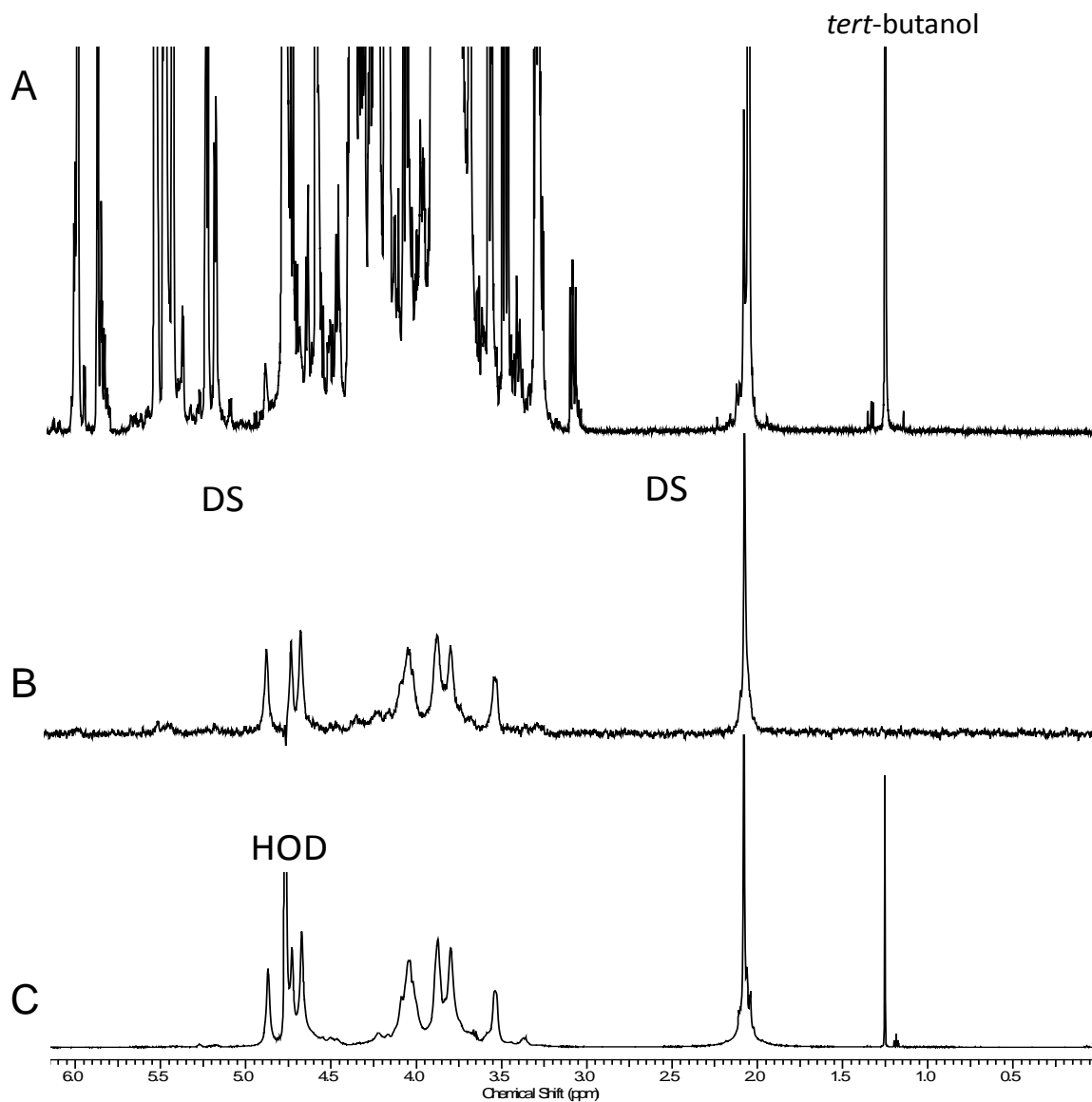


Figure 3.8. ^1H NMR spectra of (A) heparin API digest solution, (B) diffusion-edited spectrum of the DS contained in the heparin digest solution, (C) DS standard solution. The diffusion-edited spectrum was acquired with 1536 scans, gradient strength of 95%, $\Delta = 200$ ms and $\delta = 2.2$ ms.

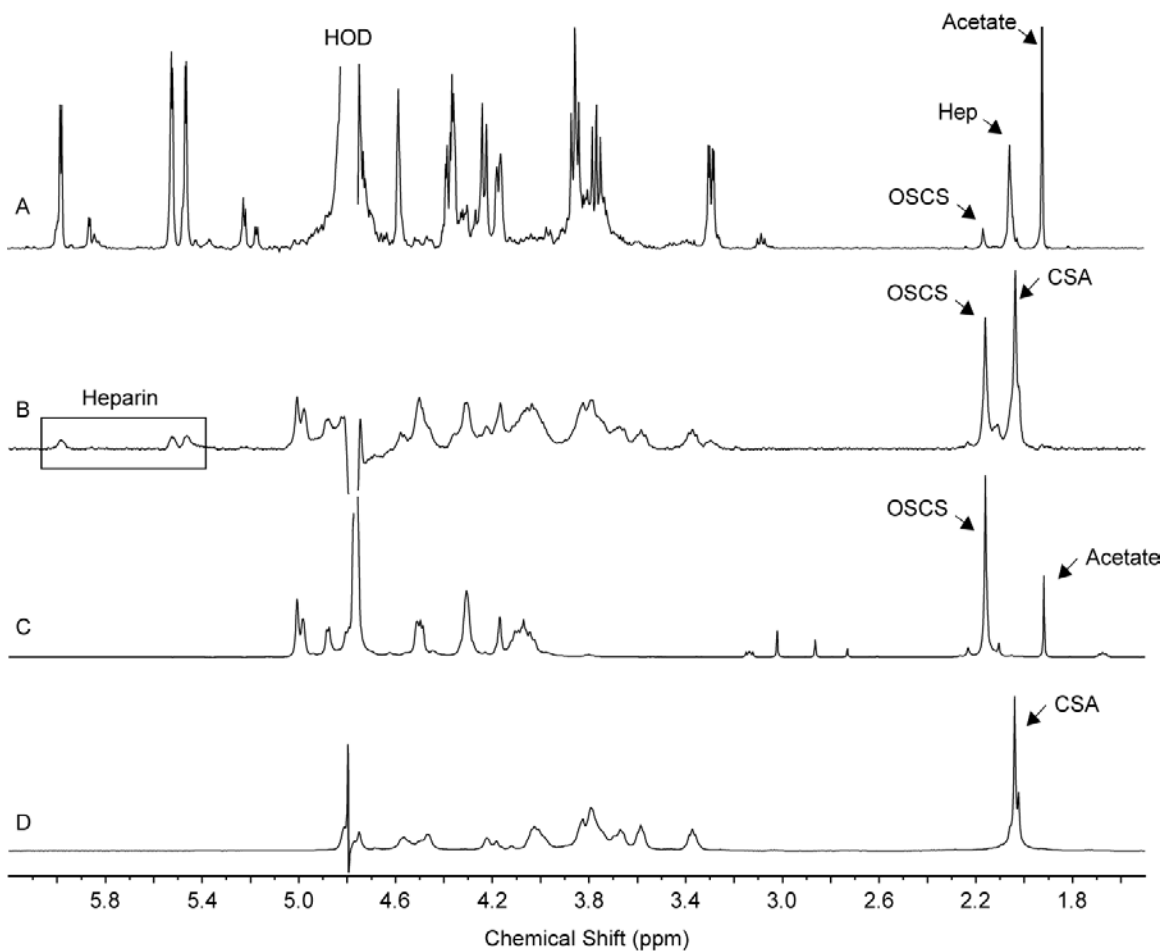


Figure 3.9. ¹H NMR spectra of (A) heparin/OSCS digest solution (B) diffusion-edited spectrum of the OSCS and CSA contained in the heparin digest solution, (C) OSCS solution prepared in our laboratory, and (D) CSA standard solution. The diffusion-edited spectrum was acquired with 2048 scans, gradient strength of 95%, $\Delta = 180$ ms and $\delta = 2$ ms. ppm that do not correspond to OSCS. In spectrum (C), the resonance at 3.142 ppm is due to TrBA and those at 2.871 and 3.027 ppm are due to DMF remaining from the synthesis of OSCS in our laboratory.

NMR spectrum of an OSCS solution synthesized in our laboratory by Christopher Jones as described in section 2.2.2.

Figure 3.10 shows an expansion of the *N*-acetyl region of spectra presented in Figure 3.9. Upon closer observation of the spectra in Figure 3.9B and C, it is evident that there are additional peaks in the region from 3.3 to 3.9. In addition to the smaller peaks from 3.3 to 3.9 ppm, an intense peak in the acetyl region at 2.041 ppm was also observed. From the measured chemical shift of the *N*-acetyl resonance and the ^1H survey spectrum (Figure 3.10B), we confirmed that in addition to OSCS (Figure 3.10C) an appreciable amount of CSA (Figure 3.10D) was also present in the solution. CSA was present as an unintentional contaminant in the heparin sample present at approximately 5% based on comparison of the intensity of the CSA *N*-acetyl peak with OSCS which was spiked into the digest solution at a known concentration. Because both OSCS and CSA are resistant to the heparinase enzymes used to digest heparin, they remained intact and therefore were resolved spectrally from the resonances of the heparin fragments which were present at a much higher abundance. A small amount of heparin was observed in the diffusion edited spectrum (Figure 3.9B), they were present at a significantly reduced intensity as a result of the diffusion gradients.

3.4 Summary

Diffusion NMR has been shown to be a powerful technique for the DOSY analysis of heparin and its impurities DS and OSCS, especially in regions of the NMR spectrum containing well-resolved resonances of the individual components. However, even in the relatively dilute GAG solutions examined in this work, the diffusion behavior of the intact biopolymers can be dominated by viscosity and molecular crowding effects.

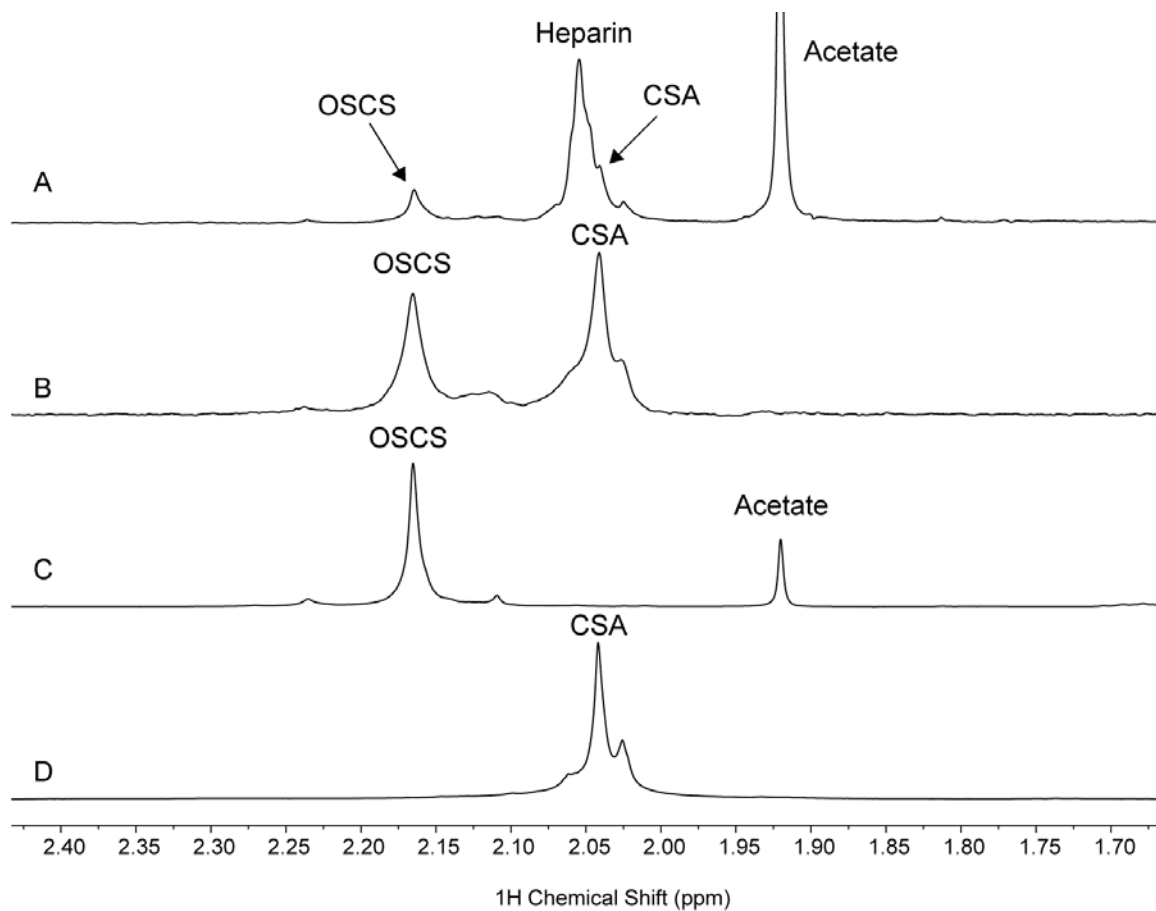


Figure 3.10. *N*-acetyl region of the ^1H NMR spectra of (A) heparin/OSCS digest solution (B) diffusion-edited spectrum of the OSCS and CSA contained in the heparin digest solution, (C) OSCS solution prepared in our laboratory, and (D) CSA standard solution.

As a consequence the NMR diffusion results obtained for solutions of intact heparin and its impurities must only be interpreted qualitatively. These limitations can be largely overcome using heparinase I to selectively digest heparin to low molecular weight oligosaccharides, significantly improving the DOSY resolution of heparin and its biopolymer impurities. Enzymatic digestion also allowed the measurement of a clean diffusion-edited spectrum of DS found naturally at low levels in a heparin API sample. Additionally in the analysis of the heparin sample contaminated with OSCS, the cocktail digestion of heparin allowed for the measurement of a clean-diffusion-edited spectrum of OSCS. Inspection of the diffusion-edited spectrum of OSCS alluded to the presence of an unexpected contaminant. The contaminant was identified as CSA which was present as a contaminant from the heparin. For low-level contaminants, especially those without resonances that are well-resolved from those of heparin, acquisition of a diffusion-edited ^1H NMR spectrum could assist in rapid identification providing that the contaminant was also resistant to the action of heparinase enzymes.

3.5 References

1. Guerrini, M.; Zhang, Z. Q.; Shriver, Z.; Naggi, A.; Masuko, S.; Langer, R.; Casu, B.; Linhardt, R. J.; Torri, G.; Sasisekharan, R. Orthogonal analytical approaches to detect potential contaminants in heparin. *Proc. Natl. Acad. Sci. U. S. A.* **2009**, *106*, 16956-16961.
2. Beyer, T.; Diehl, B.; Randel, G.; Humpfer, E.; Schäfer, H.; Spraul, M.; Schollmayer, C.; Holzgrabe, U. Quality assessment of unfractionated heparin using ¹H nuclear magnetic resonance spectroscopy. *J. Pharm. Biomed. Anal.* **2008**, *48*, 13-19.
3. Bigler, P.; Brenneisen, R. Improved impurity fingerprinting of heparin by high resolution ¹H NMR spectroscopy. *J. Pharm. Biomed. Anal.* **2009**, *49*, 1060-1064.
4. Ward, J.; Baker, J.; Miller, S.; Deborde, C.; Maucourt, M.; Biais, B.; Rolin, D.; Moing, A.; Moco, S.; Vervoort, J.; Lommen, A.; Schäfer, H.; Humpfer, E.; Beale, M. An inter-laboratory comparison demonstrates that [¹H]-NMR metabolite fingerprinting is a robust technique for collaborative plant metabolomic data collection. *Metabolomics*, *6*, 263-273.
5. Dumas, M.-E.; Maibaum, E. C.; Teague, C.; Ueshima, H.; Zhou, B.; Lindon, J. C.; Nicholson, J. K.; Stamler, J.; Elliott, P.; Chan, Q.; Holmes, E. Assessment of Analytical Reproducibility of ¹H NMR Spectroscopy Based Metabonomics for Large-Scale Epidemiological Research: the INTERMAP Study. *Anal. Chem.* **2006**, *78*, 2199-2208.
6. Dixon, A. M.; Larive, C. K. NMR Spectroscopy with Spectral Editing for the Analysis of Complex Mixtures. *Appl. Spectrosc.* **1999**, *53*, 426A-440A.
7. Johnson Jr, C. S. Diffusion ordered nuclear magnetic resonance spectroscopy: principles and applications. *Prog. Nucl. Magn. Reson. Spectrosc.* **1999**, *34*, 203-256.
8. Morris, K. F.; Johnson, C. S. Diffusion-ordered two-dimensional nuclear magnetic resonance spectroscopy. *J. Am. Chem. Soc.* **1992**, *114*, 3139-3141.
9. Barjat, H.; Morris, G. A.; Smart, S.; Swanson, A. G.; Williams, S. C. R. High-Resolution Diffusion-Ordered 2D Spectroscopy (HR-DOSY) - A New Tool for the Analysis of Complex Mixtures. *J. Magn. Reson., Ser. B* **1995**, *108*, 170-172.
10. Morris, K. F.; Stilbs, P.; Johnson, C. S. Analysis of mixtures based on molecular size and hydrophobicity by means of diffusion-ordered 2D NMR. *Anal. Chem.* **1994**, *66*, 211-215.
11. Price, K.; Lucas, L.; Larive, C. Analytical applications of NMR diffusion measurements. *Anal. Bioanal. Chem.* **2004**, *378*, 1405-1407.
12. Sitkowski, J.; Bednarek, E. b.; Bocian, W.; Kozerski, L. Assessment of Oversulfated Chondroitin Sulfate in Low Molecular Weight and Unfractionated Heparins Diffusion Ordered Nuclear Magnetic Resonance Spectroscopy Method. *J. Med. Chem.* **2008**, *51*, 7663-7665.
13. Bednarek, E.; Sitkowski, J.; Bocian, W.; Mulloy, B.; Kozerski, L. An assessment of polydispersed species in unfractionated and low molecular weight heparins by diffusion ordered nuclear magnetic resonance spectroscopy method. *J. Pharm. Biomed. Anal.* **2010**, *53*, 302-308.
14. Novoa-Carballal, R.; Fernandez-Megia, E.; Jimenez, C.; Riguera, R. NMR methods for unravelling the spectra of complex mixtures. *Nat. Prod. Rep.*, *28*, 78-98.

15. Rabenstein, D. L.; Isab, A. A. Water elimination by T_2 relaxation in ^1H spin-echo FT NMR studies of intact human erythrocytes and protein solutions. *J. Magn. Reson.* **1979**, *36*, 281-286.
16. Rabenstein, D. L.; Nakashima, T.; Bigam, G. A pulse sequence for the measurement of spin-lattice relaxation times of small molecules in protein solutions. *J. Magn. Reson.* **1979**, *34*, 669-674.
17. Hajduk, P. J.; Olejniczak, E. T.; Fesik, S. W. One-Dimensional Relaxation- and Diffusion-Edited NMR Methods for Screening Compounds That Bind to Macromolecules. *J. Am. Chem. Soc.* **1997**, *119*, 12257-12261.
18. Otto, W. H.; Larive, C. K. Improved Spin-Echo-Edited NMR Diffusion Measurements. *J. Magn. Reson.* **2001**, *153*, 273-276.
19. Khera, S.; Grillo, M.; Schnier, P.; Hollis, S. Application of diffusion-edited NMR spectroscopy for the structural characterization of drug metabolites in mixtures. *J. Pharm. Biomed. Anal.* **2010**, *51*, 164-169.
20. Kellenbach, E.; Burgering, M.; Kaspersen, F. Using Pulse Field Gradient NMR-Based Diffusion Experiments To Identify Signals of Low-Molecular-Weight Impurities. *Org. Process Res. Dev.* **1999**, *3*, 141-144.
21. Henderson, T. Feasibility study for the rapid screening of target molecules using translational diffusion coefficients: diffusion-ordered NMR spectroscopy of biological toxins. *Anal. Bioanal. Chem.* **2010**, *396*, 1465-1471.
22. Wu, D. H.; Chen, A. D.; Johnson, C. S. An Improved Diffusion-Ordered Spectroscopy Experiment Incorporating Bipolar-Gradient Pulses. *J. Magn. Reson., Ser. A* **1995**, *115*, 260-264.
23. Tanner, J. E. Use of the Stimulated Echo in NMR Diffusion Studies. *J. Chem. Phys.* **1970**, *52*, 2523-2526.
24. Pelta, M. D.; Barjat, H.; Morris, G. A.; Davis, A. L.; Hammond, S. J. Pulse sequences for high-resolution diffusion-ordered spectroscopy (HR-DOSY). *Magn. Reson. Chem.* **1998**, *36*, 706-714.
25. Nilsson, M. The DOSY Toolbox: A new tool for processing PFG NMR diffusion data. *J. Magn. Reson.* **2009**, *200*, 296-302.
26. Stejskal, E. O.; Tanner, J. E. Spin Diffusion Measurements: Spin Echoes in the Presence of a Time-Dependent Field Gradient. *J. Chem. Phys.* **1965**, *42*, 288-292.
27. Johnson Jr, C. S. Diffusion ordered nuclear magnetic resonance spectroscopy: principles and applications. *Prog. Nucl. Magn. Reson. Spectrosc.* **1999**, *34*, 203-256.
28. Huo, R.; Wehrens, R.; Duynhoven, J. v.; Buydens, L. M. C. Assessment of techniques for DOSY NMR data processing. *Anal. Chim. Acta* **2003**, *490*, 231-251.
29. Bohme, U.; Vogel, C.; Meier-Haack, J.; Scheler, U. Determination of Charge and Molecular Weight of Rigid-Rod Polyelectrolytes. *J. Phys. Chem. B* **2007**, *111*, 8344-8347.
30. Balayssac, S.; Trefi, S.; Gilard, V.; Malet-Martino, M.; Martino, R.; Delsuc, M.-A. 2D and 3D DOSY ^1H NMR, a useful tool for analysis of complex mixtures: Application to herbal drugs or dietary supplements for erectile dysfunction. *J. Pharm. Biomed. Anal.* **2009**, *50*, 602-612.

31. Monteiro, C.; Herve du Penhoat, C. Translational Diffusion of Dilute Aqueous Solutions of Sugars as Probed by NMR and Hydrodynamic Theory. *J. Phys. Chem. A* **2001**, *105*, 9827-9833.
32. Price, W. S.; Tsuchiya, F.; Arata, Y. Lysozyme Aggregation and Solution Properties Studied Using PGSE NMR Diffusion Measurements. *J. Am. Chem. Soc.* **1999**, *121*, 11503-11512.
33. Therien-Aubin, H.; Zhu, X. X.; Moorefield, C. N.; Kotta, K.; Newkome, G. R. Effect of Ionic Binding on the Self-Diffusion of Anionic Dendrimers and Hydrophilic Polymers in Aqueous Systems as Studied by Pulsed Gradient NMR Techniques. *Macromolecules* **2007**, *40*, 3644-3649.
34. Masaro, L.; Zhu, X. X. Interaction of Ethylene Glycol with Poly(vinyl alcohol) in Aqueous Systems As Studied by NMR Spectroscopy. *Langmuir* **1999**, *15*, 8356-8360.
35. Park, H. S.; Sung, J.; Chang, T. Hydrogen Bonding Effect on Probe Diffusion in Semidilute Polymer Solutions: Polymer Chain Structure Dependence. *Macromolecules* **1996**, *29*, 3216-3219.
36. Holme, K. R.; Perlin, A. S. Nuclear magnetic resonance spectra of heparin in admixture with dermatan sulfate and other glycosaminoglycans. 2-D spectra of the chondroitin sulfates. *Carbohydr. Res.* **1989**, *186*, 301-312.
37. Volpi, N. Fractionation of Heparin, Dermatan Sulfate, and Chondroitin Sulfate by Sequential Precipitation: A Method to Purify a Single Glycosaminoglycan Species from a Mixture. *Anal. Biochem.* **1994**, *218*, 382-391.
38. Johansson, L.; Skantze, U.; Lofroth, J. E. Diffusion and interaction in gels and solutions. 2. Experimental results on the obstruction effect. *Macromolecules* **1991**, *24*, 6019-6023.
39. Sloopmaekers, D.; De Jonghe, C.; Reynaers, H.; Varkevisser, F. A.; Bloys van Treslong, C. J. Static light scattering from [kappa]-carrageenan solutions. *Int. J. Biol. Macromol.* **1988**, *10*, 160-168.
40. Bernadó, P.; de la Torre, J. G.; Pons, M. Macromolecular crowding in biological systems: hydrodynamics and NMR methods. *J. Mol. Recognit.* **2004**, *17*, 397-407.
41. Ogston, A. G.; Preston, B. N.; Wells, J. D. On the Transport of Compact Particles Through Solutions of Chain-Polymers. *Proc R Soc London, A* **1973**, *333*, 297-316.
42. Zhang, Z.; Weñwer, M.; Li, B.; Kemp, M. M.; Daman, T. H.; Linhardt, R. J. Oversulfated Chondroitin Sulfate: Impact of a Heparin Impurity, Associated with Adverse Clinical Events, on Low-Molecular-Weight Heparin Preparation. *J. Med. Chem.* **2008**, *51*, 5498-5501.
43. Lindhardt, R. J.; Fitzgerald, G. L.; Cooney, C. L.; Langer, R. Mode of action of heparin lyase on heparin. *Biochimica et Biophysica Acta (BBA) - Protein Structure and Molecular Enzymology* **1982**, *702*, 197-203.
44. Chuang, W.-L.; McAllister, H.; Rabenstein, D. L. Hexasaccharides from the histamine-modified depolymerization of porcine intestinal mucosal heparin. *Carbohydr. Res.* **2002**, *337*, 935-945.
45. Limtiaco, J.; Beni, S.; Jones, C.; Langeslay, D.; Larive, C. NMR methods to monitor the enzymatic depolymerization of heparin. *Anal. Bioanal. Chem.* **2011**, *399*, 593-603.

CHAPTER FOUR

NMR Methods to Monitor the Enzymatic Depolymerization of Heparin

Based on a paper published in Analytical and Bioanalytical Chemistry

Anal. Bioanal. Chem., 2011, 399, 593-603.

This chapter describes the application of diffusion NMR, more specifically diffusion-ordered spectroscopy (DOSY), to monitor the enzymatic depolymerization of heparin using heparinase I. Diffusion NMR does not require the physical separation of the components in the reaction mixture, and instead can be used to monitor the reaction solution directly in the NMR tube. Using diffusion NMR, the enzymatic reaction can be stopped at the desired time point, maximizing the abundance of larger oligosaccharides for protein binding studies or completion of the reaction if the goal of the study is exhaustive digestion for characterization of the disaccharide composition.

4.1 Introduction: Depolymerization of Heparin

Due to heparin and heparan sulfate (HS) high degree of structural diversity, most methods used to characterize them utilize a bottom-up approach, whereby the intact polysaccharide chains are chemically or enzymatically depolymerized to smaller oligosaccharides prior to analysis. In an exhaustive digestion, heparin and HS are reduced to their disaccharide building blocks, permitting compositional analysis. Studies using larger oligosaccharides, which are more biologically relevant, are conducted on samples obtained by the partial depolymerization of the polysaccharide. In these studies, the digested oligosaccharides are first separated into size-uniform fractions, which are

further resolved to individual oligosaccharides by a charge-based separation. The purified oligosaccharides can then be characterized through the use of mass spectrometry (MS) and nuclear magnetic resonance (NMR) as discussed in Chapter 5.

Following the enzymatic or chemical depolymerization of heparin, analysis of the digests typically proceeds via the physical separation of the digest components based on differences in their size and charge. UV and fluorescence detection work well for the identification of GAGs at the disaccharide level where standards are available; however they do not provide structural information for larger components. In cases where larger oligosaccharides are targeted, digest solutions are generally size-separated by SEC to isolate corresponding di, tetra, hexa, and larger oligosaccharide fractions which are further purified to individual oligosaccharides using strong anion exchange (SAX)¹⁻⁴ or reverse-phase ion-pairing (RPIP)-HPLC.^{5, 6} Purified oligosaccharides are then structurally characterized by NMR and MS.

In this study, we used ¹H NMR spectra and diffusion NMR results in conjunction with UV absorbance at 232 nm to monitor the enzymatic depolymerization of heparin using heparinase I. DOSY NMR has been used in the analysis of intact heparin samples to evaluate purity and to identify both natural and intentional contaminants of heparin, as discussed in Chapter 3.^{7, 8} As demonstrated herein, diffusion NMR allows the investigator to follow the extent of the enzymatic reaction non-invasively and quench the digestion at the desired endpoint.

4.2 Experimental Section

4.2.1 Chemicals

Porcine intestinal mucosa heparin sodium salt grade 1-A, calcium acetate hydrate, ammonium bicarbonate, heparin disaccharide Δ UA(2S)-(1 \rightarrow 4)-GlcNS(6S) (IS) sodium salt, and tris(hydroxymethyl)aminomethane (Tris) were obtained from Sigma Chemical Company (St. Louis, MO). Heparin disaccharide IS is the product of the digestion of heparin and heparan sulfate with the enzymes heparinase I and II enzymes. Hydrochloric acid (HCl), *tert*-butanol, and sodium hydroxide were obtained from Fisher Scientific Co. (Fair Lawn, NJ). Heparinase I (EC 4.2.2.7) isolated from *Flavobacterium heparinum* was purchased from IBEX Technologies Inc. (Montreal, Quebec). HPLC grade water was purchased from Burdick and Jackson (Muskegon, MI). Deuterium oxide (D, 99.9%) was obtained from Cambridge Isotope Laboratories (Andover, MA).

4.2.2 Enzymatic Depolymerization of Heparin

Digestion of 1 g heparin was carried out in 50 mL of 100 mM Tris buffer, pH 6.8, containing 2.5 mM calcium acetate. The enzyme heparinase I (0.5 IU) was added to the mixture and incubated at 28 °C in a water bath for 66 hr. One international unit (IU) of the enzyme produces 1 μ mol of unsaturated uronic acid from porcine mucosal heparin per min at 30 °C and pH 7.0. The water bath temperature was controlled using a Fisher Scientific Isotemp 1013S scientific temperature regulator. The enzymatic reaction was quenched by placing the reaction vessel into boiling water for 5 min. The depolymerization solution was then lyophilized and reconstituted into 15 mL of the separation buffer (0.5 M NH_4HCO_3) prior to SEC separation.

4.2.3 Monitoring the Progress of the Enzymatic Depolymerization with UV Absorption

During the 66 hr enzymatic depolymerization, UV absorption measurements were taken at regular intervals (ranging from 15 min to 6 hr) to monitor the progress of the enzymatic reaction. UV measurements were performed at a wavelength of 232 nm using a Thermo Scientific NanoDrop 2000 spectrophotometer (Wilmington, DE). The NanoDrop has a 1 mm path length requiring only 1 μL of sample. For absorption measurements above 1 AU, samples were diluted by a factor of 2-4 times with the depolymerization buffer prior to analysis. At 232 nm, the molar extinction coefficient for the monounsaturated disaccharide is $5500 \text{ M}^{-1}\text{cm}^{-1}$.⁹

4.2.4 SEC Fractionation

The heparin-derived oligosaccharides were size fractionated on a column (200 cm x 0.39 cm) packed with Bio-Rad Bio-Gel P-10 resin fine (Bio-Rad Laboratories Hercules, CA) and eluted with 0.5 M NH_4HCO_3 at a flow rate of 0.08 mL/min. The total volume contained in each of the fractions collected was 4.5 mL. The progress of the separation was monitored offline by UV absorption measurements at 232 nm using the NanoDrop spectrophotometer as described above. Following SEC, similar sized fractions were pooled and stored as a lyophilized powder at $-20 \text{ }^\circ\text{C}$ for future use.

4.2.5 ^1H NMR Experiments

Solutions for NMR analysis were prepared by adding 50 μL of D_2O and 8 μL of 100 mM *tert*-butanol in D_2O to 550 μL of the depolymerization solution in a 5 mm NMR tube. Solutions were mixed by gently tapping the tube. ^1H NMR spectra were recorded

using a Bruker Avance spectrometer operating at 599.84 MHz. All experiments were performed using a broad band inverse probe with x, y, and z-gradients. Chemical shifts were referenced to *tert*-butanol (1.253 ppm) added as an internal reference. For each ^1H NMR spectrum, 64 transients were collected into 26,624 data points using a 6009 Hz spectral window and a 2 s relaxation delay. NMR spectra were acquired using the wet pulse program (WET) included with the standard Topspin release version 1.3.¹⁰ The automated Bruker shape tool was used to create the sinc pulse for selective excitation of the H_2O resonance. ^1H NMR spectra were processed using the academic edition of the ACD/Labs 1D NMR processing software, version 12.01. Prior to Fourier transformation, the free induction decays (FIDs) were zero filled to 65 536 points and apodized by multiplication with an exponential function equivalent to 1 Hz line broadening. The reaction solution was maintained at a temperature of 28 °C using the temperature control unit of the NMR spectrometer. The spectrometer was initially shimmed using a volume-matched solution of *tert*-butanol in the depolymerization buffer, with the reaction solution used for final optimization of the shims. The first spectrum was acquired at 10 min following a quick shim and optimization of the sinc shaped pulses for WET solvent suppression. Subsequent spectra were manually initiated at intervals of 10 min for the first hour of the digestion to a total interval time of 8 hr. From the ^1H NMR spectra acquired throughout the course of the digestion, the peak area of the *N*-acetyl resonance was fit using the ACD NMR processing software and the calculated areas were normalized to the fitted area of the *tert*-butanol resonance. These normalized areas were used to compare the relative intensities between the subsequent spectra.

The calibration of the z-gradient coil used for the diffusion measurements was checked using the known diffusion coefficient for lysozyme ($1.07 \times 10^{-11} \text{ m}^2/\text{s}$) at 20 °C

and a concentration of 5 mg/mL prepared in D₂O.¹¹ Diffusion spectra were acquired using the stimulated echo experiment with bipolar gradients (stebpgp1s). Diffusion (Δ) and gradient pulse times (δ) were optimized for each time-point using a one-dimensional version of the stimulated echo pulse program, stepgp1s1d. Gradient amplitudes were incremented as a square dependence from 5% to 95% into 12 or 18 gradient increments. Following acquisition, the FIDs were apodized by multiplication with an exponential function equivalent to 1.5 Hz line broadening and baseline corrected using a first order polynomial prior to DOSY processing using the DOSY Toolbox software.¹² Reference deconvolution was performed on a few spectra but resulted in significant errors in the fitting of the decay plots and was therefore not used in the processing.

Because the diffusion spectra were acquired in a solution of 90% water, it was necessary to eliminate the first spectrum corresponding to a gradient field strength of 1.686 G cm⁻¹ before DOSY processing. By eliminating the spectrum for the first gradient increment, we were able to drastically attenuate the water peak permitting the measurement of the diffusion coefficients for the nearby H-4 and anomeric proton resonances. To simplify the DOSY analysis, processing was carried out on individual spectral regions of interest corresponding to the H-4, anomeric, and *N*-acetyl resonances. We found this helpful especially when processing later experiments, after the first day of the digestion, as these spectra were observed to be more complex in terms of the size distribution of the heparin oligosaccharides. Peaks above a manually set threshold level were automatically picked by the DOSY Toolbox software for DOSY processing. Peaks were then fit to a standard monoexponential decay (HR-DOSY) with a diffusion resolution of 256 points. Fitting statistics for the pure exponential fitting to the

Stejskal-Tanner equation including fitting errors were determined and displayed following the DOSY processing.

4.3 Results and Discussion

The commercially available heparinase enzymes I, II, and III, each with unique specificity, are commonly used for heparin and HS digestions. Heparinase I cleaves the GlcNS(6S)→IdoA(2S) glycosidic bond and is considered specific for the analysis of heparin.¹³⁻¹⁵ Heparinase III is most active for 2-OH GlcA-containing glycosidic linkages and therefore is used for HS digestion.¹³ Although heparinase III tolerates 6-O sulfonation, it does not act on IdoA residues containing 2-O sulfo substituents.¹⁶ Heparinase II has broader substrate specificity cleaving a wide range of disaccharide repeat units with either 2-O sulfo or 2-OH at the uronic acid.¹³ Because heparinase II has been reported to have two distinct active sites, one which is heparinase I-like and the other heparinase III-like, it can be used for the analysis of both heparin and HS.² Exhaustive depolymerization of heparin is often carried out using a cocktail containing all three enzymes.

4.3.1 Monitoring the Enzymatic Depolymerization with UV Absorption

Cleavage of the heparin polysaccharide with heparinase enzymes introduces an unsaturated bond between C-4 and C-5 of the non-reducing end uronic acid, as shown in Figure 1.5. By exploiting the UV absorbance of the double-bond containing product, the progress of the reaction can be monitored as shown in Figure 4.1A. In our hands the results of heparinase digestions are highly variable and the extent of the reaction can be difficult to predict. The heparinase enzymes are not very stable and the point at which

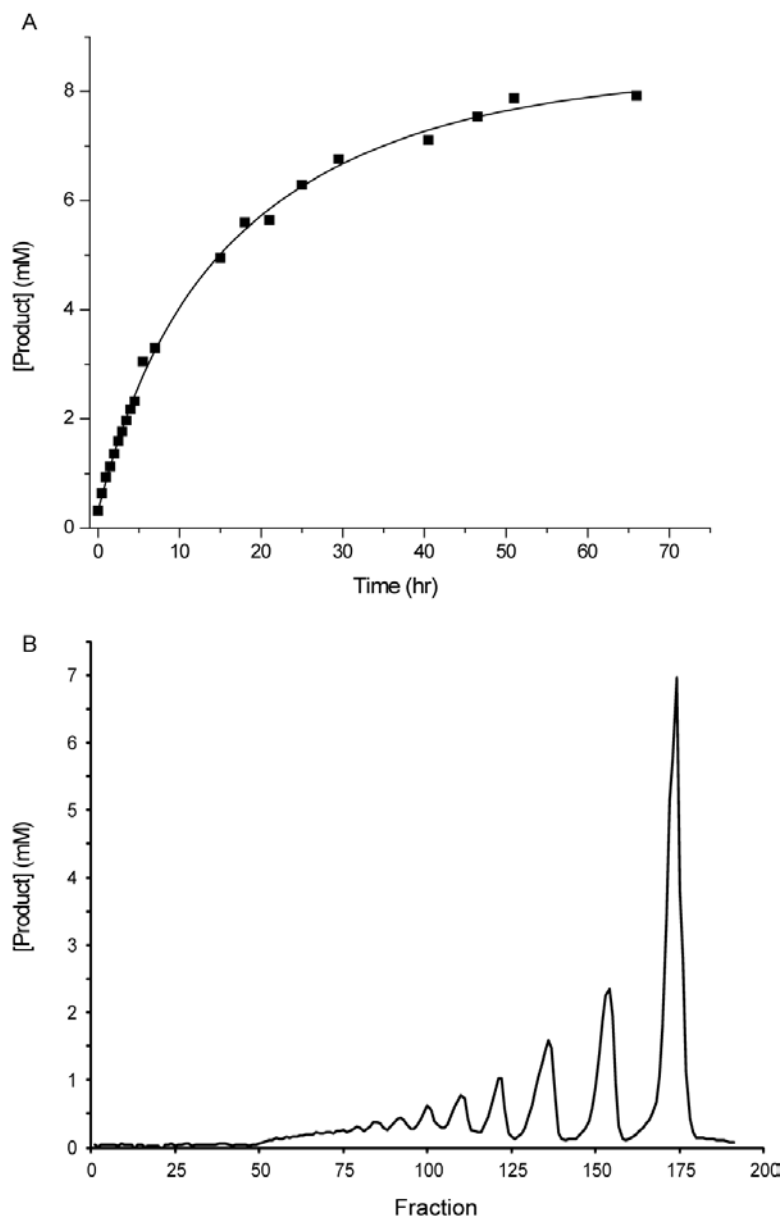


Figure 4.1. Production and size-fractionation of heparin derived oligosaccharides. (A) Progression of the enzymatic digestion measured at 232 nm using a 1 mm path length. Aliquots were taken at regular intervals (20 min to 6 hr). (B) Preparative SEC of heparin oligosaccharides following the enzymatic depolymerization of heparin with heparinase I. The labels represent the number of saccharide units in the depolymerization products with dp2 corresponding to disaccharides, dp4 to tetrasaccharides, etc. Product concentrations were calculated using the measured absorbance and the molar extinction coefficient for the monounsaturated disaccharide of $5500 \text{ M}^{-1} \text{ cm}^{-1}$.

product formation plateaus in a digestion depends both on the consumption of reactant and the loss of enzymatic activity. If the 1 g heparin sample had been completely depolymerized to disaccharides by the 50 units of heparinase I used in this experiment, a product concentration of roughly 34 mM would be predicted. Obviously the value expected would be less than this value, as some disaccharide sequences will not fit the consensus sequence required for heparinase I activity. The reaction shown in Figure 4.1A was considered complete after 66 h as indicated by a plateau in the product concentration at 7.92 mM. If the goal of this separation had been to produce mostly larger oligosaccharides for protein binding studies, it could have been desirable to quench the reaction prior to its plateau.

Following the enzymatic digestion, an SEC separation was performed to determine the size-dispersion of the resulting heparin oligosaccharides and fractionate the products based on size. The 50 mL heparinase digest solution was lyophilized, reconstituted into 15 mL of the separation buffer (0.5 M NH_4HCO_3) and applied to a preparative-scale SEC column for separation. A column void volume of 346.5 mL was observed before the initial elution of the largest class of isolated oligosaccharides, the hexadecasaccharides (dp16) present in fractions 77-81.

The progress of the size separation was monitored by UV absorbance measurements plotted as effective double bond concentration vs. SEC fraction in Figure 4.1B. The resolution obtained provided an efficient separation even for the largest oligosaccharides. As can be seen from the SEC chromatogram, completion of the reaction did not correspond to complete digestion of heparin to its corresponding disaccharide subunits. This is expected for a digestion using only heparinase I. The SEC peak with the highest concentration corresponds to the disaccharide component (dp2).

Preceding peaks correspond to larger heparin oligosaccharides ranging from tetra- (dp4) to hexadecasaccharides (dp16), with each SEC fraction containing a heterogeneous mixture of similarly-sized oligosaccharides varying in their disaccharide compositions.

4.3.2 Monitoring the Enzymatic Depolymerization of Heparin with ^1H NMR

In addition to following the enzymatic digestion using UV absorbance, ^1H NMR spectra were acquired at various points throughout the reaction. Although NMR has been used extensively in the characterization of heparin-derived oligosaccharides^{3, 17-19}, to our knowledge there has only been one study that used NMR to monitor heparin depolymerization.³ Chuang et al. used ^1H NMR to monitor the kinetics of heparinase digestions with and without histamine present and to identify the oligosaccharide fragments that were bound to histamine in the digest solution.³

In this study, ^1H NMR was also used to follow the progress of the heparinase I enzymatic digestion. The digest solution was left in the NMR probe for the duration of the reaction to maintain temperature control and to avoid extensive shimming between acquisitions. Figure 4.2 shows example ^1H NMR spectra measured as a function of reaction time. Near the start of the reaction (10 min) the spectra are essentially those of intact heparin. The heparin resonances are broad due in large part to the short T_2 values of the large biopolymer (MW ~ 12-15 kDa). Heparin resonance line widths are also affected by binding of trace paramagnetic impurities, and addition of small amounts of deuterated EDTA can significantly improve spectral quality.²⁰ However, because heparinase I requires Ca^{2+} for activity, EDTA could not be added to the reaction solution.²¹

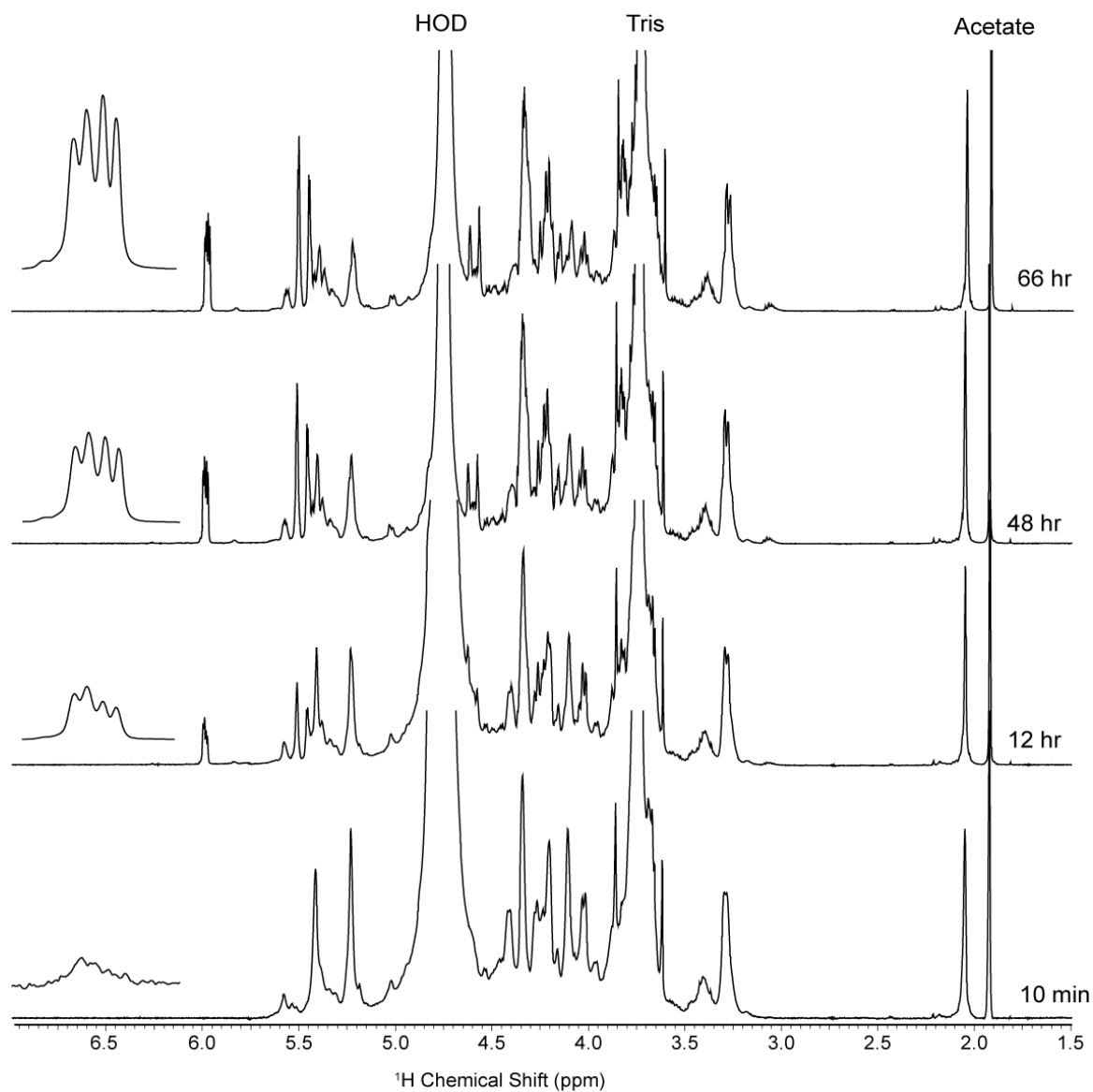


Figure 4.2. ¹H NMR spectra measured as a function of time for the depolymerization solution. Insets correspond to the H-4 resonances of the $\Delta^{4,5}$ double bond introduced during digestion. Arrows indicate the signature peaks used for the NMR diffusion measurements. Anomeric peaks at 5.460 and 5.514 ppm correspond to the formation of Δ UA(2S)-(1 \rightarrow 4)-GlcNS(6S).

As the reaction proceeded, heparin oligosaccharide resonances corresponding to the digested heparin fragments were observed at chemical shifts of 5.973, 5.981, 5.990, and 5.998 ppm consistent with results reported by Chuang.³ These resonances correspond to oligosaccharides produced by the β -elimination reaction and containing a double bond proton, $\Delta\text{UA}_{\text{H4}}$, at the C-4 position of the non-reducing end uronic acid at the cleavage site. As expected, the intensities of the $\Delta\text{UA}_{\text{H4}}$ resonances increased as the reaction progressed, although the rate of increase was different for the different peaks. The resonances at 5.990 and 5.998 ppm were observed to increase at a faster rate than the resonances at 5.973 and 5.981 ppm during the first 12 hr of the digestion. As the reaction progressed, as indicated by the increase in UV absorption, the upfield resonances continued to increase and at 48 hr the resonances at 5.973 and 5.981 ppm were similar in intensity to the resonances at 5.990 and 5.998 ppm, as shown in the inset of Figure 4.2. The two upfield resonances at 5.973 and 5.981 ppm are also more narrow, suggesting that these resonances may arise from smaller oligosaccharide fragments.

In addition to monitoring the $\Delta\text{UA}_{\text{H4}}$, we were also interested in identifying additional resonances which act as signatures of heparinase I digestion, especially resonances for the H-1 protons of the heparin oligosaccharides. Two new resonances in the anomeric region of the spectrum at 5.460 and 5.514 ppm, indicated by the arrows in Figure 4.2, were also observed to increase as the reaction progressed. In concert with the increase in intensity of these resonances, the anomeric resonances for the intact heparin at 5.235 and 5.407 ppm diminished over time. The increased intensity of the H-1 proton resonances of 5.460 and 5.514 indicate a significant increase in the amount of

Δ UA(2S)-(1 \rightarrow 4)-GlcNS(6S), disaccharide IS, the primary disaccharide building block of heparin containing a double bond as a result of the enzymatic cleavage.

4.3.3 Monitoring the Enzymatic Depolymerization of Heparin using DOSY

The NMR diffusion experiments were performed using dilute aqueous solutions of heparin. As described in chapter 3, because the diffusion behavior of solution components is related to hydrodynamic properties such as size, shape, and charge, solution components can be distinguished provided that the species have resolved resonances or significantly different diffusion coefficients.²²⁻²⁴ DOSY is commonly used to process and display diffusion data. DOSY spectra are calculated using an approximation to the inverse Laplace transform from a series of pulsed-field gradient (PFG)-NMR spectra acquired using gradient pulses with varying amplitudes. DOSY processing produces a pseudo-2D spectrum with NMR chemical shifts on the horizontal axis and calculated self-diffusion coefficients along the vertical axis, resolving the spectra of the individual components based on their diffusion behavior.²⁵⁻²⁷

DOSY NMR lends itself to monitoring reactions directly in the NMR tube. No physical separation of mixture components is required and reaction components can be identified by virtue of their ^1H NMR resonances and diffusion coefficients. These experiments used the bipolar pulse-pair stimulated echo experiment (BPPSTE).²⁸ The stimulated echo sequence avoids phase modulation of coupled resonances by storing the magnetization along the longitudinal axis during the diffusion delay, while the use of bipolar gradients reduces the effect of eddy currents and corresponding lock disturbances. Diffusion coefficients were calculated for individual resonances in the

BPPSTE spectra by measuring signal attenuation as a function of gradient amplitude. Signal intensities were fit to the Stejskal-Tanner equation (equation 1.10).

Although interactions of heparin and HS with proteins and peptides is considered primarily electrostatic involving interactions between the cationic ammonium, guanidinium, and imidazolium side chains of proteins and peptides with the anionic sites on heparin and HS, binding through unique heparin and HS structural motifs is also important for biological activity.¹³ The exhaustive digestion of heparin significantly affects the biological activity of the oligosaccharides produced by eliminating binding specificity.^{29, 30} Depolymerization reaction monitoring is currently performed using analytical scale SEC or SAX separations with UV detection to determine the oligosaccharide size distribution as a function of time.^{1, 31} These separations are time-consuming and wasteful of sample as each measurement requires extraction of an aliquot from the depolymerization reaction solution.

DOSY has traditionally been used for the analysis and characterization of mixtures and aggregates^{25, 26, 32-34}, however, the Morris group recently reported the use of DOSY to follow the acid hydrolysis of sucrose and maltotriose.^{35, 36} To our knowledge DOSY has not been used to monitor heparinase digestions, therefore we designed experiments to test the ability of DOSY to follow the heparin depolymerization reaction *in situ*. If successful, DOSY could be used to monitor the size distribution of oligosaccharides produced as the enzymatic reaction proceeds. This would allow the investigator to quench the reaction at the optimum time to maximize the yield of the larger oligosaccharides most relevant for heparin binding studies.

A portion of the DOSY spectra measured for the digest samples at 1 and 66 hr are shown in Figure 4.3A and B, respectively. At 1 hr, only two major heparin anomeric

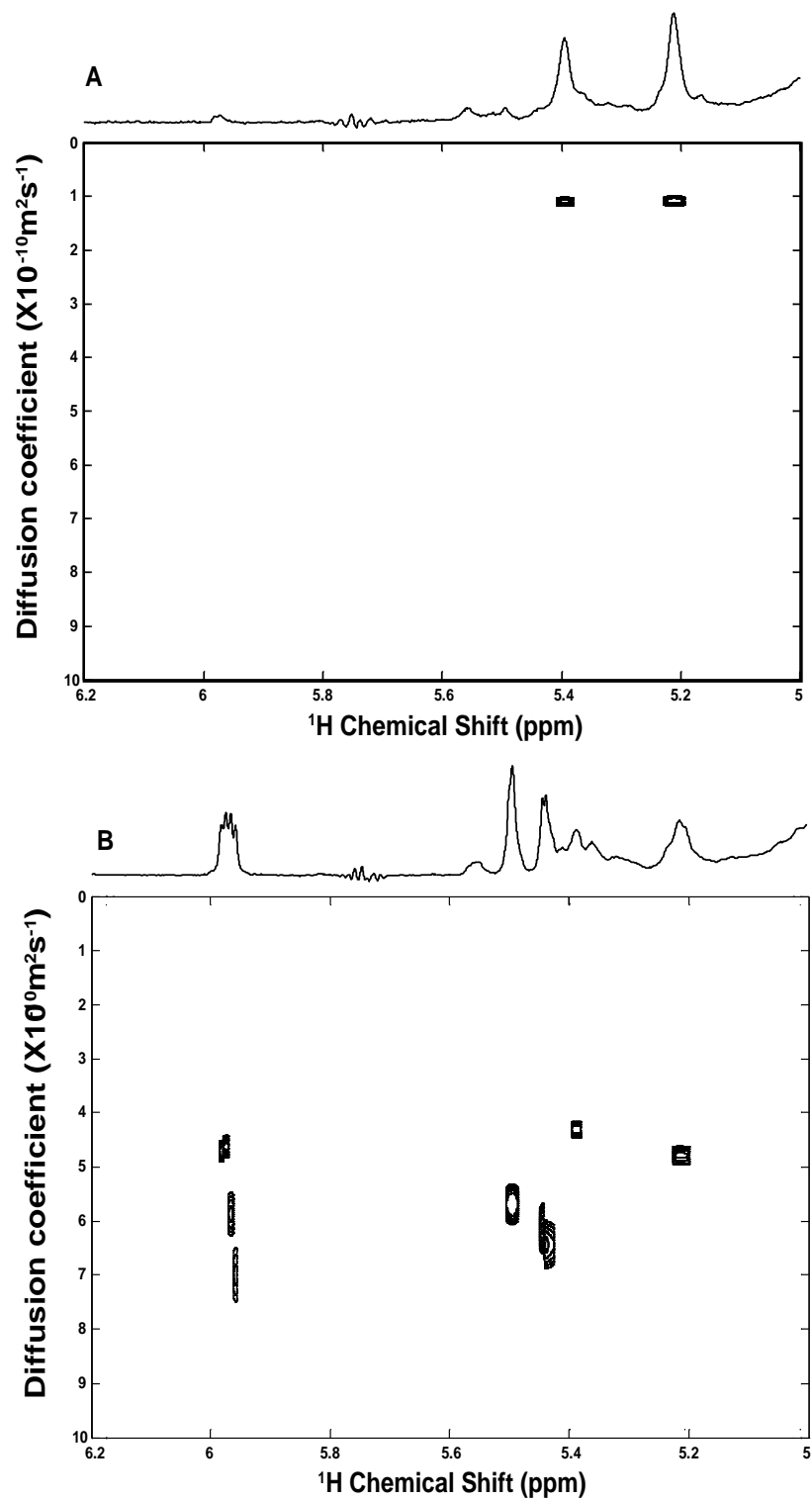


Figure 4.3. DOSY spectra for the anomeric and H-4 protons of the Δ UA residues of the heparin digest solution at (A) 1 hr and (B) 66 hr.

resonances are observed in the DOSY spectrum (Figure 4.3A). These peaks give rise to similar diffusion coefficients $1.03 \pm 0.02 \times 10^{-10}$ and $1.04 \pm 0.02 \times 10^{-10} \text{ m}^2\text{s}^{-1}$ for the proton resonances at 5.230 and 5.415 ppm, respectively. The diffusion coefficients are larger than values reported previously for intact heparin ($\sim 4.5 \times 10^{-11} \text{ m}^2\text{s}^{-1}$).⁷ This may be attributed to the slightly higher temperature used in the digestion as well as differences in the buffer concentration, heparin source, and the solution viscosities for water (1.00 mPa s) and deuterium oxide (1.25 mPa s). After 1 hr, the $\Delta\text{UA}_{\text{H4}}$ resonances can barely be detected above the noise and are too weak to provide a reliable DOSY fit.

The DOSY spectrum measured after 66 hr, Figure 4.3B, shows much greater variability in the calculated diffusion coefficients. Regions of the spectrum were fit individually to reduce the complexity of the analysis. Peaks above a manually set threshold level were automatically selected and fit with a monoexponential decay using the DOSY Toolbox software. In addition to calculating diffusion coefficients and fitting errors, residual plots for each of the fitted peaks were also available to evaluate the fitting model. From the SEC separation obtained for the bulk digestion solution at the completion of the reaction, it is evident that the digestion solution is a heterogeneous mixture dominated by smaller di- and tetrasaccharide components. Therefore, the resonances in the ^1H NMR and DOSY spectra are produced by multiple oligosaccharide components with different molecular weights but similar structures. It is possible to use routines such as CONTIN^{25, 37}, CORE³⁸, and multivariate approaches^{39, 40} to fit diffusion data measured for polydisperse components such as polymers or aggregates to a distribution of diffusion coefficients. However, for the diffusion spectra shown in Figure 4.3, a monoexponential fit of equation 1.10 to the data provides acceptable fits yielding average diffusion coefficients and reasonable fitting errors between 1.5 and 6%.

As the digestion progressed, diffusion coefficients were monitored for the anomeric resonances of the intact heparin (5.230 and 5.415 ppm), the H-4 resonances (5.973, 5.981, 5.990, and 5.998 ppm) of the cleaved product, as well as and *N*-acetyl peaks (2.048 ppm) of the heparin oligosaccharides. The values obtained over the course of the experiments are consistent with what is expected for an enzymatic digestion; as the reaction proceeded the measured diffusion coefficients for all peaks were observed to increase. This observation is expected as larger heparin oligosaccharides are continually cleaved into smaller fragments throughout the digestion thus increasing their individual mobilities in the solution. Though the diffusion coefficient for the *N*-acetyl resonance changed over the course of the digestion from an initial value of $1.04 \pm 0.01 \times 10^{-10} \text{ m}^2 \text{ s}^{-1}$ at 1 hr to $4.24 \pm 0.08 \times 10^{-10} \text{ m}^2 \text{ s}^{-1}$ at 66 hr, its intensity remained constant throughout the digestion with an average intensity of 0.377 ± 0.03 normalized to the intensity of *tert*-butanol.

Diffusion coefficients measured for the $\Delta\text{UA}_{\text{H4}}$ and the H-1 resonances associated with the digested heparin oligosaccharides also increased over the course of the digestion. Four hours following the initiation of the reaction, integration of the $\Delta\text{UA}_{\text{H4}}$ resonances at 5.990 and 5.998 ppm was possible producing diffusion coefficients of $1.68 \pm 0.19 \times 10^{-10}$ and $1.37 \pm 0.17 \times 10^{-10} \text{ m}^2 \text{ s}^{-1}$, respectively. Fitting of the $\Delta\text{UA}_{\text{H4}}$ resonances at 5.973 and 5.981 ppm was possible only after 13 hr producing diffusion coefficients of $5.77 \pm 0.76 \times 10^{-10}$ and $3.14 \pm 0.26 \times 10^{-10} \text{ m}^2 \text{ s}^{-1}$, respectively. The larger fitting errors obtained for the 4 and 13 hr data reflects the greater heterogeneity of the digestion products in these solutions and the fact that the enzymatic reaction is continuing during the 2 hr required for acquisition of the diffusion data set. At the conclusion of the digestion, the measured diffusion coefficients for the H-4 resonances

ranged from $4.87 \pm 0.15 \times 10^{-10} \text{ m}^2\text{s}^{-1}$ to $7.78 \pm 0.46 \times 10^{-10} \text{ m}^2\text{s}^{-1}$ for the peaks at 5.990 and 5.973 ppm, respectively, as shown in Figure 4.3B.

Differences observed between the diffusion coefficients determined for the *N*-acetyl, $\Delta\text{UA}_{\text{H4}}$ and anomeric resonances can be attributed to a reduced activity of the enzyme for heparin species low in sulfation, for example heparin fragments containing an acetylated glucosamine residue.¹³ Throughout the digestion, the components with upfield $\Delta\text{UA}_{\text{H4}}$ resonances (5.973 and 5.981 ppm) were observed to diffuse faster than components corresponding to the downfield resonances (5.990 and 5.998 ppm) as shown in Figure 4.3B. The $\Delta\text{UA}_{\text{H4}}$ resonance is a doublet of doublets with a larger coupling of around 4 Hz, observed in these spectra due to coupling to the H-3 proton of the uronic acid, and a <1 Hz long range coupling to H-2 not visible in these spectra due to the apodization function applied. The heterogeneity of the components giving rise to the $\Delta\text{UA}_{\text{H4}}$ peaks in the digest solution is also apparent from the varied intensities of the peaks. Clearly, even at 66 hr, the spectrum contains H-4 resonances from more than two components. Because heparin is primarily composed of the disaccharide IdoA(2S)-(1→4)-GlcNS(6S), the ¹H NMR spectrum of the IS standard dissolved in the depolymerization buffer was measured for comparison with the heparin depolymerization solution as shown in Figure 4.4. From the overlay of the two spectra, it is evident that a major component of the digestion mixture is the disaccharide IS.

Figure 4.5 was constructed using Origin Version 7.5 to compare the diffusion coefficients measured using the $\Delta\text{UA}_{\text{H4}}$ resonances as a function of reaction time. Linear regression ($R \geq 0.93$) of the data indicated a strong correlation between the diffusion

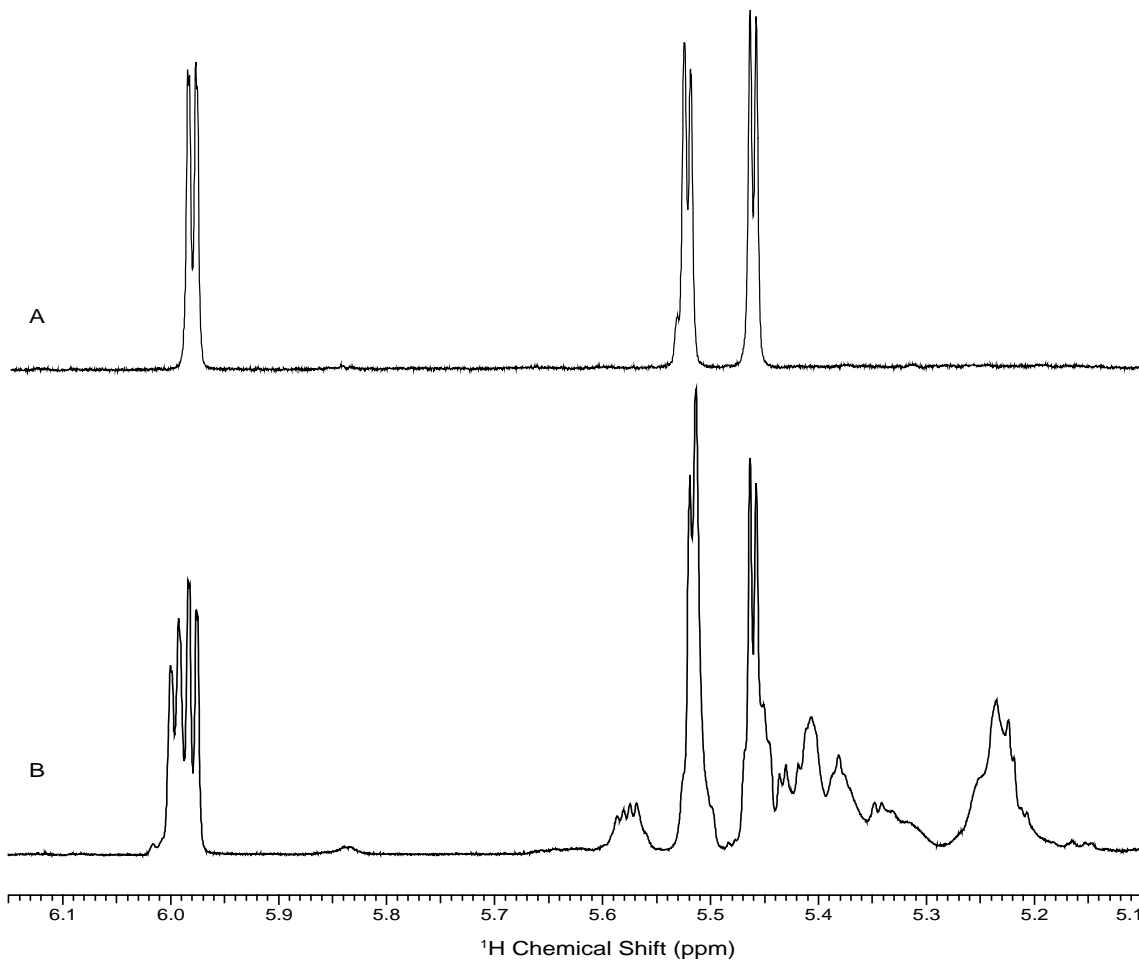


Figure 4.4. ¹H NMR spectra of the anomeric region (A) standard IS disaccharide of heparin measured in depolymerization buffer and (B) heparin depolymerization solution at time 66 hr. Spectra acquired with 64 scans using WET for the suppression of the water resonance.

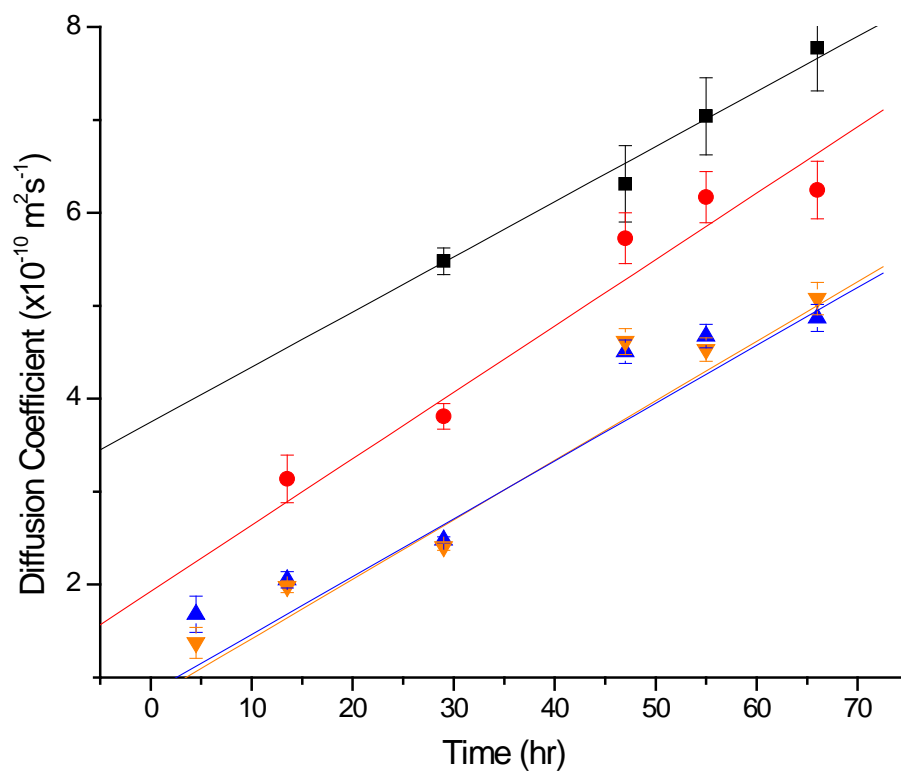


Figure 4.5. The diffusion coefficients for the H-4 protons of the Δ UA residues at 5.973 (■), 5.981 (●), 5.990 (▼), and 5.998 (▲) formed during heparinase I digestion.

coefficients and reaction time. Such a calibration plot could be useful for investigators wishing to quench the enzymatic digestion to maximize the yield of product with a desired size distribution. It is also interesting to note from the plot that although the diffusion coefficients for the resonances at 5.981, 5.990, and 5.998 ppm appear to begin level out toward the conclusion of the reaction, the diffusion coefficient measured for the resonance at 5.973 ppm continues to increase. These DOSY results may provide insight into the possible mode of action for heparinase I, as the digestion results from the repetitive binding and cleavage of larger fragments in the digest solution.

4.4 Summary

In this study, NMR provided a mechanism to monitor the enzymatic depolymerization of heparin *in-situ*. In conjunction with UV absorption measurements, DOSY provided insights into the extent of reaction and the size distribution of the heparin oligosaccharides produced along the course of the digestion. The ability to monitor diffusion coefficients, which report on the size distribution of heparin-derived oligosaccharides, provides a means for investigators to quench the reaction at an optimum time to maximize the yields of larger oligosaccharides most relevant for heparin binding studies. Following the analysis of the intact oligosaccharides using DOSY NMR we were interested in the ability of DOSY NMR to monitor the enzymatic depolymerization of heparin.

4.5 References

1. Chuang, W.-L.; McAllister, H.; Rabenstein, D. L. Chromatographic methods for product-profile analysis and isolation of oligosaccharides produced by heparinase-catalyzed depolymerization of heparin. *J. Chromatogr., A* **2001**, *932*, 65-74.
2. Pervin, A.; Gallo, C.; Jandik, K. A.; Han, X.-J.; Linhardt, R. J. Preparation and structural characterization of large heparin-derived oligosaccharides. *Glycobiology* **1995**, *5*, 83-95.
3. Chuang, W.-L.; McAllister, H.; Rabenstein, D. L. Hexasaccharides from the histamine-modified depolymerization of porcine intestinal mucosal heparin. *Carbohydr. Res.* **2002**, *337*, 935-945.
4. Imanari, T.; Toida, T.; Koshiishi, I.; Toyoda, H. High-performance Liquid Chromatographic Analysis of Glycosaminoglycan-Derived Oligosaccharides. *J. Chromatogr., A* **1996**, *720*, 275-293.
5. Thanawiroon, C.; Linhardt, R. J. Separation of a complex mixture of heparin-derived oligosaccharides using reversed-phase high-performance liquid chromatography. *J. Chromatogr., A* **2003**, *1014*, 215-223.
6. Korir, A. K.; Limtiaco, J. F. K.; Gutierrez, S. M.; Larive, C. K. Ultraperformance Ion-Pair Liquid Chromatography Coupled to Electrospray Time-of-Flight Mass Spectrometry for Compositional Profiling and Quantification of Heparin and Heparan Sulfate. *Anal. Chem.* **2008**, *80*, 1297-1306.
7. Sitkowski, J.; Bednarek, E.; Bocian, W.; Kozerski, L. Assessment of Oversulfated Chondroitin Sulfate in Low Molecular Weight and Unfractionated Heparins Diffusion Ordered Nuclear Magnetic Resonance Spectroscopy Method. *J. Med. Chem.* **2008**, *51*, 7663-7665.
8. Bednarek, E.; Sitkowski, J.; Bocian, W.; Mulloy, B.; Kozerski, L. An assessment of polydispersed species in unfractionated and low molecular weight heparins by diffusion ordered nuclear magnetic resonance spectroscopy method. *J. Pharm. Biomed. Anal.*, *53*, 302-308.
9. Rice, K. G.; Linhardt, R. J. Study of structurally defined oligosaccharide substrates of heparin and heparan monosulfate lyases. *Carbohydr. Res.* **1989**, *190*, 219-233.
10. Smallcombe, S. H.; Patt, S. L.; Keifer, P. A. WET Solvent Suppression and Its Applications to LC NMR and High-Resolution NMR Spectroscopy. *J. Magn. Reson.* **1995**, *117*, 295-303.
11. Henderson, T. Feasibility study for the rapid screening of target molecules using translational diffusion coefficients: diffusion-ordered NMR spectroscopy of biological toxins. *Anal. Bioanal. Chem.*, *396*, 1465-1471.
12. Nilsson, M. The DOSY Toolbox: A new tool for processing PFG NMR diffusion data. *J. Magn. Reson.* **2009**, *200*, 296-302.
13. Rabenstein, D. L. Heparin and heparan sulfate: structure and function. *Nat. Prod. Rep.* **2002**, *19*, 312-331.
14. Capila, I.; Linhardt, R. J. Heparin-Protein Interactions. *Angew. Chem., Int. Ed.* **2002**, *41*, 390-412.
15. Galliher, P. M.; Cooney, C. L.; Langer, R.; Linhardt, R. J. Heparinase Production by *Flavobacterium-Heparinum*. *Appl. Environ. Microbiol.* **1981**, *41*, 360-365.

16. Wei, Z.; Lyon, M.; Gallagher, J. T. Distinct Substrate Specificities of Bacterial Heparinases against N-Unsubstituted Glucosamine Residues in Heparan Sulfate. *J. Biol. Chem.* **2005**, *280*, 15742-15748.
17. Korir, A.; Larive, C. On-line NMR detection of microgram quantities of heparin-derived oligosaccharides and their structure elucidation by microcoil NMR. *Anal. Bioanal. Chem.* **2007**, *388*, 1707-1716.
18. Mikhailov, D.; Mayo, K. H.; Vlahov, I. R.; Toida, T.; Pervin, A.; Linhardt, R. J. NMR solution conformation of heparin-derived tetrasaccharide. *Biochem. J.* **1996**, *318*, 93-102.
19. Mikhailov, D.; Linhardt, R. J.; Mayo, K. H. NMR solution conformation of heparin-derived hexasaccharide. *Biochem. J.* **1997**, *328*, 51-61.
20. McEwen, I. Broadening of H-1 NMR signals in the spectra of heparin and OSCS by paramagnetic transition metal ions. The use of EDTA to sharpen the signals. *J. Pharm. Biomed. Anal.*, *51*, 733-735.
21. Shriver, Z.; Liu, D. F.; Hu, Y.; Sasisekharan, R. Biochemical investigations and mapping of the calcium-binding sites of heparinase I from *Flavobacterium heparinum*. *J. Biol. Chem.* **1999**, *274*, 4082-4088.
22. Jayawickrama, D. A.; Larive, C. K.; McCord, E. F.; Roe, D. C. Polymer additives mixture analysis using pulsed-field gradient NMR spectroscopy. *Magn. Reson. Chem.* **1998**, *36*, 755-760.
23. Derrick, T. S.; Larive, C. K. Use of PFG-NMR for Mixture Analysis: Measurement of Diffusion Coefficients of Cis and Trans Isomers of Proline-Containing Peptides. *Appl. Spectrosc.* **1999**, *53*, 1595-1600.
24. Antalek, B. Using pulsed gradient spin echo NMR for chemical mixture analysis: how to obtain optimum results. *Conc. Magn. Res.* **2002**, *14*, 225-258.
25. Morris, K. F.; Johnson, C. S. Diffusion-ordered two-dimensional nuclear magnetic resonance spectroscopy. *J. Am. Chem. Soc.* **1992**, *114*, 3139-3141.
26. Morris, K. F.; Stilbs, P.; Johnson, C. S. Analysis of mixtures based on molecular size and hydrophobicity by means of diffusion-ordered 2D NMR. *Anal. Chem.* **1994**, *66*, 211-215.
27. Barjat, H.; Morris, G. A.; Smart, S.; Swanson, A. G.; Williams, S. C. R. High-Resolution Diffusion-Ordered 2D Spectroscopy (HR-DOSY) - A New Tool for the Analysis of Complex Mixtures. *J. Magn. Reson.* **1995**, *108*, 170-172.
28. Wu, D. H.; Chen, A. D.; Johnson, C. S. An Improved Diffusion-Ordered Spectroscopy Experiment Incorporating Bipolar-Gradient Pulses. *J. Magn. Reson.* **1995**, *115*, 260-264.
29. Caldwell, E. E. O.; Nadkarni, V. D.; Fromm, J. R.; Linhardt, R. J.; Weiler, J. M. Importance of specific amino acids in protein binding sites for heparin and heparan sulfate. *Int. J. Biochem. Cell Biol.* **1996**, *28*, 203-216.
30. Yu, G.; LeBrun, L.; Gunay, N. S.; Hoppensteadt, D.; Walenga, J. M.; Fareed, J.; Linhardt, R. J. Heparinase I acts on a synthetic heparin pentasaccharide corresponding to the antithrombin III binding site. *Thromb. Res.* **2000**, *100*, 549-556.
31. Ziegler, A.; Zaia, J. Size-exclusion chromatography of heparin oligosaccharides at high and low pressure. *J. Chromatogr., B: Anal. Technol. Biomed. Life Sci.* **2006**, *837*, 76-86.

32. Politi, M.; Groves, P.; Chávez, M. I.; Cañada, F. J.; Jiménez-Barbero, J. Useful applications of DOSY experiments for the study of mushroom polysaccharides. *Carbohydr. Res.* **2006**, *341*, 84-89.
33. Huo, R.; Wehrens, R.; van Duynhoven, J.; Buydens, L. M. C. Assessment of techniques for DOSY NMR data processing. *Anal. Chim. Acta* **2003**, *490*, 231-251.
34. Balayssac, S.; Trefi, S.; Gilard, V.; Malet-Martino, M.; Martino, R.; Delsuc, M. A. 2D and 3D DOSY H-1 NMR, a useful tool for analysis of complex mixtures: Application to herbal drugs or dietary supplements for erectile dysfunction. *J. Pharm. Biomed. Anal.* **2009**, *50*, 602-612.
35. Khajeh, M.; Botana, A.; Bernstein, M. A.; Nilsson, M.; Morris, G. A. Reaction Kinetics Studied Using Diffusion-Ordered Spectroscopy and Multiway Chemometrics. *Anal. Chem.*, *82*, 2102-2108.
36. Nilsson, M.; Khajeh, M.; Botana, A.; Bernstein, M. A.; Morris, G. A. Diffusion NMR and trilinear analysis in the study of reaction kinetics. *Chem. Commun. (Cambridge, U. K.)* **2009**, 1252-1254.
37. Provencher, S. W. CONTIN - A General-Purpose Constrained Regularization Program for Inverting Noisy Linear Algebraic and Integral-Equations. *Comput. Phys. Commun.* **1982**, *27*, 229-242.
38. Stilbs, P.; Paulsen, K.; Griffiths, P. C. Global least-squares analysis of large, correlated spectral data sets: Application to component-resolved FT-PGSE NMR spectroscopy. *J. Phys. Chem.* **1996**, *100*, 8180-8189.
39. Windig, W.; Antalek, B. Direct exponential curve resolution algorithm (DECRA): A novel application of the generalized rank annihilation method for a single spectral mixture data set with exponentially decaying contribution profiles. *Chemom. Intell. Lab. Syst.* **1997**, *37*, 241-254.
40. Schulze, D.; Stilbs, P. Analysis of Multicomponent FT-PGSE Experiments by Multivariate Statistical-Methods Applied to the Complete Bandshapes. *J. Magn. Reson.* **1993**, *105*, 54-58.

CHAPTER FIVE

Structurally Unique Heparin-Derived Tetrasaccharide Isomers: Separation, Isolation and Identification using Microcoil NMR

This chapter describes the application of microcoil NMR in the characterization of mass-limited amounts of heparin-derived oligosaccharides. The isolation and purification of sufficient quantities of heparin-derived oligosaccharides for characterization by NMR is a tedious and time-consuming process. This coupled with the structural complexity and microheterogeneity of heparin and heparin sulfate (HS) makes characterization a daunting task. The methodology described herein utilizes a combination of enzymatic digestion, size-exclusion chromatography (SEC), strong anion exchange (SAX)-HPLC, reversed-phase ion-pair (RPIP)-UPLC-MS, and microcoil NMR for the efficient sequencing of heparin-derived tetrasaccharides. Complete structural characterization of microgram quantities of purified tetrasaccharide isomers was carried out through the acquisition of ^1H survey and 2D NMR spectra using a commercially available CapNMR probe. Microcoil NMR probes can provide sensitivity enhancements similar to those offered by cryogenically cooled probes at a fraction of the cost. In addition to offering an improvement in mass sensitivity, microcoil NMR can be easily coupled to separation methods such as HPLC, CE, and capillary isotachopheresis (cITP). Confirmation of the structure of the tetrasaccharides characterized by NMR was performed using RPIP-UPLC-MS.

5.1 Introduction: Structural Properties of Heparin and Heparan Sulfate

Heparin and HS are members of the glycosaminoglycan (GAG) family of carbohydrates. GAGs are unbranched, heterogeneous polysaccharides in terms of their relative molecular mass, charge density and physico-chemical properties. Among the GAGs, heparin is one of the most studied compounds due to its well known anticoagulant activity. Heparin has the highest negative charge density of any known biological molecule. Heparin and HS are comprised of variously sulfonated hexuronic acid (1→4) D-glucosamine repeating disaccharide building blocks. The uronic acid residue of heparin may be either α -L-iduronic acid (IdoA) or β -D-glucuronic acid (GlcA) and can be unsubstituted or sulfonated at the 2-O position. The glucosamine residue may be either unmodified (GlcN), *N*-sulfonated (GlcNS) or *N*-acetylated (GlcNAc) with variable patterns of *O*-sulfonation at the 3-O and 6-O positions as shown in Figure 5.1.^{1,2} Unlike nucleic acids and proteins that are biosynthesized through a template-driven assembly process, heparin and HS are actively remodeled during biosynthesis through a series of enzymatic reactions that lead to variable levels of *O*- and *N*-sulfonation and uronic acid epimerization as discussed in Section 1.1.2. The incomplete modification of the core heparin results in the bioproduction of heparin oligosaccharides with varying sequences of *N*- and *O*-sulfonation and IdoA content.³ The high degree of sequence microheterogeneity and size polydispersity makes molecular-level characterization of heparin extremely challenging.^{4,5}

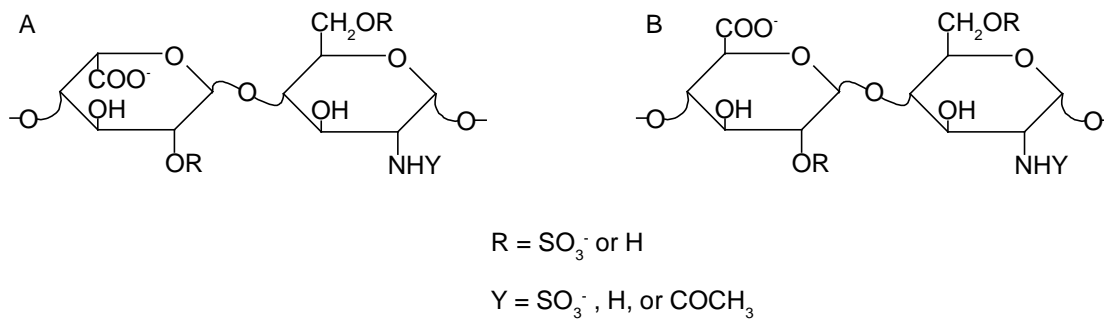


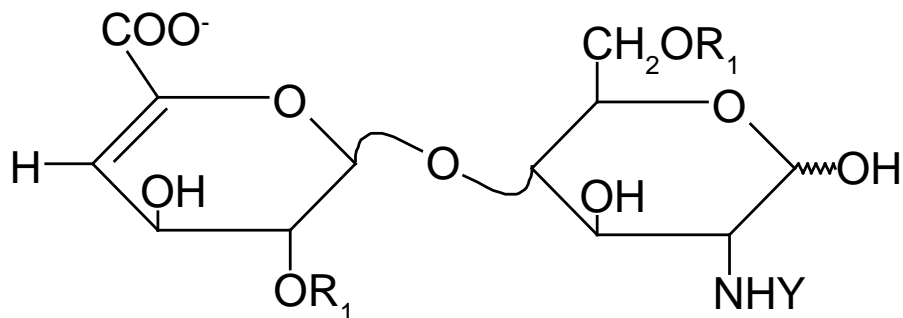
Figure 5.1. Disaccharide subunits of heparin showing the common substitution sites on the uronic acid and glucosamine residues as well as the orientation of the carboxyl moiety of the (A) iduronic acid and (B) glucuronic acid epimers.

5.1.1 Depolymerization of Heparin and HS

Due to the high degree of structural diversity associated with heparin and HS, determination of sequence information is carried out through a bottom-up approach which relies on depolymerization of the GAG via chemical or enzymatic processes through which the intact polysaccharide is reduced to smaller oligosaccharides prior to analysis. Depolymerization cleaves the polysaccharide into smaller oligosaccharide fragments that are more amenable to characterization by both MS and NMR. The depolymerization of heparin is carried out using either chemical (i.e. β -elimination, reductive deamination, and oxidation) or enzymatic means.

Commercially available enzymes used in the depolymerization of heparin include heparinase enzymes I, II, and III, each with its unique structural specificities as described in Chapter 1. In an exhaustive digestion, heparin and HS are reduced to their disaccharide building blocks using a cocktail of heparinase enzymes I, II, and III. Shown in Table 5.1, are the eleven commercially available disaccharides commonly observed following the exhaustive enzymatic depolymerization of heparin or HS. Although the direct analysis of the heparin digest solution can be accomplished using MS, most often studies perform compositional analysis using a separation method such as CE or HPLC.⁶⁻¹⁴

Frequently, the experimental goal is the isolation and characterization of larger heparin oligosaccharides, often as part of a study to explore their protein-binding properties and biological activities.¹⁵⁻¹⁹ These studies require larger heparin-derived oligosaccharides, therefore a partial depolymerization of heparin and HS is generally performed.²⁰ The partial depolymerization of heparin is achieved by shortening the reaction time and using a single enzyme for the digestion. In studies where the partial



		\underline{R}_1	\underline{R}_2	\underline{Y}
Trisulfonated	IS	SO_3^-	SO_3^-	SO_3^-
Disulfonated	IA	SO_3^-	SO_3^-	COCH_3
	IH	SO_3^-	SO_3^-	H
	IIS	H	SO_3^-	SO_3^-
	IIIS	SO_3^-	H	SO_3^-
Monosulfonated	IIA	H	SO_3^-	COCH_3
	IIIA	SO_3^-	H	COCH_3
	IIH	H	SO_3^-	H
	IIIH	SO_3^-	H	H
Nonsulfonated	IVA	H	H	COCH_3
	IVH	H	H	H

Table 5.1. Structures of commercially available heparin disaccharide standards; IA-IVA, IS-IIIS, and IH-IVH. For the presented disaccharides above the A, S, and H notation following the numeric value indicates the substitution attached to the amine of the glucosamine residue (Y) where A = COCH_3 , S = SO_3^- , and H = the nitrogen is a primary amine.

depolymerization of heparin is the goal, size and charge-based separations are necessary as the heparin depolymerization solution is a complex mixture of variously sized oligosaccharides consisting of a diverse set of positional and configurational isomers.⁴ Methods used in the separation of the heparin-derived oligosaccharides include preparative- and analytical-scale SEC for the size uniform isolation of heparin-derived oligosaccharides followed by charge-based separations including SAX-HPLC, RPIP-HPLC, and capillary electrophoresis (CE).²¹

5.1.2 Separation of Heparin-Derived Oligosaccharides

With the commercial availability of authentic heparin disaccharide standards, analysis of the disaccharide composition of heparin following exhaustive digestion is simplified using separation methods which can effectively resolve the individual disaccharides. However, when the goal of the study is in the isolation and characterization of larger heparin oligosaccharides, a single separation step is insufficient to resolve the individual components of the complex digestion mixture, requiring the use of multiple orthogonal separation methods.

5.1.2.1 SEC Separation of Heparin Depolymerization Products

Size-exclusion chromatography (SEC) is generally the first separation step in the analysis of partially depolymerized heparin. SEC reduces the sample complexity by separating the heparin-derived oligosaccharides into size-uniform fractions corresponding to di-, tetra-, hexa-, and larger oligosaccharides.^{20, 21} These size-uniform fractions are subjected to additional charged-based separations to further purify oligosaccharides into their single-components.^{19, 20} Preparative SEC can be carried out

on a scale ranging from 100 mg to 1 g, allowing for the resolution of different sized fractions.²² Preparative SEC separations generally take on the order of days to complete and are therefore unsuitable for the rapid characterization of heparin. In contrast, analytical SEC separations require only a few hours to achieve similar or even better resolution than preparative SEC while using microgram amounts of material making this technique amenable to the rapid analysis of heparin and HS samples available in mass-limited amounts.²²

5.1.2.2 SAX-HPLC Separation of Size-Uniform Heparin Oligosaccharide Fractions

SAX-HPLC offers a robust approach for the separation and analysis of heparin- and HS-derived oligosaccharides and is commonly used for the separation of GAG oligosaccharides following enzymatic depolymerization.²³⁻²⁶ In comparison to other modes of separation used in heparin analysis, SAX columns provide the highest resolution while also providing greater sample loading capacities. In this study, the greater capacity of the semi-prep SAX column allowed efficient isolation of the purified components. This is especially important when isolating materials for characterization by NMR which traditionally requires milligram amounts of material for complete characterization by 2D NMR techniques. The trade off for the improved resolution and sample loading capacity is the longer analysis time required for SAX-HPLC and the high-ionic strength mobile phase, generally 2 M NaCl, necessary for the elution of the highly charged heparin oligosaccharides. Because of the large concentration of NaCl used in the separation, SAX-HPLC is not easily coupled to detection by MS or NMR. Heparin

and HS oligosaccharides isolated using SAX-HPLC must therefore be desalted prior to analysis by MS or NMR.

5.1.2.3 RPIP-HPLC Separation of Size-Uniform Heparin Oligosaccharides

The increasing popularity of RPIP-HPLC in the separation of heparin and HS oligosaccharides stems from the widespread availability of reversed-phase HPLC columns and the relative ease of coupling RPIP-HPLC to a variety of detection methods including UV, fluorescence, and MS. Separations by RPIP-HPLC are typically performed on an octadecyl (C₁₈) column using a lipophilic alkyl ammonium salt as the ion pairing reagent (IPR). As explained in Section 2.3.1, the IPR aids in the retention and resolution of hydrophilic analytes through an electrostatic mechanism. For heparin and HS this involves the interaction of the cationic ammonium group of the IPR with the anionic carboxylate and sulfonate functional groups of heparin and HS. The heparin-IPR complex is relatively neutral and hydrophobic, which facilitates interaction with the hydrophobic stationary phase of the reversed-phase HPLC column.²⁷⁻²⁹

Although earlier separations utilized quarternary ammonium salts such as tetrabutylammonium as the IPR, incorporation of more volatile reagents such as tri- and dibutylamine has made RPIP-HPLC more amenable to detection by MS. Hyphenation of RPIP-HPLC with MS significantly improves the sensitivity when compared to UV absorbance and electrochemical methods while providing structural information of the analytes.^{6, 8, 30-32} Though SAX-HPLC offers better resolution, because of its ability to be directly coupled to MS for detection, RPIP-HPLC is often preferred for the rapid separation and analysis of heparin oligosaccharides.

5.1.3 Characterization of Heparin Components by NMR

NMR spectroscopy is highly sensitive to minor variations in molecular structure, making it an important technique for heparin characterization. A simple ^1H survey spectrum can both reveal the number of monosaccharide residues present and provide a tentative compositional analysis based on the comparison of ^1H chemical shifts and reference data.^{1, 15, 33} Although the ^1H survey spectrum can provide important information about sample purity and composition, complete structural characterization of isolated oligosaccharides requires two-dimensional NMR experiments such as correlation spectroscopy (COSY), total correlation spectroscopy (TOCSY), and rotating-frame Overhauser effect spectroscopy (ROESY).²⁴ With the powerful arsenal of two-dimensional experimental techniques available, NMR spectroscopy can be used to determine the sequence of the component monosaccharide residues and unambiguously assign sites of *N*-acetylation as well as of *N*- and *O*-sulfonation along the oligosaccharide chain. Most importantly, NMR spectroscopy can also specify the orientation of the anomeric linkage connecting the various disaccharide subunits and easily distinguishes IdoA and GlcA residues that may be important for specific protein binding.

Because of its high level of microheterogeneity and polydisperse nature, the complete structural characterization of unfractionated heparin continues to be a major challenge. Therefore, NMR measurements are usually reserved for the characterization of purified single oligosaccharides obtained by chemical or enzymatic depolymerization, following size- and charge-based separations. Interpretation of NMR spectral data is facilitated by molecular-weight and fragmentation information provided by MS.

5.1.3.1 Two-dimensional NMR Analysis of Heparin Oligosaccharides

Structural characterization of heparin-derived oligosaccharides is typically initiated by identification of the individual monosaccharide subunits in the oligosaccharide chain using scalar couplings to provide through-bond connectivities. These connectivities can be obtained through a number of two-dimensional NMR experiments, including COSY and TOCSY experiments, as well as heteronuclear single quantum coherence (HSQC) and multiple quantum coherence (HMBC) spectroscopy experiments.^{24, 34-36} Through the COSY spectrum, connections between coupled protons on adjacent carbon atoms within a monosaccharide ring can be identified. The well-resolved anomeric resonances and the H4 resonance of the $\Delta^{4,5}$ UA residue of oligosaccharides produced by enzymatic cleavage provide an entry point for analysis of the COSY spectrum. However, the limited ^1H NMR chemical shift dispersion of carbohydrates can make interpretation of the COSY data challenging, even for medium-sized oligosaccharides. Because the TOCSY experiment transfers ^1H scalar coupling information throughout a spin system, the TOCSY spectrum allows detection of the connectivity of all the protons within each monosaccharide residue through the well-resolved anomeric resonances. Through comparison of reference data with the ^1H chemical shifts obtained from the TOCSY spectrum the structural identities of the monosaccharide residues can be deduced. The HSQC and HMBC experiments provide additional information about the type, number, and position of C-H bonds and offer improved spectral resolution by taking advantage of the greater dispersion of ^{13}C chemical shifts.

Following assignment of the resonances of the individual monosaccharide residues, the oligosaccharide sequence is determined through dipolar coupling information obtained by the ROESY experiment. The ROESY spectrum can also distinguish IdoA

and GlcA through unique interresidue cross peaks. In the ROESY spectrum, cross peaks arise between resonances of the H1 and the H4 protons of adjacent residues connected via the glycosidic bond, which reveals the relative positions of the monosaccharide residues within the full chain. The correlations observed by the COSY, TOCSY, and ROESY spectra are illustrated in Figure 5.2.

5.2 Experimental Section

5.2.1 Chemicals

Porcine intestinal mucosa heparin sodium salt, grade 1-A, calcium acetate hydrate, tris(hydroxymethyl)aminomethane (Tris), tributylamine (TrBA), and acetonitrile (optima grade) were obtained from Sigma Chemical Company (St. Louis, MO). Hydrochloric acid (HCl), *tert*-butanol, sodium chloride, sodium hydroxide, dibasic sodium phosphate, phosphoric acid, ammonium acetate, ammonium bicarbonate, ammonium formate, formic acid, and acetic acid were purchased from Fisher Scientific Co. (Fair Lawn, NJ). Sephadex G-10 (superfine) was purchased from GE Healthcare (Pittsburgh, PA). Heparinase I enzyme (EC 4.2.2.7) from recombinant *Flavobacterium heparinum* was purchased from IBEX Technologies Inc. (Montreal, Quebec). HPLC grade water was purchased from Burdick and Jackson (Muskegon, MI). Low paramagnetic deuterium oxide (D, 99.9%), chloroform-*d* (D, 99.8%), DMSO-*d*6 (D, 99.9%), EDTA-*d*16 (D, 98%) and TMSP-2,2,3,3-*d*4 (D, 98%) were purchased from Cambridge Isotope Laboratories (Andover, MA).

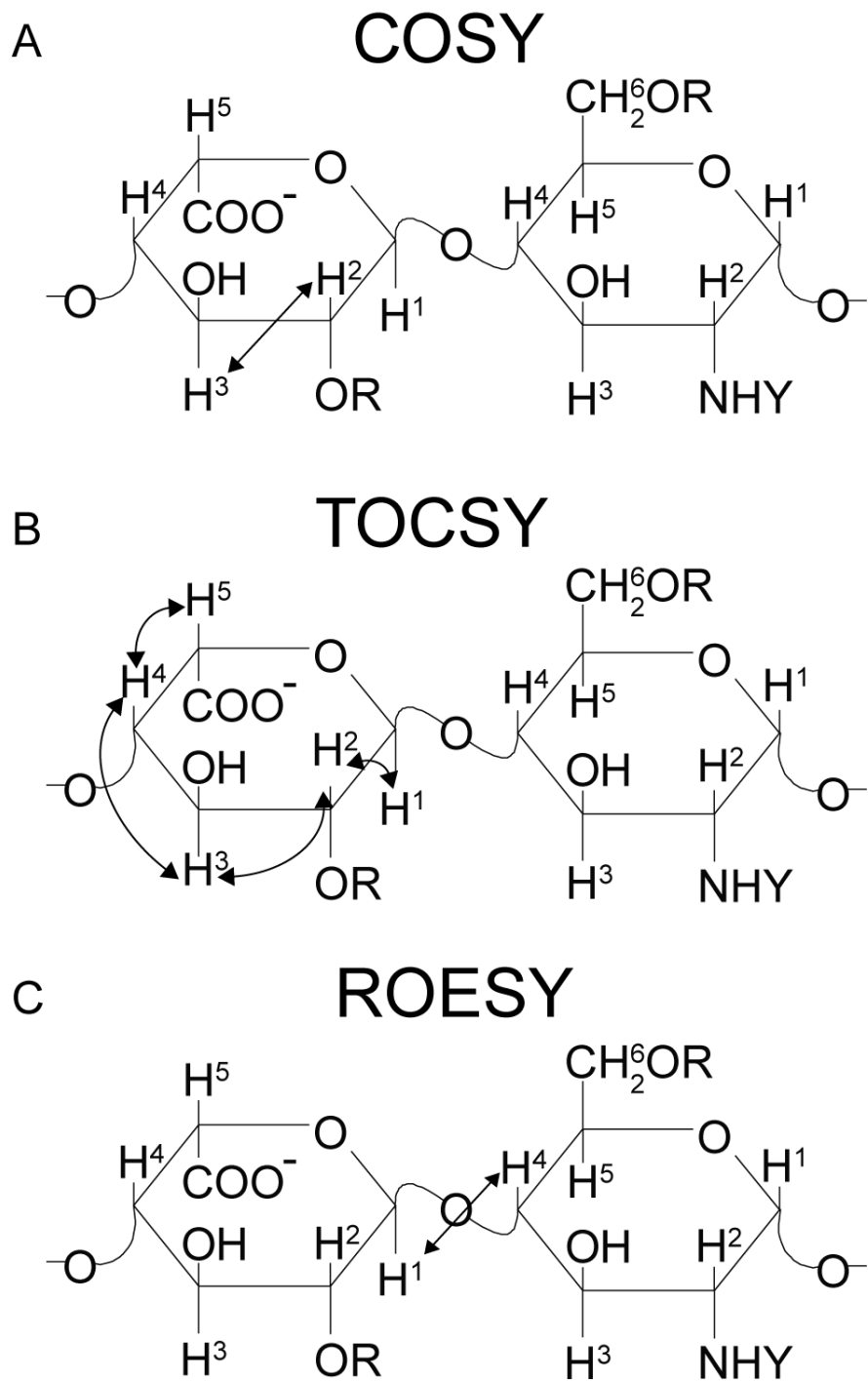


Figure 5.2. Diagram illustrating the ^1H correlations observed using the pulse sequences (A) COSY, (B) TOCSY, and (C) ROESY.

5.2.2 Enzymatic Depolymerization of Heparin

The enzymatic depolymerization of heparin was performed by Derek Langeslay at UCR. Digestion of 1 g of heparin was carried out in 50 mL of 100 mM pH 6.8 Tris buffer containing 2.5 mM calcium acetate. The enzyme heparinase I (0.5 IU) was added to the mixture and incubated at 28 °C in a water bath for 66 hr. The water bath temperature was controlled using a Fisher Scientific Isotemp 1013S scientific temperature regulator. To monitor the progress of the enzymatic reaction, UV measurements were performed at 232 nm using a Thermo Scientific NanoDrop 2000 spectrophotometer (Wilmington, DE). At 232 nm, the molar extinction coefficient for the monounsaturated disaccharide is $5500 \text{ M}^{-1}\text{cm}^{-1}$.³⁷ At the conclusion of the enzymatic reaction, the digest solution was quenched by placing the reaction vessel into boiling water for 5 min. The depolymerization solution was then lyophilized and reconstituted into 15 mL of the separation buffer (0.5 M NH_4HCO_3) prior to SEC fractionation.

5.2.3 SEC Separation

The heparin-derived oligosaccharides present in the heparinase I digest were size-fractionated on a 3.0 × 200 cm column packed with Bio-Rad Bio-Gel P-10 resin fine (Bio-Rad Laboratories Hercules, CA) and eluted with 0.5 M NH_4HCO_3 at a flow rate of 0.08 mL/min. The eluent was collected into 4.5 mL fractions. The progress of the separation was monitored off-line by UV absorption measurements at 232 nm using the NanoDrop spectrophotometer as described above. Following SEC, similar sized fractions were pooled and stored as a lyophilized powder at -20 °C until SAX-HPLC separation.

5.2.4 SAX-HPLC Separation

SAX-HPLC separations of tetrasaccharides were performed using a Dionex 500 ion chromatography system equipped with a GP40 gradient pump and an AD20 UV–Vis detector using a CarboPac PA1 semi-preparative scale column (9 mm x 25 cm) purchased from Dionex (Sunnyvale, CA). The lyophilized SEC fractions containing the various tetrasaccharides were re-dissolved in HPLC grade water and 500 μ L injected into the HPLC system. Approximately 15 injections were performed to isolate material for NMR analysis. The time necessary to isolate a sufficient amount of material was about a week. Tetrasaccharides were separated using a NaCl gradient profile developed by Szabolcs Beni. Separations were performed with a 50 mM pH 7.0 phosphate buffer (eluent A) and 2.0 M NaCl in 50 mM pH 7.0 phosphate buffer (eluent B) at a flow-rate of 2.5 mL/min for 90 minutes. The gradient profile applied is as follows: 0 min: 100% A, 0% B; 10 min: 71% A, 29% B; 80 min: 39% A, 61% B. After each run, the column was washed with solvent B for 10 min to elute any impurities, followed by solvent A for 20 min to equilibrate the column. Separated tetrasaccharide peaks were collected into vials and after the desired number of injections each fraction was further purified by re-injection to concentrate the analyte and reduce the NaCl content. Prior to reinjection, the collected peaks were diluted with eluent A to reduce the NaCl concentration to below 0.3 M, and the entire solution was pumped through the semi-preparative column as the mobile phase. This step allows the tetrasaccharides to be retained on the column while the excess NaCl is eluted. The analyte was then eluted from the SAX column with the NaCl gradient used in its isolation. The purified tetrasaccharides were lyophilized to dryness and redissolved with the minimum amount of HPLC grade water to obtain a small volume better suited for desalting.

5.2.5 Desalting Procedure

Although much of the NaCl was removed by reinjection of the isolated peaks onto the SAX column, further desalting was necessary. The tetrasaccharide samples were desalted by Szabolcs Beni on a 1.6 × 70 cm Sephadex G-10 (superfine) column using HPLC grade water as the eluent and a flow-rate of 0.15 mL/min. The SAX fractions were lyophilized and reconstituted in the minimum amount of water to obtain a saturated solution. The retention of the column for NaCl was determined by monitoring the conductivity of the eluent throughout the desalting step. Fractions (1.5 mL) were collected from the Sephadex G10 column and lyophilized. These samples were reconstituted into 100 μL of water for UV absorbance measurements at 232 nm. Fractions containing the desalted tetrasaccharides were aliquoted for analysis by NMR and MS, lyophilized, and stored at -20 °C for subsequent use.

5.2.6 Microcoil NMR Analysis

Isolated tetrasaccharides were reconstituted in 50 μL low paramagnetic D₂O and lyophilized to replace exchangeable protons with deuterium. As a final step immediately prior to NMR analysis, samples were reconstituted in 20 μL low paramagnetic D₂O and 5 μL DMSO-*d*₆, as a keeper solvent, and lyophilized to concentrate the sample at the bottom of the sample vial.³⁸ The lyophilized samples were reconstituted in 3.5 μL pD 7.4 phosphate buffer containing 10 mM EDTA-*d*₁₆ and TMSP-*d*₄ as the chemical shift reference (0 ppm). The solution pD was calculated using the pH meter reading (pH*) and the equation $pD = pH^* + 0.4$.³⁹ EDTA-*d*₁₆ was added as a chelating agent to scavenge trace paramagnetic impurities, a practice that has been shown to improve resonance line widths of heparin.⁴⁰ A 3.0 μL aliquot of the sample was sandwiched between deuterated

chloroform plugs in a 25 μL Hamilton syringe and injected into the double resonance (^1H , ^{13}C) Protasis/MRM microcoil NMR probe (Marlboro, MA). This probe has a flow-cell volume of 5 μL and an active volume of 1.5 μL . The sample was positioned within the active volume of the microcoil by monitoring the D_2O lock signal. Following analysis, NMR samples were collected from the microcoil probe and reduced to dryness by speed vacuum and stored at $-20\text{ }^\circ\text{C}$.

NMR spectra were recorded using a Bruker Avance spectrometer operating at 599.84 MHz for ^1H . For each ^1H NMR spectrum, 64 transients were collected into 24576 data points using a 6613 Hz spectral window and a 3 s relaxation delay. ^1H NMR spectra were acquired using either presaturation (zgpr) or WET solvent suppression included with the standard Topspin release version 1.3. For WET solvent suppression, the automated Bruker shape tool was used to create the sinc pulse for the selective excitation of the HOD resonance.

Two-dimensional COSY, TOCSY, and ROESY experiments were carried out on the isolated samples delivered to the CapNMR flow cell. In each experiment, a spectral width of 3 kHz was used in both dimensions and 32 scans per increment were acquired. Presaturation of the solvent resonance was used to reduce the intensity of the residual HOD signal. Double-quantum filtered COSY (cosydfphpr) spectra were obtained by acquisition of a 2048×256 data matrix using a relaxation delay of 1.5 s. The COSY data set was apodized using a sinebell squared function with zero-filling to 4096 points in F2 and 2048 points in F1. TOCSY (mlevphpr) spectra were acquired into a 2048×320 data matrix using a relaxation delay of 1.6 s and a mixing time of 200 ms. The TOCSY spectra were apodized by multiplication with a cosine function and zero-filled to 4096 points in F2. Both the TOCSY and ROESY data were linear predicted to 2048 points in

F1. ROESY (roesyphpr.2) spectra were acquired into a 2048 × 320 data matrix using a relaxation delay of 1.5 s and mixing time of 350 ms. The ROESY spin lock was applied as a continuous low power pulse with a field strength of 2.5 kHz. The ROESY spectra were apodized by multiplication with a cosine squared function and zero-filled to 4096 points.

Following the completion of the NMR measurements, samples were pushed out of the probe using 50 μL CDCl_3 followed by 50 μL D_2O and collected. The collected samples were then frozen with dry ice and lyophilized overnight. Lyophilized samples were reconstituted into 100 μL of water and UV absorbance measurements at 232 nm were performed to determine the amount of material analyzed using NMR.

5.2.7 NMR Sensitivity Measurements

Experiments to compare the sensitivity of two microcoil NMR probes were performed using a sucrose sample containing 20 μg dissolved in 3 μL for analysis in the CapNMR probe and in 5 μL for the analysis in the Bruker 1 mm TXI triple resonance microprobe. A 100 mg/mL sucrose stock solution was prepared into D_2O and diluted to the necessary concentrations with D_2O . Sodium azide at a concentration of 0.35 mM was added to the stock solution to inhibit bacterial growth during storage. Prior to analysis, the stock sucrose solution was stored at -20°C . NMR spectra for sensitivity comparisons were acquired using a standard pulse and acquire experiment (zg). For each ^1H NMR spectrum, 128 transients were collected into 36864 data points using a 6613 Hz spectral window and a 2 s relaxation delay corresponding to a total acquisition time of 14 min. Prior to Fourier transformation, the free induction decays (FIDs) were zero-filled to 65536 points and apodized by multiplication with an exponential function

equivalent to 0.5 Hz line broadening. NMR experiments using the Bruker 1 mm TXI triple resonance microprobe were performed on a Bruker Avance spectrometer operating at 600.13 MHz for ^1H . Though the CapNMR and microprobe experiments were carried out on different spectrometers, the sensitivity of the two spectrometers should be comparable and should not have a significant effect on the probe comparison.

5.2.8 RPIP-UPLC Separation

All chromatographic separations were performed using a 2.1 × 100 mm Acquity UPLC BEH C₁₈ column with 1.7 μm particles purchased from Waters Corporation (Milford, MA). A guard column using the same material was also employed. The column temperature was maintained at 25 °C throughout the separation, and a flow rate of 0.5 mL/min was used with 10 μL injections. Samples for MS analysis were reconstituted in water to prepare a tetrasaccharide solution with approximate concentrations of 0.2 mM and 0.1 mM for the mixture and the individual tetrasaccharides, respectively. A binary solvent system was used for gradient elution. Solvent A consisted of 5% acetonitrile in water while solvent B consisted of 80% acetonitrile in water. Both eluents contained 20 mM TrBA and 2.5 mM ammonium formate buffer. The pH was adjusted to 6.0 prior to the addition of the required volume of acetonitrile. The separation was started at 30% B and the organic composition increased linearly to 47% B over 4 min. The organic composition was held at 47% B for 2 min and then increased linearly from 47 to 90% B over the next 6 min. The eluent composition was finally increased to 100% B over 1 min and held for 2 min to remove any highly retained components before returning the column to its starting condition over the next 2 min for a total run time of 17 min. A 5 min equilibration was utilized prior to the next injection.

5.2.9 Mass Spectrometry

Total ion chromatograms were obtained using a Waters ESI quadrupole time-of-flight mass spectrometer (Q-TOF-MS). Data acquisition was performed using MassLynx 4.1 software. All spectra were obtained in negative ion mode using the following instrument parameters: capillary voltage 3 kV; cone voltage 12 V; source temperature 120 °C; desolvation temperature 200 °C; extraction cone voltage 1 V; radio frequency lens 0.5 V; interscan delay 0.1 s; m/z range 230–1500. Solvent delay from 0-3 min and 15-17 min were used to minimize contamination of the MS source.

5.3 Results and Discussion

Heparin and HS are highly heterogeneous with respect to their molecular size, disaccharide composition, and sulfonation pattern, all of which can vary according to tissue and species of origin. As a result of the structural diversity of heparin and HS, most methods used for their structural characterization utilize a bottom-up approach, in which the intact polysaccharide is chemically or enzymatically depolymerized to smaller oligosaccharides prior to analysis.^{6, 26} In this study, intact heparin was digested to its smaller oligosaccharide fragments using the enzyme heparinase I. Heparinase enzymes are highly specific with respect to the uronic acid configuration and degree of sulfonation at the cleavage site.^{41, 42} The heparinase I enzyme used in this study cleaves the [1→4] glycosidic bond between a glucosamine residue that is *N*-sulfonated (GlcNS) and an iduronic acid sulfonated at the 2-O position (IdoA2S),^{42, 43} the most common substitution motif observed in unfractionated heparin from porcine intestinal mucosa. Figure 1.5 illustrates the depolymerization of heparin to its corresponding oligosaccharide subunits. The enzymatic depolymerization of heparin occurs through a β -elimination reaction

yielding oligosaccharide fragments that are unsaturated at the C-4,5 position of the non-reducing end of the terminated hexuronic acid residues.⁴⁴ This unsaturated bond produces a characteristic absorption maximum at 232 nm, thus allowing UV detection.⁴⁴

In studies where determination of the disaccharide composition is the goal, intact heparin is exhaustively digested with a cocktail of heparinase enzymes I, II, and III.^{6, 21, 45-47} Exhaustive heparin digestion yields almost exclusively disaccharides and with the availability of authentic heparin disaccharide standards, compositional analysis of the digested heparin can be achieved simply by using HPLC^{6, 48-51} or CE^{21, 52-54} generally coupled to UV absorption or fluorescence spectroscopy for detection and quantification. If the experimental goal is to isolate and characterize larger heparin oligosaccharide fragments, often as part of a study to explore their protein binding properties or biological activity, partial digestion of the intact heparin is performed. Partial depolymerization of heparin results in a complex mixture of variably-sized oligosaccharides consisting of a diverse set of positional and configurational isomers.⁵⁵ For these samples, a single mode of separation is ineffective in resolving the individual mixture components, therefore, multiple orthogonal separation approaches are required.

5.3.1 Separation and Isolation of Heparin-Derived Tetrasaccharides

Following the enzymatic digestion of heparin, the resulting solution of oligosaccharides was separated into size-uniform fractions using SEC. The SEC column was effective in baseline separating the components into peaks ranging from disaccharides (dp2) to hexadecasaccharides (dp16) as shown in Figure 5.3A. Because of the specificity of the enzymatic reaction, primarily even numbered oligomers were produced, although small quantities of trisaccharides have also been reported.⁵⁶

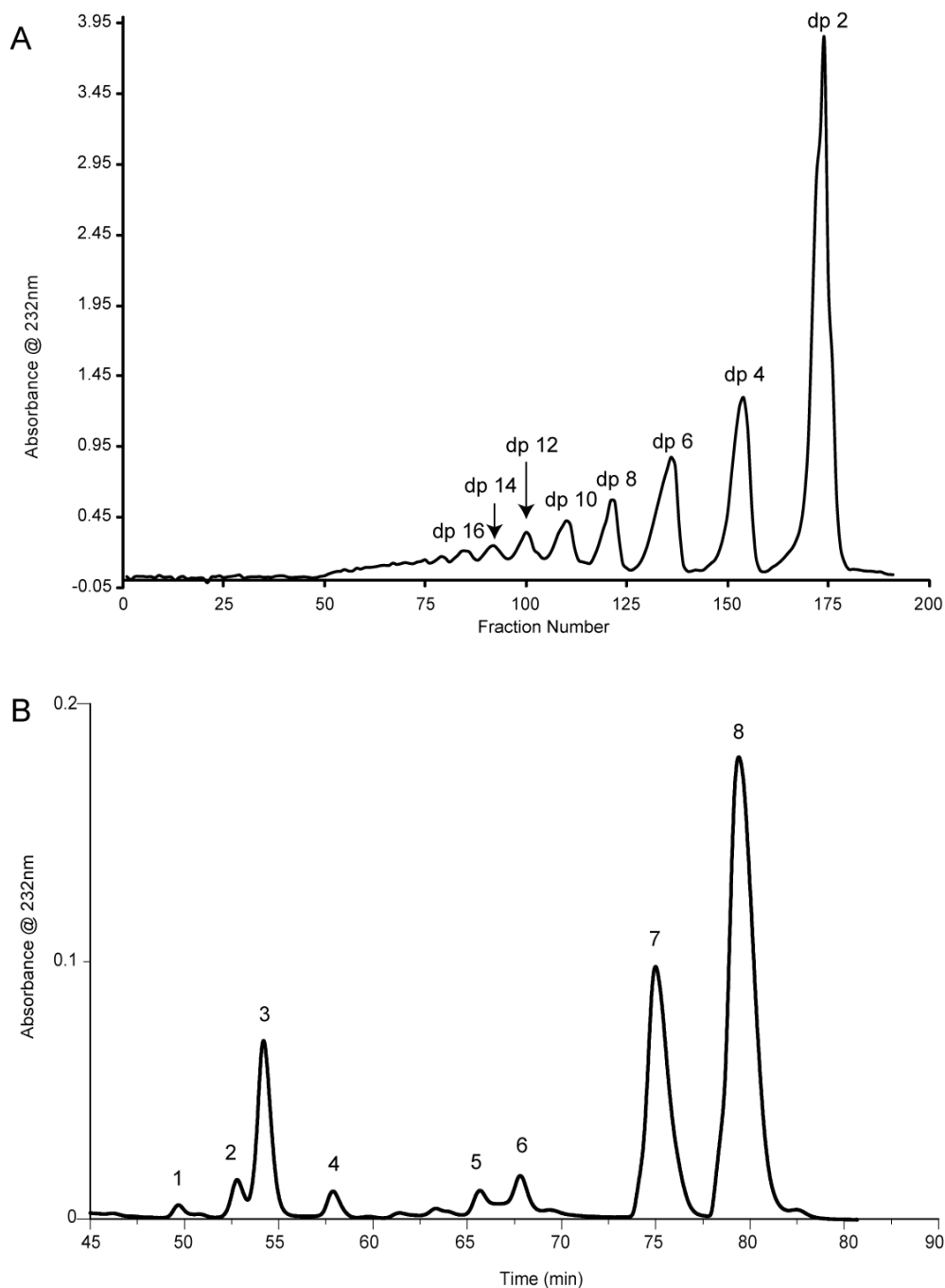


Figure 5.3. (A) SEC separation of heparin digest with off-line detection at 232 nm. Well-resolved peaks corresponding to size-uniform depolymerization products (dp) are detected for di- (dp2) to hexadecasaccharides (dp16). (B) UV-detected SAX chromatogram at 232 nm for the SEC fraction of heparin-derived tetrasaccharides using a 2.0 M NaCl gradient for elution. Identified tetrasaccharides are labeled according to their order of elution and corresponding masses presented in Table 5.2.

Similar sized SEC fractions were pooled and subjected to further fractionation using SAX chromatography on a CarboPac PA1 semi-preparative column as described by Chuang and co-workers, with the resulting chromatogram shown in Figure 5.3B.^{15, 23} The numbered peaks correspond to the tetrasaccharides isolated for structural characterization in this work. The chromatogram shown in Figure 5.3B demonstrates the high resolution achieved by the SAX separation. Sample purity is especially important when analyzing heparin oligosaccharides by NMR as spectral overlap can complicate oligosaccharide characterization because of the limited ¹H chemical shift dispersion in carbohydrate NMR spectra. An additional consideration for choosing SAX-HPLC for the isolation of heparin tetrasaccharides was the loading capacity possible with the CarboPac PA1 semi-prep column.

Compared with RPIP-HPLC discussed in section 4.3.2, SAX does not require an ion-pairing reagent (IPR) such as tetrabutylammonium (TBA) or the more volatile TrBA commonly used in RPIP-UPLC-MS.⁶ In our experience isolating materials for NMR analysis using RPIP-UPLC with TrBA as the IPR, it can be very difficult to completely remove the IPR prior to NMR analysis. For samples isolated in minute amounts for microcoil NMR analysis, the TrBA contaminant can limit the receiver gain values that can be used. In contrast, SAX separations require large concentrations of salt for elution and it was therefore necessary to desalt isolated peaks with a Sephadex G-10 column prior to NMR analysis. Removal of the large amounts of salt permitted us to tune and match the CapNMR probe for each of the samples analyzed.

Using SAX-HPLC, 3 major and 5 minor peaks were separated (Figure 5.3B) with baseline resolution between most of the peaks. From their retention times, we hypothesized that the peaks between 54 and 75 min correspond to pentasulfonated

tetrasaccharides while the largest peak at 80 min corresponds to the hexasulfonated tetrasaccharide, Δ UA(2S)-GlcNS(6S)-IdoA(2S)-GlcNS(6S). The high level of sulfonation observed in the isolated peaks is expected as about 70% of heparin isolated from porcine intestinal mucosa is comprised of the disaccharide IdoA(2S)-GlcNS(6S), a trisulfonated heparin disaccharide.¹

5.3.2 RPIP-UPLC-MS Analysis of the SEC Tetrasaccharide Fraction

RPIP-UPLC coupled to mass spectrometry was used in the preliminary analysis of tetrasaccharides present in the SEC fraction, as shown in Figure 5.4. Though RPIP-UPLC-MS was effective in separating the heparin-derived tetrasaccharides, better resolution was achieved by the SAX-HPLC separation as demonstrated in Figure 5.3B. Using mass spectrometry we confirmed the identity of the most abundant peak as the hexasulfonated tetrasaccharide Δ UA(2S)-GlcNS(6S)-IdoA(2S)-GlcNS(6S) having a unique m/z of 575.96 Da for the molecular ion $[M-2H]^{2-}$. The smaller peaks eluting from 6.6-7.4 min in Figure 5.4 each have m/z values of 535.98 Da corresponding to tetrasaccharides containing one sulfonate group less than the hexasulfonated species. Considering the various positions of sulfonate substitution and uronic acid configuration, there are 12 possible compounds that could correspond to this m/z , disregarding the anomeric configuration at the reducing-end.

Mass spectrometry has been used in the complete structural characterization of heparin hexasaccharides by Schenauer and coworkers.⁵⁷ This approach required further enzymatic digestion of the isolated and purified hexasaccharides to their corresponding tetrasaccharide and disaccharide subunits to generate sequence

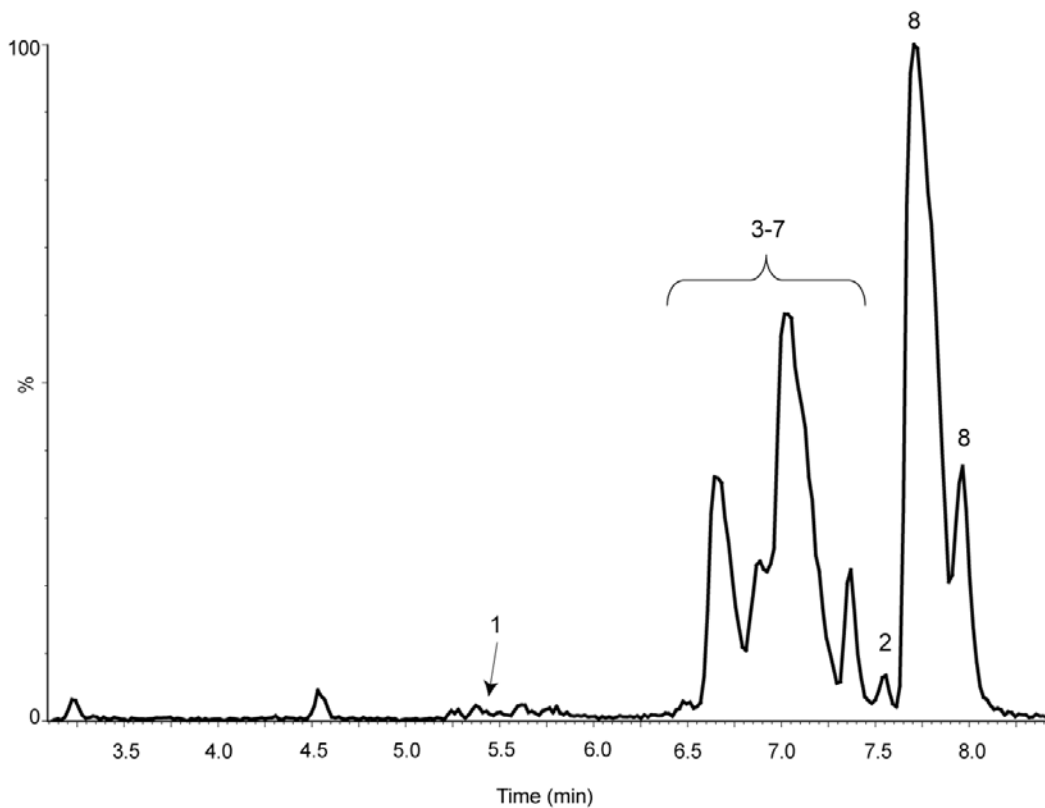


Figure 5.4. Total ion chromatogram of an optimized RPIP-UPLC/MS separation for the SEC fraction of heparin-derived tetrasaccharides. RPIP-UPLC resolves the α and β anomers of the reducing end residue, complicating the separation and contributing to the poor resolution of this separation.

information as the differential cleavage sites of heparinase enzymes can be used to identify neighboring disaccharides. This method may be efficient for the characterization of a few unique heparin-derived oligosaccharides especially in studies in which heparin is digested in the presence of its binding partner,¹⁵ but would be expensive for the characterization of multiple heparin-derived oligosaccharides. More importantly, information on the configuration of the internal uronic acid residues is lost as a result of the second enzymatic digestion. Studies by Mikhailov and coworkers have demonstrated the biological importance of the configuration of the internal uronic acid residue.^{58, 59} In their ¹H NMR studies of the solution structure of the hexasulfonated heparin-derived tetrasaccharide Δ UA(2S)-GlcNS(6S)-UA(2S)-GlcNS(6S), they observed that the tetrasaccharide containing β -D-glucuronic acid at the non-reducing-end disaccharide has considerably less biological activity than similar oligosaccharides containing an α -L-iduronic acid residue.⁵⁹ These authors attributed the unique heparin binding properties and thus biological activity of the α -L-iduronic acid containing tetrasaccharides to the greater flexibility of this residue.⁵⁹

In recent papers by Amster and coworkers, electron detachment dissociation (EDD) was used in the characterization of heparin-derived tetrasaccharides.^{60, 61} Ion activation methods, such as EDD and electron-induced dissociation (EID), have recently found widespread application in the characterization of biomolecules.⁶²⁻⁶⁵ Because GAGs readily form negative ions, Amster and coworkers investigated the utility of EDD in the fragmentation of a select group of multiply-charged heparan sulfate-derived tetrasaccharides; Δ UA-GlcNH-GlcA-GlcNAc^{60, 61}, Δ UA-GlcNAc-GlcA-GlcNAc⁶⁰, Δ UA-GlcNS-GlcA-GlcNAc^{60, 61}, Δ UA-GlcNS-IdoA-GlcNAc(6S)⁶⁰, Δ UA-GlcNS-IdoA-GlcNAc⁶¹, and Δ UA-GlcNH-IdoA-GlcNAc⁶¹. In EDD, multiply-charged negative ions are irradiated

with electrons of moderate energy (15-20 eV) resulting in the loss of an electron and the subsequent ion fragmentation. Electron activation of precursor ions resulted in the complete cleavage of glycosidic bonds as well as abundant cross-ring cleavage, greatly improving the capability of MS to determine sites of sulfonation and acetylation compared with collisionally activated dissociation (CAD) and infrared multiphoton dissociation (IRMPD).⁶⁰ In addition, characteristic fragmentation patterns and product ions also permitted the discrimination between GlcA and IdoA containing heparan sulfate oligosaccharides.⁶¹ Though EDD was successfully used in the structural analysis of heparan sulfate-derived tetrasaccharides, in our studies of heparin-derived tetrasaccharides using ESI-TOF-MS characteristic cross-ring and glycosidic bond cleavage product ions were not observed and it was therefore necessary to use 2D NMR techniques in order to determine the uronic acid epimers.

5.3.3 ¹H NMR Characterization of Saccharides

NMR spectroscopy has been successfully used in the characterization of complex carbohydrates providing complementary information to that obtained through MS analysis and allowing for the complete structural characterization even when multiple isomers are present. The standard strategy for the determination of the oligosaccharide primary structure by NMR involves the identification of each monosaccharide residue using scalar connectivities by 2D COSY and TOCSY. Positions of *N*- and *O*- sulfonation are inferred by the analysis of chemical shifts using reference chemical shift data.³³ Following identification of the monosaccharide residues, the oligosaccharide sequence is then determined by measurement of dipolar coupling using the ROESY experiment.

NMR spectroscopy is an essential tool used in the chemical analysis of heparin-derived oligosaccharides providing molecular level information required for complete structural characterization. However its application is limited by its relatively poor limit of detection especially when compared to other analytical techniques such as mass spectrometry. Although a ^1H survey spectrum can be measured with less material, two-dimensional NMR experiments, especially ROESY, typically require concentrations of on the order of 50-100 μM for analysis in conventional, room-temperature 5-mm probes using the most accessible magnets (i.e., 11.7 or 14 T), although cryogenically-cooled probes, novel sample tube geometries and higher magnetic fields offer significant improvements in sensitivity.⁶⁶⁻⁶⁸ This has historically limited the application of NMR to characterization of the more abundant heparin oligosaccharides.^{24, 46, 69} Although signal averaging can be used to extend the mass-limitations of detection in NMR experiments, there are practical limits (in our experience ~ 2 days) especially for experiments like ROESY that are sensitive to the laboratory environment.

5.3.4 Microcoil NMR

The high aqueous solubility of saccharides makes these samples particularly amenable to analysis by microcoil NMR. Compared with conventional 5-mm probes, microcoil NMR probes can offer a 2-fold improvement in mass-sensitivity for a given sample mass even when Shigemi tubes are employed. The improved mass sensitivity of microcoil NMR probes reduces sample consumption while increasing the speed with which the analysis is carried out. In addition, for samples that must be isolated through laborious procedures, a significant savings can be achieved in the time and effort required to isolate sufficient quantities of sample for NMR characterization.

In these experiments, a 3 μL aliquot of the reconstituted tetrasaccharide was sandwiched between plugs of deuterated chloroform (CDCl_3) in the injection syringe and manually transferred to the active volume of the CapNMR probe using an approach similar to the segmented flow technique described by Kautz et al.⁷⁰ Segmented flow minimizes dispersion of the sample permitting the use of the minimum sample volume required to obtain high resolution spectra, typically twice the volume of the microcoil observe volume.⁷¹ Positioning the sample plug into the active volume of the flow cell was accomplished by monitoring the deuterium lock channel as the sample was transferred into the probe. Upon introduction of the sample into the microcoil, the lock level was observed to reach a maximum similar to the deuterium lock level observed by the complete filling of the CapNMR microcoil with the D_2O buffer. Following the introduction of the sample into the probe, survey spectra were acquired to evaluate sample purity and ensure a sufficient S/N for subsequent 2D NMR analysis using the COSY, TOCSY, ROESY, and in some cases the natural abundance ^1H - ^{13}C HSQC experiments.

5.3.5 NMR Sensitivity Comparison

To compare the sensitivity enhancement achieved by segmented flow using CDCl_3 , ^1H NMR spectra were acquired using the same mass amount of sucrose in D_2O with and without CDCl_3 focusing. Protasis currently recommends samples be introduced using a push volume method in which the sample at a volume of 3-5 μL is positioned within the active volume of the flow probe using the sample buffer as a push solvent. Sucrose at a mass amount of 20 μg was positioned into the active volume of the flow probe using the push volume technique and the ^1H NMR spectrum was measured (Figure 5.5A). The S/N ratio was calculated for the anomeric resonance at 5.43 ppm as

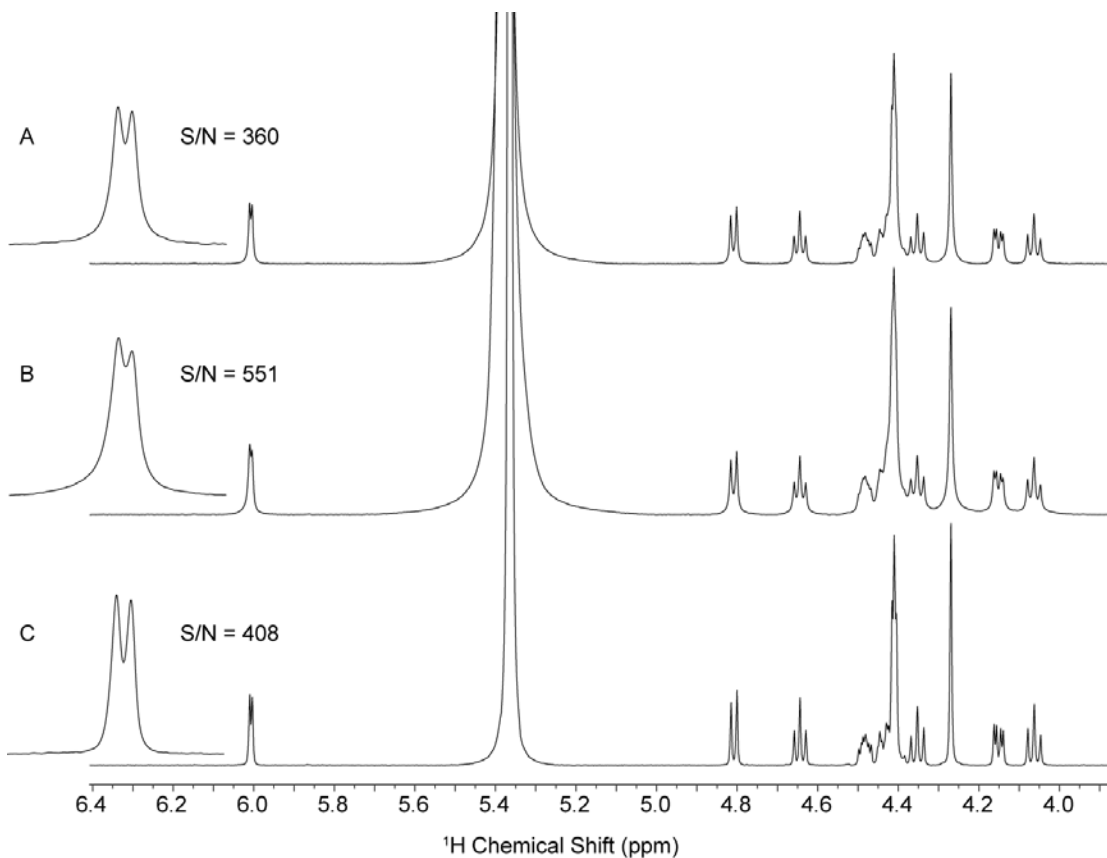


Figure 5.5. ^1H NMR spectra comparing the observed S/N and line shapes for 20 μg of sucrose in D_2O using (A) CapNMR probe using solvent push volume technique, (B) CapNMR probe using sample focusing with chloroform-*d*, and (C) a Bruker 1 mm MicroProbe with disposable capillary insert. S/N calculations were determined using the region 5.2-5.6 ppm as the signal region corresponding to the anomeric resonance of sucrose and 6.0-6.5 ppm as the noise region far removed from any peaks belonging to sucrose.

this peak was sufficiently resolved from the residual HOD resonance (4.79 ppm) to provide an accurate assessment of S/N. The S/N measured using the push volume technique was 360 while the S/N ratio for the sample sandwiching technique (Figure 5.5B) was 551. In addition to comparing the sensitivity of the two sample introduction methods for the CapNMR probe, we also recorded a similar spectrum, shown in Figure 5.5C, using a disposable 1 mm capillary in a Bruker 1 mm NMR microprobe with a minimum sample volume of 5 μ L. Using the 1 mm Bruker probe, a S/N ratio of 408 was obtained, which is similar to the value determined using the push volume technique with the CapNMR probe. Though better line shapes were observed with the 1 mm Bruker probe, a S/N improvement of 35% was obtained using chloroform focusing in the CapNMR probe, so this approach was utilized in our NMR measurements of the isolated tetrasaccharides.

5.3.6 NMR Characterization of Heparin Tetrasaccharides

The ^1H NMR spectrum for SAX peak 4 shown in Figure 5.6 was measured with 21 μ g of a heparin-derived tetrasaccharide giving 9 μ g in the active volume of the microcoil probe. In addition to the characteristic $\Delta\text{UA}_{\text{H4}}$ proton signal at 6.02 ppm of the non-reducing end uronic acid, four anomeric proton resonances are well resolved at 5.53, 5.45, 5.42, and 5.22 ppm. Chemical shift analysis can be used in the preliminary identification of the tetrasaccharide, and the intensity of the resonances can indicate whether the sample is of sufficient concentration for further characterization by 2D NMR experiments. The chemical shift of the anomeric resonance of an internal 2-O sulfonated iduronic acid (IdoA2S) is expected in the 5.2 ppm region whereas a 2-O sulfonated

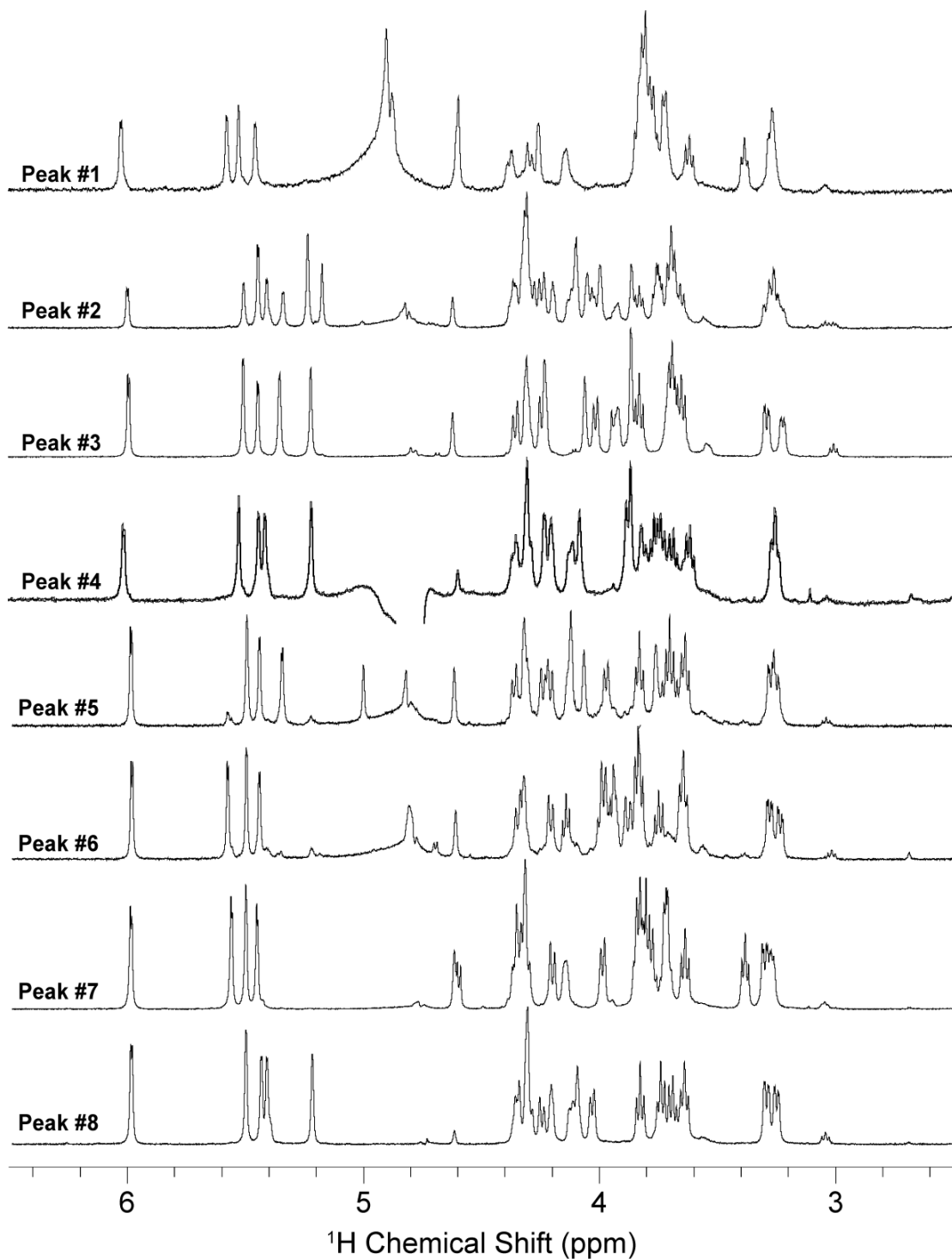


Figure 5.6. CapNMR ^1H spectra measured for the tetrasaccharide peaks isolated using SAX-HPLC.

glucuronic acid (GlcA2S) would have a signal around 4.6 ppm. Therefore, the resonance at 5.22 ppm suggests that the internal uronic acid residue is IdoA2S. The ^1H NMR spectrum can also provide information about the *N*-substituent of the glucosamine residues; *N*-acetylation can be deduced from the presence of a singlet resonances around 2 ppm.

Although important structural information can be obtained by careful interpretation of the ^1H survey spectrum, definitive resonance assignment requires measurement of 2D NMR spectra. The common strategy in assigning resonances of heparin oligosaccharides takes advantage of the well-resolved anomeric resonances along with the distinctive chemical shift of the $\Delta\text{UA}_{\text{H4}}$ of the uronic acid provides a unique entry point into the 2D data for spectral interpretation. Figures 5.7A, B, and C correspond to the COSY, TOCSY, and ROESY spectra, respectively, for SAX peak 4. These 2D spectra were acquired in 42 hours with 21 μg of material in the microcoil probe. In the spectra presented in Figure 5.7, the $\Delta\text{UA}_{\text{H4}}$ proton of the unsaturated uronic acid appears at 6.02 ppm as labeled in the COSY spectrum shown in Figure 4.10A. Using the COSY spectrum, the scalar connectivity to $\Delta\text{UA}_{\text{H3}}$ (4.24), $\Delta\text{UA}_{\text{H2}}$ (4.61), and subsequently, $\Delta\text{UA}_{\text{H1}}$ (5.53), can be traced establishing the connectivity within the monosaccharide residue A. This was then repeated for all subsequent monosaccharide residues.

The assignment of chemical shifts with closely resonating protons required the use of the TOCSY experiment. The TOCSY spectrum, Figure 5.7B, was necessary for the assignment of the resonances for the glucosamine residues and was also used to

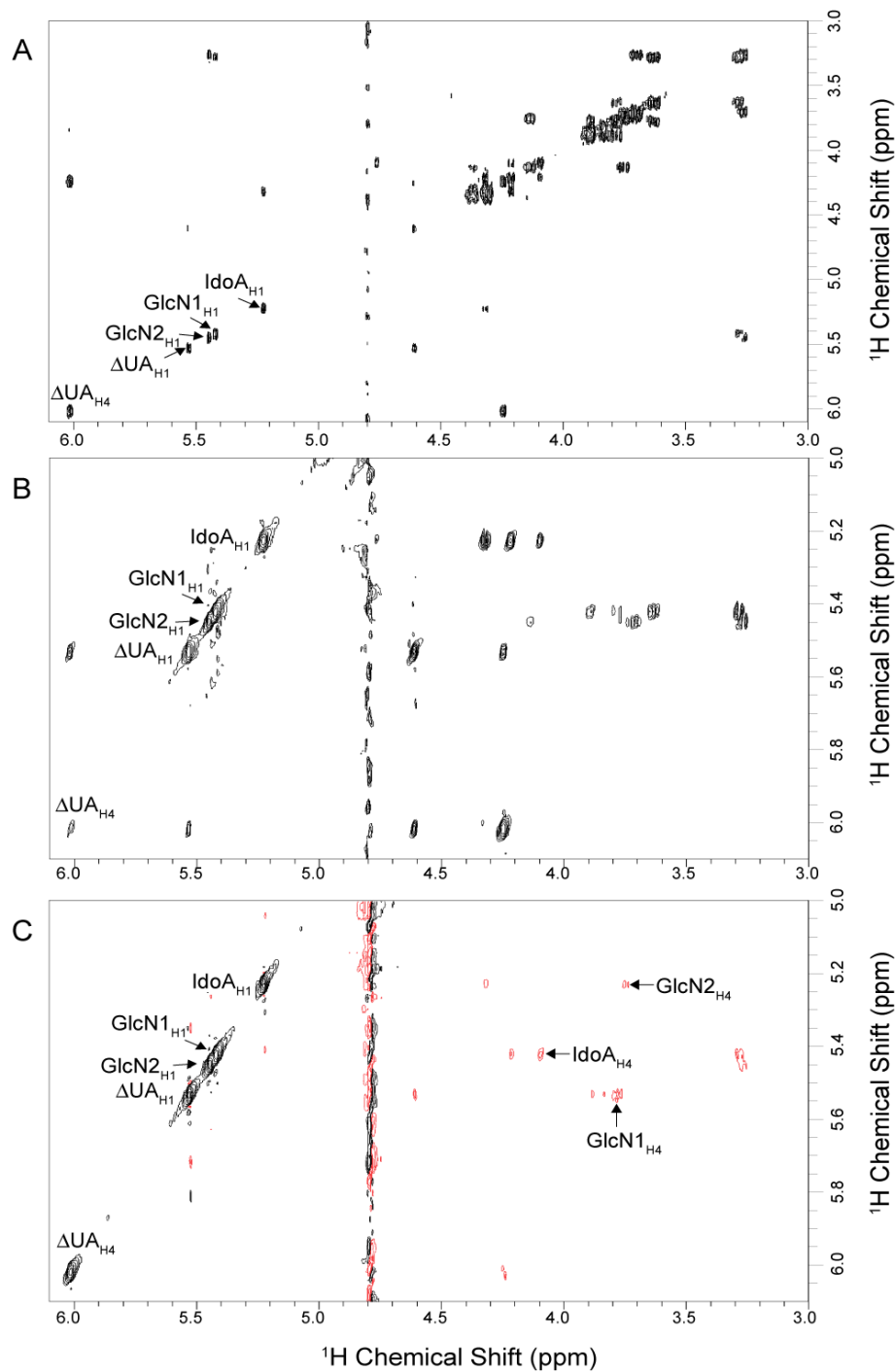


Figure 5.7. CapNMR spectra measured with 21 μg of $\Delta\text{UA}(2\text{S})\text{-GlcNS-IdoA}(2\text{S})\text{-GlcNS}(6\text{S})$ isolated as SAX peak 4. Portions of the (A) COSY, (B) TOCSY and (C) ROESY spectra showing cross peaks to the well-resolved anomeric resonances used to establish the structure of the tetrasaccharide. All spectra were acquired within a 42 hr period.

confirm the COSY assignments. In the TOCSY spectrum, cross peaks are observed among most protons within each of the monosaccharide residue as the magnetization is efficiently transferred within their respective spin systems. Figure 5.7B is a portion of the TOCSY spectrum for SAX peak 4 showing cross-peaks to the well resolved anomeric resonances. As a result of the small amount of material used in the acquisition of the 2D spectra, correlations between the anomeric resonance of the reducing end glucosamine at 5.45 ppm and its H6 protons were not present above the noise and it was therefore necessary to use TOCSY correlations with the H2 proton at 3.26 ppm in order to confirm sulfonation at the 6-O position of the reducing-end glucosamine residue. Chemical shifts established using both COSY and TOCSY experiments is presented in Table 5.2. Comparison of chemical shift data with values presented in the literature eluded to the structural identities of the individual monosaccharide residues.³³ The ROESY experiment was used to establish connectivities and spatial positions of the individual monosaccharide residues within the intact tetrasaccharide. In the ROESY experiment, cross peaks are observed between resonances of the H1 protons and the H4 protons of the next residue, connected via a glycosidic bond. Shown in Figure 5.7C is a portion of the ROESY spectrum showing the important cross peaks from $\Delta\text{UA}_{\text{H1}}$ to GlcN1_{H4} , GlcN1_{H1} to IdoA_{H4} , and finally IdoA_{H1} to GlcN2_{H4} . From the measured chemical shifts for SAX peak 4, summarized in Table 5.2, and ROESY cross peaks the identity of the tetrasaccharide was determined to be $\Delta\text{UA}(2\text{S})\text{-GlcNS-IdoA}(2\text{S})\text{-GlcNS}(6\text{S})$. This structure is consistent with the specificity of the heparinase I enzyme which requires a 2-O-sulfonated residue at the non-reducing end of the digested heparin fragment. NMR spectra for SAX peak 4 was presented as it corresponds to the smallest fraction isolated

Table 5.2. ¹H Chemical shifts of the tetrasaccharides isolated using SAX-HPLC

SAX Peak Number	Proton	NMR Chemical shifts (ppm)			
		ΔUA(2S)-	-GlcNS-	-GlcA-	-GlcNS(6S)
1		ΔUA(2S)-	-GlcNS-	-GlcA-	-GlcNS(6S)
	1	5.54	5.58	4.61	5.46
	2	4.61	3.29	3.40	3.28
	3	4.27	3.63	3.85	3.73
	4	6.03	3.79	3.79	3.75
	5		3.83	3.81	4.16
	6		3.82		4.31
6'		3.84		4.39	
2		IdoA(2S)-	-GlcNS(6S)-	-IdoA(2S)-	-GlcNS(6S)
	1	5.18	5.41	5.24	5.45
	2	4.31	3.29	4.33	3.26
	3	4.11	3.71	4.21	3.70
	4	4.00	3.77	4.11	3.76
	5	4.84	4.05	4.82	4.14
	6		4.27		4.31
6'		4.33		4.38	
3		ΔUA(2S)-	-GlcNS(6S)-	-IdoA(2S)-	-GlcNS
	1	5.51	5.36	5.23	5.45
	2	4.63	3.31	4.31	3.24
	3	4.32	3.67	4.24	3.70
	4	5.99	3.84	4.07	3.72
	5		4.03	4.80	3.88
	6		4.25		3.83
6'		4.36		3.93	
4		ΔUA(2S)-	-GlcNS-	-IdoA(2S)-	-GlcNS(6S)
	1	5.53	5.42	5.22	5.45
	2	4.61	3.28	4.32	3.26
	3	4.24	3.63	4.22	3.70
	4	6.02	3.78	4.10	3.76
	5		3.79	4.77	4.13
	6		3.83		4.32
6'		3.89		4.38	
5		ΔUA(2S)-	-GlcNS(6S)-	-IdoA-	-GlcNS(6S)
	1	5.50	5.36	5.01	5.45
	2	4.63	3.29	3.77	3.26
	3	4.33	3.65	4.13	3.72
	4	6.00	3.85	4.08	3.76
	5		3.99	4.79	4.14
	6		4.22		4.26
6'		4.37		4.33	
6		ΔUA(2S)-	-GlcNS(6S)-	-GlcA(2S)-	-GlcNS
	1	5.51	5.59	4.71	5.45
	2	4.62	3.30	4.15	3.25
	3	4.33	3.66	4.00	3.76
	4	5.99	3.84	3.84	3.66
	5		3.99	3.85	3.95
	6		4.22		3.89
6'		4.36		3.96	

7		Δ UA(2S)-	-GlcNS(6S)-	-GlcA-	-GlcNS(6S)
	1	5.51	5.57	4.61	5.46
	2	4.63	3.31	3.39	3.28
	3	4.33	3.65	3.86	3.72
	4	6.00	3.84	3.80	3.72
	5		4.00	3.82	4.15
	6		4.21		4.32
	6'		4.35		4.37
8		Δ UA(2S)-	-GlcNS(6S)-	-IdoA(2S)-	-GlcNS(6S)
	1	5.51	5.42	5.23	5.44
	2	4.62	3.30	4.32	3.26
	3	4.32	3.65	4.22	3.70
	4	5.99	3.84	4.10	3.76
	5		4.05	4.80	4.14
	6		4.25		4.31
	6'		4.35		4.35

in this study, thus demonstrating the utility of microcoil NMR in the characterization of mass-limited amounts of sample.

Most of the isolated SAX fractions were composed of a single component as demonstrated by their ^1H survey spectra (Figure 5.6) and were readily characterized using 2D NMR techniques presented above. Table 5.2 summarizes the ^1H chemical shift data for the isolated tetrasaccharides recorded using 2D COSY and TOCSY with the CapNMR probe. Although most of the fractions consisted of a single component, examination of the ^1H NMR survey spectrum obtained for SAX peak 2 (Figure 5.6) indicated that it was probably composed of two different tetrasaccharides present at roughly equal concentrations. It is interesting, that integration of the anomeric resonances and the $\Delta\text{UA}_{\text{H4}}$, presented in Figure 5.8, suggests that only one of the tetrasaccharides present in the fraction contains a double-bond at the non-reducing end uronic acid residue. Further analysis of the ^1H NMR spectra measured for SAX peaks 2 and 3 (Figures 5.6) alludes to the possibility that one of the components in SAX peak 2 is the closely eluting SAX peak 3 as observed in the SAX chromatogram (Figure 5.3B).

In order to confirm the identity of the contaminant in SAX peak 2 as being SAX peak 3, their TOCSY and ROESY spectra were compared. Shown in Figure 5.9 are expansions of the TOCSY (Figure 5.9A) and ROESY (Figure 5.9B) spectra used in the structural characterization of SAX peak 3. Characterization of SAX peak 3 was performed as demonstrated above, whereas, the $\Delta\text{UA}_{\text{H4}}$ proton of the unsaturated uronic acid and the well-resolved anomeric resonances of the tetrasaccharide provided an entry point for spectral determination and comparison of measured chemical shift data with values presented in the literature relating to the identities of the individual monosaccharide residues. From the measured chemical shifts, summarized in Table

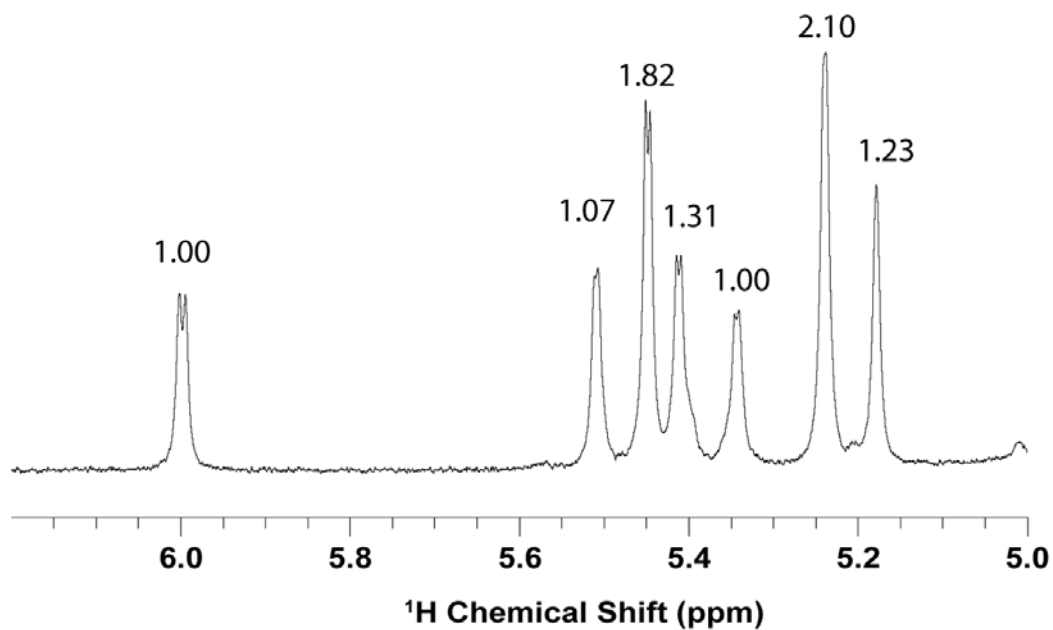


Figure 5.8. ¹H NMR spectrum for SAX peak 2 showing the anomeric and $\Delta\text{UA}_{\text{H4}}$ chemical shift region. The measured integrals displayed above each peak were normalized to the area of the $\Delta\text{UA}_{\text{H4}}$ resonance.

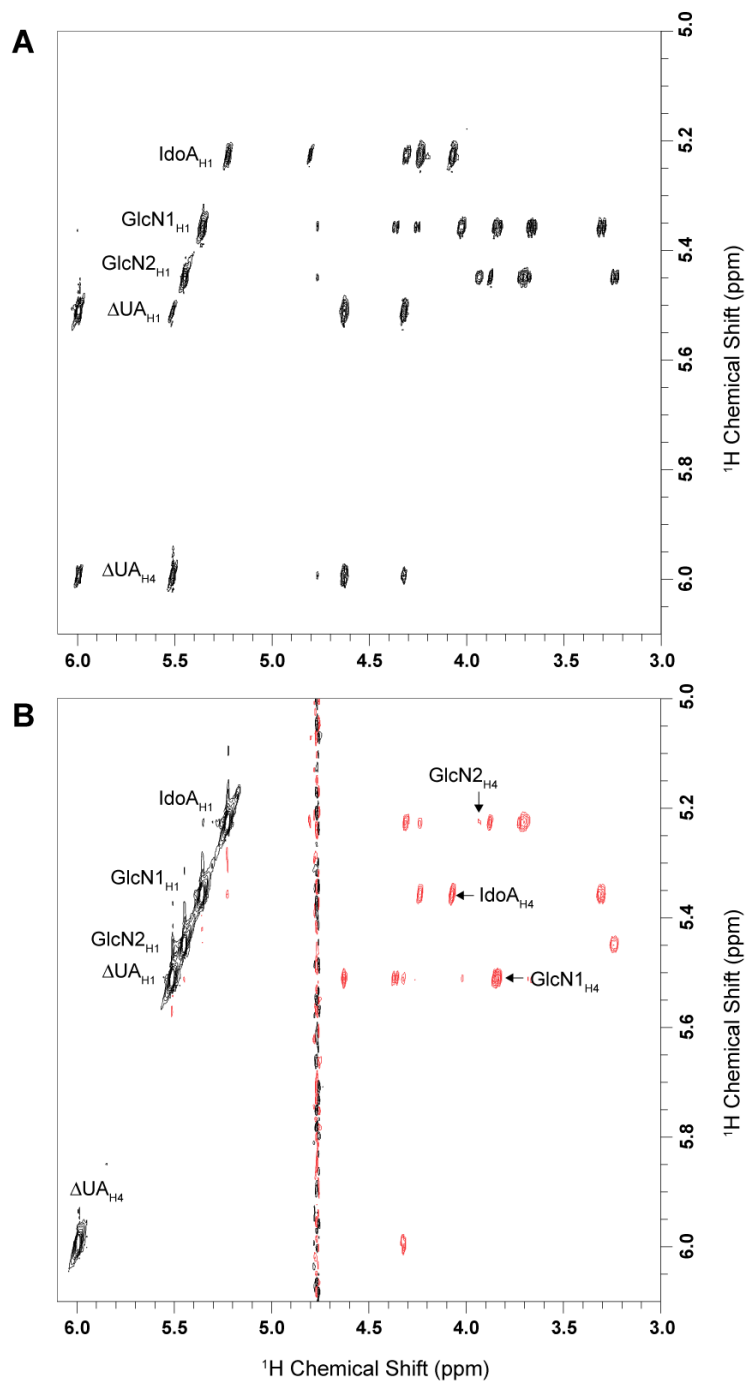


Figure 5.9. CapNMR ¹H spectra measured for ΔUA(2S)-GlcNS(6S)-IdoA(2S)-GlcNS isolated as SAX peak 3. Portions of the (A) TOCSY and (B) ROESY spectra measured for this sample.

5.2, and the ROESY cross-peaks the identity of the tetrasaccharide was determined to be Δ UA(2S)-GlcNS(6S)-IdoA(2S)-GlcNS.

Figure 5.10 show an expansion of the TOCSY (Figure 5.10A) and ROESY (Figure 5.10B) spectra acquired for SAX peak 2. Most peaks corresponding to the unknown component can be differentiated from those of SAX peak 3 shown in Figure 5.9 A. Peaks corresponding to SAX peak 3 are labeled according to their anomeric and Δ UA_{H4} resonances. From the measured ¹H integrals (Figure 5.8) and the observed number of TOCSY cross-peaks for the glucosamine anomeric resonance at 5.45 ppm and the iduronic acid resonance at 5.23 ppm (Figure 5.10A) of peak 2, it is evident that the resonances at 5.23 and 5.45 ppm contain protons from both tetrasaccharides, peak 2 and 3. Based on the integrals (Figure 5.8) and the assumptions that peak 2 is composed of two independent tetrasaccharide components and one of the components in the peak is the closely eluting peak 3, we assigned the Δ UA_{H4} resonance at 5.99 ppm and the anomeric resonances at 5.51 (Δ UA_{H1}) and 5.36 ppm (GlcN1_{H1}) as belonging to only peak 3.

Characterization of peak 2 was slightly complicated as a result of the assignment of the Δ UA_{H4} resonance at 5.99 ppm to peak 3. As with the other isolated tetrasaccharides, characterization of peak 2 progressed via the assignment of the individual monosaccharide residues using the 2D COSY and TOCSY spectra. From the measured chemical shifts of peak 2 (Table 5.2), two iduronic acid residues were observed. Through the ROESY spectrum (Figure 5.10B), the iduronic acid anomeric resonance at 5.23 ppm was determined to be from the internal uronic acid residue containing a ROESY cross-peaks to the H-1 proton of the terminal glucosamine (3.77 ppm) while the anomeric resonance at 5.17 ppm corresponded to the terminal uronic

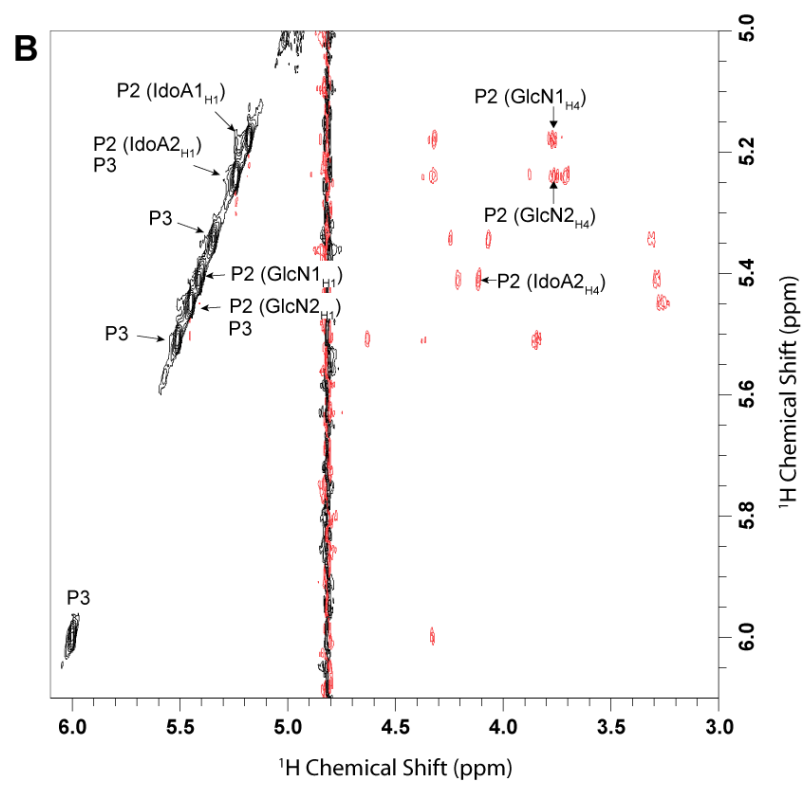
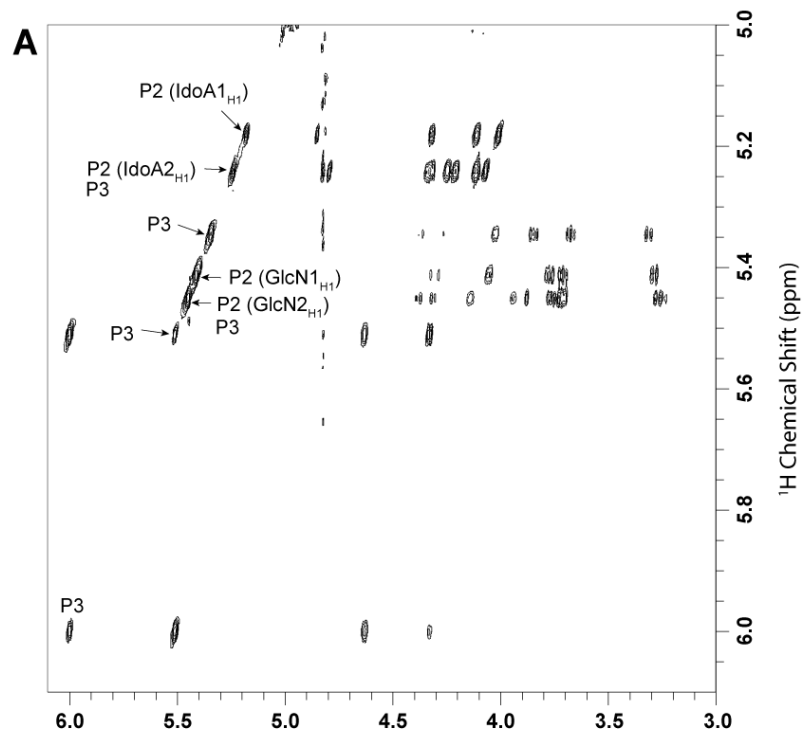


Figure 5.10. CapNMR ^1H spectra measured for SAX peak 2 Portions of the (B) TOCSY and (C) ROESY spectra measured for this sample. The spectrum was acquired within a 24 hr period for a sample containing 49 μg of isolated sample. Cross peaks due to $\Delta\text{UA}(2\text{S})\text{-GlcNS}(6\text{S})\text{-IdoA}(2\text{S})\text{-GlcNS}$ (labeled P3) are assigned in Figure 5.9.

acid residue having a ROESY cross-peak to the internal glucosamine (3.78 ppm). The absence of a characteristic $\Delta\text{UA}_{\text{H4}}$ resonance helped to establish the idea that this tetrasaccharide lacked the characteristic double-bond resulting from the enzymatic depolymerization of heparin. This suggests that the unknown component in SAX peak 2 may originate from the natural non-reducing terminus of the heparin polysaccharide.

Following acquisition of the NMR spectra, the sample was pushed out of the microcoil NMR probe and collected. To confirm the identities of the tetrasaccharides characterized by NMR, the SAX peaks were also analyzed using RPIP-UPLC-MS. The total ion chromatogram (TIC) for SAX peak 2 is shown in Figure 5.11A with the mass spectra of the individual peaks given in Figures 5.11B and 5.11C. Splitting of the tetrasaccharide peaks in the RPIP-UPLC-MS separation of SAX peak 2 (Figure 5.11A) is a result of the separation of the α and β anomeric forms of the individual tetrasaccharides. The peaks at 6.44 and 6.76 min correspond to the α and β anomeric forms, respectively, of peak 3 while the peaks at 7.30 and 7.55 min correspond to the α and β anomeric forms, respectively, of peak 2. RPIP-UPLC-MS analysis of the SAX peak eluting at 53 min (Figure 5.3B) matches the retention time (6.44 min) and m/z (535.98 Da) of the doubly-charged molecular ion $[\text{M}-2\text{H}]^{2-}$ observed for $\Delta\text{UA}(2\text{S})\text{-GlcNS}(6\text{S})\text{-IdoA}(2\text{S})\text{-GlcNS}$ in SAX peak 3. As shown in Figure 5.11A and Figure 5.11C, peak 2 elutes at 7.30 min and has a doubly-charged molecular ion $[\text{M}-2\text{H}]^{2-}$ of 584.96 Da. This unique molecular ion is consistent with a hexasulfated tetrasaccharide lacking the characteristic double bond at the nonreducing end uronic acid residue. From the measured chemical shifts, summarized in Table 5.2, the monosaccharide sequence information provided by ROESY, and complementary MS information the identity of the tetrasaccharide was determined to be $\text{IdoA}(2\text{S})\text{-GlcNS}(6\text{S})\text{-IdoA}(2\text{S})\text{-GlcNS}(6\text{S})$. This

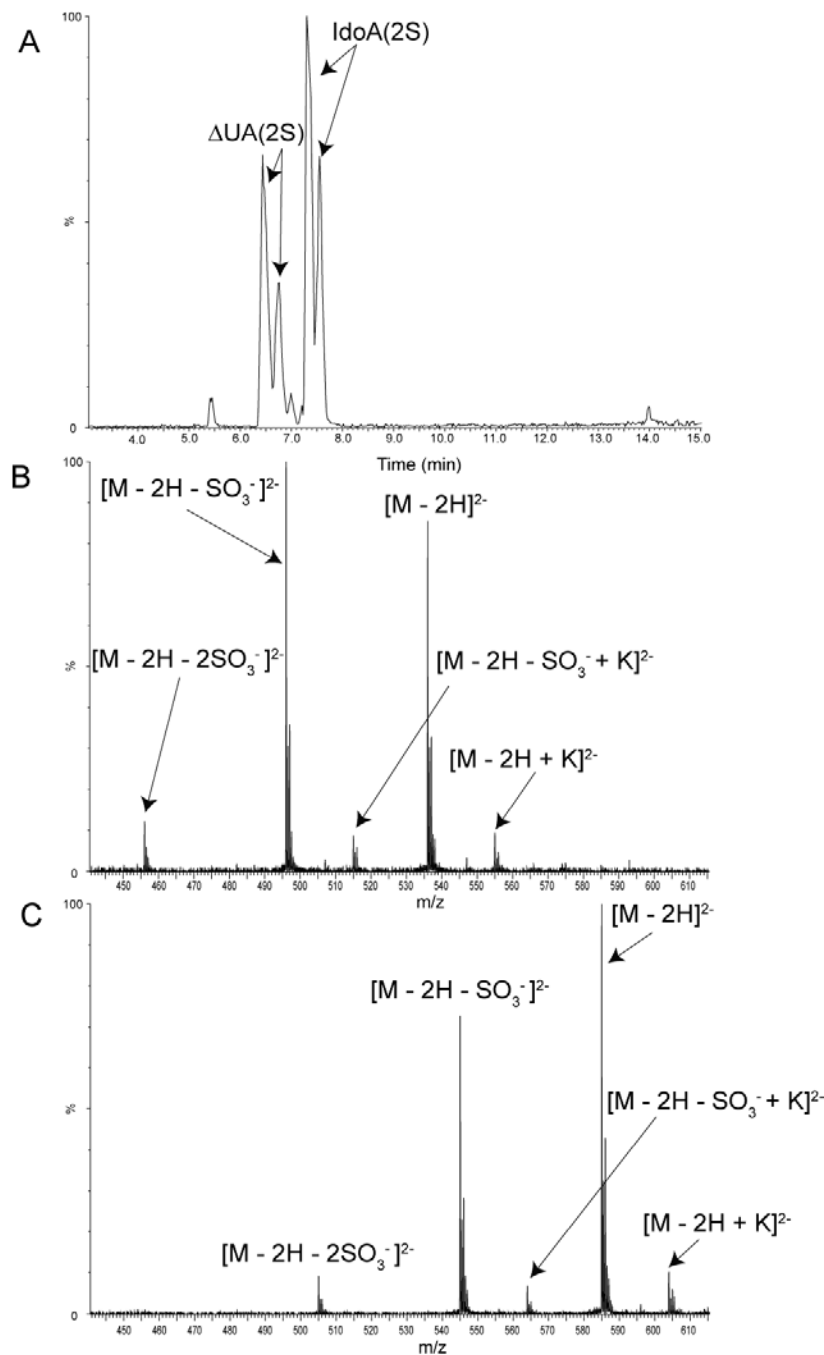


Figure 5.11. (A) Total ion chromatogram of the RPIP-UPLC/MS separation of SAX peak 2 containing tetrasaccharides $\Delta\text{UA}(2\text{S})\text{-GlcNS}(6\text{S})\text{-IdoA}(2\text{S})\text{-GlcNS}$ and $\text{IdoA}(2\text{S})\text{-GlcNS}(6\text{S})\text{-IdoA}(2\text{S})\text{-GlcNS}(6\text{S})$ along with their mass spectra (B) and (C), respectively. The RPIP-UPLC conditions used resolve the α and β anomers of the reducing end residue, complicating the separation.

tetrasaccharide sequence is unique, lacking a unsaturated uronic acid at the non-reducing end of the heparin-derived oligosaccharide. To our knowledge this tetrasaccharides has not been reported in the literature.

It is interesting to note that although IdoA(2S)-GlcNS(6S)-IdoA(2S)-GlcNS(6S), SAX peak 2, is a hexasulfonated tetrasaccharide, it elutes much earlier in the SAX chromatogram (Figure 5.3B) than the corresponding double-bond containing hexasulfonated tetrasaccharide, Δ UA(2S)-GlcNS(6S)-IdoA(2S)-GlcNS(6S), and also prior to all of the pentasulfated species we identified. This suggests a critical role of the double bond and the concomitant change in ring-conformation on retention of oligosaccharides in the charged-based SAX separation. Though a considerable difference in SAX retention times was observed as a result of the double-bond at the non-reducing end uronate residue, in the RPIP-HPLC separation both hexasulfonated tetrasaccharides, IdoA(2S)-GlcNS(6S)-IdoA(2S)-GlcNS(6S) (7.51 min) and Δ UA(2S)-GlcNS(6S)-IdoA(2S)-GlcNS(6S) (7.76 min), are observed to elute after the pentasulfonated tetrasaccharides as would be expected with charge based separations.

Shown in Table 5.3 are the identities of all of the isolated tetrasaccharides, their SAX-HPLC retention times, RPIP-UPLC retention times, the mass amounts used in their characterization by CapNMR, and their characteristic m/z values measured by RPIP-UPLC-MS. Most of the tetrasaccharides summarized in Table 5.3 are commonly observed in a heparinase digested mixture as the majority of the individual fragments are highly sulfonated. The most abundant tetrasaccharide is the hexasulfonated tetrasaccharide, Δ UA(2S)-GlcNS(6S)-IdoA(2S)-GlcNS(6S), SAX peak 8, which was originally characterized by ^1H and ^{13}C NMR in the mid 80's.^{69, 72} As the heparin biopolymer is rich in this highly sulfonated sequence, literature corresponding to the

Table 5.3. SAX retention times, RPIP-UPLC retention times, m/z of the molecular ion $[M-2H]^{-2}$, the mass used in the microcoil NMR experiments and the identities of the heparin-derived tetrasaccharides determined, and references previously reporting this compound.

Number	SAX Retention Time	RPIP-UPLC Retention Time	Molecular Ion m/z	Mass for CapNMR Experiments	Tetrasaccharide Identity	References
1	49 min	5.58 min	496.02 Da	34 μ g	Δ UA(2S)-GlcNS-GlcA-GlcNS(6S)	Merchant1985, Yamada1995
2	53	7.51	584.96	49	IdoA(2S)-GlcNS(6S)-IdoA(2S)-GlcNS(6S)	NA
3	54	6.61	535.98	149	Δ UA(2S)-GlcNS(6S)-IdoA(2S)-GlcNS	Yamada1994Ya mada1995 Xiao2011
4	58	6.78	535.98	21	Δ UA(2S)-GlcNS-IdoA(2S)-GlcNS(6S)	Rice1989 Yamada1995
5	66	6.90	535.98	40	Δ UA(2S)-GlcNS(6S)-IdoA-GlcNS(6S)	NA
6	68	6.99	535.98	81	Δ UA(2S)-GlcNS(6S)-GlcA(2S)-GlcNS	Yamada1995
7	75	7.08	535.98	192	Δ UA(2S)-GlcNS(6S)-GlcA-GlcNS(6S)	Merchant1985, Rice1989 Yamada1994 Yamada1995 Xiao2011
8	80	7.76	575.96	413	Δ UA(2S)-GlcNS(6S)-IdoA(2S)-GlcNS(6S)	Merchant1985, Rice1989 Yamada1994 Yamada1995 Xiao2011

characterization of this tetrasaccharide is extensive and diverse. This includes studies on the conformation and flexibility of the monosaccharide residues within the chain as well as the influence that these residues has on its overall binding.^{59, 73, 74} Earlier investigations of the highly sulfonated tetrasaccharides necessitated milligram amounts of each compound for unambiguous identifications. Merchant and co-workers used a 360 MHz NMR for the characterization of 5 major tetrasaccharides. Samples were obtained via the fractionation of a mixture of 25 mg of tetrasaccharides on SAX-HPLC. The tetra- and the pentasulfonated tetrasaccharides corresponding to the SAX peaks 1 and 7 (Figure 5.3B and Table 5.3), were identified in this study.⁶⁹ Another study by Rice and co-workers successfully isolated and characterized 3 structurally unique tetrasaccharides.³⁷ In addition to the most abundant SAX peaks 7 and 8 they also characterized the minor compound Δ UA(2S)-GlcNS-IdoA(2S)-GlcNS(6S) corresponding to SAX peak 4, albeit the characterization of the isolated compounds by 2D COSY and ¹³C-¹H correlation spectroscopy required milligram quantities of material.³⁷ As higher field NMR magnets came into general use, the identification of less abundant structures became feasible. In 1995, Yamada and co-workers published the structures of eleven tetrasaccharides; the tetrasaccharides characterized included 6 of the 8 tetrasaccharides observed in our SAX separation. The 2 tetrasaccharides not observed were IdoA(2S)-GlcNS(6S)-IdoA(2S)-GlcNS(6S) and Δ UA(2S)-GlcNS(6S)-IdoA-GlcNS(6S) corresponding to peaks 2 and 5, respectively. Characterization of the 11 tetrasaccharides was accomplished using a 500 MHz NMR in addition to FAB-MS.⁴⁵ Though the mass amounts of material used in the characterization of the tetrasaccharides was not reported we suspect that milligram amounts were required. From their study, they concluded that the internal 2-O-sulfonated uronic acid residues

are not exclusively iduronic acid by digestion experiments performed on the isolated tetrasaccharides.⁴⁵ A 2-O-sulfonated glucuronic acid was also observed in this study corresponding to peak 6 (Table 5.3). To our knowledge the tetrasaccharides corresponding to SAX peaks 2 and 5 (Table 5.3) have never been reported as discrete structures. The pentasulfonated tetrasaccharide, Δ UA(2S)-GlcNS(6S)-IdoA-GlcNS(6S) (SAX peak 5), is the diastereomeric pair of Δ UA(2S)-GlcNS(6S)-GlcA-GlcNS(6S), peak 7, containing an internal GlcNS(6S)-IdoA motif. This motif serves as a substrate for the heparinase II enzyme and therefore can only be present in heparin digestion solutions utilizing only the heparinase I enzyme. The tetrasaccharide, IdoA(2S)-GlcNS(6S)-IdoA(2S)-GlcNS(6S) (SAX peak 2), may represent the terminus of a biosynthetically formed native heparin chain or a newly formed non-reducing terminus exposed by endo- β -glucuronidase involved in the post-synthetic fragmentation of macromolecular heparin. There is only one fully characterized unsaturated heparin-derived compound in the literature with characteristic chemical shifts and MS data, a saturated tetrasulfated trisaccharide described by Yamada et al.⁴⁶ This saturated trisaccharide fragment was observed to co-elute with an unsaturated trisulfated tetrasaccharide, it was therefore necessary to assign chemical shifts using 2D TOCSY and COSY techniques, as reasonable heteronuclear correlations experiments of oligosaccharides using conventional 5 mm tubes on a 500 MHz instrument necessitates at least one order of magnitude more sample compared to CapNMR probes.

The identification of tetrasaccharides is relatively straightforward considering the mass of individual structures one can isolate and purify from a heparinase digested mixture, however the main advantage of microcoil-based structural characterization of individual structures resides in its extension to much larger heparin- or heparan sulfate

oligosaccharides where the accessibility of unique structures with the purity desired for NMR and MS experiments are mass-limited.

From Table 5.3 it is interesting to note that in addition to separating the tetrasaccharide sulfation isomers, we were also able to separate the different IdoA and GlcA acid epimers. Following the identification of the isolated tetrasaccharides, we observed that compounds containing an internal GlcA residue have longer SAX retention times than their IdoA-containing counterparts having the same sulfonation positions and net negative charge. The same elution order was similarly observed by Schenauer and coworkers in the case of two less charged HS-derived hexasaccharides, Δ UA-GlcNS-IdoA2S-GlcNS-IdoA-GlcNAc and Δ UA-GlcNS-IdoA2S-GlcNS-GlcA-GlcNAc, which differ only in their C5 epimerization of the uronic acid at the reducing end disaccharide.³⁰ These observations confirm that the configuration of the internal uronic acid residue plays a crucial role in the interaction between the oligosaccharides and the stationary phase of the SAX column.

5.4 Summary

The results presented demonstrate the potential of microcoil NMR for the structure determination of isolated heparin tetrasaccharide isomers. Focusing the reconstituted sample between an immiscible plug of deuterated chloroform provided an improvement in mass sensitivity of 53% compared with the push volume technique and 35% compared with a 1-mm probe using capillary tubes. The complete structural elucidation of two diastereomer pairs and various penta- and hexasulfonated heparin tetrasaccharides were carried out using minute amounts (as low as 21 μ g) of purified samples. A unique, hexasulfated tetrasaccharide IdoA(2S)-GlcNS(6S)-IdoA(2S)-

GlcNS(6S) was identified besides the well known hexasulfonated Δ UA(2S)-GlcNS(6S)-IdoA(2S)-GlcNS(6S), where the non-reducing end lacks the double bond introduced by heparinase I. The tetrasaccharide Δ UA(2S)-GlcNS(6S)-IdoA-GlcNS(6S) among the five pentasulfonated tetrasaccharide has not been reported previously as a discrete structure.

5.5 References

1. Rabenstein, D. L. Heparin and heparan sulfate: structure and function. *Nat. Prod. Rep.* **2002**, *19*, 312-331.
2. Jones, C. J.; Beni, S.; Limtiaco, J. F. K.; Langeslay, D. J.; Larive, C. K. Heparin Characterization: Challenges and Solutions. *Annu. Rev. Anal. Chem.* **2011**, *4*, Submitted.
3. Capila, I.; Linhardt, R. J. Heparin - Protein interactions. *Angew. Chem.-Int. Edit.* **2002**, *41*, 391-412.
4. Korir, A.; Larive, C. Advances in the separation, sensitive detection, and characterization of heparin and heparan sulfate. *Anal. Bioanal. Chem.* **2009**, *393*, 155-169.
5. Beni, S.; Limtiaco, J.; Larive, C. Analysis and characterization of heparin impurities. *Anal. Bioanal. Chem.* **2010**, *In Press*.
6. Korir, A. K.; Limtiaco, J. F. K.; Gutierrez, S. M.; Larive, C. K. Ultrapformance ion-pair liquid chromatography coupled to electrospray time-of-flight mass spectrometry for compositional profiling and quantification of heparin and heparan sulfate. *Anal. Chem.* **2008**, *80*, 1297-1306.
7. Gunay, N. S.; Linhardt, R. J. Capillary electrophoretic separation of heparin oligosaccharides under conditions amenable to mass spectrometric detection. *J. Chromatogr. A* **2003**, *1014*, 225-233.
8. Henriksen, J.; Roepstorff, P.; Ringborg, L. H. Ion-pairing reversed-phased chromatography/mass spectrometry of heparin. *Carbohydr. Res.* **2006**, *341*, 382-387.
9. Thanawiroon, C.; Rice, K. G.; Toida, T.; Linhardt, R. J. Liquid Chromatography/Mass Spectrometry Sequencing Approach for Highly Sulfated Heparin-derived Oligosaccharides. *J. Biol. Chem.* **2004**, *279*, 2608-2615.
10. Yang, B.; Weyers, A.; Baik, J. Y.; Sterner, E.; Sharfstein, S.; Mousa, S. A.; Zhang, F.; Dordick, J. S.; Linhardt, R. J. Ultra-performance ion-pairing liquid chromatography with on-line electrospray ion trap mass spectrometry for heparin disaccharide analysis. *Anal. Biochem.* **2011**, *In Press, Corrected Proof*.
11. Zaia, J. On-line separations combined with MS for analysis of glycosaminoglycans. *Mass Spectrom. Rev.* **2009**, *28*, 254-272.
12. Eldridge, S. L.; Higgins, L. A.; Dickey, B. J.; Larive, C. K. Insights into the Capillary Electrophoresis Separation of Heparin Disaccharides from Nuclear Magnetic Resonance, pKa, and Electrophoretic Mobility Measurements. *Anal. Chem.* **2009**, *81*, 7406-7415.
13. Thanawiroon, C.; Linhardt, R. J. Separation of a complex mixture of heparin-derived oligosaccharides using reversed-phase high-performance liquid chromatography. *J. Chromatogr. A* **2003**, *1014*, 215-223.
14. Karamanos, N. K.; Vanky, P.; Tzanakakis, G. N.; Tseggenidis, T.; Hjerpe, A. Ion-pair high-performance liquid chromatography for determining disaccharide composition in heparin and heparan sulphate. *J. Chromatogr. A* **1997**, *765*, 169-179.
15. Chuang, W.-L.; McAllister, H.; Rabenstein, D. L. Hexasaccharides from the histamine-modified depolymerization of porcine intestinal mucosal heparin. *Carbohydr. Res.* **2002**, *337*, 935-945.

16. Lindahl, U.; Backstrom, G.; Thunberg, L.; Leder, I. G. Evidence for a 3-O-sulfated D-glucosamine residue in the antithrombin-binding sequence of heparin. *Proc. Natl. Acad. Sci. U. S. A.* **1980**, *77*, 6551-6555.
17. Marchetti, M.; Vignoli, A.; Russo, L.; Balducci, D.; Pagnoncelli, M.; Barbui, T.; Falanga, A. Endothelial capillary tube formation and cell proliferation induced by tumor cells are affected by low molecular weight heparins and unfractionated heparin. *Thromb. Res.* **2008**, *121*, 637-645.
18. Futamura, M.; Dhanasekaran, P.; Handa, T.; Phillips, M. C.; Lund-Katz, S.; Saito, H. Two-step Mechanism of Binding of Apolipoprotein E to Heparin. *J. Biol. Chem.* **2005**, *280*, 5414-5422.
19. Naimy, H.; Leymarie, N.; Bowman, M. J.; Zaia, J. Characterization of Heparin Oligosaccharides Binding Specifically to Antithrombin III Using Mass Spectrometry. *Biochemistry* **2008**, *47*, 3155-3161.
20. Chai, W.; Luo, J.; Lim, C. K.; Lawson, A. M. Characterization of Heparin Oligosaccharide Mixtures as Ammonium Salts Using Electrospray Mass Spectrometry. *Anal. Chem.* **1998**, *70*, 2060-2066.
21. Eldridge, S. L.; Korir, A. K.; Gutierrez, S. M.; Campos, F.; Limtiaco, J. F. K.; Larive, C. K. Heterogeneity of depolymerized heparin SEC fractions: to pool or not to pool? *Carbohydr. Res.* **2008**, *343*, 2963-2970.
22. Ziegler, A.; Zaia, J. Size-exclusion chromatography of heparin oligosaccharides at high and low pressure. *Journal of Chromatography B* **2006**, *837*, 76-86.
23. Chuang, W.-L.; McAllister, H.; Rabenstein, D. L. Chromatographic methods for product-profile analysis and isolation of oligosaccharides produced by heparinase-catalyzed depolymerization of heparin. *J. Chromatogr. A* **2001**, *932*, 65-74.
24. Pervin, A.; Gallo, C.; Jandik, K. A.; Han, X.-J.; Linhardt, R. J. Preparation and structural characterization of large heparin-derived oligosaccharides. *Glycobiology* **1995**, *5*, 83-95.
25. Imanari, T.; Toida, T.; Koshiishi, I.; Toyoda, H. High-performance liquid chromatographic analysis of glycosaminoglycan-derived oligosaccharides. *J. Chromatogr. A* **1996**, *720*, 275-293.
26. Rice, K. G.; Kim, Y. S.; Grant, A. C.; Merchant, Z. M.; Linhardt, R. J. High-performance liquid chromatographic separation of heparin-derived oligosaccharides. *Anal. Biochem.* **1985**, *150*, 325-331.
27. Cecchi, T. Ion Pairing Chromatography. *Crit. Rev. Anal. Chem.* **2008**, *38*, 161-213.
28. Stahlberg, J. Ion-Pair Chromatography and Related Techniques. *J. Am. Chem. Soc.* **2010**, *132*, 1732-1732.
29. Cecchi, T.; Pucciarelli, F.; Passamonti, P. Extended Thermodynamic Approach to Ion Interaction Chromatography. *Anal. Chem.* **2001**, *73*, 2632-2639.
30. Doneanu, C. E.; Chen, W.; Gebler, J. C. Analysis of Oligosaccharides Derived from Heparin by Ion-Pair Reversed-Phase Chromatography/Mass Spectrometry. *Anal. Chem.* **2009**, *81*, 3485-3499.
31. Kuberan, B.; Lech, M.; Zhang, L.; Wu, Z. L.; Beeler, D. L.; Rosenberg, R. D. Analysis of Heparan Sulfate Oligosaccharides with Ion Pair-Reverse Phase Capillary High Performance Liquid Chromatography-Microelectrospray Ionization Time-of-Flight Mass Spectrometry. *J. Am. Chem. Soc.* **2002**, *124*, 8707-8718.

32. Zhang, Z.; Xie, J.; Liu, H.; Liu, J.; Linhardt, R. J. Quantification of Heparan Sulfate Disaccharides Using Ion-Pairing Reversed-Phase Microflow High-Performance Liquid Chromatography with Electrospray Ionization Trap Mass Spectrometry. *Anal. Chem.* **2009**, *81*, 4349-4355.
33. Chuang, W.-L.; Christ, M. D.; Rabenstein, D. L. Determination of the Primary Structures of Heparin- and Heparan Sulfate-Derived Oligosaccharides Using Band-Selective Homonuclear-Decoupled Two-Dimensional ¹H NMR Experiments. *Anal. Chem.* **2001**, *73*, 2310-2316.
34. Mascellani, G.; Guerrini, M.; Torri, G.; Liverani, L.; Spelta, F.; Bianchini, P. Characterization of di- and monosulfated, unsaturated heparin disaccharides with terminal N-sulfated 1,6-anhydro-[beta]-d-glucosamine or N-sulfated 1,6-anhydro-[beta]-d-mannosamine residues. *Carbohydr. Res.* **2007**, *342*, 835-842.
35. Yamada, S.; Yoshida, K.; Sugiura, M.; Sugahara, K. One- and Two-Dimensional ¹H-NMR Characterization of Two Series of Sulfated Disaccharides Prepared from Chondroitin Sulfate and Heparan Sulfate/Heparin by Bacterial Eliminas Digestion. *J. Biochem. (Tokyo, Jpn.)* **1992**, *112*, 440-447.
36. Yates, E. A.; Santini, F.; Guerrini, M.; Naggi, A.; Torri, G.; Casu, B. ¹H and ¹³C NMR spectral assignments of the major sequences of twelve systematically modified heparin derivatives. *Carbohydr. Res.* **1996**, *294*, 15-27.
37. Rice, K. G.; Linhardt, R. J. Study of structurally defined oligosaccharide substrates of heparin and heparan monosulfate lyases. *Carbohydr. Res.* **1989**, *190*, 219-233.
38. Lin, Y.; Schiavo, S.; Orjala, J.; Vouros, P.; Kautz, R. Microscale LC-MS-NMR Platform Applied to the Identification of Active Cyanobacterial Metabolites. *Anal. Chem.* **2008**, *80*, 8045-8054.
39. Glasoe, P. K.; Long, F. A. Use of Glass Electrodes to Measure Acidities in Deuterium Oxide 1,2. *J. Phys. Chem.* **1960**, *64*, 188-190.
40. McEwen, I. Broadening of ¹H NMR signals in the spectra of heparin and OSCS by paramagnetic transition metal ions. The use of EDTA to sharpen the signals. *J. Pharm. Biomed. Anal.* **2010**, *51*, 733-735.
41. Linhardt, R. J.; Turnbull, J. E.; Wang, H. M.; Loganathan, D.; Gallagher, J. T. Examination of the Substrate-Specificity of Heparin and Heparan-Sulfate Lyases. *Biochemistry* **1990**, *29*, 2611-2617.
42. Desai, U. R.; Wang, H. M.; Linhardt, R. J. Specificity Studies on the Heparin Lyases from Flavobacterium-Heparinum. *Biochemistry* **1993**, *32*, 8140-8145.
43. Galliher, P. M.; Cooney, C. L.; Langer, R.; Linhardt, R. J. Heparinase production by Flavobacterium heparinum. *Appl. Environ. Microbiol.* **1981**, *41*, 360-365.
44. Lohse, D. L.; Linhardt, R. J. Purification and Characterization of Heparin Lyases from Flavobacterium-Heparinum. *J. Biol. Chem.* **1992**, *267*, 24347-24355.
45. Yamada, S.; Murakami, T.; Tsuda, H.; Yoshida, K.; Sugahara, K. Isolation of the porcine heparin tetrasaccharides with glucuronate 2-O- sulfate. Heparinase cleaves glucuronate 2-O-sulfate-containing disaccharides in highly sulfated blocks in heparin *J. Biol. Chem.* **1995**, *270*, 8696-8705.
46. Yamada, S.; Sakamoto, K.; Tsuda, H.; Yoshida, K.; Sugahara, K.; Khoo, K.-H.; Morris, H. R.; Dell, A. Structural studies on the tri- and tetrasaccharides isolated from porcine intestinal heparin and characterization of heparinase/heparitinases using them as substrates. *Glycobiology* **1994**, *4*, 69-78.

47. Ampofo, S. A.; Wang, H. M.; Linhardt, R. J. Disaccharide compositional analysis of heparin and heparan sulfate using capillary zone electrophoresis. *Anal. Biochem.* **1991**, *199*, 249-255.
48. Kerns, R. J.; Linhardt, R. J. Separation of Hydroxyl Protected Heparin Derived Disaccharides Using Reversed-phase High-Performance Liquid-Chromatography. *J. Chromatogr. A* **1995**, *705*, 369-373.
49. Volpi, N.; Cusmano, M.; Venturelli, T. Qualitative and quantitative studies of heparin and chondroitin sulfates in normal human plasma. *Biochim. Biophys. Acta, Gen. Subj.* **1995**, *1243*, 49-58.
50. Kinoshita, A.; Sugahara, K. Microanalysis of Glycosaminoglycan-Derived Oligosaccharides Labeled with a Fluorophore 2-Aminobenzamide by High-Performance Liquid Chromatography: Application to Disaccharide Composition Analysis and Exosequencing of Oligosaccharides. *Anal. Biochem.* **1999**, *269*, 367-378.
51. Vives, R. R.; Pye, D. A.; Salmivirta, M.; Hopwood, J. J.; Lindahl, U.; Gallagher, J. T. Sequence analysis of heparan sulphate and heparin oligosaccharides. *Biochem. J.* **1999**, *339*, 767-773.
52. Desai, U. R.; Wang, H. M.; Ampofo, S. A.; Linhardt, R. J. Oligosaccharide Composition of Heparin and Low-Molecular-Weight Heparins by Capillary Electrophoresis. *Anal. Biochem.* **1993**, *213*, 120-127.
53. Ruiz-Calero, V.; Puignou, L.; Galceran, M. T. Use of reversed polarity and a pressure gradient in the analysis of disaccharide composition of heparin by capillary electrophoresis. *J. Chromatogr. A* **1998**, *828*, 497-508.
54. Militsopoulou, M.; Lamari, F. N.; Hjerpe, A.; Karamanos, N. K. Determination of twelve heparin- and heparan sulfate-derived disaccharides as 2-aminoacridone derivatives by capillary zone electrophoresis using ultraviolet and laser-induced fluorescence detection. *Electrophoresis* **2002**, *23*, 1104-1109.
55. Limtiaco, J.; Beni, S.; Jones, C.; Langeslay, D.; Larive, C. NMR methods to monitor the enzymatic depolymerization of heparin. *Anal. Bioanal. Chem.* **2010**, *399*, 593-603.
56. Ziegler, A.; Zaia, J. Size-exclusion chromatography of heparin oligosaccharides at high and low pressure. *J. Chromatogr., B: Anal. Technol. Biomed. Life Sci.* **2006**, *837*, 76-86.
57. Schenauer, M. R.; Meissen, J. K.; Seo, Y.; Ames, J. B.; Leary, J. A. Heparan Sulfate Separation, Sequencing, and Isomeric Differentiation: Ion Mobility Spectrometry Reveals Specific Iduronic and Glucuronic Acid-Containing Hexasaccharides. *Anal. Chem.* **2009**, *81*, 10179-10185.
58. Mikhailov, D.; Linhardt, R. J.; Mayo, K. H. NMR solution conformation of heparin-derived hexasaccharide. *Biochem. J.* **1997**, *328*, 51-61.
59. Mikhailov, D.; Mayo, K. H.; Vlahov, I. R.; Toida, T.; Pervin, A.; Linhardt, R. J. NMR solution conformation of heparin-derived tetrasaccharide. *Biochem. J.* **1996**, *318*, 93-102.
60. Wolff, J. J.; Amster, I. J.; Chi, L.; Linhardt, R. J. Electron Detachment Dissociation of Glycosaminoglycan Tetrasaccharides. *J. Am. Soc. Mass Spectrom.* **2007**, *18*, 234-244.
61. Wolff, J. J.; Chi, L.; Linhardt, R. J.; Amster, I. J. Distinguishing Glucuronic from Iduronic Acid in Glycosaminoglycan Tetrasaccharides by Using Electron Detachment Dissociation. *Anal. Chem.* **2007**, *79*, 2015-2022.

62. Anusiewicz, I.; Jasionowski, M.; Skurski, P.; Simons, J. Backbone and Side-Chain Cleavages in Electron Detachment Dissociation (EDD). *The Journal of Physical Chemistry A* **2005**, *109*, 11332-11337.
63. Yang, J.; Mo, J.; Adamson, J. T.; Hakansson, K. Characterization of Oligodeoxynucleotides by Electron Detachment Dissociation Fourier Transform Ion Cyclotron Resonance Mass Spectrometry. *Anal. Chem.* **2005**, *77*, 1876-1882.
64. Wolff, J. J.; Laremore, T. N.; Busch, A. M.; Linhardt, R. J.; Amster, I. J. Electron Detachment Dissociation of Dermatan Sulfate Oligosaccharides. *J. Am. Soc. Mass Spectrom.* **2008**, *19*, 294-304.
65. Wolff, J. J.; Laremore, T. N.; Aslam, H.; Linhardt, R. J.; Amster, I. J. Electron-Induced Dissociation of Glycosaminoglycan Tetrasaccharides. *J. Am. Soc. Mass Spectrom.* **2008**, *19*, 1449-1458.
66. Styles, P.; Soffe, N. F.; Scott, C. A.; Crag, D. A.; Row, F.; White, D. J.; White, P. C. J. A high-resolution NMR probe in which the coil and preamplifier are cooled with liquid helium. *J. Magn. Reson.* **1984**, *60*, 397-404.
67. Robosky, L.; Reily, M.; Avizonis, D. Improving NMR sensitivity by use of salt-tolerant cryogenically cooled probes. *Anal. Bioanal. Chem.* **2007**, *387*, 529-532.
68. Szántay, J. C.; Béni, Z.; Balogh, G.; Gáti, T. The changing role of NMR spectroscopy in off-line impurity identification: A conceptual view. *TrAC Trends in Analytical Chemistry* **2006**, *25*, 806-820.
69. Merchant, Z. M.; Kim, Y. S.; Rice, K. G.; Linhardt, R. J. Structure of Heparin-Derived Tetrasaccharides. *Biochem. J.* **1985**, *229*, 369-377.
70. Kautz, R. A.; Goetzinger, W. K.; Karger, B. L. High-Throughput Microcoil NMR of Compound Libraries Using Zero-Dispersion Segmented Flow Analysis. *J. Comb. Chem.* **2004**, *7*, 14-20.
71. Behnia, B.; Webb, A. G. Limited-Sample NMR Using Solenoidal Microcoils, Perfluorocarbon Plugs, and Capillary Spinning. *Anal. Chem.* **1998**, *70*, 5326-5331.
72. Linker, A.; Hovingh, P. Structural studies on heparin. Tetrasaccharides obtained by heparinase degradation. *Carbohydr. Res.* **1984**, *127*, 75-94.
73. Jin, L.; Hricovíni, M.; Deakin, J. A.; Lyon, M.; Uhrin, D. Residual dipolar coupling investigation of a heparin tetrasaccharide confirms the limited effect of flexibility of the iduronic acid on the molecular shape of heparin. *Glycobiology* **2009**, *19*, 1185-1196.
74. Tjong, S.-C.; Chen, T.-S.; Huang, W.-N.; Wu, W.-g. Structures of Heparin-Derived Tetrasaccharide Bound to Cobra Cardiotoxins: Heparin Binding at a Single Protein Site With Diverse Side Chain Interactions. *Biochemistry* **2007**, *46*, 9941-9952.

CHAPTER SIX

IMPACT-HNMBC Measurements of Amino Sugars

Based on a paper published in the Journal of Magnetic Resonance

J. Magn. Reson., 2011, 209, 323-331.

This chapter describes the development of an *improved and accelerated constant-time proton nitrogen multiple-bond correlation* (IMPACT-HNMBC) pulse sequence and its application in the measurement of ^{15}N chemical shifts as well as long-range ^{15}N - ^1H correlations of amino sugars. The sensitivity and resolution of the gradient-enhanced *heteronuclear multiple bond correlation* (ge-HMBC) pulse sequence¹, *improved and accelerated constant-time heteronuclear multiple-bond correlation* (IMPACT-HMBC) pulse sequence², and the modified pulse sequence with the ^1J -filters removed, IMPACT-HNMBC, were compared. ^{15}N chemical shifts and long-range proton correlations are reported using the IMPACT-HNMBC experiment for *N*-acetyl-glucosamine, *N*-acetyl-galactosamine, and for a series of glucosamine analogs with an *N*-sulfo substitution, unmodified amino group, and 6-*O*-sulfonation. Additionally, ^{15}N - ^2H couplings are also reported for the *N*-acetylated sugars: *N*-acetyl-galactosamine (GalNAc), *N*-acetyl-glucosamine (GlcNAc), and *N*-acetyl-glucosamine-6-*O*-sulfate (GlcNAc6S) in D_2O solutions.

6.1 Introduction: Inverse Detected NMR Experiments for Heteronuclear Correlation

Inverse detected multidimensional NMR experiments such as the *heteronuclear single quantum coherence* (HSQC)³ and the HMBC pulse sequences are routinely used in NMR analysis to improve the sensitivity of nuclei where the low magnetogyric ratios coupled with a low natural abundance complicate acquisition. These experiments are commonly used for structural characterization as they yield information similar to that of direct detection experiments (e.g., HETCOR⁴) but with a significant enhancement in signal intensity. Signal enhancements related to γ_H/γ_X are expected using these inverse detected experiments, where γ_H and γ_X are the magnetogyric ratio of the proton and the heteronuclei (i.e. ¹³C or ¹⁵N), respectively.

While heteronuclei such as ¹³C and ¹⁵N lack the high natural abundance of ¹H, often requiring isotopic enrichment procedures to improve signal intensity, they have the advantage of a large chemical shift range thus providing a much better resolution of chemically distinct sites.⁵ The improved resolution available with heteronuclear NMR experiments is especially advantageous in the analysis of carbohydrates where the greater dispersion in the ¹³C chemical shift facilitates the assignment of the individual spin systems as well as the identification of ring modifications.⁶

6.1.1 Single-bond heteronuclear [¹H-¹⁵N] correlation experiments in GAG analysis

Despite the biological importance of heparin, heparin sulfate (HS), chondroitin sulfate and the other glycosaminoglycans (GAGs),^{7, 8} until recently relatively little information had been reported about the ¹⁵N chemical shifts of the amino sugars in these

biopolymers. The low natural abundance of ^{15}N (0.37%), its negative NOE with nearby protons, and long T_1 relaxation times make direct detection of ^{15}N challenging. These limitations are easily overcome by inverse detected experiments, for example, HSQC spectroscopy, which detects ^{15}N through the resonances of directly-bonded protons.⁹⁻¹¹ There are several examples of the use of HSQC to characterize GAG-derived materials. Sigulinsky et al. used the HSQC experiment in the characterization of ^{15}N -labeled heparosan, a biopolymer with repeating disaccharide residues β -D-glucuronic acid (GlcA) linked to an *N*-acetyl-D-glucosamine (GlcNAc) biosynthesized through bacterial expression systems.^{12, 13} Blundell et al. reported the complete ^1H , ^{13}C and ^{15}N resonance assignments at 900 MHz for a family of hyaluronic acid oligosaccharides at natural abundance. These authors used [^1H - ^{15}N]-HSQC spectra to distinguish the locations of hyaluronic acid GlcNAc residues within a hexasaccharide chain. They observed separate ^{15}N signatures from terminal and internal GlcNAc residues.¹⁴ In a recent report, Pomin et al. used HSQC for detection of ^{15}N -labeled *N*-acetyl-D-galactosamine (GalNAc) in chondroitin sulfate and dermatan sulfate (DS) as well as GlcNAc in heparan sulfate (HS) isolated from cultured mouse lung endothelial and Chinese hamster ovary cells (CHO) cells to which ^{15}N -labeled glutamine was added as a precursor.¹⁵ Pomin et al. noted that HSQC experiments with HS were less useful for structural characterization, as only the GlcNAc residues could be detected by this approach.¹⁵ Although these authors were unable to detect the ^{15}N resonances of either the *N*-sulfo-D-glucosamine (GlcNS) or D-glucosamine (GlcN) residues of HS because of the fast exchange of the nitrogen-bonded protons with water, Zhang et al. reported the detection of a very weak resonance assigned to GlcNS in the HSQC spectrum of uniformly $^{13}\text{C}/^{15}\text{N}$ labeled *N*-sulfo heparosan in D_2O .¹⁶ The structure for GlcN is shown in Figure 6.1 along with

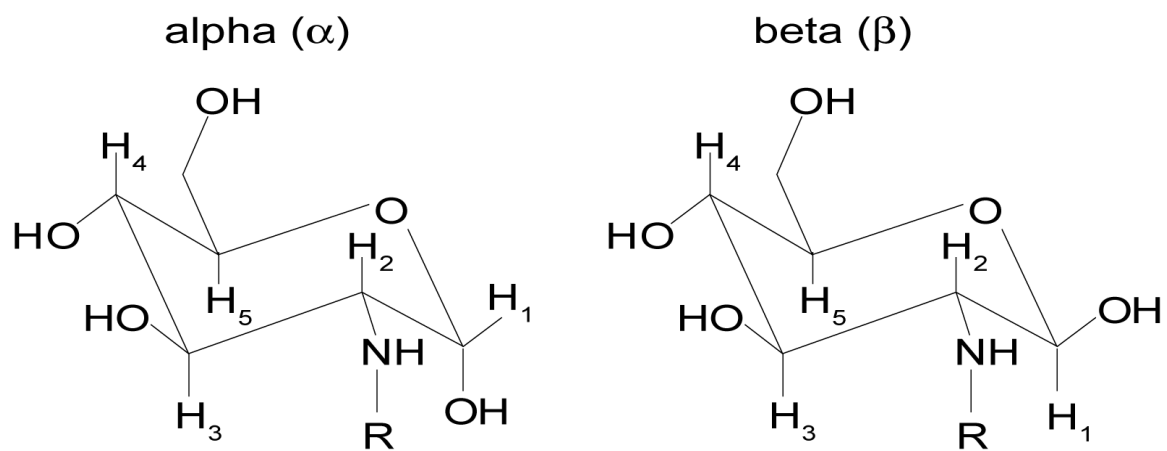


Figure 6.1. Structures of both the alpha (α) and beta (β) anomeric forms of GlcN along with the ^1H numbering scheme used to represent the peaks in the 2D NMR spectra. R: H, SO_3^- , COCH_3

numbering scheme used in the identification of the protons in the presented NMR spectra.

6.1.2 Multiple-bond heteronuclear [^1H - ^{15}N] correlation experiments in GAG analysis

An alternative strategy explored in this study is the use of HMBC experiments to detect ^{15}N chemical shifts through long-range couplings. Such [^1H - ^{13}C]-HMBC experiments are widely employed in the structural characterization of organic compounds.^{11, 17-19} Although applications of [^1H - ^{15}N]-HMBC are less prominent in the literature, characterization of nitrogen containing natural products using this approach is well-accepted and has been the subject of a thorough review by Martin and Haddon.²⁰

6.2 Experimental Section

6.2.1 Chemicals

The sugars examined in this study all contained ^{15}N at natural abundance levels. GlcN hydrochloride and *N*-acetyl-D-glucosamine-6-*O*-sulfate (GlcNAc6S) were purchased from Sigma-Aldrich (St. Louis, MO). GlcNS, *N*-sulfo-D-glucosamine-6-*O*-sulfate (GlcNS6S), and D-glucosamine-6-*O*-sulfate (GlcN6S) were purchased from V-Labs (Covington, LA). GlcNAc was purchased from Alfa Aesar (Ward Hill, MA) while GalNAc was purchased from Acros Organics (Geel, Belgium). The lyophilized powders were reconstituted in D_2O and the solution pD adjusted to 7.40 with 0.1 M DCl and NaOD. Sodium 3-(trimethylsilyl)propionate-2,2,3,3-*d*4 (TMSP, Cambridge Isotope Laboratories) was added as an internal chemical shift reference (0 ppm) and the samples diluted as needed to give a final concentration between 100 mM and 500 mM.

6.2.2 NMR experiments

6.2.2.1 ^1H NMR experiments

NMR spectra were recorded at 25°C using a Bruker Avance spectrometer operating at 599.84 MHz for ^1H and 60.79 MHz for ^{15}N . All NMR experiments were performed using a broadband inverse probe with x, y, and z gradients. ^1H NMR spectra were acquired with 64 transients into 32 768 data points using a 6.6 kHz spectral window and a 2 s relaxation delay. Proton survey spectra were acquired using presaturation to suppress the residual HOD resonance and were processed using Topspin version 1.3. Prior to Fourier transformation, the free induction decays (FIDs) were zero-filled to 65 536 points and apodized by multiplication with an exponential function equivalent to 0.5 Hz line broadening.

6.2.2.2 [^1H - ^{15}N]-HMBC experiments

[^1H - ^{15}N]-HMBC spectra were acquired with an acquisition time of 0.3408 s and a relaxation delay of 2.0 s. Initial parameter sets were optimized using a GlcNAc solution, since the ^{15}N chemical shift of this monosaccharide is easily detected by HSQC. A sample of 500 mM GlcNAc in D_2O was used in the comparison of the different pulse sequences. For the glucosamine mixture solution, GlcN, GlcNAc, and GlcNS were each present at 100 mM. To facilitate detection of sugar resonances close to the solvent peak, D_2O was selected as the solvent for most measurements. For the pulse sequence comparison, 32 scans were acquired into 2048 data points in F_2 with 128 t_1 increments using spectral widths of 3004 Hz and 1215 Hz in the ^1H and ^{15}N dimensions, respectively. The IMPACT-HNMBC spectrum for the glucosamine mixture was acquired with 512 t_1 increments and a spectral width of 3004 Hz and 9115 Hz in the ^1H and ^{15}N dimensions,

respectively. A total of 32 scans were acquired for each increment. Subsequent spectra for the GlcN analogs at a concentration of 200 mM were acquired with 220 t_1 increments and a spectral width of 1215 Hz in the ^{15}N dimension. For the GalNAc sample at 500 mM, 32 scans were acquired into 2048 data points in F_2 and 256 t_1 increments using a spectral width of 3004 Hz and 1215 Hz in the ^1H and ^{15}N dimensions, respectively. Data processing of 2D spectra was performed using the MestReNova NMR suite version 6.2.0 (Santiago de Compostela, Spain). Spectra were apodized in both dimensions with a sinebell function shifted by 90° and zero-filled in the F_1 dimension to 1024 data points. Indirect referencing in the ^{15}N dimension was accomplished using the TMSP resonance in the ^1H NMR spectra.²¹ The signal-to-noise ratios for comparison of the IMPACT-HMBC and IMPACT-HNMBC experiments were determined using the Topspin signal-to-noise processing command (SINO). The signal-to-noise ratios were calculated by summing the projections along F_2 for both the α (122.83 ppm) and β (122.11 ppm) anomers of GlcNAc.^{3, 22}

6.2.2.3 Characterization of the α and β anomers of GalNAc

The HSQC spectrum of 250 mM GalNAc in 90% $\text{H}_2\text{O}/10\%$ D_2O was acquired with 80 scans into 2048 data points in F_2 and 300 t_1 increments with a spectral width of 6009 Hz and 1215 Hz in the ^1H and ^{15}N dimensions, respectively. For purposes of ^1H resonance assignment, DQF-COSY spectra were acquired for all samples with 16 transients into 2048 data points in the F_2 dimension and 256 t_1 increments. COSY spectra were measured with a spectral width of 3 kHz and an acquisition time of 0.3408 sec per t_1 increment.

6.3 Results and Discussion

6.3.1 HMBC Pulse Sequences

The HMBC experiment is a powerful tool for structural elucidation of synthetic compounds and natural products. It allows connections to be made from protons via long-range couplings to carbon nuclei, even those without directly bonded protons such as carbonyl carbons and the quaternary carbons of phenyl rings. A common strategy in structure elucidation is to identify molecular building blocks using homonuclear ^1H - ^1H couplings to assign the resonances within spin systems, and then to stitch the spin systems together using a combination of [^1H - ^{13}C]-HSQC and HMBC correlations. In this process, one-bond couplings are identified in the HSQC spectrum and are correlated with the longer-range HMBC connectivities. Because the HMBC spectra reveal connections through two, three, or occasionally four bonds, the spectra can be crowded and one-bond filters are often incorporated to suppress the cross peaks from directly bonded protons. A commonly implemented version of this experiment is the gradient-enhanced (ge)-HMBC pulse sequence shown in Figure 6.2A.²³⁻²⁵

For complex structures or crowded spectra, the poor digital resolution in the F_1 dimension of the 2D HMBC spectrum can make it difficult to resolve ^{13}C resonances that are close in chemical shift. This problem can be subverted using a band selective version of the experiment in which only the crowded ^{13}C spectral region of interest is excited and the spectrum acquired with greater F_1 digital resolution. However, the improved resolution is compromised by skewing of the cross peaks is observed as a result of proton-proton J-coupling modulation. Claridge and Victoria introduced a band-selective constant-time (CT) pulse sequence that eliminates this modulation due to

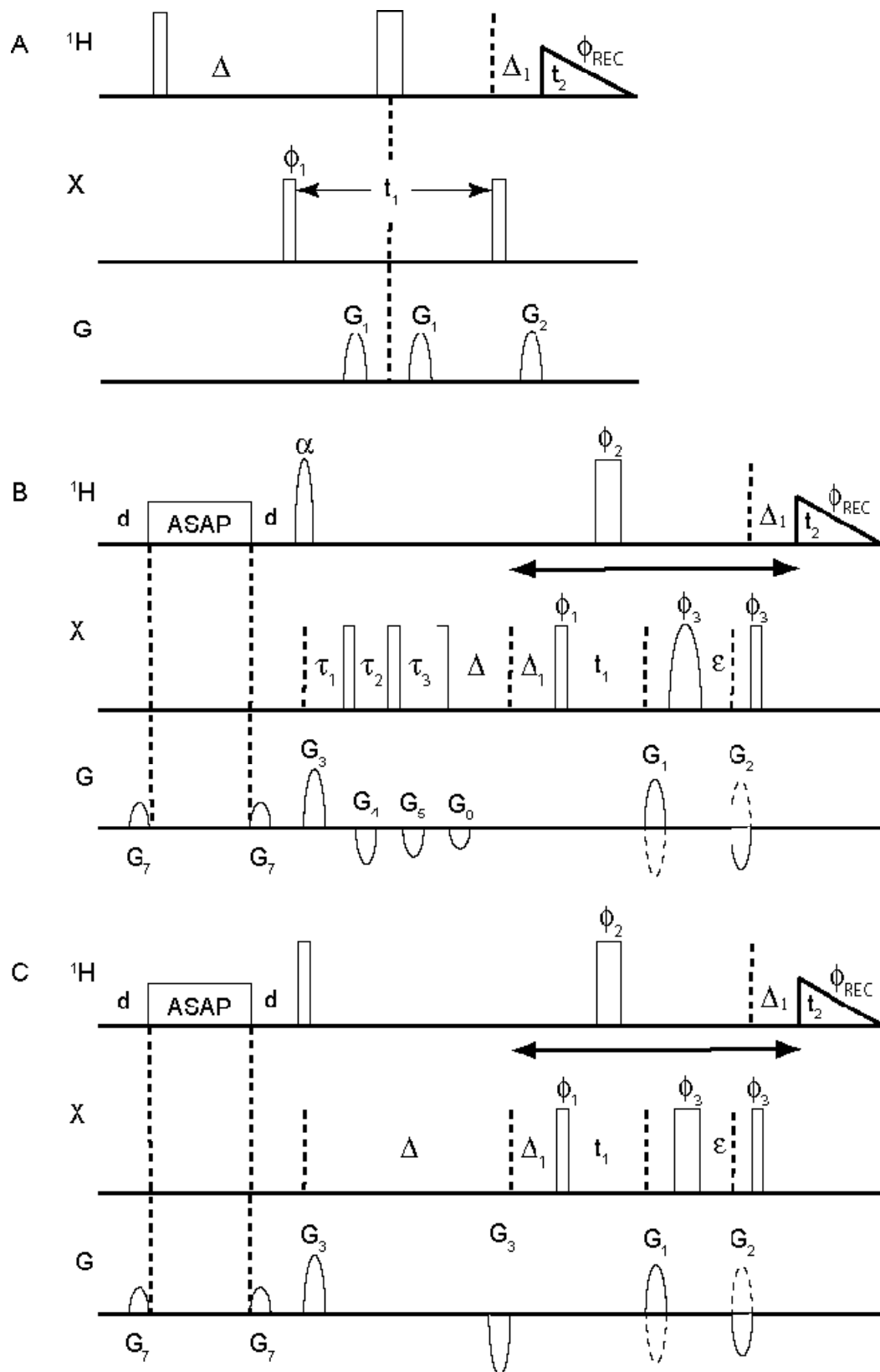


Figure 6.2. The NMR pulse sequences for the (A) ge-HMBC, (B) IMPACT-HMBC, and (C) IMPACT-HNMBC experiments. Narrow open bars indicate 90° pulses and wider bars 180° pulses. In the IMPACT-HNMBC pulse sequence, the first pulse on the ^1H channel, originally a sine shaped pulse, is replaced by a broadband 90° pulse while the 180° pulse on the ^{15}N channel was either a broadband or band-selective Q3 Gaussian pulse. Additionally, the three step low-pass ^1J filter was removed to reduce T_2 losses and improve the S/N in nitrogen detected experiments.

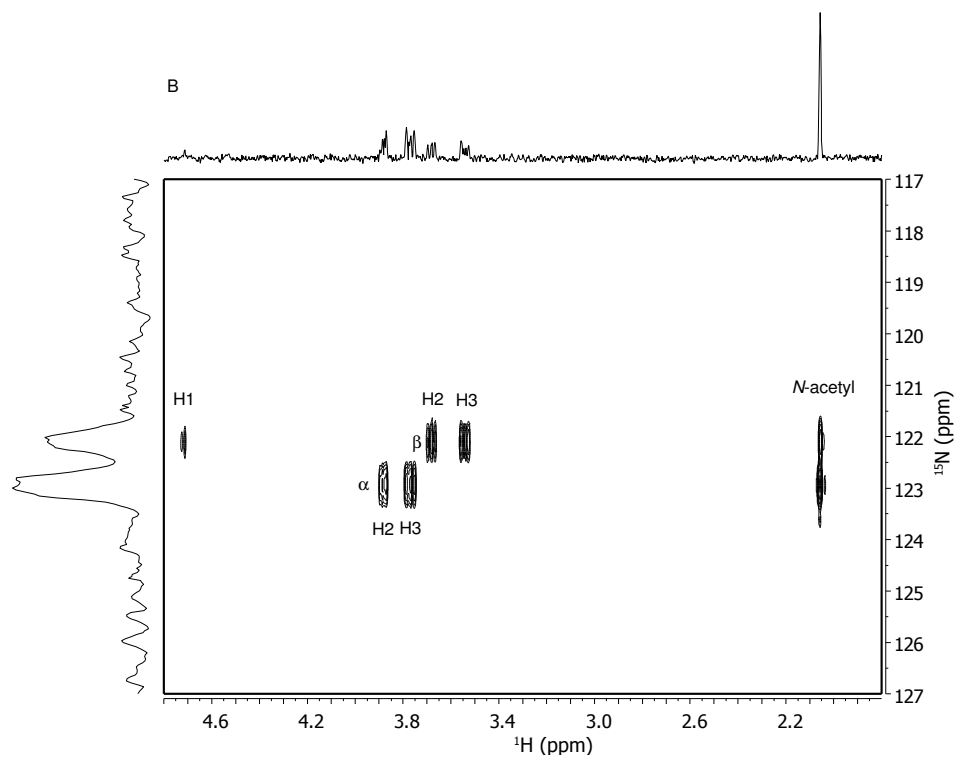
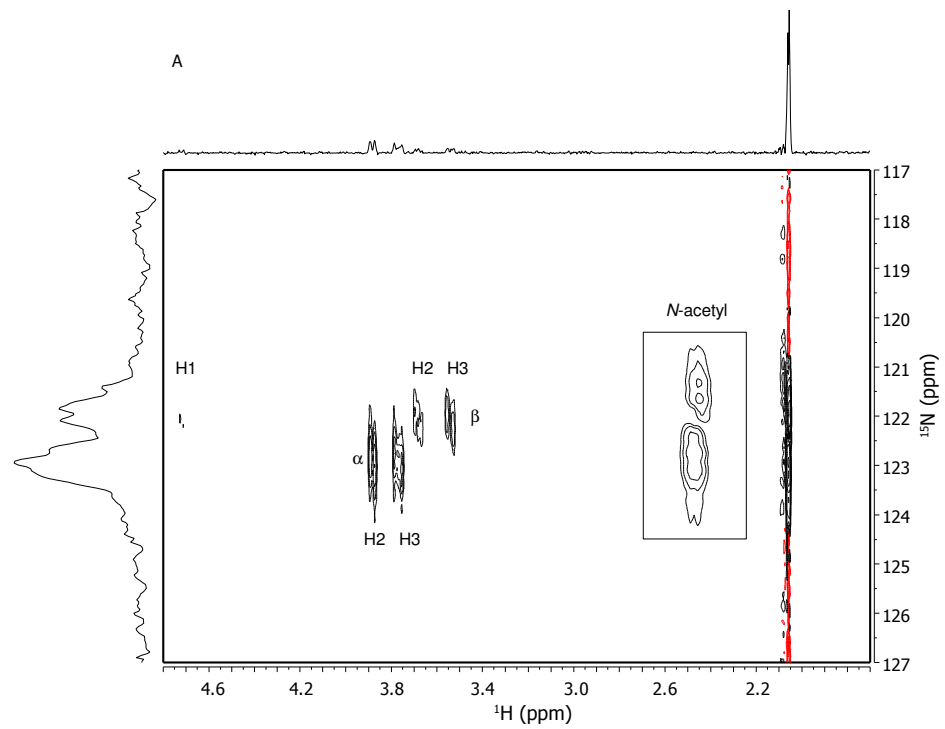
homonuclear couplings, greatly improving the resolution of cross peaks in the resulting CT-HMBC spectrum.²⁶ Building on this idea, Furrer recently reported the IMPACT-HMBC experiment illustrated in Figure 6.2B.² The IMPACT-HMBC pulse sequence uses a constant-time evolution period to minimize cross peak skew introduced by evolution of ^1H - ^1H couplings during the $1/(2J)$ delay and incorporates an ASAP period that reduces F_1 noise while enhancing sensitivity by minimizing the recycle delay used in this experiment.

The goal of this study is to measure ^{15}N chemical shifts of amino sugars through long-range ^1H - ^{15}N couplings. While the pulse sequences shown in Figure 6.2A and B can be used to measure [^1H - ^{15}N]-HMBC spectra, they are not ideal. Because the long-range ^1H - ^{15}N couplings we hope to detect are very small (2-3 Hz), skew from ^1H - ^1H J-modulation should be even more pronounced than in ^1H - ^{13}C experiments, so a constant-time experiment should be beneficial. In [^1H - ^{15}N]-HMBC spectra we do not expect interferences from one-bond couplings and removal of the 1J filters should improve sensitivity.²⁷ Figure 6.2C illustrates a modified pulse sequence we refer to as IMPACT-HNMBC, following the convention of Farley²⁷ and Williamson²⁸. In this pulse sequence, the filters designed to suppress one-bond couplings have been eliminated and the gradient pulses contained within these filters collapsed into a single gradient pulse. Although Figure 6.2C shows the pulse sequence with a non-selective 180° nitrogen inversion pulse, a band-selective pulse can be substituted if greater selectivity in the ^{15}N dimension is desired.

6.3.2 HMBC pulse sequence comparison

Figure 6.3 shows the results obtained for the pulse sequences illustrated in Figure 6.2 using a D₂O solution containing 500 mM GlcNAc at ¹⁵N natural abundance. Each spectrum was acquired using identical parameters with a total acquisition time of 3 hr for each experiment. These spectra contain several long-range ¹H-¹⁵N correlations. Figure 6.3A shows the spectrum produced by the ge-HMBC pulse sequence. Strong cross peaks are observed for the *N*-acetyl protons with weaker cross peaks to the H2 and H3 protons of the sugar ring. The two ¹⁵N chemical shifts result from the presence of α and β GlcNAc anomers. As shown in the insert in Figure 6.3A, because of the singlet nature of the *N*-acetyl resonance these cross peaks are not susceptible to skewing. However the cross peaks to the H2 and H3 protons of the glucosamine ring show a strong variation with proton chemical shift due to ¹H-¹H coupling modulation.

Figure 6.3B shows the results obtained with the IMPACT-HMBC pulse sequence. The ASAP feature of this pulse sequence greatly reduces the F₁ noise ridges from the *N*-acetyl singlet resonance. Compared with the ge-HMBC results in Figure 6.3, this constant-time pulse sequence provides improved sensitivity and resolution in the ¹H dimension by eliminating cross peak skew due to ¹H-¹H coupling.²⁹ As expected, the ¹⁵N projection in Figure 6.3B now contains only two nitrogen peaks, due to the α and β anomers. For the β -anomer, the cross peak between ¹⁵N and H1, clearly detected in Figure 6.3B, appears to be only noise in the ge-HMBC spectrum in Figure 6.3A. Removal of the one-bond J-filters in the IMPACT-HNMBC pulse sequence further enhances the signal-to-noise ratio (S/N) of the spectrum shown in Figure 6.3C by reducing transverse relaxation losses. Although it can be difficult to assess sensitivity



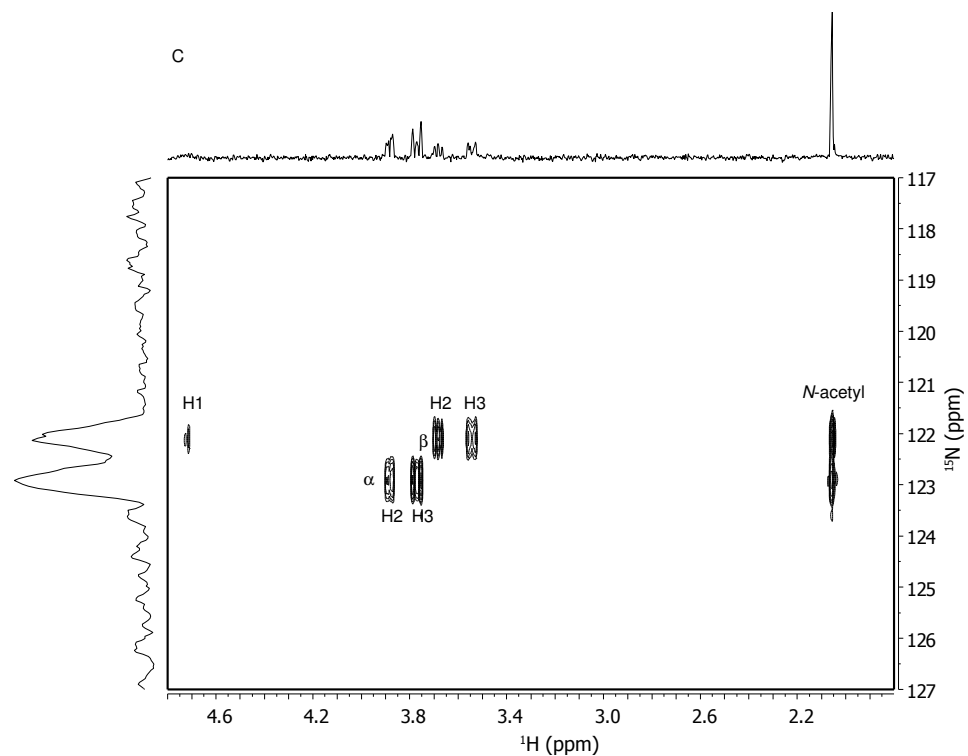


Figure 6.3. Two dimensional HMBC NMR spectra of GlcNAc recorded on a 600 MHz NMR spectrometer using the (A) ge-HMBC, (B) IMPACT-HMBC, and (C) IMPACT-HNMBC pulse sequences. Spectra were measured using 128 increments and 32 transients with a spectral window of 3004 Hz in F_2 and 1215 Hz in F_1 . The measurement time for each of the experiments was approximately 3 hr.

gains from the contour plots alone, the projections in the ^1H dimension reflect the S/N improvements provided by the IMPACT-HNMBC pulse sequence when compared with the ge-HMBC and IMPACT-HMBC experiments. Signal-to-noise improvements from 7% to 36% were observed for the cross peaks in the IMPACT-HNMBC experiment when compared to the IMPACT-HMBC experiments acquired in the same amount of time. The differences in signal intensities observed among the different peaks in the spectra may result from the efficiency of long-range transfer among the protons within the compound. It is expected that the improvement in signal intensity obtained by the IMPACT-HNMBC experiment would be more pronounced when investigating larger compounds where the delay for long-range transfer leads to excessive signal loss by transverse relaxation.³⁰

6.3.3 IMPACT-HNMBC of *N*-modified glucosamines

Although the results shown in Figure 6.3C are promising, the ^{15}N chemical shift of GlcNAc could have been more easily measured using the HSQC experiment. The potential power of this approach is in the detection of ^{15}N chemical shifts through long-range ^1H - ^{15}N couplings in situations where rapid chemical exchange prevents detection of the directly bonded protons using HSQC. Therefore, to test the utility of the IMPACT-HNMBC experiment, we prepared a solution containing three glucosamine analogs, GlcNAc, GlcNS and GlcN, each at concentrations of 100 mM. Figure 6.4A shows the ^1H NMR spectra of these compounds individually and as a mixture. The spectrum of the mixture aptly illustrates the problem of proton resonance overlap due to the limited dispersion common in carbohydrate NMR.

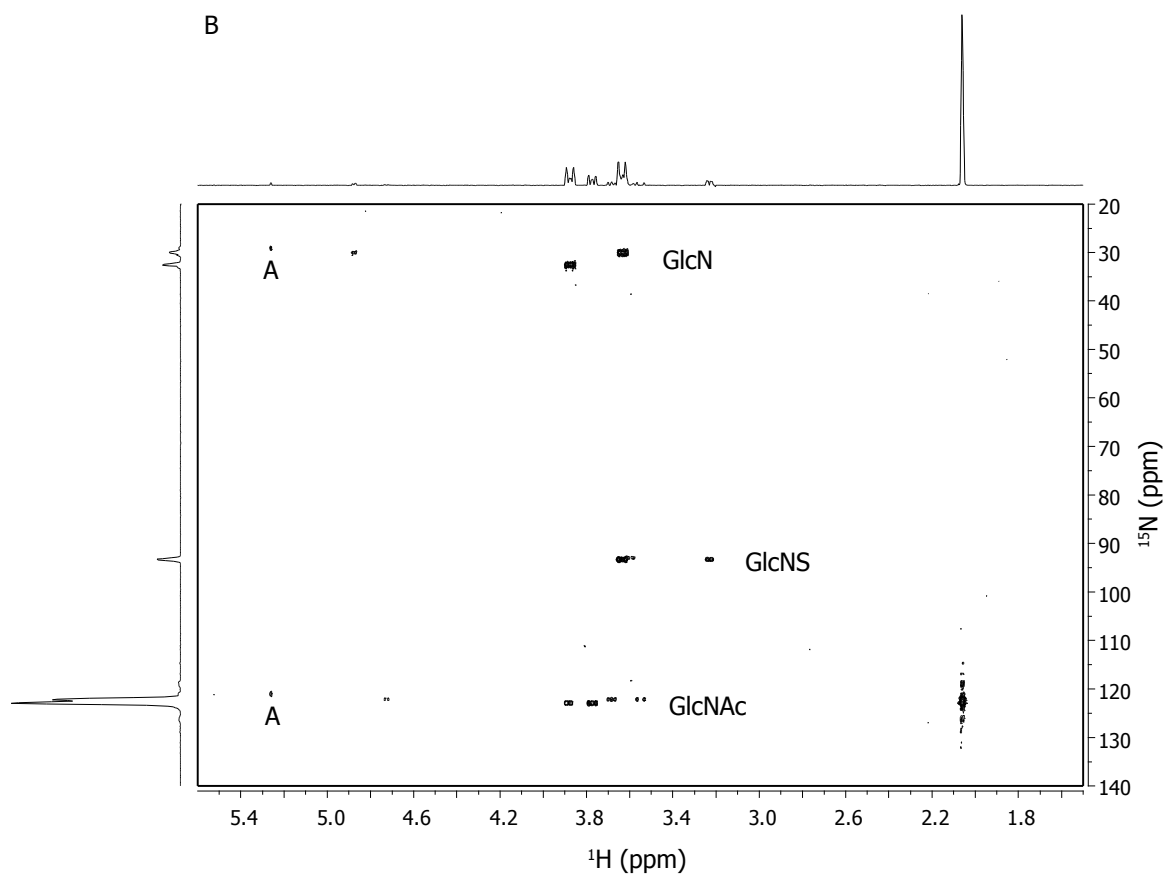
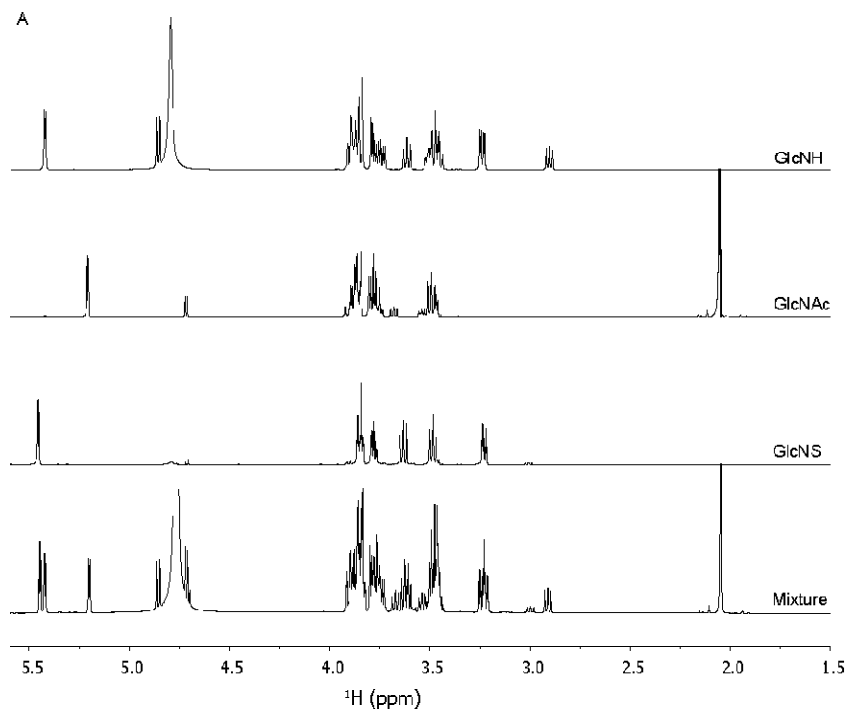


Figure 6.4. (A) ^1H NMR spectrum and (B) IMPACT-HNMBC of a mixture containing GlcN, GlcNS, and GlcNAc each at a concentration of 100 mM in D_2O . The spectrum was acquired with a spectral width of 3004 Hz in the ^1H dimension and 9115 Hz in the ^{15}N dimension in 12 hr. The peaks labeled with an A in the IMPACT-HNMBC correspond to spectral artifacts that are not present in IMPACT-HNMBC spectra acquired of the individual amino sugars.

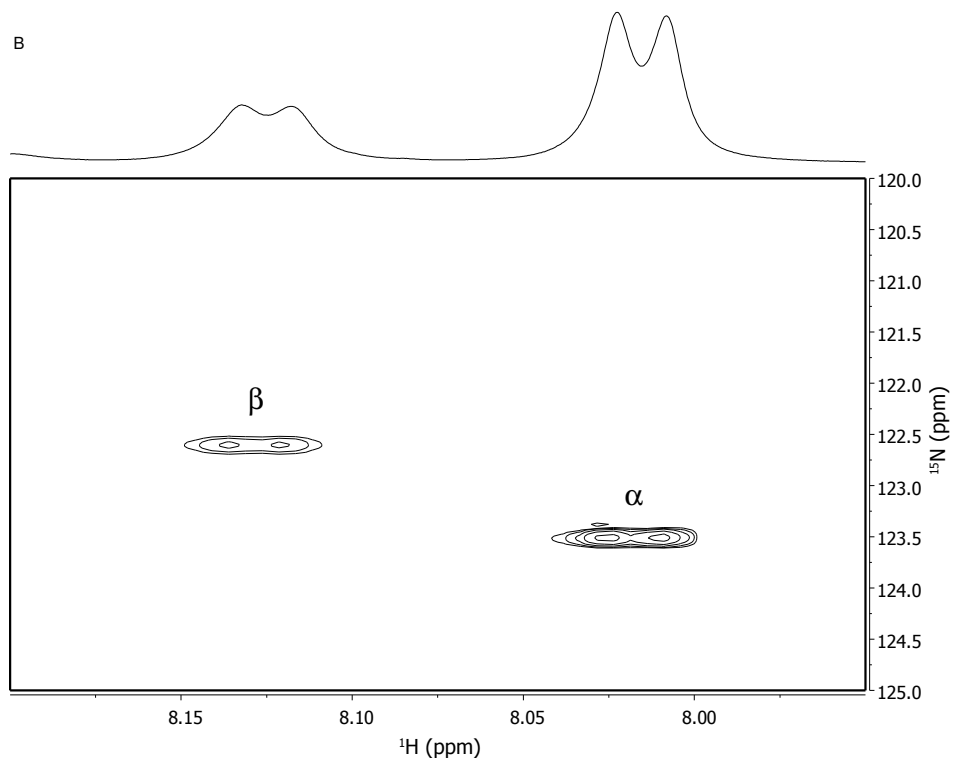
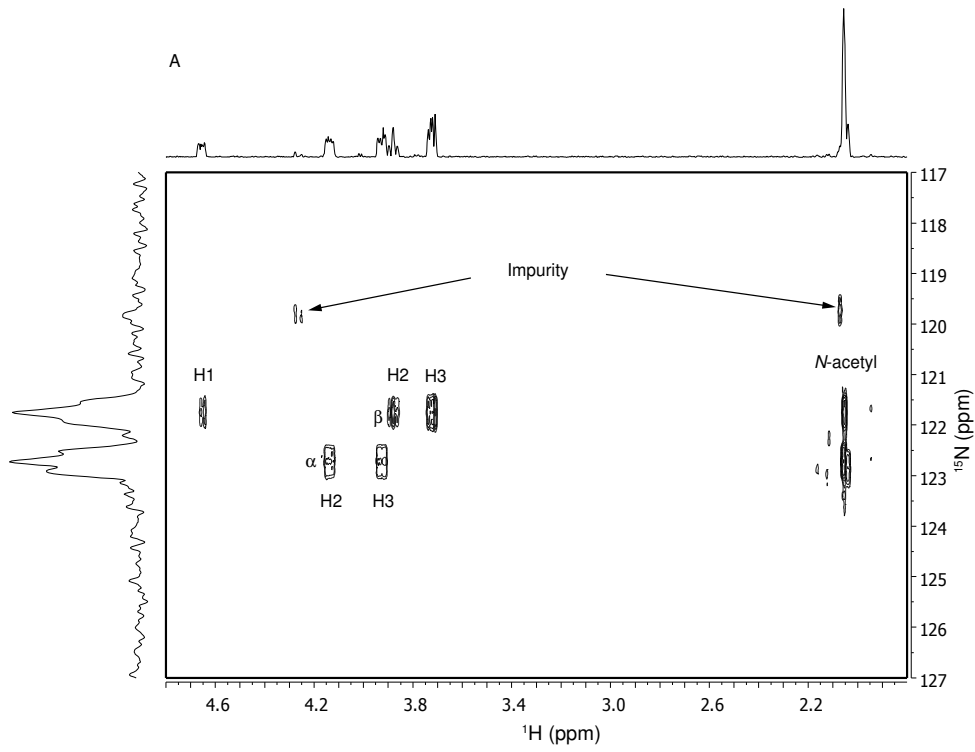
Shown in Figure 6.4B is the IMPACT-HNMBC spectrum measured for the mixture of glucosamine analogs. This spectrum was acquired using an evolution delay of 167 ms, corresponding to an average coupling constant of 3.0 Hz. The sensitivity of the ^{15}N chemical shift to nitrogen substitution is quite dramatic. The ^{15}N chemical shifts observed for this solution ranged from 122.83 ppm (α) and 122.11 (β) for GlcNAc, to 32.49 (α) and 29.93 (β) for GlcN. To our knowledge, this is the first report of the ^{15}N chemical shift of GlcN measured in solution, although Tzou reported ^{15}N chemical shifts for the amino form of GlcN of 16.9 (α) and 15.0 (β) using solid state NMR.³¹ For GlcNS the α anomer was observed with a ^{15}N chemical shift of 93.21 ppm while the less intense β anomer was observed at 92.90 ppm. Compared with Figure 6.4A, the ^1H projection is greatly simplified since only those protons within 2 or 3 bonds of the ^{15}N are detected. It is also interesting that the different glucosamine analogs show different coupling patterns to nearby glucosamine ring protons.

Although it appears from the ^{15}N projection in Figure 6.4B that the sensitivity of the experiment is greater for GlcNAc than for GlcNS or GlcN, this is an artifact of the intense GlcNAc *N*-acetyl resonance. If the projection is derived only from the glucosamine ring cross peaks, the intensities of the peaks in the ^{15}N projection are comparable. Two peak artifacts were also observed in the IMPACT-HNMBC spectrum indicated by the asterisks. We confirmed these peaks as artifacts using previously acquired IMPACT-HNMBC spectra of the individual components. In spectra of the individual components, the artifact peaks were absent.

We have previously reported that the population of the α and β anomers in heparin disaccharides depends on the nature of the substituent on the glucosamine nitrogen³² and the results in Figure 6.4B reinforce that conclusion. The ratio (β/α)

estimated from the peaks in the ^{15}N projection of the IMPACT-HNMBC spectrum (Figure 6.4B) for GlcN, GlcNS, and GlcNAc were 0.58, 0.05, and 0.68, respectively, a trend similar to that observed by Eldridge et al. in the ^1H NMR spectra of heparin disaccharides.³² In GlcNS the bulky *N*-sulfo substitution likely reduces the stability of the β anomer due to steric effects.

Figure 6.5A shows the high-resolution IMPACT-HNMBC spectrum acquired for a solution of 500 mM GalNAc in D_2O with 256 t_1 increments using a spectral width of 1215 Hz in F_1 . In addition to the detection of both the α and β anomers of GalNAc, we also detected a minor contaminant at a ^{15}N chemical shift of 119.73 ppm as shown in Figure 6.5A. For comparison, the HSQC spectrum of GalNAc measured in 90% $\text{H}_2\text{O}/10\%$ D_2O is shown in Figure 6.5B. As in the case of the glucosamine analogs, two ^{15}N chemical shifts are detected corresponding to the α and β anomeric forms of GalNAc. Comparison of the ^{15}N chemical shifts of GalNAc in 100% D_2O and 90% $\text{H}_2\text{O}/10\%$ D_2O reveals an upfield shift of 0.74 and 0.80 ppm for the α and β anomers, respectively, as a result of deuterium substitution. This solvent-dependent difference in nitrogen chemical shifts has been reported previously following exchange of nitrogen-bound ^1H with ^2H in protein amide groups.^{33, 34} Based on the pattern of long-range couplings observed in Figure 6.5A and its greater abundance, we initially assigned the more intense downfield ^{15}N resonance in Figure 6.5B to the α anomer. The ^1H - ^{15}N coupling constants measured for the GalNAc anomeric proton (H1) of 3.65 Hz (α) and 8.45 Hz (β) are also consistent with this assignment. After realizing that our assignment of the ^{15}N chemical shifts of the GalNAc anomers was opposite to that reported by Pomin et al., we measured a COSY spectrum of this solution (Figure 6.5C) which confirmed our assignments. Our



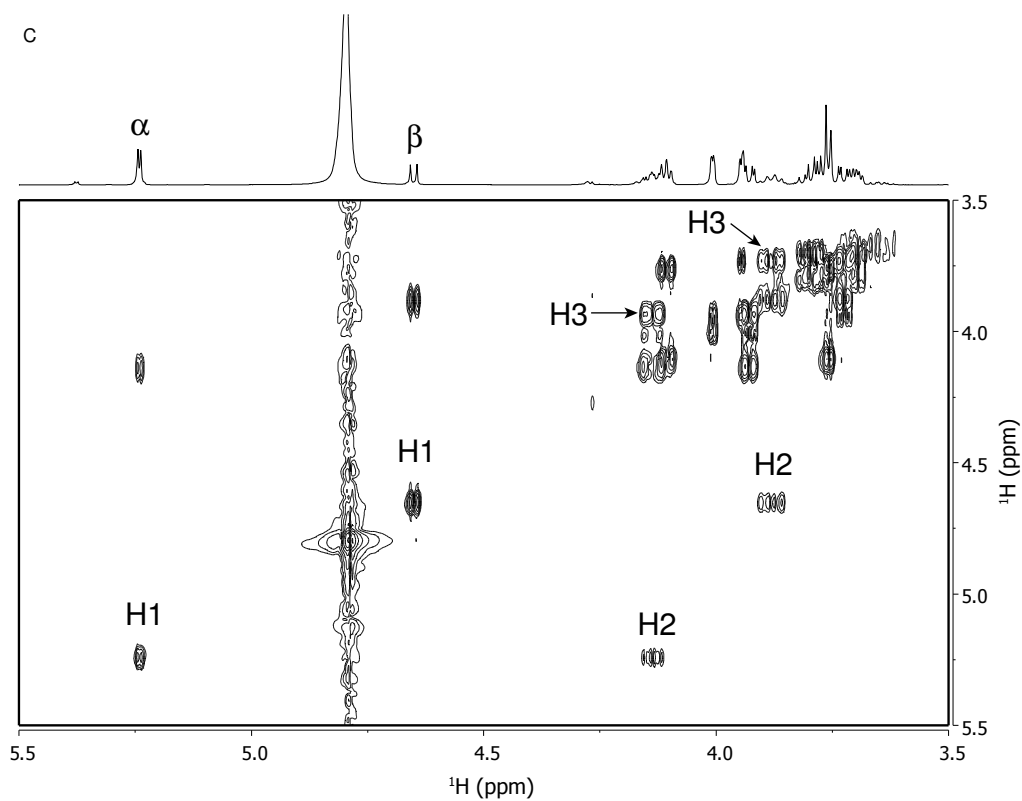


Figure 6.5. Two dimensional NMR spectra of GalNAc: (A) IMPACT-HNMBC at 500 mM GalNAc in D_2O , (B) portion of the HSQC, and (C) DQF-COSY at 250 mM in 90% $\text{H}_2\text{O}/10\% \text{D}_2\text{O}$, confirming the assignment of the α and β anomeric forms.

6.3.4 ^{15}N - ^2H splitting with IMPACT-HNMBC

It is interesting that in the ^{15}N projection in Figure 6.5A, each ^{15}N resonance appears as a triplet. Measurement of the IMPACT-HNMBC spectrum in 90% H_2O /10% D_2O (Figure 6.6) removes the coupling in F_1 and the ^{15}N projection of GalNAc shows only sharp singlet peaks. This is expected as the HMBC experiment, which is based on the spin-echo experiment (Section 1.6.1), is designed to refocus ^1H - ^{15}N couplings. We also did not observe modulation of the ^{15}N projection in similar spectra acquired for the GlcN or GlcNS samples, where fast deuterium exchange is expected. Although this ^{15}N multiplicity is not well-resolved in Figure 6.3C, acquisition of spectra with higher digital resolution in F_1 for D_2O solutions of GlcNAc and GlcNAc6S (Figure 6.7A and B, respectively) also produced triplets in the indirect dimension. We attribute this multiplicity to ^2H - ^{15}N coupling and measured coupling constants of 12.6 Hz and 12.7 Hz for GalNAc and GlcNAc, respectively. Using an average ^{15}N - ^1H coupling constant of 90 Hz³⁵, splitting patterns observed using IMPACT-HNMBC relate well to the ^1J coupling constants estimated for ^{15}N and ^2H of 13.8 Hz using $\gamma_{\text{H}}/\gamma_{\text{D}} \approx 6.5$. Although a 1:1:1 triplet pattern would normally be expected for coupling to a spin 1 nucleus like deuterium, in these spectra the center resonance of the triplet is of greater intensity than the two outer bands. These intensity variations are most likely due to differences in the quadrupolar relaxation of the different spin states of ^2H , which are compounded by the long ^1H - ^{15}N coupling delay used in the HMBC experiment.

IMPACT-HNMBC spectra were also recorded for a series of glucosamine analogs selected to examine the effect of 6-*O* sulfonation, a common motif in heparin and HS, on ^{15}N chemical shift. Table 6.1 summarizes the ^{15}N chemical shifts obtained for all the compounds studied along with the chemical shifts of the protons detected by long-

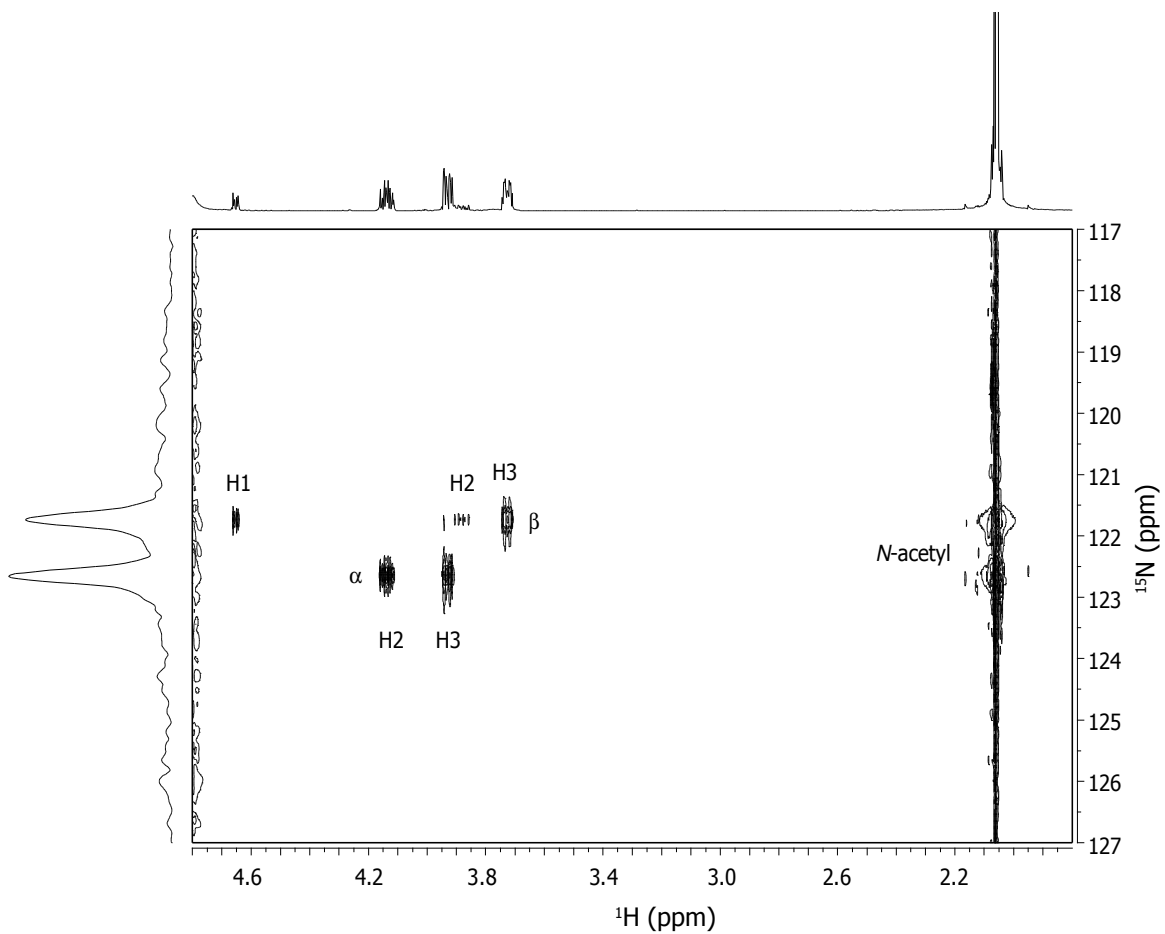


Figure 6.6. IMPACT-HNMRBC spectrum of 634 mM GalNAc in 90% $\text{H}_2\text{O}/10\%\text{D}_2\text{O}$ acquired with 2048 data points in F_2 and 256 t_1 increments. The spectrum was acquired with 74 scans per t_1 increment resulting in a total acquisition time of 14 hr. The peaks in the ^{15}N projection appear as sharp singlet resonances.

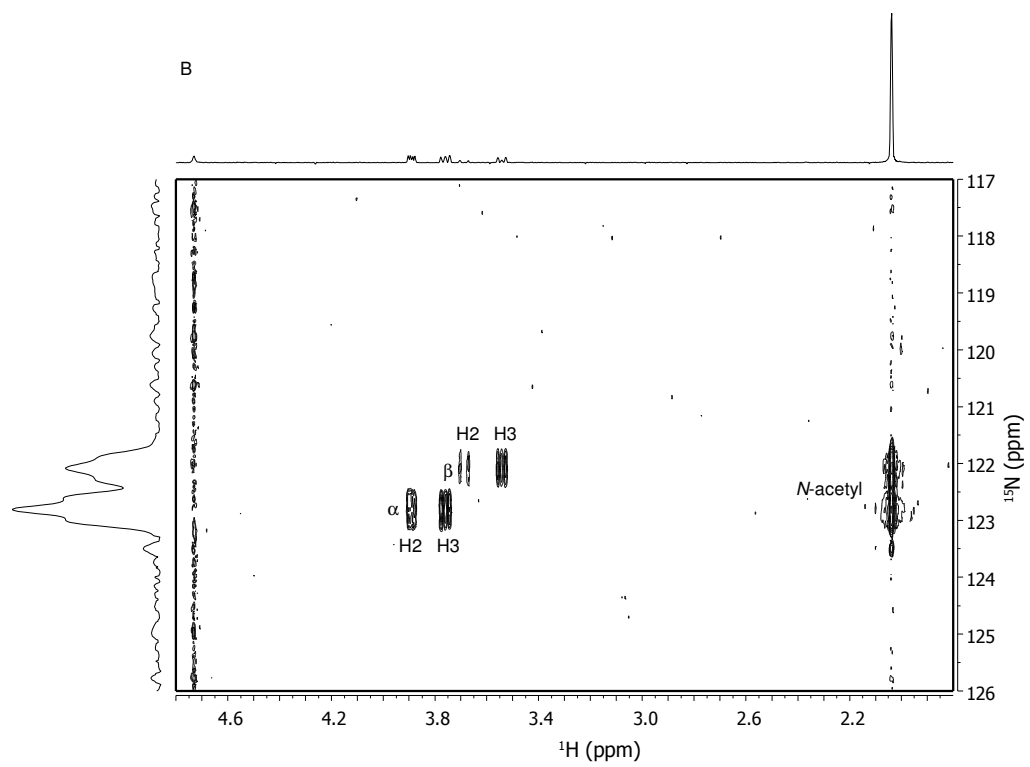
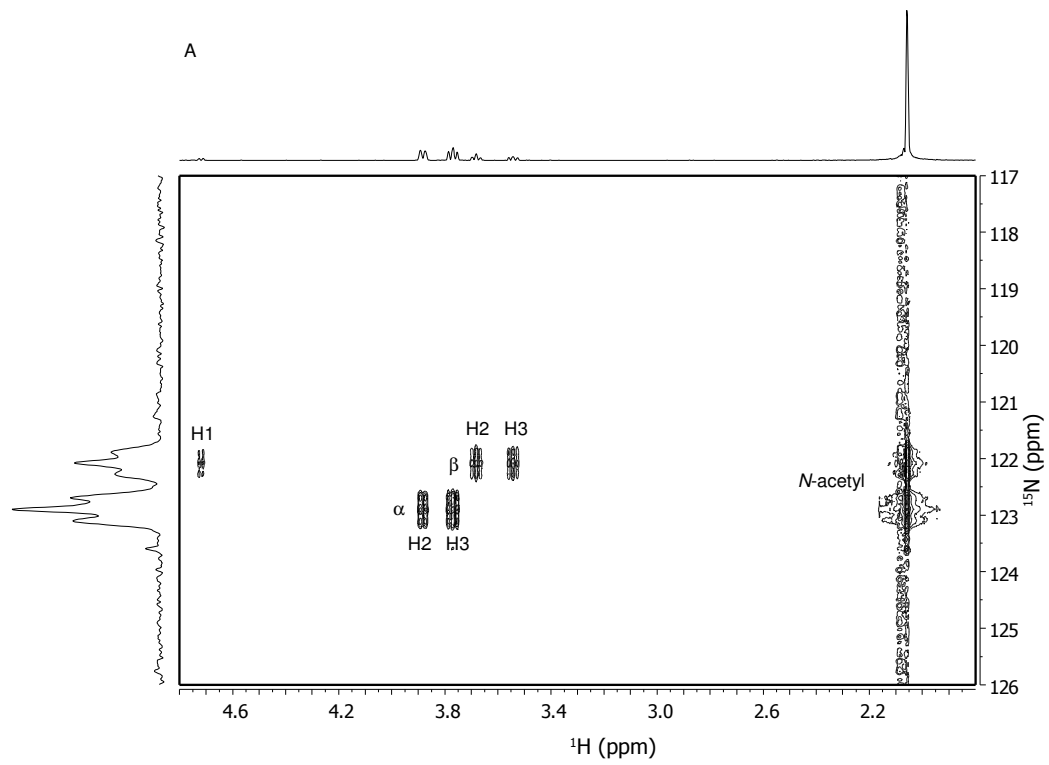
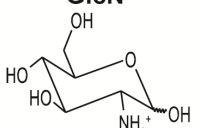
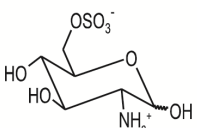
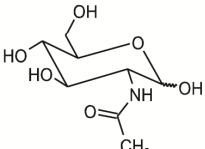
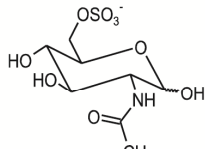
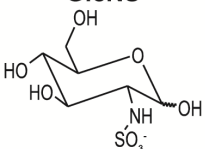
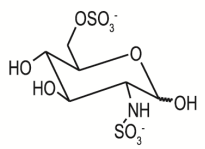
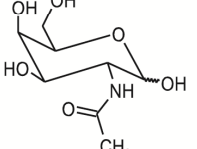


Figure 6.7. IMPACT-HNMBC spectra acquired with 2048 data points in F_2 and 256 t_1 increments; A) 500 mM GlcNAc, B) 200 mM GlcNAc6S. Solutions were prepared in D_2O . In both spectra, the peaks in the ^{15}N projection appear as triplets as a result of J-modulation due to 2H - ^{15}N coupling.

Chemical Shift (ppm)						
Amino Sugar	Anomer	¹⁵ N	H1	H2	H3	N-acetyl
GlcN 	α	32.49			3.874	
	β	29.93	4.873*		3.631	
GlcN6S 	α	32.35			3.879	
	β	29.71			3.626	
GlcNAc 	α	122.83		3.88	3.768	2.056
	β	122.11	4.716	3.68	3.546	2.054
GlcNAc6S 	α	122.70		3.909	3.779	2.056
	β	121.97		3.706	3.56	2.056
GlcNS 	α	93.21		3.229	3.634	
	β	92.90			3.596	
GlcNS6S 	α	93.20		3.254	3.645	
	β	92.74			3.608	
GalNAc 	α	122.78		4.137	3.926	2.057
	β	121.81	4.652	3.879	3.723	2.055

* indicates a very weak signal, detected just above the noise floor

Table 6.1. Amino sugar ¹⁵N chemical shifts and long-range ¹H correlations observed in the IMPACT-HNMBC spectra measured in D₂O solution.

range ^1H - ^{15}N correlations. Although the ^{15}N chemical shift of GalNAc and GlcNAc are quite similar, they can be easily distinguished by their ^1H chemical shifts. It is interesting that the β anomers of GlcNAc and GalNAc show cross peaks to 3 ring protons, H1, H2, and H3, while the α anomer, and indeed most of the analogs examined, show only two cross peaks to H2 and H3. Although *N*-sulfonation results in a significant change in the ^{15}N chemical shift of GlcN, 6-*O* sulfo substitution has no apparent effect on the local environment of the amino nitrogen.

6.4 Summary

The work demonstrates the detection of ^{15}N in amino sugars through long-range couplings to carbon-bound protons of the sugar ring. Comparison of the *ge*-HMBC, IMPACT-HMBC and a modified IMPACT-HNMBC pulse sequence revealed improved sensitivity, resolution and reduced F_1 noise with the IMPACT-HNMBC experiment modified to remove ^1J -filters. Although this approach is less sensitive than using the HSQC experiment to measure ^{15}N chemical shifts through directly bonded protons, the IMPACT-HNMBC experiment has the advantage of being applicable to molecules for which fast exchange precludes efficient detection of N-H resonances, for example in amino sugars containing an *N*-sulfo substitution or an unmodified amino group, common motifs in heparin and HS.

The compounds examined in this study are inexpensive and commercially available. Application of this approach to more complex oligosaccharides will likely require that the experiments be carried out on sub-milligram quantities of isolated material. Clearly the use of ^{15}N -specific labeling will be required to make such measurements practical. Additional instrumental improvements in S/N can also help

increase the sensitivity of these measurements. The experiments reported herein used a 5-mm room temperature broad-band inverse probe. Additional gains in sensitivity could be achieved by performing the measurements in a higher magnetic field, using a cryogenically cooled probe or a microcoil probe with a reduced detection volume.

6.5. Acknowledgements

The authors especially thank Prof. Leonard Mueller for insightful discussions in regards to ^2H - ^{15}N coupling.

6.6 References

1. Bax, A.; Summers, M. F. Proton and carbon-13 assignments from sensitivity-enhanced detection of heteronuclear multiple-bond connectivity by 2D multiple quantum NMR. *J. Am. Chem. Soc.* **1986**, *108*, 2093-2094.
2. Furrer, J. A robust, sensitive, and versatile HMBC experiment for rapid structure elucidation by NMR: IMPACT-HMBC. *Chem. Commun. (Cambridge, U. K.)* **2010**, *46*, 3396-3398.
3. Kay, L.; Keifer, P.; Saarinen, T. Pure absorption gradient enhanced heteronuclear single quantum correlation spectroscopy with improved sensitivity. *J. Am. Chem. Soc.* **1992**, *114*, 10663-10665.
4. Freeman, R.; Morris, G. A. Experimental chemical shift correlation maps in nuclear magnetic resonance spectroscopy. *J. Chem. Soc., Chem. Commun.* **1978**, 684-686.
5. Schnell, I.; Langer, B.; Söntjens, S. H. M.; van Genderen, M. H. P.; Sijbesma, R. P.; Spiess, H. W. Inverse Detection and Heteronuclear Editing in ¹H-¹⁵N Correlation and ¹H-¹H Double-Quantum NMR Spectroscopy in the Solid State under Fast MAS. *J. Magn. Reson.* **2001**, *150*, 57-70.
6. Duus, J. O.; Gotfredsen, C. H.; Bock, K. Carbohydrate Structural Determination by NMR Spectroscopy: Modern Methods and Limitations. *Chem. Rev. (Washington, DC, U. S.)* **2000**, *100*, 4589-4614.
7. Jackson, R. L.; Busch, S. J.; Cardin, A. D. Glycosaminoglycans: molecular properties, protein interactions, and role in physiological processes. *Physiol. Rev.* **1991**, *71*, 481-539.
8. Capila, I.; Linhardt, R. J. Heparin-Protein Interactions. *Angew. Chem., Int. Ed.* **2002**, *41*, 390-412.
9. Bodenhausen, G.; Ruben, D. J. Natural abundance nitrogen-15 NMR by enhanced heteronuclear spectroscopy. *Chem. Phys. Lett.* **1980**, *69*, 185-189.
10. Bax, A.; Griffey, R. H.; Hawkins, B. L. Correlation of proton and nitrogen-15 chemical shifts by multiple quantum NMR. *J. Magn. Reson.* **1983**, *55*, 301-315.
11. Martin, G. E.; Crouch, R. C. Inverse-Detected Two-Dimensional Nmr Methods: Applications in Natural Products Chemistry. *J. Nat. Prod.* **1991**, *54*, 1-70.
12. Sigulinsky, C.; Babu, P.; Victor, X. V.; Kuberan, B. Preparation and characterization of ¹⁵N-enriched, size-defined heparan sulfate precursor oligosaccharides. *Carbohydr. Res.* **2010**, *345*, 250-256.
13. Tran, V.; Nguyen, T.; Raman, K.; Kuberan, B. Applications of isotopes in advancing structural and functional heparanomics. *Anal. Bioanal. Chem.* **2010**, 1-12.
14. Blundell, C. D.; DeAngelis, P. L.; Day, A. J.; Almond, A. Use of ¹⁵N-NMR to resolve molecular details in isotopically-enriched carbohydrates: sequence-specific observations in hyaluronan oligomers up to decasaccharides. *Glycobiology* **2004**, *14*, 999-1009.
15. Pomin, V. H.; Sharp, J. S.; Li, X.; Wang, L.; Prestegard, J. H. Characterization of Glycosaminoglycans by ¹⁵N NMR Spectroscopy and in Vivo Isotopic Labeling. *Anal. Chem.* **2010**, *82*, 4078-4088.
16. Zhang, Z.; McCallum, S. A.; Xie, J.; Nieto, L.; Corzana, F.; Jimenez-Barbero, J. s.; Chen, M.; Liu, J.; Linhardt, R. J. Solution Structures of Chemoenzymatically

- Synthesized Heparin and Its Precursors. *J. Am. Chem. Soc.* **2008**, *130*, 12998-13007.
17. Bax, A.; Marion, D. Improved resolution and sensitivity in ¹H-detected heteronuclear multiple-bond correlation spectroscopy. *J. Magn. Reson.* **1988**, *78*, 186-191.
 18. Fulcrand, H.; Benabdeljalil, C.; Rigaud, J.; Cheynier, V.; Moutounet, M. A new class of wine pigments generated by reaction between pyruvic acid and grape anthocyanins. *Phytochemistry* **1998**, *47*, 1401-1407.
 19. Shen, C. C.; Chang, Y. S.; Ho, L. K. Nuclear-Magnetic-Resonance Studies of 5,7-Dihydroxyflavonoids. *Phytochemistry* **1993**, *34*, 843-845.
 20. Martin, G. E.; Hadden, C. E. Long-Range ¹H-¹⁵N Heteronuclear Shift Correlation at Natural Abundance. *J. Nat. Prod.* **2000**, *63*, 543-585.
 21. Wishart, D. S.; Bigam, C. G.; Yao, J.; Abildgaard, F.; Dyson, H. J.; Oldfield, E.; Markley, J. L.; Sykes, B. D. ¹H, ¹³C and ¹⁵N chemical shift referencing in biomolecular NMR. *J. Biomol. NMR* **1995**, *6*, 135-140.
 22. Palmer, A. G.; Cavanagh, J.; Wright, P. E.; Rance, M. Sensitivity improvement in proton-detected two-dimensional heteronuclear correlation NMR spectroscopy. *J. Magn. Reson.* **1991**, *93*, 151-170.
 23. Parella, T.; Sanchezferrando, F.; Virgili, A. Purge Scheme for Efficient Suppression of Direct Responses in Gradient-Enhanced HMBC Spectra. *J. Magn. Reson.* **1995**, *112*, 241-245.
 24. Ruiz-Cabello, J.; Vuister, G. W.; Moonen, C. T. W.; van Gelderen, P.; Cohen, J. S.; van Zijl, P. C. M. Gradient-enhanced heteronuclear correlation spectroscopy. Theory and experimental aspects. *J. Magn. Reson.* **1992**, *100*, 282-302.
 25. Schleucher, J.; Schwendinger, M.; Sattler, M.; Schmidt, P.; Schedletzky, O.; Glaser, S. J.; Sørensen, O. W.; Griesinger, C. A general enhancement scheme in heteronuclear multidimensional NMR employing pulsed field gradients. *J. Biomol. NMR* **1994**, *4*, 301-306.
 26. Claridge, T. D. W.; Perez-Victoria, I. Enhanced ¹³C resolution in semi-selective HMBC: a band-selective, constant-time HMBC for complex organic structure elucidation by NMR. *Org. Biomol. Chem.* **2003**, *1*, 3632-3634.
 27. Farley, K. A.; Walker, G. S.; Martin, G. E. Long-range two-dimensional H-1-N-13 heteronuclear shift correlation at natural abundance using GHNMQC. A study of the reverse transcriptase inhibitor delavirdine. *Magn. Reson. Chem.* **1997**, *35*, 671-679.
 28. Williamson, R. T.; Sitachitta, N.; Gerwick, W. H. Biosynthesis of the marine cyanobacterial metabolite barbamide. 2: Elucidation of the origin of the thiazole ring by application of a new GHNMQC experiment. *Tetrahedron Lett.* **1999**, *40*, 5175-5178.
 29. Furihata, K.; Seto, H. Constant time HMBC (CT-HMBC), a new HMBC technique useful for improving separation of cross peaks. *Tetrahedron Lett.* **1998**, *39*, 7337-7340.
 30. Phan, A. T.; an Long-range imino proton-¹³C J-couplings and the through-bond correlation of imino and non-exchangeable protons in unlabeled DNA. *J. Biomol. NMR* **2000**, *16*, 175-178.
 31. Tzou, D.-L. M. A solid-state NMR application of the anomeric effect in carbohydrates: galactosamine, glucosamine, and N-acetyl-glucosamine. *Solid State Nucl. Magn. Reson.* **2005**, *27*, 209-214.

32. Eldridge, S. L.; Higgins, L. A.; Dickey, B. J.; Larive, C. K. Insights into the Capillary Electrophoresis Separation of Heparin Disaccharides from Nuclear Magnetic Resonance, pKa, and Electrophoretic Mobility Measurements. *Anal. Chem.* **2009**, *81*, 7406-7415.
33. Hansen, P. E. Isotope effects on chemical shifts of proteins and peptides. *Magn. Reson. Chem.* **2000**, *38*, 1-10.
34. Lycka, A.; Hansen, P. E. Deuterium isotope effects on ^{14}N and ^{15}N nuclear shielding in simple nitrogen-containing compounds. *Magn. Reson. Chem.* **1985**, *23*, 973-976.
35. Yao, L.; Ying, J.; Bax, A. Improved accuracy of ^{15}N - ^1H scalar and residual dipolar couplings from gradient-enhanced IPAP-HSQC experiments on protonated proteins. *J. Biomol. NMR* **2009**, *43*, 161-170.

CHAPTER SEVEN

Conclusion and Future Directions

7.1 Conclusions

The utility of NMR spectroscopy in the identification of OSCS as the adulterant of heparin prompted the FDA and the US pharmacopeia to incorporate NMR in the routine screening of heparin. The availability of an OSCS standard furthered the development of NMR techniques for the analysis and characterization of heparin and its contaminants, helping to safeguard heparin against adulteration by OSCS in the future. In this dissertation we demonstrate the utility of NMR spectroscopy, specifically LC-NMR and diffusion NMR, for the analysis of intact glycosaminoglycans (GAGs) including heparin, DS, CSA, and OSCS. In chapter 2, weak-anion exchange chromatography (WAX)-HPLC-NMR is used for the separation of the intact polysaccharides on an amino-bonded WAX column. Using WAX-HPLC, we were able to get baseline resolution of the three components, heparin, DS + CSA, and OSCS, eliminating problems of spectral interpretation arising from resonance overlap. Because WAX-HPLC operates by a displacement-based mechanism, we were able to semi-quantitatively trap OSCS onto the column offering a mechanism to concentrate OSCS before NMR analysis and significantly improving the overall sensitivity of this method. Although we demonstrated the utility of this method with known heparin contaminants, the approach can be generalized to any unknown anionic contaminant, providing that it can be chromatographically resolved from heparin. NMR was used for the detection and characterization of the sample components, providing conclusive identification of the eluting polysaccharides based on their characteristic NMR fingerprints.

In Chapter 3, the application of diffusion NMR techniques for the *in-situ* separation of heparin contaminants was described. Compared with the physical separation effected by WAX HPLC-NMR, diffusion NMR provides a pseudo-separation spectroscopically. The advantages of diffusion NMR for the routine screening of solutions are in its ease of implementation and non-destructive nature, permitting further analysis by other methods. Using diffusion-ordered spectroscopy (DOSY), we were unable to completely resolve intact heparin from either DS or OSCS, despite their different molecular weights. The impact that solution viscosity had on the measured diffusion coefficients was investigated. We observed that even in fairly dilute GAG solutions, the diffusion behavior of the intact biopolymers can be dominated by viscosity and molecular crowding. Therefore, NMR diffusion results obtained for the intact biopolymer solutions must be interpreted qualitatively. To improve the DOSY resolution of heparin and its impurities, heparinase enzymes were added to the solution to reduce the heparin polysaccharide to smaller oligosaccharides which diffuse much faster than the intact DS and OSCS impurities. Following the enzymatic depolymerization of heparin, diffusion-editing was used to selectively attenuate the resonances of the faster diffusing heparin oligosaccharides while allowing acquisition of a ^1H NMR spectrum of the intact GAG contaminant.

Diffusion NMR was also used in Chapter 4 to monitor the enzymatic depolymerization of heparin with heparinase I. This approach provides investigators the opportunity to monitor and quench the reaction at a point where larger oligosaccharides, which are more relevant for protein-binding studies, dominate the depolymerization products.

The requirement of relatively large sample amounts for analysis with NMR spectroscopy and the multiple separation steps for the isolation of pure oligosaccharides continues to be a bottleneck in efforts aimed at the characterization of heparin's microstructure. The microcoil NMR approach described in Chapter 5 allows for the acquisition of NMR spectra for microgram quantities of heparin-derived oligosaccharides. Using microcoil NMR, quantities of up to 2-3 times less material is required when compared to conventional 5 mm NMR tubes. A further improvement in sensitivity was obtained by sandwiching the analyte solution between plugs of deuterated chloroform, improving the probe fill factor and sensitivity by about another factor of 2. This method of sample introduction also provided an efficient means of delivering and positioning the sample within the active volume of the CapNMR probe by monitoring of the deuterium lock. While the sensitivity gains achieved with this approach are relatively modest, because heparin oligosaccharides are isolated through lengthy and laborious procedures, a 5-fold sensitivity increase can translate to a significant reduction in the time and effort necessary to isolate sufficient quantities of oligosaccharides for NMR characterization.

In Chapter 6, we demonstrate the utility of the IMPACT-HNMBC pulse sequence in the detection of ^{15}N in amino sugars through long-range couplings to carbon-bound protons of the sugar ring. Although this approach is considerably less sensitive than using the HSQC experiment to measure ^{15}N chemical shifts through the directly bonded protons, the IMPACT-HNMBC experiment has the advantage of being applicable to molecules for which fast exchange precludes efficient detection of N-H resonances, for example in amino sugars containing an *N*-sulfo substitution or an unmodified amino group.

7.2 Future Directions

7.2.1 Capillary Isotachophoresis (cITP)-NMR

The potential of CE for the separation of heparin and OSCS has been demonstrated through its use to screen contaminated heparin lots. The application of CE in the analysis of contaminated batches of heparin was aided by the presence of a significant quantity of OSCS in contaminated samples, as baseline resolution of the heparin and OSCS peaks was not achieved by this method. Optimization of CE in the separation of heparin contaminated solutions by Wielgos et al.¹ and Somsen et al.² have improved the limits of detection to 0.1% of the total heparin. This is significantly better than the 1-5% necessary for reliable determination in the initial CE separation.³

Our research group has pioneered the development of cITP-NMR and has demonstrated its use for analysis of heparin di- and tetrasaccharides.^{4, 5} In these experiments we take advantage of the ability of cITP to concentrate trace components while effecting a separation based on differences in electrophoretic mobility. For example, in on-line cITP-NMR experiments, our group has demonstrated the ability to obtain ¹H NMR spectra of acetaminophen impurities at the 0.1% level without any interference from the parent drug.⁶ The separation and analysis of contaminated heparin samples by cITP would be complicated by the heterogeneity of heparin itself and would likely be effective only if the electrophoretic mobilities of the components differ significantly as should be the case when OSCS is the contaminant. Most investigators using cITP employ it as a preconcentration method on the front end of a CE separation. In this application, cITP selectively concentrates ionic species which are then separated using the superior resolution of the CE.

The electrophoretic mobility of the GAGs is controlled largely by the net charge per disaccharide subunit with the net charge determined by the number of negative (SO_3^- and COO^-) moieties and any positive charges due to free amino groups on the glucosamine. For example, in cITP-NMR experiments the heparin IS disaccharide and hexasulfonated tetrasaccharide co-migrate.^{4, 5} We expect that a highly sulfonated impurity like OSCS to be focused ahead of less sulfonated components such as heparin and DS.

7.2.2 Heteronuclear Hartmann-Hahn (HEHAHA)

In addition to the contamination of heparin with OSCS and DS, chemical modification of heparin during the manufacturing process can be another source of heparin impurities, for example those introduced by *O*-acetylation.⁷ Such impurities are likely to be present at low levels and can be challenging to identify due to their structural similarity to heparin. A novel heteronuclear NMR experiment, HEHAHA, introduced by Jones and Bendiak,⁸ has been used for characterization of the primary structure of oligosaccharides as well as to determine positions of modification. This experiment uses doubly ^{13}C -labeled acetyl groups to establish correlations between protons on the sugar rings and *O*-acetyl moieties.^{8, 9} A selective version of this experiment, SHEHAHA, accomplishes magnetization transfer between the carbonyl ^{13}C and the proximal proton on the sugar ring while suppressing proton-proton TOCSY relay to the other sugar ring protons, allowing unambiguous assignment of the location of the *O*-acetyl group.¹⁰

Using HEHAHA, we expect to get a more efficient transfer of magnetization between nuclei when compared to delay based transfer methods such as HSQC and HMBC as presented in Chapter 6. The efficiency of the transfer in the HEHAHA

experiment is based on matching of the Hartmann-Hahn condition for the isotopically labeled ^{13}C and ^1H using a spin-lock sequence as is found in the 2D TOCSY experiment. Additionally, cross peak multiplet patterns appear in-phase and purely absorptive. From the multiplet pattern, scalar couplings between the ring protons can be accurately measured and used to define the stereochemistry of the sugar ring.⁹

7.2.3 Hyperpolarization

Hyperpolarization techniques have been demonstrated to significantly improve the sensitivity of NMR spectroscopy.¹¹⁻¹³ A number of hyperpolarization techniques are available to boost the sensitivity of NMR, the most logical hyperpolarization technique in the analysis of heparin would be to carry out the microwave irradiation *in situ*, at high field strengths, and phase in which the sample is to be studied. However the inefficiency of the electron-nuclear spin transfer mechanism in liquids at high fields, compounded by the short relaxation times of the spins in solution, makes hyperpolarization of the molecule in the solution state highly impractical.¹² Therefore, hyperpolarization transfer techniques are carried out in an *ex situ* manner where the sample is irradiated as a solid at cryogenic temperatures and the hyperpolarized sample is subsequently melted and transferred into the NMR for detection.¹³⁻¹⁶

Signal enhancements of up to 44,400 for ^{13}C and 23,500 for ^{15}N are attainable using *ex situ* polarization techniques.¹⁶ With the introduction of single scan multidimensional NMR pulse sequences, ^{15}N heteronuclear correlation experiments can now be performed with mass-limited amounts of labeled materials in the ms time frame.^{17, 18} Hyperpolarization would significantly improve our ability to measure ^{15}N chemical shift in the intact heparin polymer as well as for depolymerized heparin

oligosaccharides corresponding to different structural features. This includes substitutions at the amino position as well as modification throughout the glucosamine ring.

7.3 References

1. Wielgos, T.; Havel, K.; Ivanova, N.; Weinberger, R. Determination of impurities in heparin by capillary electrophoresis using high molarity phosphate buffers. *J. Pharm. Biomed. Anal.* **2009**, *49*, 319-326.
2. Somsen, G. W.; Tak, Y. H.; Toraño, J. S.; Jongen, P. M. J. M.; de Jong, G. J. Determination of oversulfated chondroitin sulfate and dermatan sulfate impurities in heparin by capillary electrophoresis. *J. Chromatogr., A* **2009**, *1216*, 4107-4112.
3. Patel, R. P.; Narkowicz, C.; Hutchinson, J. P.; Hilder, E. F.; Jacobson, G. A. A simple capillary electrophoresis method for the rapid separation and determination of intact low molecular weight and unfractionated heparins. *J. Pharm. Biomed. Anal.* **2008**, *46*, 30-35.
4. Korir, A. K.; Almeida, V. K.; Malkin, D. S.; Larive, C. K. Separation and Analysis of Nanomole Quantities of Heparin Oligosaccharides Using On-Line Capillary Isotachopheresis Coupled with NMR Detection. *Anal. Chem.* **2005**, *77*, 5998-6003.
5. Korir, A.; Larive, C. On-line NMR detection of microgram quantities of heparin-derived oligosaccharides and their structure elucidation by microcoil NMR. *Anal. Bioanal. Chem.* **2007**, *388*, 1707-1716.
6. Eldridge, S. L.; Almeida, V. K.; Korir, A. K.; Larive, C. K. Separation and Analysis of Trace Degradants in a Pharmaceutical Formulation Using On-Line Capillary Isotachopheresis-NMR. *Anal. Chem.* **2007**, *79*, 8446-8453.
7. Guerrini, M.; Zhang, Z.; Shriver, Z.; Naggi, A.; Masuko, S.; Langer, R.; Casu, B.; Linhardt, R. J.; Torri, G.; Sasisekharan, R. Orthogonal analytical approaches to detect potential contaminants in heparin. *Proc. Natl. Acad. Sci. U. S. A.* **2009**, *106*, 16956-16961.
8. Jones, D. N. M.; Bendiak, B. Novel multi-dimensional heteronuclear NMR techniques for the study of ¹³C-O-acetylated oligosaccharides: Expanding the dimensions for carbohydrate structures. *J. Biomol. NMR* **1999**, *15*, 157-168.
9. Bendiak, B.; Fang, T. T.; Jones, D. N. M. An effective strategy for structural elucidation of oligosaccharides through NMR spectroscopy combined with peracetylation using doubly ¹³C-labeled acetyl groups. *Can. J. Chem.* **2002**, *80*, 1032-1050.
10. Meng, X.; Nguyen, W. H.; Nowick, J. S.; Shaka, A. J. Selective heteronuclear Hartmann-Hahn: A multiple-pulse sequence for selective magnetization transfer in the structural elucidation of "isotagged" oligosaccharides. *J. Magn. Reson.* **2010**, *203*, 73-80.
11. Maly, T.; Debelouchina, G. T.; Bajaj, V. S.; Hu, K.-N.; Joo, C.-G.; MakJurkauskas, M. L.; Sirigiri, J. R.; van der Wel, P. C. A.; Herzfeld, J.; Temkin, R. J.; Griffin, R. G. Dynamic nuclear polarization at high magnetic fields. *J. Chem. Phys.* **2008**, *128*, 052211-052219.
12. Frydman, L.; Blazina, D. Ultrafast two-dimensional nuclear magnetic resonance spectroscopy of hyperpolarized solutions. *Nat. Phys.* **2007**, *3*, 415-419.
13. Hall, D. A.; Maus, D. C.; Gerfen, G. J.; Inati, S. J.; Becerra, L. R.; Dahlquist, F. W.; Griffin, R. G. Polarization-Enhanced NMR Spectroscopy of Biomolecules in Frozen Solution. *Science* **1997**, *276*, 930-932.

14. Becerra, L. R.; Gerfen, G. J.; Bellew, B. F.; Bryant, J. A.; Hall, D. A.; Inati, S. J.; Weber, R. T.; Un, S.; Prisner, T. F.; McDermott, A. E.; Fishbein, K. W.; Kreisler, K. E.; Temkin, R. J.; Singel, D. J.; Griffin, R. G. A Spectrometer for Dynamic Nuclear Polarization and Electron Paramagnetic Resonance at High Frequencies. *J. Magn. Reson.* **1995**, *117*, 28-40.
15. Wolber, J.; Ellner, F.; Fridlund, B.; Gram, A.; Jóhannesson, H.; Hansson, G.; Hansson, L. H.; Lerche, M. H.; Månsson, S.; Servin, R.; Thaning, M.; Golman, K.; Ardenkjær-Larsen, J. H. Generating highly polarized nuclear spins in solution using dynamic nuclear polarization. *Nucl. Instrum. Methods Phys. Res., Sect. A* **2004**, *526*, 173-181.
16. Ardenkjær-Larsen, J. H.; Fridlund, B.; Gram, A.; Hansson, G.; Hansson, L.; Lerche, M. H.; Servin, R.; Thaning, M.; Golman, K. Increase in signal-to-noise ratio of > 10,000 times in liquid-state NMR. *Proc. Natl. Acad. Sci. U. S. A.* **2003**, *100*, 10158-10163.
17. Shrot, Y.; Shapira, B.; Frydman, L. Ultrafast 2D NMR spectroscopy using a continuous spatial encoding of the spin interactions. *J. Magn. Reson.* **2004**, *171*, 163-170.
18. Frydman, L.; Lupulescu, A.; Scherf, T. Principles and Features of Single-Scan Two-Dimensional NMR Spectroscopy. *J. Am. Chem. Soc.* **2003**, *125*, 9204-9217.